

Tissue scale electrophysiological-mechanical continuum modelling for white matter transcranial ultrasound neuromodulation

Ciara Felix

Oriel College

Department of Engineering Science

University of Oxford

Supervised by:

Professor Antoine Jérusalem

Thesis for the degree of

Doctor of Philosophy

2022

Acknowledgements

Throughout my DPhil, I have received a great deal of support, guidance and assistance. First of all, I would like to give my sincere gratitude to my supervisor, Professor Antoine Jérusalem, for not only giving me the opportunity to study a DPhil in his research group, but also for sharing his knowledge, expertise and network, which had been very invaluable in my research. I would like to thank Dr. Haoyu Chen for acting as my second supervisor and for giving me enormous assistance and guidance in developing the theoretical framework for the flexoelectric tissue model. I would like to thank Dr. Davide Folloni for his tremendous help in post-processing DTI data, using probabilistic tractography, creating tractography masks, and for his much needed advice and knowledge on experimental ultrasound neuromodulation. I would like to thank Dr. Bradley Treeby for his help in using *k*-Wave and for providing constructive input on my work. Thank you to Dr. Lennart Verhagen and Dr. Jerome Sallet for their guidance on ultrasound neuromodulation as well, and for providing the experimental data for my project. I would like to thank Dr. Daniel García-González for patiently guiding me in the first year of my DPhil and helping me figure out the direction of my project. Furthermore, I would like to kindly acknowledge the EPSRC DTA studentship (Reference number EP/N509711/1) from UKRI (United Kingdom Research and Innovation) for their financial support on my research project.

I would like to recognise all the help and support that have been given to me by members of my research group. I would like to thank Ice for all the support she gave me in our first year of DPhil together, and for helping me in all aspects of my work. I would like to thank Caroline for the time she dedicated to read my transfer report and always giving a very detailed feedback. Thank you to Miren for spreading her enthusiasm for research, for inspiring us with her work in IBME,

and for always being there to offer uplifting advice. Thank you to Celine for spreading her positivity not just to me but also to everyone else, and for always being there to support and encourage me whenever I need it. Thank you to Sara for always having the time to listen, help and answer all my questions, and for spending the time to go over my work and provide suggestions and feedback. Thank you to Yanis for always being willing to help with anything and answering all my questions. Thank you to Aaron for helping me learn how to use Abaqus and for spending a lot of time working with me on radiation force. Thank you to Kamel and Sylvin for all their help on finite element method. I would also like to thank Casey, Hannah, Alonso, Juliet, Amir, Anna, Emily, Charlotte and Sahand for all the encouragement and help they have given me.

I would like to thank all my friends and family who have helped and supported me throughout my DPhil. Specifically, thank you to Barbara, Trish and Tammy for always being there for me. Thank you to my parents, Dennis and Annalyn, and my siblings, Marian and Carl, for always believing in me. Thank you to my aunt, Tita Ning, for always encouraging and supporting me as well as always reminding me to never give up. Thank you to my grandparents, Lola Poleng, Lola Ising, Lolo Max and Lolo Dyeng, for their love and for being great inspirations in my life. Thank you to Tito Romy, Tita Chai, Gabriel, Enzo, Olivia, Miguel, Tita Theen, Tito Oji, Tita Carizza, Tito Niel and Tita Majo for all their love and support. Last but not the least, I would like to thank Alex for his never-ending support, advice and encouragement as well as for always pushing me to be better and believe in myself.

Abstract

Neurological disorders are a substantial health and economic burden worldwide. Low-intensity transcranial ultrasound stimulation (TUS) is now considered as one of the most promising treatments for neurological disorders due to its high spatial resolution compared to other non-invasive neuromodulation methods. While for many decades now, ultrasound has been known to be able to influence or modulate neuronal activities in the brain, its underlying mechanisms are still poorly understood. Maybe not fully unrelated, while nerve impulses have traditionally been considered to be a purely electrical phenomenon, a growing body of evidence is now pointing towards additional thermodynamic changes occuring alongside the action potential. Numerous models have been proposed to study this electromechanical coupling phenomenon. Among these, the flexoelectric theory is postulating that a temporal variation of strain gradient in the membrane leads to current creation. Whether or not this hypothesis is fully accurate microscopically in the context of TUS, it offers a phenomenological framework that could be used at the organ scale to quantify electrical induction in the presence of minute mechanical vibrations. However, the flexoelectric theory relies on formulations directly built on the microstructural description of the underlying dielectric polarisation. In membranes, this constrains the flexoelectricity modelling to simple membrane morphologies and prevents the simulation of flexoelectricity in large scale assemblies of multiple biological cells. To this end, this work proposes a homogenised bulk flexoelectric model focussing on the continuum level formulations of bundles of flexoelectric cylinders. This model was calibrated against a microscale formulation to ensure multiscale compatibility, but it can be directly used at the macroscale for the description of strain-gradient induced electromechanical coupling without the need to account for the microstructural polarisation.

A 1D proof of concept is first proposed, followed by 2D and 3D formulations of the homogenised bulk flexoelectric model. The homogenised model is used for brain white matter tracts in the context of TUS, where ultrasound induced electrical activity arising within the tracts is simulated in a human head model in 2D and a monkey head model in 3D. In the latter case, a direct comparison against experimental models is proposed. In particular, this study proposes a way to predict the loss of brain region correlation during TUS. To conclude, the framework proposed here has the potential to fully capture multiphysics phenomena such as in TUS. The results from this study provide a theoretical building block to identify the desirable ultrasound parameters for clinical and/or experimental applications that can be used for the successful treatment of neurological disorders.

Table of Contents

1 Introduction **1**

2 Literature review **7**

2.1 Neurological disorders and their treatment 7

2.1.1 Neurological disorders 7

2.1.2 Conventional treatments of neurological disorders 9

2.1.3 Use of ultrasound for treatment of neurological disorders . 11

2.1.4 Research studies on low-intensity focussed TUS 12

2.1.4.1 Earlier studies 13

2.1.4.2 Recent small animal studies 15

2.1.4.3 Recent large animal studies 18

2.1.4.4 Recent primate studies 19

2.1.4.5 Recent human studies 21

2.1.5 Applications of TUS 23

2.1.5.1 Research limitations 23

2.1.5.2 Mechanisms of ultrasound 29

2.1.5.3 Ultrasound simulation methods 32

2.2 Electromechanical coupling in neurons 34

2.2.1 Neurons and action potential 34

2.2.2 Electrical models of nerve excitation 37

2.2.2.1 H-H model 37

2.2.2.2 Simplification of the H-H model 40

2.2.3 Non-electrical aspects of nerve excitation and alternative models 40

2.2.3.1 Heimburg and Jackson model 42

2.2.3.2 Rvachev model 44
2.2.3.3 El Hady and Machta model 45
2.2.3.4 Engelbrecht model 46
2.2.3.5 Flexoelectricity 47
2.3 Conclusion 49

3 1D axonal model **51**
3.1 Electromechanical coupled model 51
3.2 Finite difference method 54
3.3 Fourier pseudospectral method 56
3.4 Results and discussion 60

4 Theoretical framework **65**
4.1 Density and orientation of axons 65
4.2 Electrophysiological model 67
4.3 Mechanical model 70
4.4 Flexoelectric coupling model 71
4.5 The *k*-space pseudospectral method 74
4.6 Finite element formulation 78
4.6.1 2D model 78
4.6.2 3D model 83
4.7 Summary 87

5 Implementation and application to TUS **89**
5.1 2D human model 89
5.1.1 Validation 89
5.1.2 Application to TUS 92
5.2 3D macaque monkey model 98
5.3 Discussion 106

5.3.1 TUS configuration effect 108
5.3.2 TUS functional effect 110

6 Conclusion **118**
6.1 Summary 118
6.2 Limitations and future work 119

A 2D model **122**

B 3D model **128**

List of Figures

2.1 Cavitation in the leaflet of membranes where the leaflets of the mebrane are a) contracted and b) expanded. 32
2.2 Structure of a neuron. 35
2.3 Generation of an action potential. 37
2.4 Equivalent circuit for H-H model. 39
2.5 Gel and fluid phases of the lipid membrane. 43
2.6 Process of nerve impulse propagation in Engelbrecht model. . . . 47
2.7 Induced polarisation on the membrane due to non-uniform deformation. 48

3.1 Schematic of the 1D axonal model. 52
3.2 Finite difference method. 62
3.3 Fourier pseudospectral method. 62

4.1 The unit fibre orientation vector $\mathbf{a}_{axon}$ using spherical coordinates. 69
4.2 Continuum bulk flexoelectricity framework: a) membrane polarisation $\mathbf{P}$ (naturally orthogonal to the membrane) arises from bending of the axons; b) in the bulk, the homogenised bulk polarisation $\tilde{\mathbf{P}}$ is defined at the tissue level (here with three axons of volume V_1, V_2 and V_3 and surface S_1, S_2 and S_3) and coincides with its membrane counterpart when projected orthogonally to the membrane. 72
4.3 Schematic of the staggered grid. 77
4.4 8-node 2D quadrilateral element in the isoparametric reference frame (ξ, η). 78

4.5 20-node 3D brick element in the isoparametric reference frame (ξ, η, ζ). 83

5.1 (a) 2D Abaqus model of one axon, and (b) 2D MATLAB homogenised model ($250\ \mu m$ length and number of elements in the x-direction not to scale). 90

5.2 Induced current per unit length calculated by membrane flexoelectric effect and the proposed homogenised volumetric flexoelectric effect at 24.5 ns. 91

5.3 TUS in k-Wave with three transducer orientations, and the grid discretisation of the brain (blue and red dots correspond to the supplementary motor area (SMA) and Brodmann area 9-46, respectively; p, ux, uy, dx, dy are the pressure, velocities in x and y and displacements in x- and y-directions. 94

5.4 (a) White matter tract between the target region, SMA, and Broadmann area 9-46, (b) induced current for each element within the white matter tract for each transducer configuration after steady state is reached, (c) corresponding induced maximum power, (d) corresponding induced steady state average power, and total generated steady state average power for the whole tract for each transducer position, and (e) the peak pressure in the SMA and Broadmann area 9-46; three transducer configurations: leaning towards the front ("front") sending waves towards the back of the skull, sitting directly on top of the skull ("top"), and leaning towards the back ("back") thus sending waves towards the front of the skull. 96

5.5 The different ROIs in the monkey brain, and the position of the transducer and coupling cone on the head. 101

5.6 (a) Total steady state maximum and average current for the white matter tracts, (b) total steady state maximum and average power for the tracts, (c) total steady state maximum and average power for the tracts from the FHN model, (d) induced steady state maximum and average current for each voxel showing the first three voxels and last three voxels within each tract, (e) corresponding induced steady state maximum and average power for each voxel, and (f) corresponding induced steady state maximum and average power for each voxel from the FHN model. 103

5.7 Peak pressure at each ROI. 104

5.8 (a) Relative change between the experimental control and ACC TUS in the connectivity fingerprint of ACC, and (b) absolute change between the experimental control and ACC TUS in the connectivity fingerprint of ACC. 112

List of Abbreviations

1D . . . . . One-dimensional

2D . . . . . Two-dimensional

3D . . . . . Three-dimensional

ACC . . . . . Anterior cingulate cortex

ATP . . . . . Adenosine triphosphate

BBB . . . . . Blood-brain barrier

BOLD . . . . . Blood-oxygen-level-dependent

Ca^{2+} . . . . . Calcium

CSF . . . . . Cerebral spinal fluid

DALY . . . . . Disability-adjusted life-years

DBS . . . . . Deep brain stimulation

DTI . . . . . Diffusion tensor imaging

EEG . . . . . Electroencephalogram

FHN . . . . . Fitzhugh-Nagumo

fMRI . . . . . Functional magnetic resonance imaging

GABA . . . . . Gamma aminobutyric acid

H-H . . . . . Hodgkin and Huxley

HIFU . . . . . High-intensity focussed ultrasound

INCS . . . . . Iterative Nonlinear Contrast Source

K^+ . . . . . Potassium

MRI . . . . . Magnetic resonance imaging

Na^+ . . . . . Sodium

NICE . . . . . Neuronal intramembrane cavitation excitation

PML . . . . . Perfectly matched layer

rs-fMRI . . . . . Resting-state functional magnetic resonance imaging

ROI . . . . . Region of interest

RVE . . . . . Representative volume element

SCC . . . . . Subcallosal cingulate

SMA . . . . . Supplementary motor area

tDCS . . . . . Transcranial direct current stimulation

TMS . . . . . Transcranial magnetic stimulation

TUS . . . . . Transcranial ultrasound stimulation

VNS . . . . . Vagus nerve stimulation

1 | Introduction

Neurological disorders such as Alzeimer's disease, Parkinson's disease and epilepsy are diseases of the central and peripheral nervous systems, and are important causes of disability and fatality (World Health Organisation, 2018). In particular, neurological disorders have been reported to be the leading cause group of disability-adjusted life-years (DALYs) and the second leading cause group of death worldwide (GBD 2016 Neurology Collaborators, 2019; GBD 2015 Neurological Disorders Collaborator Group, 2017). About a third of the global population is estimated to be affected by neurological disorders across their lifespans (World Health Organisation, 2018). The growth in world population number as well as the rise in life expectancy have resulted in more people reaching ages where neurological disorders are most prevalent (GBD 2016 Neurology Collaborators, 2019). These disorders can be expected to present an increasing challenge for the ageing populations, and cause serious threats to public health and health service delivery. Hence, its prevention, treatment and management are of utmost importance.

While pharmacological interventions remain to be the main focus of treatment for neurological disorders (Leinenga et al., 2016), a number of non-pharmacological procedures have been developed throughout the years. Surgical methods are the pioneering techniques while neuromodulation methods such as deep brain stimulation (DBS) (Perlmutter and Mink, 2006), transcranial direct current stimulation (tDCS) (Boggio et al., 2006), and transcranial magnetic stimulation (TMS) (Fatemi-Ardekani, 2008) have received widespread acceptance for treating neurological disorders (Wagner et al., 2007). DBS is a reversible method that can alter the brain activity in a controlled manner (Naor et al., 2016). However, this is an invasive method due to the need for implanted electrodes (Barbarisi et al., 2011), and

thus comes with a recognised risk of complications and side effects (Dobrakowski et al., 2014). On the other hand, while tDCS and TMS are non-invasive neuromodulation methods, they have relatively low spatial resolution and cannot reach the deep areas in the brain as well as the invasive methods can (Kropotov, 2016; Kirton and Gilbert, 2016).

Ultrasound, which is an acoustic wave above 20 kHz (Howard et al., 2005), is increasingly being considered as a potentially powerful tool for neurological disorder treatment (Sassaroli and Vykhodtseva, 2016). This is because ultrasound has many advantages including being regarded as non-invasive (Clement, 2004; Hynynen and Jolesz, 1998) with potential effects on biological tissues (Dobrakowski et al., 2014). It can minimise the occurrence of complications compared to other methods and it does not require the implantation of electrodes (Li and Cook, 2018; Wang et al., 2017; Deffieux et al., 2013b). Additionally, it has an increased spatial selectivity over tDCS and TMS (Folloni et al., 2019b; Fouragnan et al., 2019; Bystritsky et al., 2011) and therefore, has the ability to target the deeper structures within the brain (Wang et al., 2019; Blackmore et al., 2019; Darrow et al., 2019; Tyler et al., 2018; Fini and Tyler, 2017). The use of high-intensity focussed ultrasound (HIFU) can disrupt the blood-brain barrier (BBB) to allow drug delivery to the brain (Meng et al., 2019; Airan et al., 2017; Leinenga et al., 2016). By producing thermal effects, it is extremely effective for ablative purposes (Legon et al., 2014, 2012; Dalecki, 2004). But regardless of its benefits, HIFU destroys the targeted tissue which poses inherent risks and causes irreversible damage to the brain (Tyler et al., 2018).

To prevent this tissue damage from HIFU, researchers have focussed their attention on studying the use of low-intensity focussed transcranial ultrasound stimulation (LIFU or TUS) (Krishna et al., 2019; Tyler et al., 2018; Khanna et al., 2017; Mueller et al., 2014). TUS has been considered to be a promising new genera-

tion treatment for neurological disorders (Naor et al., 2016). This has been the subject of growing investigations as lower intensities are less likely to produce thermal effects, but can still induce prominent mechanical bio-effects on cells and tissues (Fini and Tyler, 2017; Legon et al., 2012; Dalecki, 2004). Furthermore, TUS can modulate the functions of the brain and probe neurological processes from a cellular level all the way up to macroscale level (Amiez et al., 2006) with sub-millimeter resolution (Darrow, 2019; Darrow et al., 2019; Baek et al., 2017; Naor et al., 2016), further increasing the interest in its clinical applications (Sanguinetti et al., 2020; Monti et al., 2016; Bystritsky and Korb, 2015). Many studies have shown that TUS can safely and non-invasively modulate the neuronal activity within the brain (Wang et al., 2019; Tyler et al., 2018; Sassaroli and Vykhodtseva, 2016; Tyler, 2011; Tufail et al., 2010; Tyler et al., 2008; Khraiche et al., 2008) and induce various responses in animals (Sato et al., 2018; Kamimura, 2016; Chu et al., 2015; Deffieux et al., 2013a) such as causing behavioral changes and improving sensory discrimination abilities (Folloni et al., 2019b; Fouragnan et al., 2019; Legon et al., 2014; Tufail et al., 2010). In addition, *in-vitro* and *in-vivo* experiments in animals and humans have reported that TUS induced excitation and/or inhibition of neuronal activities (Darrow et al., 2019; Naor et al., 2016) depending on the applied ultrasound parameters (Legon et al., 2018a; Lee et al., 2016a; Hameroff et al., 2013).

A variation of ultrasound parameters however, have been used by different research groups to study TUS on a variety of animal subjects and brain regions, which produced a range of observed effects (Baek et al., 2017). Therefore, their experimental results cannot be directly compared with each other (Darrow et al., 2019; Baek et al., 2017; ter Haar, 2007). This heterogeneity of effects makes it difficult to have a full understanding of the main underlying mechanisms of ultrasound (Darrow et al., 2019; Naor et al., 2016), and its exact effects on the neuronal

activities in the brain are still under exploration. A better control of TUS thus, requires a better understanding of the electromechanical coupling occurring in neurons (Naor et al., 2016; Sassaroli and Vykhodtseva, 2016) and how this coupling arises due to TUS. Experimental studies in animals and more recently, in humans are currently being conducted to further understand the use of low-intensity TUS as a neuromodulation tool.

Numerous evidences from earlier experimental studies have shown that neuronal activity is not only associated with electrical and chemical changes but mechanical and other thermodynamic changes are also involved through electromechanical coupling (Tasaki et al., 1989; Tasaki, 1988; Iwasa et al., 1980; Iwasa and Tasaki, 1980). These observations have opened various research questions on the understanding of nerve impulse propagation in neurons from a thermodynamic perspective (Anderson et al., 2009). Different numerical models have been proposed and developed to study this coupling in healthy and damaged neurons (Garcia-Gonzalez and Jérusalem, 2019; Kwong et al., 2019; Cinelli et al., 2018; García-Grajales et al., 2015; Drapaca, 2015; Jérusalem et al., 2013). Despite the models' differences and sometimes contradictory approaches, they can help to provide some insight into the multi-physics of neurons and better the knowledge in this area of research. However, there is currently no widely accepted model that takes account of all the aspects of a nerve impulse and rationalises the electromechanical coupling phenomenon in neurons especially in the context of TUS.

Flexoelectricity is a commonly observed effect in biological membranes. It has been considered as one of the key mechanisms in many electromechanical coupling phenomena (Krichen and Sharma, 2016; Petrov, 2006, 2002). In neurons, it has been suggested that both the membrane movement and polarisation induced by an action potential could be related to flexoelectricity (Petrov and Mircevová, 1986; Petrov, 1975). Building on this, Chen et al. (2019) have proposed an elec-

tromechanical model using flexoelectricity as a possible mechanism of TUS. This model however, only focusses on the membrane level. Although it can capture some of the key characteristics of ultrasound-induced electrical activity, the need to account for the microstructural description of the underlying dielectric polarisation restricts this model to cellular observations and precludes any simulation of large scale assemblies of multiple biological cells. Furthermore, while other coupling mechanisms might be at play and membrane flexoelectricity might not be the driving neuromodulation mechanism, the current experimental observations of electrophysiological activity being induced by minute mechanical vibration at the organ scale further highlights the need for a phenomenological continuum flexoelectric framework that does not require to explicitly account for the underlying microstructure.

Hence, the aim of this research project is to numerically investigate the electromechanical coupling phenomenon in neurons and how this manifests at the macroscale level in the context of TUS. In particular, in light of recent results suggesting the important role of white matter neuromodulation (Hamani et al., 2011; Mayberg et al., 2005), the proposed work here focusses on white matter tracts. This work contributes to the advancement of knowledge on the use of ultrasound as a neuromodulation tool and its potential to help with the successful treatment of neurological disorders. The specific objectives are:

i) To develop a one dimensional (1D) electromechanical axonal model using direct flexoelectricity as the coupling mechanism for proof of concept;

ii) To develop a homogenised bulk flexoelectric tissue model to capture the electromechanical coupling at the macroscale level for bundles of flexoelectric cylinders, and provide a scalable multi-physics numerical model focussing on continuum level formulations;

iii) To implement the homogenised model in two dimension (2D) and three di-

mension (3D) for the validation of the approach and its application to brain white matter tracts in the context of TUS, and for testing it against real experimental studies.

A review of the literature is presented in Chapter 2 and the specific objectives are presented in Chapters 3, 4 and 5, respectively. Chapter 6 then concludes the work including possible future directions of the work.

2 | Literature review

This literature review details how neurological disorders are currently being treated and how TUS is increasingly considered as a promising, safe and alternative candidate. This chapter also outlines the various models that have been developed to investigate the electromechanical coupling phenomenon in neurons and how this coupling can arise from the application of TUS.

2.1 Neurological disorders and their treatment

Neurological disorders are increasingly becoming a huge concern to society. Different methods of treatment have been introduced over the years to help mitigate this challenge (Gibbs et al., 2018).

2.1.1 Neurological disorders

Neurological disorders are diseases of the central and peripheral nervous systems (World Health Organisation, 2018) and include stroke, Alzheimer's disease and other dementias, Parkinson's disease, epilepsy, multiple sclerosis, migraine, tension-type headache, medication overuse headache, meningitis, tetanus, encephalitis, brain and nervous system cancer, motor neuron disease, and a residual category of other neurological disorders that include diseases such as, muscular dystrophy and Huntington's disease (GBD 2016 Neurology Collaborators, 2019; GBD 2015 Neurological Disorders Collaborator Group, 2017). Around a third of the population in the world is estimated to be affected by neurological disorders across their lifespans, where rates are found to be highest in low and middle income countries (World Health Organisation, 2018).

In 2016, the neurological disorders included in the systematic analysis for the

Global Burden of Disease Study (GBD 2016 Neurology Collaborators, 2019) were the principal cause in 16.5% of total global deaths accounting to 9 million deaths. These disorders were also responsible for 276 million DALYs which was 11.6% of global DALYs for all diseases. Neurological disorder DALYs exceeded the DALYs from other diseases or disorders such as physical injuries, cardiovascular disease excluding stroke, cancer, and mental and substance use disorders. The four disorders that contributed the most to neurological DALYs were stroke (42.2%), migraine (16.3%), Alzheimer's disease and other dementias (10.4%), and meningitis (7.9%). The age-standardised DALY rates were higher in males (male-to-female ratio 1.12) but more common disorders such as migraine, multiple sclerosis, and tension-type headache caused more burden in females (male-to-female ratio 0.7) (GBD 2016 Neurology Collaborators, 2019; GBD 2015 Neurological Disorders Collaborator Group, 2017).

Overall, the burden of neurological disorders has substantially increased despite the decline in mortality rates from stroke and communicable neurological disorders. The increase in life expectancy and rising population growth (GBD 2016 Neurology Collaborators, 2019) is leading to a staggering health and economic burden (Gibbs et al., 2018), as people with neurological conditions who need care by expert clinicians will continue to grow in the future (GBD 2016 Neurology Collaborators, 2019). In Europe, 35% of total disease burden account for neurological disorders. This amounts to a yearly cost of 800 billion euros, where 60% of the cost are related to direct healthcare and non-medical costs (Di Luca et al., 2018). Thus, it is very important to focus on the prevention, treatment and management of neurological diseases to reduce its threat to public health and health service delivery.

2.1.2 Conventional treatments of neurological disorders

Pharmacological interventions are the primary treatment for neurological disorders (Leinenga et al., 2016). However, local injections of pharmacologic agents, such as muscimol (Amiez et al., 2006) and micro-stimulation (Histed et al., 2009) are inherently invasive and can cause unwanted side effects (Polanía et al., 2018). Because of this, a number of non-pharmacological procedures have been developed throughout the years. Surgical methods are the pioneering techniques and they have been widely used particularly on patients with unilateral tremor resistance to pharmacological treatment (Dobrakowski et al., 2014). Subsequently, the introduction of neuromodulation methods such as DBS (Perlmutter and Mink, 2006), tDCS (Boggio et al., 2006), and TMS (Fatemi-Ardekani, 2008) have received widespread acceptance due to their efficacy in the treatment of neurological and psychiatric diseases (Wagner et al., 2007). DBS can alter the brain activity in a controlled and reversible manner (Naor et al., 2016), and has been used for treating Parkinson's disease, essential tremors, and neuropathic pain (Wagner et al., 2007). A similar method to DBS is vagus nerve stimulation (VNS). This has been used to treat epilepsy and depression (Groves and J., 2005). Both DBS and VNS however, involve the use of implantable electrodes, which is associated with more morbidity due to the requirement for surgery, consistent battery replacements, and immunosuppression (Barbarisi et al., 2011; Wagner et al., 2007). Together with other methods such as radiofrequency ablation and radiosurgery, DBS is found to be highly invasive or can cause exposure to ionising radiation when used to treat Parkinson's disease and essential tremors (Barbarisi et al., 2011). DBS is also associated with a recognised risk of complications and side effects including infection, haemorrhage and damage to the surrounding brain tissue (Dobrakowski et al., 2014).

Although the invasive methods are improving, TMS (Lee et al., 2012) and tDCS (Nitsche et al., 2009) have been gaining more attention. This is because they are non-invasive methods and they avoid the complications involved in DBS and VNS. TMS and tDCS however, have a few disadvantages e.g., they are not able to reach and stimulate the deep structures in the brain as well as the invasive methods can (Wright et al., 2017). They can also lead to side effects and symptoms such as tingling sensations, headaches, fatigues, nausea and metallic taste in the mouth for tDCS (Kropotov, 2016), and facial twitching, skin redness and anxiety for TMS (Kirton and Gilbert, 2016).

Nevertheless, no matter how effective a particular method is at treating neurological disorders, it is still very important to take account of the patients' preferences when it comes to determining which method would be best to use to treat them. For example, although invasive treatments such as DBS and VNS can effectively target the deep regions within the brain, some patient may not want to undergo any of these invasive treatments. This is because they may find the procedures frightening or risky since they are invasive. Therefore, a patient suffering from a particular neurological disorder may choose an alternative treatment which may be less effective, as long as the treatment seems to be less risky or less invasive. This means that patients may be more prepared to potentially suffer from negative side effects from a non-invasive treatment rather than potentially get complications from an invasive treatment. Consequently, when treating a patient with a specific neurological disorder, the focus should not only be on the effectiveness of the treatment e.g., its ability to focus on a specific brain target region and how well it can treat the disorder but also the patient's personal preferences.

2.1.3 Use of ultrasound for treatment of neurological disorders

Ultrasound is increasingly being considered as a potentially powerful candidate for neurological disorder treatment (Sassaroli and Vykhodtseva, 2016). Ultrasound is defined as an acoustic wave above $\sim$20 kHz which is beyond the frequency range of human hearing (Howard et al., 2005). For neuromodulation, an electrical waveform is emitted from a pulse generator, which is carried and amplified in the ultrasound transducer. This excites the piezoelectric element inside and mechanically oscillates the active face it is coupled to (Fomenko et al., 2018; King et al., 2013; Younan et al., 2013). Ultrasound can propagate through the skull (Clement, 2004; Hynynen and Jolesz, 1998), focus on a small target region, and interact with biological tissues through thermal and/or non-thermal mechanisms, which all minimises the occurrence of complications compared to other methods (Dobrakowski et al., 2014). It does not require the implantation of an electrode (Li and Cook, 2018; Wang et al., 2017; Deffieux et al., 2013b) compared to DBS, and it can provide an increased spatial selectivity over other non-invasive neuromodulation methods such as tDCS and TMS (Folloni et al., 2019b; Fouragnan et al., 2019; Bystritsky et al., 2011). It also has the potential to target tissues anywhere in the body with sub-millimetre precision (Wang et al., 2019; Blackmore et al., 2019; Darrow et al., 2019; Tyler et al., 2018; Fini and Tyler, 2017; Tufail et al., 2010; Gavrilov and Tsirulnikov, 2012).

Focussed ultrasound has been shown to disrupt the BBB in the brain through mechanical mechanisms. This can involve generating a lesion on the targeted area and disrupting the BBB within the periphery of the lesion. The opening of the BBB allows drug delivery to the brain (Meng et al., 2019; Airan et al., 2017; Leinenga et al., 2016) ranging from small molecule drugs (Treat et al., 2007) to viral vectors (Alonso et al., 2013) by combining these intravenously injected ultra-

sound contrast agents with shorter focussed ultrasound pulses (McDannold et al., 2012; Sheikov et al., 2008; Hynynen et al., 2005). This means that focussed ultrasound can be utilised for pharmacologic neuromodulation of specific brain regions (Constans et al., 2020; Airan et al., 2017).

HIFU is extremely effective at focally and rapidly heating tissues therefore, it is very useful for ablative purposes such as for treating brain cancers (Dalecki, 2004; Legon et al., 2014; Martin et al., 2014; Legon et al., 2012; Martin et al., 2009) and other neurological disorders where ablating a specific area can result in significant symptom improvements (Wang et al., 2015; Lipsman et al., 2014). Furthermore, HIFU has been reported to treat essential tremors, neuropathic pain and Parkinson's disease, and it can be used for targeted procedures in the thalamus, subthalamus and globus pallidus regions (Dobrakowski et al., 2014).

HIFU however, still poses inherent risks because heating the brain tissue causes irreversible damage (Tyler et al., 2018). Ultrasound at lower intensities on the other hand, have been shown to be able to modulate neurons directly (Tufail et al., 2010; Khraiche et al., 2008; Tyler et al., 2008) and induce prominent mechanical bio-effects without the addition of therapeutic agents (Blackmore et al., 2019). This has allowed low-intensity TUS to gain a lot of attention from researchers and considered to be a new generation treatment for neurological disorders (Naor et al., 2016).

2.1.4 Research studies on low-intensity focussed TUS

Recent investigational work has focussed on studying the use of low-intensity focussed TUS[1] to potentially treat neurological disorders while preventing the tissue damage inherent to HIFU (Krishna et al., 2019; Tyler et al., 2018; Khanna et al.,

[1]Here and subsequently, the term TUS is used in the context of low-intensity.

2017; Mueller et al., 2014). Many studies have shown that TUS can safely and non-invasively modulate the neuronal activity within the brain (Wang et al., 2019; Tyler et al., 2018; Sassaroli and Vykhodtseva, 2016; Tyler, 2011; Tufail et al., 2010; Tyler et al., 2008; Khraiche et al., 2008) inducing changes in the responses of animals (Sato et al., 2018; Kamimura, 2016; Chu et al., 2015; Deffieux et al., 2013a) such as causing behavioral changes and improving sensory discrimination abilities (Folloni et al., 2019b; Fouragnan et al., 2019; Legon et al., 2014; Tufail et al., 2010). This has further sparked interest to study TUS for applications in the rapidly growing field of neuromodulation. *In-vitro* and *in-vivo* experiments in animals and humans have shown that TUS can cause the excitation and/or inhibition of neuronal activities (Darrow et al., 2019; Naor et al., 2016), where the neuronal responses seem to be dependent on the parameters of the applied ultrasound (Legon et al., 2018a; Lee et al., 2016a; Hameroff et al., 2013). Moreover, TUS is thought to be a better alternative method for the treatment of neurological disorders and psychiatric diseases, and for the scientific investigation of the neuronal mechanisms of cognitive, sensory, and motor functions (Fini and Tyler, 2017).

In the following, a literature review of neuromodulation studies in the context of TUS is provided. Note that some work focussed on HIFU is also discussed when relevant.

2.1.4.1 Earlier studies

The first reported neuromodulatory effect of ultrasound was conducted by Harvey (1929) in the early 20^{th} century. His work showed that direct application of HIFU could enhance the firing rate of amphibian cardiac preparations. In this study, he observed 'sub-minimal twitching of the gastrocnemius muscle' on a frog's sciatic nerve. Since then, exploratory studies by a number of researchers have mostly

focussed on investigating the effects of ultrasound on peripheral nerves (Wright et al., 2002; Mihran et al., 1990; Fry, 1968; Lele, 1963) and only a few studies looked into the effects on the central nervous system tissues (Tsirulnikov et al., 1988; Wall et al., 1953).

In the 1950's, the Fry brothers and colleagues demonstrated that in addition to causing thermal lesions at high intensities (Fry, 1954), ultrasound delivered to the craniotomised feline's lateral geniculate nucleus at sub-heating intensities could reversibly suppress visual evoked potentials when the cat's eyes were stimulated by light (Fry et al., 1958). A partial reduction of the evoked potential occurred straight after ultrasound exposure and a complete recovery of visual functions occurred within 30 $mins$ after the exposure (Fry et al., 1958). This was one of the first observations on the effects of focussed ultrasound on the neuronal activity in brains (Naor et al., 2016). It was also found that the ultrasound effects on the chemical synapses were one of the earliest changes to happen. This provided a potential explanation for the functional changes detected immediately after ultrasound application (Borrelli et al., 1981). Furthermore, Lele (1963) performed extensive studies on the effects of focussed ultrasound on the peripheral nerves of cats, monkeys, and humans. Depending on the exposure conditions used, three different effects on the action potential were observed. These effects were reversible enhancement, progressive inhibition, and irreversible inhibition. It was suggested that the ultrasound-induced effects on the nerve fibres can be reproduced when heat is applied to specific regions of the nerves.

In another experiment where ultrasound was applied to the optic tract and lateral geniculate nucleus junction, it was observed that the visual evoked potentials in both the visual cortex and the optic tract were suppressed to some extent. The degree of recovery varied depending on the ultrasound parameters used in the experiments (Adrianov et al., 1984; Uranova et al., 1979). In some cases, the effects

of ultrasound on the visual cortex were delayed for about 4 to 5 $mins$ compared to the optic tract. A proposed explanation for this delay is the spreading depolarisation. This is an electrochemical wave that propagates through the neuronal tissue at about 2 to 5 mm/min. Spreading depolarisation can trigger a disruption in the neuronal bioelectrical activity and can cause massive surges of the extracellular K^+ ions. This suggestion was tested on a rat brain where the possibility of the ultrasound inducing a negative shift of direct current potential and the initiation of the spreading depolarisation in the cortical and sub-cortical structures such as the cerebral cortex, caudate nucleus, thalamus and hippocampus were confirmed by the same research group (Vykhodtseva et al., 2007; Vykhodtseva and Koroleva, 2006, 1986).

Although the early studies elegantly showed that ultrasound can be used as a neurophysiological mapping tool within an intact brain, the transducers used were bulky and insufficiently powered to penetrate the mammalian skull (Fomenko et al., 2018). The skull is highly reflective, diffractive, and absorptive of ultrasound therefore, it produces a significant barrier for the delivery of ultrasound to the brain, in particularly above 1 MHz (Li et al., 2016). These effects can vary widely across different regions of the skull with differing thickness and concavity (Darrow et al., 2019; Haritonova et al., 2015; Kyriakou et al., 2014; Hynynen et al., 2004).

2.1.4.2 Recent small animal studies

Recent technology improvement in transducer designs such as miniaturization (Li et al., 2018; Qiu et al., 2017) and phased arrays (Hynynen et al., 2004), have allowed transcranial targeting at sub-millimetre scale and have spurred renewed interest in the field of TUS (Tyler et al., 2018; Dallapiazza et al., 2018; Naor et al., 2016). Over the last few decades, researchers have investigated the effects of ul-

trasound on different areas in the animal spinal cord, cortex, subcortical structures, and peripheral nerves (Dallapiazza et al., 2018; Downs et al., 2017; Wattiez et al., 2017; Yuan et al., 2016; Hakimova et al., 2015; King et al., 2014; Deffieux et al., 2013b; King et al., 2013; Muratore and Vaitekunas, 2012; Tufail et al., 2011; Min et al., 2011a; Yoo et al., 2011a,b; Tufail et al., 2010; Foley et al., 2008). A general shift towards targeting the central nervous system tissues started when Tyler and colleagues stimulated hippocampal slices at lower intensities compared to those used on peripheral nerves (Tyler et al., 2008). After this, several other studies were conducted in the living brain by stimulating the motor activity (Tufail et al., 2010) influencing gamma aminobutyric acid (GABA) release (Yang et al., 2012), reversibly inhibiting epileptic activity (Min et al., 2011a) and stimulating somatosensory sensations (Lee et al., 2015a) for the study of neuronal activity (Tyler et al., 2008; Wahab et al., 2012) and brain functions (King et al., 2014, 2013; Younan et al., 2013).

In particular, Muratore et al. (2009) showed that short pulses of low-intensity ultrasound can trigger neurons in mouse hippocampal slice cultures to generate action potentials. These *in-vitro* studies were followed by a number of *in-vivo* studies in anaesthetised rodent and rabbit models. Additionally, reproducible contralateral muscle group movements were observed in mice (King et al., 2014, 2013), rats (Kim et al., 2014a), and rabbits (Yoo et al., 2011a) when sonicating their motor cortices under low levels of anaesthesia. The brain regions with successful stimulation corresponded to distant regions from the anatomical motor cortex (Fomenko et al., 2018). This discrepancy may be due to the size of the animal brain, the relative size of the acoustic focus in contrast to the brain, far-field ultrasound effects and additional skull spatial distortions (Younan et al., 2013). Numerical simulations and *ex-vivo* transcranial pressure measurements showed that a rat skull can attenuate up to 11% of ultrasound and low frequency sonica-

tions can cause the ultrasound field's peaks to move away from focus (Younan et al., 2013).

The effects of inhibition and excitation were both observed from induced muscle activity, evoked potentials, microelectrode recordings and functional magnetic resonance imaging (fMRI). Electrophysiological studies have shown that ultrasound can have short- and long-lasting inhibitory effects on neuronal pathways (Kim et al., 2015, 2014b; Mehić et al., 2014; Younan et al., 2013; King et al., 2013; Yoo et al., 2011a). Visually evoked potentials from ultrasound has been demonstrated to be suppressed in rats (Kim et al., 2015), rabbits (Yoo et al., 2011a), and cats (Barnard et al., 1955) in *in-vivo* models. The suppression of seizure-like activity in various animal models of epilepsy has also been investigated. For an intracerebral kainic acid-induced medial temporal lobe epilepsy in a mouse model, electrographic seizures were suppressed using a single 1 ms ultrasound pulse containing 200 acoustic cycles of 200 kHz repeated at a pulse repetition frequency of 0.5 kHz, and caused a reduction in recurrent seizures (Hakimova et al., 2015). In addition, using the same seizure model in rats, a small pilot study showed that seizure activity terminated after the hippocampus was targeted using a magnetic resonance imaging (MRI)-guided sonication at 690 kHz with a pulse repetition frequency of 100 Hz for 1 min (Yoo et al., 2010). Similarly, a reduction in the duration of pentylenetetrazol-induced acute seizures was observed in anaesthetised rats when sonicating the thalamic region (Min et al., 2011a) as well as, an increase in extracellular dopamine and serotonin levels in the frontal cortex (Min et al., 2011b). However, the use of anaesthesia is a significant limitation when using rodent models of epilepsy for TUS as it can prevent the movements of the animals, which causes both the seizure frequency and ultrasound efficacy to be suppressed (Kim et al., 2014a; Yoo et al., 2011b).

Pulsed and continuous ultrasound waves were also applied to the somato-motor

cortical areas to investigate the motor responses in mice (Kamimura et al., 2015; Mehić et al., 2014; King et al., 2013; Tufail et al., 2010), rabbits (Yoo et al., 2011a) and rats (Kim et al., 2014b,a; Younan et al., 2013). This affected non-cortical areas such as the hippocampus by inducing extracellular spikes and local field potentials (Tufail et al., 2010). Pulsed-wave bursts of 650-690 kHz on the thalamus of rats caused a reduction in epileptic seizures and electroencephalogram (EEG) bursts (Min et al., 2011a), as well as increased levels of frontal lobe GABA, dopamine and serotonin (Yang et al., 2012; Min et al., 2011b). Overall, *in-vivo* small animal studies have been very useful in the development of TUS procedures but these studies are limited by the formation of standing wave patterns within the animals' small skulls (Younan et al., 2013) and the requirement for maintaining low anaesthesia levels (King et al., 2013). These limitations have ultimately motivated researchers to rapidly develop experimental applications in larger animals, primates and humans (Mueller and Tyler, 2014).

2.1.4.3 Recent large animal studies

Larger animals have a more voluminous brain so targeting using region-specific low-intensity TUS can be validated to discrete neuroanatomic targets. Larger cranial volume sonications may also lessen the acoustic reverberations and standing waves that were suggested to unfavourably impact the precise targeting within the small animal skulls (Younan et al., 2013; Tang and Clement, 2010). Sheep skulls are similar to human skulls because they have similar rounded cranial convexity as well as similar skull thickness of around 4-5 mm (Lee et al., 2016b, 2015b). Sonication of the primary visual cortex have shown to induce EEG evoked potentials in anaesthetised sheep, while sonication of the sensorimotor cortex have shown to induce contralateral hindlimb electromyographic evoked potentials (Lee et al., 2016b). Although this incurred no adverse neurological damage, prolonged

sonication exposure in animals caused cerebral micro-haemorrhages on haematoxylin and eosin *post-mortem* staining but with no evidence of edoema or necrosis (Lee et al., 2016b). Furthermore, in a study by Dallapiazza et al. (2018) using an anaesthetised swine model, targeting the somatosensory thalamic nuclei with low-intensity TUS elicited trigeminal and tibial somatosensory evoked potentials. Following the ultrasound exposure, a peak suppression was observed for 5 $mins$ which returned to the baseline activity after 10 $mins$. Compared to the sheep studies, microscopic evidence of tissue damage was not found using histological staining when targeting the thalamus. Precise targeting of the thalamic nuclei was demonstrated with accuracy and specificity on the millimetre scale.

2.1.4.4 Recent primate studies

Primates have similar skull curvature to human skull and more specifically, a macaque monkey brain has similar neuroanatomic relationships with human brain regardless of absolute size differences (Fomenko et al., 2018). The primate skull is thicker than small animal skull such as of rodents, so the spatial dispersion and reflection of the pressure field is about 42% when using typical sonication parameters (Deffieux et al., 2013b; Choi et al., 2007).

In a study by Deffieux et al. (2013a), the frontal eye field region of the frontal cortex was targeted using low-intensity TUS in awake, behaving macaques using a 320 kHz scalp-mounted delivery paradigm from a single transducer. These macaques were trained to perform visual tasks such as saccadic eye movements. This demonstrated that ultrasound can lead to a significant transient modulation of anti-saccade latencies in the contralateral visual field and slower eye movements. To account for their finding, they postulated a focussed ultrasound-induced disruption of processing across the frontal eye field (Deffieux et al., 2013a). A further study showed that there were stimulus-locked effects on saccade latency (Deffieux

et al., 2013b). A study by Wattiez et al. (2017) using frontal eye field sonication showed that, in the supplementary eye field, which is a reciprocally-connected brain region, ultrasound can affect the single-neuron discharge frequency. In another study by Yang et al. (2018) using lightly anaesthesised macaques, MRI-guided ultrasound of 250 kHz with pulse repetition frequency of 2 kHz, duty cycle of 50%, and duration of 20 ms was applied to the primary somatosensory cortex. The resulting fMRI blood oxygen level dependent (BOLD) activation was compared to the tactile stimulation. They found that ultrasound was able to induce haemodynamic signal changes in the same cortical areas as with the tactile stimuli. However, this had a larger peak magnitude of around 0.8% and a shorter peak latency by 1 s. In addition, sonications of subcortical structures such as the putamen were also conducted in macaque monkeys (Downs et al., 2017). This promoted small improvements in the speed and accuracy of the macaques when performing visuospatial motor tasks.

These studies however, have only reported short-lived neuromodulatory effects. To be able to deliver ultrasound's full potential for research and therapy, inducing longer-lasting effects or changes are required to be achieved. A study by Verhagen et al. (2019) showed that when targeting the supplementary motor area (SMA) and the frontal polar cortex, an ultrasound protocol of 250 kHz with 30 ms ultrasound bursts every 100 ms can induce offline ultrasound effects which can last over an hour. Furthermore, they found that ultrasound caused the stimulated areas to interact more selectively with the rest of the brain and show regionally specific effects. This is in contrast with what would normally happen at rest, where the brain areas would reflect their activity in their interconnected regions. These ultrasound effects were found to be temporary with no related microstructural changes. A similar study was conducted by Folloni et al. (2019b) but instead targeting the anterior cingulate cortex (ACC) and the amygdala. This demonstrated that there

were long-lasting ultrasound effects that caused a change in the relationship of the targeted regions with the other areas of the brain that they are interconnected with. In addition, because there was an extended period of action observed after stimulation, it was suggested that there were no direct auditory effects, and the dissociable and focal effects on neural activity could not be explained by auditory confounds. This is in contrast with a few experiments in rodents where it was proposed that acoustic transmission through cochlear fluids may induce the activation of a secondary auditory pathway, which could be responsible for the diffuse and non-specific electrophysiological and behavioural outcomes (Guo et al., 2018; Sato et al., 2018; Ai et al., 2016).

The understanding on how long-lasting offline effects are achieved is very relevant in TUS studies particularly, in the treatment of epilepsy where longer-lasting therapeutic effects are desirable to reduce the number and duration of seizures. A study by Zou et al. (2020) on acute epileptic monkeys showed that TUS at a frequency of 800 kHz, a pulse repetition frequency of 500 Hz, and acoustic pressure of 1.74 MPa for 15 $mins$ can cause inhibitory effects that could last for 7 $hours$. It was observed that there was an increase in the expression of c-Fos protein in GABAergic neurons suggesting that TUS may be able to enhance GABAergic neuron activity and increase the inhibitory postsynaptic inputs (Lin et al., 2020). Furthermore, it was suggested that TUS could be affecting the activity of ion channels and synaptic receptors at a single cell or brain network level and this may be reducing the propagation of epileptic discharges across the brain (Hakimova et al., 2015).

2.1.4.5 Recent human studies

After Deffieux and coworkers demonstrated neuromodulation with the primate brain, human experiments quickly followed (Deffieux et al., 2013b) to begin the

exploration of electrophysiological, imaging, and behavioural effects of ultrasound on the human brain activity (Legon et al., 2018a; Ai et al., 2016). Pilot studies in healthy human volunteers have elicited a broad range of suppressive and inhibitory effects on cortical and subcortical target areas (Lee et al., 2016a; Legon et al., 2014). Hameroff et al. (2013) were the first to conduct a study on human subjects. Their study was conducted as a double-blinded trial where ultrasound with low-intensity and a high frequency of 8 MHz was applied using a clinical imaging transducer for 15 s to the scalp region overlying the frontal-temporal cortex. Their findings showed that ultrasound can cause non-specific mood effects on the subjects. Studies by Lee et al. (2015a), Mueller et al. (2014) and Legon et al. (2014) that followed confirmed the modulation of human somatosensory cortex activity. They also recorded amplitude reductions and spectral content changes in the somatosensory evoked potentials. Targeting the primary somatosensory cortex can enhance the performance on sensory discrimination tasks without influencing the task attention or response bias (Lee et al., 2015a; Mueller et al., 2014; Legon et al., 2014).

To date, only Monti et al. (2016) reported a neuromodulatory treatment for brain pathology for thalamic stimulation in a patient with severe traumatic brain injury from a vehicular accident. After the injury, significant brain contusions led to a poor initial level of consciousness and a persistent minimally conscious state for 19 days. A 65 kHz transducer was positioned over the temporal bone window which delivered 10 sonications, each lasting 20 s with a pulse repetition frequency of 100 Hz and intensity of 720 mW/cm^2. It was reported that the patient improved 2 days after the sonication following a gradual recovery in terms of speech and ambulation. But because there were no controls or other subjects used in this study, a spontaneous recovery could not be ruled out.

Legon et al. (2018a) were the first to convincingly demonstrate human subcorti-

cal target neuromodulation. They used a single-element transducer to target the sensory thalamus through the temporal bone. It was observed that the amplitudes of characteristic P14 thalamic somatorsensory evoked potentials were attenuated. The beta and gamma cortical oscillations were modulated which was consistent with previous studies (Lee et al., 2015a; Mueller et al., 2014). Furthermore, their study on the primary human motor cortex showed that a simultaneous 0.5 MHz low-intensity ultrasound and TMS can attenuate the motor evoked potential amplitude and reduce intracortical facilitation (Legon et al., 2018b). However, this did not show any effects on intracortical inhibition. A behavioural task asking the subjects to press a button when they see a visual stimulus on the screen showed that contralateral motor cortex sonication significantly shortened the response time of the subjects Legon et al. (2018b).

2.1.5 Applications of TUS

The rapidly increasing number of findings showing that ultrasound waves can modulate the function of neuronal circuits makes it apparent that TUS has a great potential to have a non-invasive and spatially confined influence on both deep and fairly superficial neuronal structures (Sassaroli and Vykhodtseva, 2016). However, its limitations should be carefully considered and further understanding of its mechanisms are still required for its safety. To further investigate these, ultrasound simulations are being studied to complement the experimental work on TUS.

2.1.5.1 Research limitations

To date, evidence from experimental studies have demonstrated that TUS is a safe method. However, appropriate safety precautions are still being taken when using ultrasound to modulate the brain or its neuronal functions (Naor et al., 2016;

Sassaroli and Vykhodtseva, 2016). This is because the full spectrum of safe and effective parameters are still being identified and optimised. The major practical challenges and limitations associated with the experimental study of TUS especially in small animals are strong anaesthesia effects, and standing waves within the skull (Naor et al., 2016).

Anaesthesia such as ketamine and isoflurane has been shown to suppress ultrasound elicited motor responses thereby, blocking the animal's cortical neuron activity (Han et al., 2018). A reduction of the isoflurane dose to 0.1% allowed TUS to be conducted on semi-awake animals due to the light state of anaesthesia (King et al., 2013). However, in some experiments, it was reported that the ultrasound transducer generated auditory artifacts and audible buzzing sounds, which might have affected the experiments in animals (Guo et al., 2018; Sato et al., 2018) and humans (Legon et al., 2018b, 2014; Mueller et al., 2014). This means that careful considerations such as signal smoothing are needed when using low levels of anaesthesia (Mohammadi et al., 2019) to avoid such confounds. Furthermore, it has been observed from DBS studies that anaesthesia can affect the spontaneous background firing and neuronal spike activity patterns in the brain, and also potentiate the inhibitory actions of GABA, causing effects such as global depression in neuronal discharge (Chakrabarti et al., 2014; Grant et al., 2015). In a repetitive TMS study in rats, isoflurane, dexmedetomindine and propofol caused significant different effects on the functional connectivity of the brain, particularly between the sensorimotor cortex and thalamus (Boonzaier et al., 2017).

Although small animals such as rats or rodents have thin skull bones which allow ultrasound to penetrate their brains, there is poor characterisation of the ultrasound field. This is because their small cranial volumes lead to reflections off the opposite side of the skull which can form standing waves leading to complex fields and pressure hotspots away from the target region (Constans et al., 2017; Younan

et al., 2013). However, not a lot of effort has been done in controlling or correcting these reflections. This leads to conflicting results from a variety of models which are very difficult to compare. The biological complexity of the brain tissue also makes it harder to identify the ultrasound parameters needed for a successful neuromodulation (Gavrilov and Tsirulnikov, 2012; Colucci et al., 2009).

The presence of hair on the head can contribute to loss of ultrasound focus on the target region. Therefore, it is a current practise to shave the subject's head before conducting TUS experiments. On the contrary, a study by Eames et al. (2014) showed that hair had a negligible effect on focal spot thermal rise at 220 kHz and a there was a 17% drop in temperature elevation when using 710 kHz. The results also showed that hair induces minimal loss compared to the skull. Air bubbles however, can be trapped in the hair which can reflect ultrasound and also absorb ultrasound energy (Eames et al., 2014). To create a full contact with the scalp without the presence of air, a coupling medium is typically used between the transducer and the head to prevent loss of ultrasound focus. A coupling medium such as gel or degassed water allows high transmission of wave and low reflection, with an attenuation coefficient and acoustic impedance close to that of the scalp skin (Casarotto et al., 2004). Furthermore, to prevent the loss of focus due to head movements, a stereotactic frame is usually used to ensure that the focus of ultrasound stays on the target region and is not affected by movement of the head (Kusunose et al., 2021).

When scaling up from small to large animals and humans, the head is still shaved to prevent air bubbles being trapped in the hair. A stereotactic frame is also used to prevent the movement of the head while sonicating. These requirements need consideration especially when conducting studies on humans as they may not want to have their heads shaved or use stereotactic frames. Therefore, it is very important for the subjects to first fully understand what the procedure entails and its benefits

before giving their consent.

Large animals and humans have thicker skulls and this can also present another challenge. Thicker skulls can increase the attenuation and aberration of the acoustic wave (Fry, 1978; White et al., 1978) shifting the focus of ultrasound inside the brain. The skull is a multi-layered structure. It has a a hard cortical shell, and a blood- and fat-filled inner cancellous bone layer. The structure of the inner layer of the skull causes strong scattering of the acoustic wave at frequencies above 1 MHz (Pinton et al., 2010). This limits the viable frequency range for transcranial ultrasound propagation (Blackmore et al., 2019).

In spite of this challenge, the development of multi-element arrays which features hundreds to thousands of individual transducers (Hynynen et al., 2006, 2004) has enabled the ultrasound wave to be corrected to compensate for the aberrations and effectively focus on deep brain regions. Many researchers however, do not use these transducer arrays since they are highly complex and expensive (Blackmore et al., 2019). Nevertheless, many TUS studies still investigate brain regions situated close to the cortical surface (Lee et al., 2016a; Legon et al., 2014) where transducer arrays may not be required (Ye et al., 2016; King et al., 2013; Tufail et al., 2010) and simple transducers can be used instead at a lower cost. Here, computational models can be useful to complement experiments that use simpler conditions, such as single-element transducers (Constans et al., 2017; Mueller et al., 2017; Robertson et al., 2017).

However, some brain regions are likely to still remain difficult to target and access using single-element transducers due to the heterogeneity of the skull overlying the target regions. For these, an acoustic lens can be used, which can be effective at correcting for the induced aberrations and reforming the acoustic focus over the target region (Maimbourg et al., 2018). The lens has a variable thickness for

adjusting the phase of the incident wave based on the material's sound speed and is therefore, target specific (Blackmore et al., 2019).

TUS experimental studies have used a wide range of ultrasound frequencies between 220 kHz and 1.9 MHz for effective neuromodulation without causing neurologic injury (Naor et al., 2016; Kim et al., 2014a; King et al., 2013; Deffieux et al., 2013b; Manlapaz et al., 1964). The magnitude and direction of modulation has been observed to be dependent on different factors such as fundamental frequency, targeted volume, sonication intensity, pulsing frequency and duration, duty cycle, and level of anaesthesia (Yoo et al., 2011b). Even small changes in these parameters can easily have profound effects on the neuromodulation (Fomenko et al., 2018; Kubanek, 2018; King et al., 2013; Younan et al., 2013). High frequencies of ultrasound (greater than 1 MHz) can result in unwanted transcranial attenuation and scattering of ultrasound waves (Sun and Hynynen, 1998). *Ex-vivo* experiments with human skulls have shown that less than 700 kHz is the optimum frequency for transcranial transmission (Mueller et al., 2017; Chang et al., 2016; Clement and Hynynen, 2002). Although continuous sonication (100% duty cycle) has shown to stimulate brain activity in some studies (Kim et al., 2014a; Hameroff et al., 2013; Tsui et al., 2005; Barnard et al., 1955), a pulsed delivery is more favourable. This is because it has a lower risk of heating the tissues and it has lower thresholds for neuronal activation (Tufail et al., 2010; Horder et al., 1998). Preclinical studies have shown that longer durations of sonication are likely to cause inhibition of cortical neurons, and shorter durations are likely to cause excitation (M.Plaksin et al., 2016; Kim et al., 2014a). For ensuring the safety of ultrasound neuromodulation, the chosen sonication intensity is preferred to be as low as possible so that the thermal and mechanical tissue damage caused by ultrasound can be further minimised. The brain is very sensitive to temperature elevations and it has been highlighted that an increase of only $4°C$

for 5 $mins$ within the brain can already cause irreversible damage (Horder et al., 1998).

But depending on the incident waveform, the absorption of ultrasound can also result in thermal neuromodulation. A few degrees of temperature change can affect the neuronal activity, where the action potential amplitude and duration, excitation thresholds, spiking rates and afterhypolarisation kinetics are altered (Lee et al., 2005; Thompson et al., 1985; Chapman, 1967; Guttman, 1966). Temperature simulations in several rodent set-ups however, have shown that temperature effects can generally be ignored (Constans et al., 2017). In particular, recent brain studies have observed that rises in temperature are only typically less than a tenth of a degree (Tufail et al., 2010; Khraiche et al., 2008). Although, it was reported by Constans et al. (2017) that there was a rise in temperature of $7°C$ due to thermal diffusion from the skull bone into the brain when simulating using the ultrasound parameters from Kamimura (2016)'s study. Therefore, it is vital that off-target temperature rises do not occur through skull-induced heating.

The impact of the ultrasound stimulation protocol is a function of the animal model being used and the exact features of the ultrasound frequencies, pulse shape, duration, and ongoing brain activity (Airan and Butts Pauly, 2018). Techniques such as mapping cavitation, temperature and displacement are examples of how ultrasound parameters can be controlled to achieve targeted neuronal excitation and inhibition (Kamimura et al., 2020). But further investigations are still required so that essential translational information can be provided for this method including its safety (Blackmore et al., 2019; di Biase et al., 2019; Pasquinelli et al., 2019; Yoon et al., 2019; Bystritsky and Korb, 2015).

2.1.5.2 Mechanisms of ultrasound

In spite of the progress in ultrasound application, very little is known about its mechanisms. It is not well understood how mechanical forces impart actions upon neuronal functions. However, it is known that various cellular and molecular components can sense and transduce the mechanical signals in neurons and brain circuits (Tyler, 2012). These include viscoelastic plasma membrane, mechano-sensitive ion channels, and cytoskeletal proteins such as actin and microtubules that can generate and sense intracellular force as well as, extracellular matrix proteins that can provide adhering and coupling forces between cells (Tyler, 2012).

Because of the many different regions in a neuron, it is not easy to predict how the ultrasound energy is being translated into a cellular response. One of the possible intermediaries are the ion channels, as they are one of the components involved in the nerve depolarisation response (Wright et al., 2015). Through conformational changes, ion channels opening or closing can affect their radius and hydrophobic thickness. They can be more or less sensitive to mechanical forces from the surrounding membrane, a process known as mechano-sensitivity (Ursell et al., 2007). This deformation of the membrane and proteins can affect the ion channel kinetics and/or the membrane capacitance. This induces transmembrane currents that generate the action potentials (Tyler, 2011; Johns, 2002).

Recent studies suggests that glial cells have a critical role in the brain for neuronal function (Fields, 2015; Min and Nevian, 2012). Experimental studies have shown that ultrasound can activate mechanosensitive ion channels (Qiu et al., 2019; Prieto et al., 2018; Kubanek et al., 2016; Tyler et al., 2008) and other brain cell types such as astrocytes (Oh et al., 2019), where a mechanical stimulus can excite calcium waves in glial cells, making them a potential target for TUS in the brain (Newman and Zahs, 1998). Subcellular responses such as sodium and calcium

transient generation are evident in glial cells following TUS suggesting that glial cells may have increased sensitivity to ultrasound (Tyler et al., 2008).

The main theory for TUS is that ion channels are both the direct receiver of the ultrasound force and the only biological effectors involved in the action potential generation (Wright et al., 2017). However, it has also been found that ultrasound affects the chemical synapses (Borrelli et al., 1981). On the other hand, according to Wulff et al. (1951), there are five influences of ultrasound propagation in living tissues. These are heating from absorption of acoustic energy, periodic pressure changes, radiation pressure, streaming or flow in viscous media, and high temperatures and pressures associated with cavitation. Ultrasound can heat tissues using HIFU (Elias et al., 2013; McDannold et al., 2010; Martin et al., 2009) while recent studies using lower intensities show that there is a very low chance of heating and inertial cavitation forming (Lee et al., 2015a; Deffieux et al., 2013a; Tufail et al., 2010). Although other researchers found that it is possible to have stable cavitation of pre-existing bubbles (ter Haar et al., 1986, 1982).

A neuronal intramembrane cavitation excitation (NICE) model has been proposed as a possible mechanism of ultrasound (Plaksin et al., 2014; Krasovitski et al., 2011). This model uses a modified Hodgkin and Huxley (H-H) model and includes a bilayer sonophore that describes the response of the lipid membrane to ultrasound (Krasovitski et al., 2011). This predicts that the absorbed ultrasound can cause expansions and contractions in the intramembrane space between the two leaflets of the lipid membrane as seen in Figure 2.1. This can cause a membrane area change that is proportional to the applied pressure amplitude and inversely proportional to the square root of the frequency (Krasovitski et al., 2011). By linking this model to the electromechanical coupling phenomenon, the membrane capacitance changes within the model can create currents that induce the action potential (Plaksin et al., 2014). This model is proposed as an explanation

of the other experimentally observed phenomena of a nerve impulse (Mueller and Tyler, 2014). Ultrasound is assumed to induce intramembrane cavitation or cause nanobubble formation in between the two leaflets of the membrane at cavitation thresholds. The negative pressure of the ultrasound wave can pull the two monolayers of the membrane apart and the positive pressure of the ultrasound can push the monolayers of the membrane towards each other. The nanobubbles can be created from the dissolved gas accumulating in the hydrophobic zone and they can expand and contract periodically. These oscillations of the nanobubbles can cause changes in the local curvature of the membrane (Plaksin et al., 2014). Furthermore, it was observed that there are reductions in the amplitude and conduction velocity of electrically evoked action potentials in the giant axon of earthworms after sonicating them with ultrasound pulse trains. The use of acoustic intensities below the cavitation thresholds suggests that it is the acoustic radiation force (the net force provided by the oscillating pressure in the inhomogeneous material) effects that modulate or suppress the nervous system activities (Wahab et al., 2012). A similar conclusion is reached by Prieto et al. (2013) by investigating the isolated lipid membrane model's dynamic responses to ultrasound.

Moreover, all the proposed mechanisms of ultrasound would be occurring to some extent in the complex environment of tissues but the importance of each one will vary depending on the ultrasound parameters being applied and the structure of the tissue being targeted. Since in the case of neuromodulation, the mode of action and method of energy transduction is still left very open, there is a requirement for better understanding of the electromechanical coupling occurring in neurons (Naor et al., 2016; Sassaroli and Vykhodtseva, 2016).

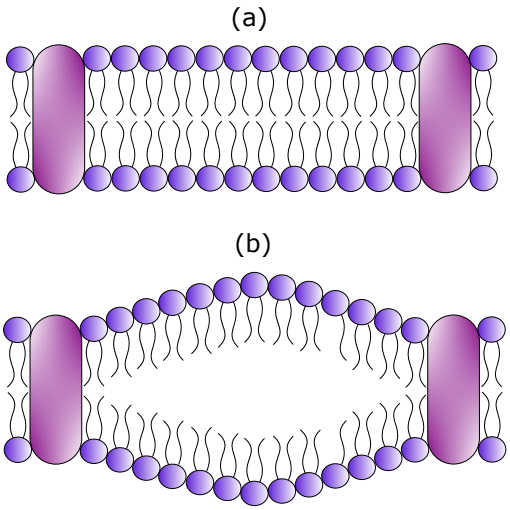


Figure 2.1: Cavitation in the leaflet of membranes where the leaflets of the membrane are a) contracted and b) expanded.

2.1.5.3 Ultrasound simulation methods

The experimental studies on TUS has sparked interest in its computational modelling as it can examine the effects of ultrasound on the neuronal activity of the brain without the need to account for the risks that ultrasound can impart on the subjects. The numerical models and theories that have been developed for the electromechanical coupling effects including flexoelectricity however, will be covered in Section 2.2.3.

Currently, there are different methods that have been developed for the simulation of non-linear, pulsed acoustic fields excited by medical transducers (Verweij et al., 2014; Verweij and Huijssen, 2011). Forward-wave methods are the most commonly used but due to their nature, they can only deal with waves that travel away from the source. Heterogeneities are generally not dealt with so they have difficulties in dealing with realistic features of ultrasound simulations such as, tissue heterogeneities, power law losses or steered beams (Demi et al., 2014). On the other hand, full-wave methods can directly solve the basic acoustic equations

using the finite difference or finite element method. A preferred direction of propagation is not necessary and it can also deal with medium heterogeneities very easily. However, the implementation of the full-wave methods still needs at least 10 to 20 grid points per smallest wavelength and per shortest period. This can result in computational grids that are too large to process for a realistic computational domain (Demi et al., 2014).

Two full-wave methods have been developed that do not suffer from the above restrictions. The first method is called *k*-Wave (Treeby and Cox, 2010), which is a toolbox in MATLAB (MathWorks, 2017). It utilises a Fourier pseudospectral method, where the spatial grid points are largely reduced by performing the spatial derivatives in the Fourier domain. The second method is the Iterative Non-linear Contrast Source (INCS) method. It is an integral equation method, where the number of spatial and temporal grid points is decreased by applying appropriate filtering in occurring spatio-temporal convolution operation. These two methods can both deal with non-linear waves propagating in an arbitrary direction in heterogeneous media with power losses. Therefore, they are both very useful in the study of TUS. The only approximations made in these methods are related to the discretisation of the computational domain (Demi et al., 2014). The performances of *k*-Wave and INCS have been demonstrated in a number of published studies and they have shown that they are able to deal very well with realistic models of situations encountered in non-linear medical ultrasound. In contrast, *k*-Wave and INCS are based on different computational principles so it is unlikely that they would both suffer from the same systematic error. Quantitatively comparing these two methods for different situations has established that both methods are correct and highly accurate (Demi et al., 2014).

Nonetheless, these simulation methods only focus on simulating ultrasound and they do not look into ultrasound effects on the electrophysiology of the brain.

Thus, there is a need for computational modelling of ultrasound that can further investigate its effects on the brain activity by looking into the electromechanical coupling that arises in neurons.

2.2 Electromechanical coupling in neurons

A nerve impulse was initially and often still considered to be a purely electrical phenomenon. However, other aspects associated with action potential such as mechanical and thermal changes have been observed conjointly to the action potential (Tasaki et al., 1989; Iwasa and Tasaki, 1980). Different electrical and alternative models of a nerve impulse have been developed to study the action potential while accounting for the coupling between the action potential and other changes associated with multi-physics.

2.2.1 Neurons and action potential

For complex organisms, the communication between neurons within the neuronal network in the nervous system and between neurons and other cells within the body is necessary for their functionality and survival (Bishop, 1956). The human body consists of billions of neurons and specifically, there are $\sim$86 billions of neurons in the human brain (Herculano-Houzel, 2012). Depending on the key physiological roles, the nervous systems is divided into two parts: the central nervous system (CNS) consisting of the brain and spinal cord, and the peripheral nervous system (Fletcher, 2014).

A neuron, illustrated in Figure 2.2, has a polar structure where one end receives incoming information and the other end makes contact with other neurons or cells to pass information along. Typically, a neuron consists of a soma which is around 20 μm in diameter containing the cell nucleus. Extending from the soma are den-

drites that receive incoming information from the pre-synaptic neurons. The long process emerging from the soma is the axon which divides into terminal branches, each forming a synapse or a junction with a post-synaptic cell. Myelinated axons are insulated with a discontinuous sheath of myelin formed by glial cells and separated by the nodes of Ranvier (Sassaroli and Vykhodtseva, 2016; Kevenaar and Hoogenraad, 2016; Fletcher, 2014). The fibre diameter in humans can range from 0.16 to 9 μm (Liewald et al., 2014). All sections of the neuron are vital for the transfer of information within the whole body.

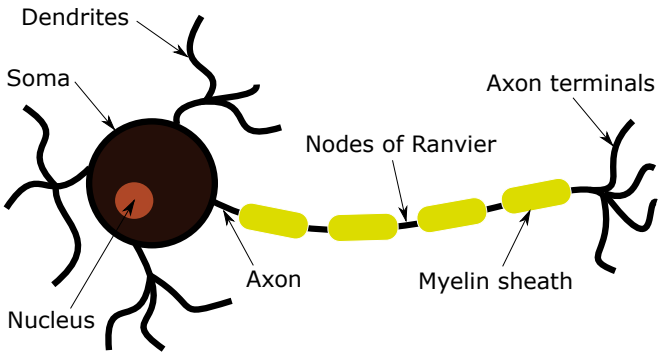


Figure 2.2: Structure of a neuron.

The way information is transferred from one end of a neuron to another is through an active electrophysiological response of the membrane: the action potential defined as a large and rapid reversible fluctuation in the membrane potential that propagates along the length of the axon (Fletcher, 2008). This property of neurons allows for rapid responses to changes in the internal and external environment. Ion protein channels on the plasma membrane of neurons underlie the electrical signalling by enabling the generation and propagation of these action potentials by generating changes in the electrical potential difference across the membrane (Sassaroli and Vykhodtseva, 2016).

The two main ions involved in the resting state and generation of action potentials are sodium (Na^+) ions and potassium (K^+) ions. The resting state of the mem-

brane is established by actively pumping the Na^+ ions out of the cell using the energy from the adenosine triphosphate (ATP) molecules through the Na^+/K^+-ATPase protein (Lodish et al., 2000; Johnston and Wu, 1994). The K^+ ions are simultaneously pumped into the cell at a 3:2 ratio with the Na^+ ions (Fletcher, 2008). The membrane has a resting potential difference between approximately -30 and -70 mV (Lodish et al., 2000) where the inside of the cell is negative relative to the outside due to the presence of the leak K^+ ion channels in the membrane (Fletcher, 2008). The membrane is depolarised when the threshold potential is reached by a positive stimulus, which is $\sim$20 mV. The abrupt opening of the voltage-gated Na^+ ion channels triggers an action potential by allowing Na^+ ions to move inside the cell causing the depolarisation of the membrane. An efflux of K^+ ions rapidly restores the membrane to its resting state causing a repolarisation of the membrane. This is mediated by the leak K^+ ion channels and the voltage-gated K^+ ion channels, which open as the voltage-gated Na^+ ion channels are closing. Further stimuli cannot trigger another depolarisation immediately after this because voltage-gated Na^+ ion channels become temporarily unresponsive for a period of time, called the refractory period (Sassaroli and Vykhodtseva, 2016; Fletcher, 2008; Lodish et al., 2000). The voltage-gated K^+ ion channels remain open causing the membrane potential to temporarily be slightly more negative than the normal resting potential. The normal resting state is restored when the voltage-gated K^+ ion channels close. This period of hyper-polarisation is called an undershoot and denotes a phase of decreased responsiveness related to the refractory period. This means that a larger stimulus than usual would be required to cause a depolarisation as the inside of the cell is more negative than the normal resting potential. Furthermore, the action potential is self-propagating so a depolarisation of a small region of the membrane can trigger the opening of adjacent Na^+ ion channels along the length of the axon creating a wave of depolarisation

(Fletcher, 2008). Typically, an action potential can propagate with a velocity of between 0.1 and 100 m/s (Engelbrecht et al., 2018b; Sassaroli and Vykhodtseva, 2016; Lodish et al., 2000) but unmyelinated axons can conduct from 0.5 to 10 m/s and myelinated axons can conduct even up to 150 m/s (Purves et al., 2001). An action potential has a duration of 1 to 20 ms (Sassaroli and Vykhodtseva, 2016; Liewald et al., 2014; Lodish et al., 2000) corresponding to action potential lengths from a few millimetres to a few centimetres (Sassaroli and Vykhodtseva, 2016). Figure 2.3 shows the changes in ion concentration and electrical potential inside the cell during an action potential.

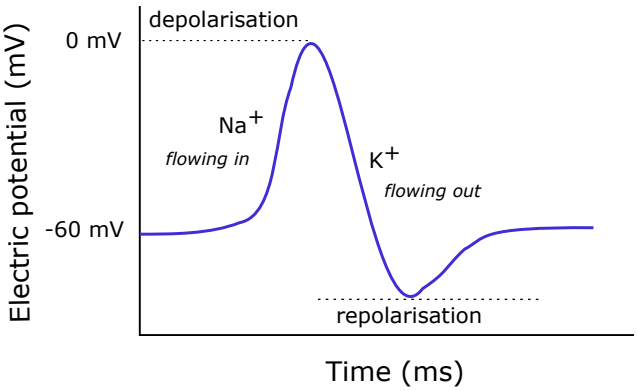


Figure 2.3: Generation of an action potential.

2.2.2 Electrical models of nerve excitation

Several models of electrophysiology demonstrating how action potentials are initiated and propagated within cells and tissues have been developed. Over the years, they have contributed a great deal to the study of excitable systems.

2.2.2.1 H-H model

Action potentials were originally considered to be a purely electrical phenomenon. The H-H model (Hodgkin and Huxley, 1952) has served as a foundation for neuro-

scientific research for the past seventy years (Catterall et al., 2012).

The model builds upon efforts to study the electrophysiology of single neurons by using a squid giant axon in the 1930s (Young, 1938). From there, Hodgkin and Huxley started recording the action potentials from inside the nerve fibres of squid giant axons (Hodgkin and Huxley, 1939). They tested the hypothesis that voltage-sensitive Na^+ ion and K^+ ion permeability changes are both important for the induction of action potential. They conducted this experiment using the voltage-clamp technique, where the ion currents through the membrane of the axon were measured by controlling the voltage across the membrane (Hodgkin and Huxley, 1952). Subsequent studies supported Hodgkin and Huxley's discovery of the two independent membrane mechanisms by demonstrating that depolarising the membrane can cause an influx of Na^+ ions into the cell, followed by an efflux of K^+ ions (Narahashi et al., 1964; Tasaki and Hagiwara, 1957). In addition, the time-course and the underlying permeability changes of the action potential was described mathematically. The H-H model phenomenologically describes the electrical behaviour of an axonal membrane, where the conducted experiments were used for calibration (Hodgkin and Huxley, 1952). The model is based on the conductance of ion-selective channels which acts as resistors, and a lipid bilayer membrane which acts as a capacitor (Mueller and Tyler, 2014), see Figure 2.4. The concentration gradient across the membrane gives rise to the ionic currents. This model agrees with the different properties of the action potential such as, amplitude, threshold, velocity and refractory period (Phillips et al., 2012).

From these assumptions, the total current equation is

$$I = C_M \frac{\delta v}{\delta t} + h_K \omega^4 (v - v_K) + h_{Na} \Omega^3 \eta (v - v_{Na}) + h_L (v - v_L) \qquad (2.1)$$

where, v is the electrical potential of the membrane, h_K $h_{Na}$and h_L are the maxi-

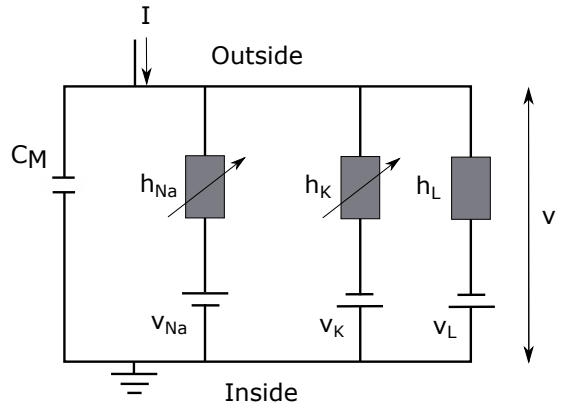


Figure 2.4: Equivalent circuit for H-H model.

mum conductance values for the Na^+, K^+ and leakage (L) ionic current, and v_K, v_{Na} and v_L are the differences between equilibrium and membrane electrical potential. The coefficients, ω, Ω and η are the gating variables and their values vary with voltage and time. The overall equation has four contributing terms: a capacity current, a K^+ ion current, a Na^+ ion current, and a L ion current. The leakage term represents the sum of smaller currents for other ions (Drukarch et al., 2018; Hodgkin and Huxley, 1952).

However, in Hodgkin and Huxley's voltage-clamp experiments, no action potential propagation was observed as the voltage clamp only considered a patch of membrane. To address this problem, Rall carried out neurophysiological experiments with spinal motor neurons and coupled the cable theory to the H-H model (Rall, 2010). This replicated the generation, propagation, and shape of the action potential that was observed from the experimental data as it showed the propagation of a voltage pulse along the cylindrical membrane through the passive spreading of electrical currents to the adjacent segments of the axon (Sassaroli and Vykhodtseva, 2016).

2.2.2.2 Simplification of the H-H model

The H-H model has been extended and applied to a wide range of excitable cells since its development and it is a widely accepted model for describing action potentials (Mueller and Tyler, 2014). However, because it has a four-variable formula, a direct use of the model requires the knowledge of many parameters (Postnikov and Titkova, 2016).

Fitzhugh and Nagumo developed a simplified two-variable version of the H-H model, which includes the essential behaviour of the action potential. Similar to the H-H model, the Fitzhugh-Nagumo (FHN) model has also contributed immensely to the study of excitable systems (Fitzhugh, 1961). A model for the simulation of cardiac excitation called the Aliev-Panfilov model was also developed, which retained the simplicity of the FHN model. It adequately represents the action potential shape and restitution property of the cardiac tissue, while avoiding the cyclic behaviour of the FHN model (Aliev and Panfilov, 1996).

2.2.3 Non-electrical aspects of nerve excitation and alternative models

The H-H model phenomenologically describes the electrical physics of the action potential and does not include the non-electrical aspects of nerve impulses, such as the mechanical and thermodynamic variables that have been experimentally observed (Mueller and Tyler, 2014). Therefore, over the years, the H-H model has been challenged (Appali et al., 2012) as substantial experimental evidences showed that the action potential is accompanied by axonal radius, pressure and length changes (Iwasa and Tasaki, 1980) as well as, reversible heat changes (Tasaki et al., 1989).

The first study on the mechanical aspects of nerve impulses was conducted by Hill (1950), where he observed that an electrical stimulation of the sepia giant nerve fibre caused an increase in the nerve fibre diameter. This observation was then supported by the results he obtained from the crayfish giant axon experiments (Hill et al., 1977). Additionally, Iwasa and colleagues were able to confirm Hill's results (Iwasa and Tasaki, 1980; Iwasa et al., 1980) where they demonstrated that during the action potential, the giant squid axon swelled up and returned to its initial state afterwards (Tasaki and Iwasa, 1982). Terakawa recorded an increase in the intracellular pressure in both intact and perfused squid giant axons, followed by a decrease in intracellular pressure (Terakawa, 1985). Recent studies confirmed that the dimensional changes in the nerve fibres occur in phase with the action potential (Gonzalez-Perez et al., 2016; Oh et al., 2012; Nguyen et al., 2012). Le Bihan (2007) proposed that the ionic transmembrane contributing to the observed transient cellular expansions may be playing a functional role in neuronal activation through complex interactions with the cytoskeleton. This was supported by the experiments mentioned above. Another study on the thermal aspect of action potential showed that the released heat during the depolarisation phase of the action potential is found to be compensated by the heat uptake in the repolarisation phase (Zohar et al., 1998; Tasaki et al., 1989). Although, several previous experiments mentioned that not all of the heat released during the action potential was absorbed during repolarisation (Howarth et al., 1968).

Due to the limitations of the H-H model, new models of nerve impulses have been proposed for the study of neuronal excitability as an attempt to have an overall representation of the nerve impulse. There are established models that can describe the relationship between mechanical and electro-chemical signalling in tissues outside of brain neuroscience (Eyckmans et al., 2011; Sachs, 2010). For example, the roles of mechanical forces and the stretch-activated channels are well

established for cardiac excitation (McCain and Parker, 2011; Morris, 2011; Ward et al., 2008). Many researchers have developed hypotheses and models to provide an explanation on the electromechanical coupling in nerve impulses in neuronal tissues. However, the physical basis for the observed non-electrical changes in this case remains mostly hypothetical and not fully understood. Further theoretical and experimental work are needed to provide more evidence that the proposed models can act as a comprehensive physical explanation of nerve impulses (Mueller and Tyler, 2014).

2.2.3.1 Heimburg and Jackson model

In 1912, Wilke proposed a pressure wave theory suggesting that mechanical impulses underlie the propagation of information in nerves. The electrical oscillations were suggested to accompany these mechanical impulses (Wilke, 1912). This inspired Heimburg and Jackson to develop a soliton model that considers the action potential to be an adiabatic, mechanical density pulse. The focus of this model was shifted from membrane proteins such as ion channels, which according to the H-H model play an important role in nerve impulse generation and propagation, to membrane lipids instead (Holland et al., 2019). The 'solitary wave propagates with little loss of energy and also maintains its shape and speed after colliding with another such wave' (Heimburg and Jackson, 2005). This soliton model suggests that during the nerve impulse propagation, the axon swells, heat is released and then reabsorbed along with an electrical potential difference across the membrane, all occurring simultaneously. This can therefore, be considered to be a more complete explanation to the phenomenon that a nerve impulse has both thermodynamic and electrophysiological aspects (Drukarch et al., 2018).

From the thermodynamic stand point, the lipid membrane is found phenomenologically in the fluid state with some domains in the gel phase. It displays re-

versible phase transitions from the liquid to the gel phase and vice versa (Sassaroli and Vykhodtseva, 2016; Heimburg and Jackson, 2005), see Figure 2.5. Changes in temperature, voltage, pressure and chemical potentials such as pH and calcium concentration can influence the phase transitions of lipid membranes (Sassaroli and Vykhodtseva, 2016). The proteins however, do not function as active components in the model of soliton propagation through the phospholipid bilayer. Thus, the role of the proteins in the electrical propagation of nerve impulses is ignored. Including the proteins in the soliton model by combining it with the H-H model is not as straightforward as some researchers have imagined because the two models are considered to be separate mechanisms (Mueller and Tyler, 2014).

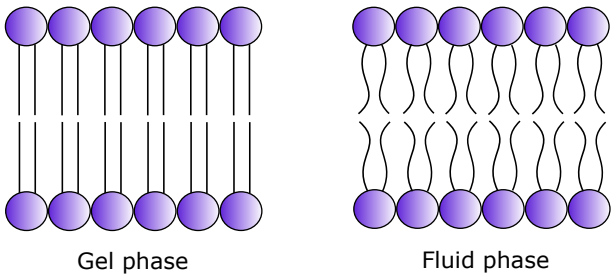


Figure 2.5: Gel and fluid phases of the lipid membrane.

Adding to the potential controversy of putting aside the role of ion channels, two colliding solitons pass through each other with minimal loss of energy, while the collision of action potentials has been known to annihilate the propagation of nerve impulses due to the refractory period (Lautrup et al., 2011). This observation was challenged by Gonzalez-Perez et al. (2016, 2014), where they demonstrated that action potentials can penetrate each other in invertebrate neurons thus, agreeing with the prediction of the soliton model. Follman and colleagues tried to replicate this finding but their observation showed no soliton-like behaviour such as reflection or crossing of the action potentials (Follmann et al., 2015). Lastly, the soliton model implies that the nerve impulse is an adiabatic process, meaning that heat changes are completely reversible. Even though Hodgkin and Huxley gave

experimental evidences in favour of this (Hodgkin and Huxley, 1952), most studies suggest that not all the heat released is absorbed back during the repolarisation phase (Anderson et al., 2009). Due to the technical limitations of the experimental techniques used to measure the temperature changes accompanying the nerve impulse, conclusions about this can still not be drawn with certainty (Anderson et al., 2009).

2.2.3.2 Rvachev model

Rvachev proposed a model that assumes axoplasmic pressure waves that co-propagate with the action potential can cause lipid bilayer to expand. This expansion can activate the mechano-sensitive Na^+ channels and enable the membrane to be depolarised. The influx of calcium (Ca^{2+}) ions into the neuronal cytoplasm is thought to cause the subaxolemmal actin-myosin filaments to contract, which accelerates the propagation of the axoplasmic pressure pulse (Rvachev, 2010). A number of studies confirmed that the activity of voltage-gated Na^+ ion channels can be modulated by mechanical stresses (Beyder et al., 2010; Wang et al., 2009). According to a 'bilayer mechanism' theory, the perturbations in membrane mechanics such as the changes in the membrane lateral pressure can stimulate changes in the conformational structure of ion channels. This can thereby, modulate their opening and total membrane conductance (Tyler, 2012). Additionally, according to the 'tethered mechanism' theory, the ion channels are anchored to the subaxolemmal cytoskeleton and could directly sense mechanical displacements through these filament connections (Xu et al., 2013).

Similar to the soliton model, Rvachev's model is able to give some explanation to the non-electrical phenomena of the nerve impulse, which are not included in the H-H model. The model includes the dependence of the nerve impulse velocity on the axon diameter and the degree of myelination. This provides a framework

that allows for the understanding of the contribution of ion channel proteins to nerve impulse initiation and propagation, which the soliton model cannot provide (Drukarch et al., 2018).

2.2.3.3 El Hady and Machta model

El Hady and Machta proposed a computational model where a travelling wave of action potential produces varying electrostatic forces across the membrane. This in turn, results in co-propagating displacements, called action waves, to emerge from the surface wave speed (El Hady and Machta, 2015). This model suggests that as the potential energy stored in the membrane elastic properties and the cytoskeleton is converted into kinetic energy carried by the axoplasmic fluid, mechanical displacements arise. As a result of the physical process of electrostriction (Gilbert, 1975; Biondi et al., 1972), they proposed that the depolarisation of the membrane causes the mechanical changes, regardless if they have physiological significance. Unlike the model by Rvachev (Rvachev, 2010), their model do not need augmentation of the mechanical pulse by cytoskeleton contractions. But it is likely that the mechanical waves could feedback to the action potential through the mechanically sensitive ion channels and cytoskeletal ultra-structure.

This model agrees with the experiments that there is a reversible heat change during a nerve impulse and predicts that heat is released during the depolarisation phase, where the Na^+ ions travel down their concentration and potential gradients. It also predicts the absorption of heat during the repolarisation phase as the K^+ ions move down their concentration gradients thereby, moving out of the cell. This model suggests that there is a net production of heat during the nerve impulse meaning that not all the heat is absorbed back. Furthermore, the simulation results from this model agrees with a variety of experimental results on the magnitude of membrane displacement (Drukarch et al., 2018; El Hady and Machta, 2015).

2.2.3.4 Engelbrecht model

Engelbrecht and colleagues proposed an approach that integrates the H-H model (Hodgkin and Huxley, 1952) and the soliton model (Heimburg and Jackson, 2005) in a general unifying model for all relevant manifestations of the nerve impulse and their interactions with each other. Thus, this model can be used to extensively study the electromechanical coupling of waves in nerve fibres. The three waves involved in this model are: an electrical pulse, a pressure wave in the axoplasmic fluid of the nerve fibre, and a mechanical wave in the neuronal membrane. These are described mathematically and coupled through coupling forces (Engelbrecht et al., 2018b,a, 2016), see Figure 2.6. The action potential which is modelled as an electrical pulse using a modified FHN model (Nagumo et al., 1962; Fitzhugh, 1961) is assumed to trigger all the processes. This modified FHN model includes the mechanical activation parameters that describe the mechano-sensitivity of the ion channels. The electrical pulse is coupled to the mechanical waves, which take account of the longitudinal and transverse waves in the membrane as well as the pressure wave in the axoplasm. A modified non-linear soliton model is used to model the longitudinal wave. The transverse wave is related to the longitudinal wave through modelling using the theory of rods. To model the pressure wave in the axoplasm, a model of pressure waves in an elastic cylinder tube with added viscous damping is described by a 1D Navier-Stokes equation. For the coupling effect, a number of coupling forces are added into the governing equations depending on the spatial and temporal changes of the voltage (Engelbrecht et al., 2018b,a, 2016). This mathematical model can be used to predict the characteristics of nerve impulse propagation (Engelbrecht et al., 2018a).

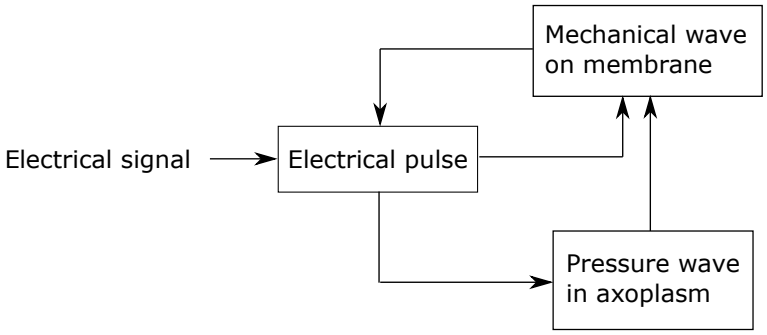


Figure 2.6: Process of nerve impulse propagation in Engelbrecht model.

2.2.3.5 Flexoelectricity

There is growing evidence that flexoelectricity is also one of the key mechanisms in the coupling between mechanical deformation and electrophysiology, especially in biological cells (Krichen and Sharma, 2016; Ahmadpoor et al., 2013). This phenomenon was first recognised in liquid crystals and was introduced as an atypical piezoelectricity where an out-of-plane bending modifies the electrical field inside the liquid crystal (Harden et al., 2006; Raphael et al., 2000; Meyer, 1969). Since then, flexoelectricity has also been widely observed in other dielectric materials including crystalline materials (Zubko et al., 2013), semiconductors (Narvaez et al., 2016), polymers (Chu et al., 2015), bones (Vasquez-Sancho et al., 2018) and biomembranes (Ahmadpoor and Sharma, 2015; Petrov, 2006). Generally, flexoelectricity is considered to be the coupling between polarisation and strain gradients in dielectric materials (Zubko et al., 2013). When these materials are deformed non-uniformly, the local centrosymmetries break inducing a change in polarisation (Krichen and Sharma, 2016; Zubko et al., 2013; Tagantsev, 1986), see Figure 2.7. The recent attention on flexoelectricity is primarily due to its proposed effects in biological functions such as vesicle equilibrium (Gao et al., 2008), tether formation (Brownell et al., 2010; Glassinger et al., 2005), thermal fluctuation (Liu and Sharma, 2013), ion transport (Petrov et al., 1993), cochlear

amplification and sharp frequency discrimination, and outer hair cell electromotility (Liu and Sharma, 2013; Deng et al., 2014; Breneman et al., 2009; Spector et al., 2006; Brownell et al., 2001; Raphael et al., 2000).

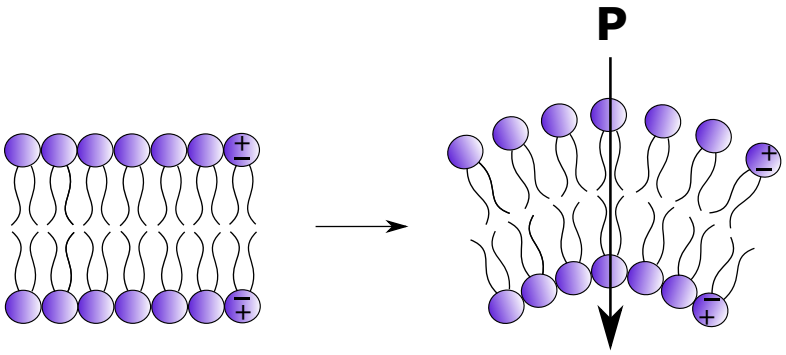


Figure 2.7: Induced polarisation on the membrane due to non-uniform deformation.

Biological flexoelectricity is a phenomenon that refers to the curvature-dependent polarisation of the membrane (Petrov, 2006). This takes into account the deformation of the membrane and provides a basic electromechanical mechanism that enables biomembranes to exchange responsiveness between electrical and mechanical stimuli (Cole, 1941). Flexoelectricity is a bi-directional phenomenon as it includes both the direct flexoelectricity referring to a spontaneous electric polarisation in a dielectric material induced by an applied mechanical strain gradient, and the reverse flexoelectricity referring to the strain gradient induced by an electrical field applied across the dielectric material (Bruhn et al., 2016; Krichen and Sharma, 2016; Harden et al., 2008; Raphael et al., 2000).

Petrov proposed that the mechanical changes associated with the action potential arise from the flexoelectrical property of the cell membrane (Agnes and Nandor, 2013). In this hypothesis, the voltage-gated ion channels play an important role in the generation and propagation of the action potential whereas, the role of the lipid phase transition is ignored. Ionic currents are induced by a sufficient membrane

depolarisation through the voltage-gated ion channels, as suggested by the H-H model. At the same time, the changes in the membrane curvature are induced through the reverse flexoelectric effect. This allows Petrov to consider that the action potential as a flexoelectric wave (Agnes and Nandor, 2013; Petrov, 2006). As a result, it is suggested that flexoelectricity is very likely to be involved in several membrane functions that manipulate the curvature of a membrane, e.g., exocytosis, endocytosis and cell migration, which relates membrane mechanics and electrodynamics (Mueller and Tyler, 2014).

2.3 Conclusion

In recent years, extensive progress has been made in the studies of physiology of the central nervous system, the identification of the functional roles of specific brain structures and the exploration of large-scale network dynamics (Dayan et al., 2013). Among the wealth of techniques available to probe and interact with the brain functions, neuromodulation is poised to become the most promising tool for the exploration of neurological processes in the brain with a precision ranging from cellular level all the way up to the macroscale level (Amiez et al., 2006). While the transient manipulation of activities in rodents (Vanduffel, 2016; Sternson and Roth, 2014) is increasingly becoming accessible, the manipulation of brain activities in the primate brain is less widely available and remain accessible to comparatively few researchers in a limited number of research centres worldwide (Galvan et al., 2018; Vanduffel, 2016; Krug et al., 2015). In addition, experimental studies especially on larger animals and humans are very costly and require extensive long-term care and training before, during and after the experiments have been conducted. Therefore, computational studies have become a convenient method to support and complement the experimental work on TUS.

Currently, computational modelling of TUS is still solely focussed at simulating ultrasound without coupling with the electrophysiology of the brain (Pouget et al., 2020; Folloni et al., 2019b; Verhagen et al., 2019). In addition, the electromechanical models that have been developed only focus on the electromechanical coupling that naturally occurs in neurons during the action potential as opposed to occurring with the intervention of external mechanical stimuli (and in particular here, ultrasound). Finally, these models are solely focussed on the cellular scale, and do not straightforwardly scale up to the network or organ scale. This means that ultrasound effects on the brain activity is currently not being investigated computationally. The issues and risks involved in experimental studies as well as the lack of electrophysiology modelling to study the effects of ultrasound on the brain activity further emphasises the need for a tissue model to understand the electromechanical coupling phenomenon at the organ scale especially in the context of TUS.

3 | 1D axonal model

This chapter presents a 1D axonal model serving as a proof of concept for the electromechanical coupling phenomenon in neurons using direct flexoelectricity. The axonal model is implemented using two methods namely, the explicit finite difference method and the Fourier pseudospectral method, used in the ultrasound propagation simulator, *k*-Wave (Treeby and Cox, 2010) which is commonly used in TUS studies.

3.1 Electromechanical coupled model

The 1D axonal model (see Figure 3.1) describes the propagation of the action potential along the length of the axon when subjected to a longitudinal displacement. This overall model consists of a mechanical pulse model, a flexoelectric coupling model linking the electric polarisation to the axonal mechanical strain gradient, and an electrophysiological pulse model. The axon is assumed to be a symmetric, incompressible, isotropic and homogeneous cylinder. Here, a cylindrical coordinate system (r, θ, z) is used and the axon is truncated to $z \in [-L, L]$ with time $t \in [0, T]$, where the space and time step increments are $\Delta z = L/M$ and Δt, respectively. This defines $z_j = j\Delta x$ and $t_n = n\Delta t$ with nodes $j = -M, ..., M$ and time steps $n = 0, ..., N$.

For the mechanical pulse model, a wave equation is used (Pierce, 1998):

$$\frac{\partial^2 \delta_z}{\partial t^2} = c^2 \frac{\partial^2 \delta_z}{\partial z^2} \tag{3.1}$$

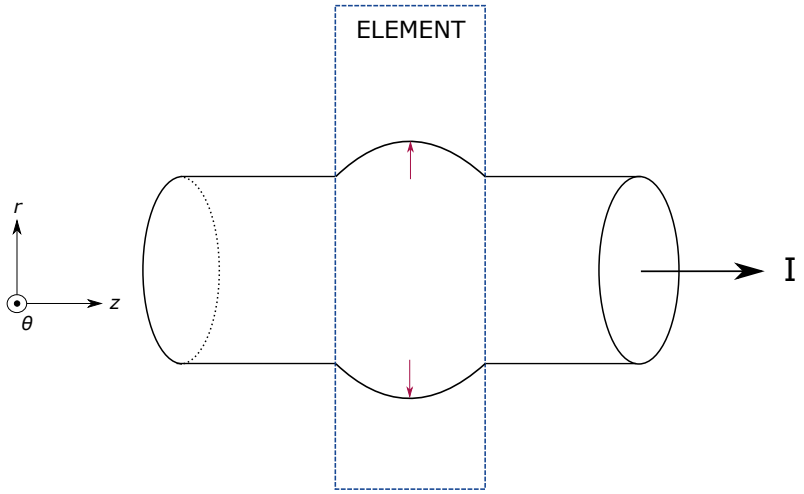


Figure 3.1: Schematic of the 1D axonal model.

where the wave speed c is given as:

$$c = \sqrt{\frac{K}{\rho}} \tag{3.2}$$

δ_z is the displacement of axon in the longitudinal direction z, K is the bulk modulus, and ρ is the material density. From the application of a displacement on the first node from the initial time to a certain time, the deformation of a slice of axon assuming incompressibility (no volume change) is:

$$\begin{aligned} \pi r_a^2 dz &= \pi \left(r_a + \delta_r\right)^2 \left(dz + d\delta_z\right) \\ 1 &= \left(1 + \frac{\delta_r}{r_a}\right)^2 \left(1 + \frac{d\delta_z}{dz}\right) \\ 1 &= {\lambda_\theta}^2 \lambda_z \\ \lambda_\theta &= \sqrt{\frac{1}{\lambda_z}} \end{aligned} \tag{3.3}$$

where r_a is the radius of the axon, δ_r is the displacement in the radial direction r, λ_z is the longitudinal stretch, and λ_θ is the circumferential stretch (Slaughter,

2002).

The circumferential strain ε_θ is given by the logarithm of the circumferential stretch λ_θ:

$$\varepsilon_\theta = ln(\lambda_\theta) \tag{3.4}$$

The resulting electric polarisation P (Zubko et al., 2013) from the strain gradient is given by making use of the flexoelectric coefficient f:

$$P = f\frac{\partial \varepsilon_\theta}{\partial z} \tag{3.5}$$

and the current density J (Grant and Phillips, 2008) which is the the amount of polarisation per unit time is given by:

$$J = \frac{\partial P}{\partial t} \tag{3.6}$$

Using the initial cross-sectional area A_0 of the axon and making use of Equation (3.3), the cross-sectional area A of the axon is given by:

$$A = \frac{A_0}{\lambda_z} \tag{3.7}$$

This leads to the induced current I which is the rate of flow of polarisation:

$$I = J \cdot A \tag{3.8}$$

This current can then be added to the electrophysiological model chosen here to follow the dimensionless Aliev-Panfilov equation (Aliev and Panfilov, 1996):

$$\begin{aligned}\frac{\partial v}{\partial t} &= D\frac{\partial^2 v}{\partial z^2} - k_1 v(v-a_1)(v-1) - vr + I \\ \frac{\partial r}{\partial t} &= \left(\epsilon + \frac{\alpha_1 r}{(v+\alpha_2)}\right)(-r - k_2 v(v-b_1-1))\end{aligned} \tag{3.9}$$

where v is the electrical potential, r is the recovery variable, and D is the diffusion coefficient. In addition, k_1, k_2, a_1, b_1, ϵ, α_1, and α_2 are the constant parameters of the model.

3.2 Finite difference method

To implement the model using the explicit finite difference method, the first and second derivatives of a function s with respect to the longitudinal coordinate z, where $s\left(z_j, t^n\right) = s_j^n$, are approximated by (LeVeque, 2007):

$$\frac{\partial s}{\partial z} = \frac{s_{j+1}^n - s_j^n}{\Delta z} \tag{3.10}$$

$$\frac{\partial^2 s}{\partial z^2} = \frac{s_{j+1}^n - 2s_j^n + s_{j-1}^n}{\Delta z^2} \tag{3.11}$$

and the first and second derivatives with respect to the time t are approximated by:

$$\frac{\partial s}{\partial t} = \frac{s_j^{n+1} - s_j^n}{\Delta t} \tag{3.12}$$

$$\frac{\partial^2 s}{\partial t^2} = \frac{s_j^{n+1} - 2s_j^n + s_j^{n-1}}{\Delta t^2} \tag{3.13}$$

Using this method, the wave equation in Equation (3.1) is discretised as:

$$\frac{{\delta_z}_j^{n+1} - 2{\delta_z}_j^{n} + {\delta_z}_j^{n-1}}{\Delta t^2} = c^2 \frac{{\delta_z}_{j+1}^{n} - 2{\delta_z}_j^{n} + {\delta_z}_{j-1}^{n}}{\Delta z^2} \tag{3.14}$$

and the longitudinal displacement δ_z on each node for each time step is updated explicitly with:

$${\delta_z}_j^{n+1} = 2{\delta_z}_j^{n} - {\delta_z}_j^{n-1} + \Delta t^2 c^2 \frac{{\delta_z}_{j+1}^{n} - 2{\delta_z}_j^{n} + {\delta_z}_{j-1}^{n}}{\Delta z^2} \tag{3.15}$$

The Aliev-Panfilov equation (Aliev and Panfilov, 1996) in Equation (3.9) is discretised as:

$$\begin{aligned}
\frac{r_j^{n+1} - r_j^n}{\Delta t} &= \left(\epsilon + \frac{\alpha_1 r_j^n}{(v_j^n + \alpha_1)}\right)\left(-r_j^n - k_2 v_j^n (v_j^n - b_1 - 1)\right) \\
\frac{v_j^{n+1} - v_j^n}{\Delta t} &= D\frac{v_{j+1}^n - 2v_j^n + v_{j-1}^n}{\Delta z^2} - k_1 v_j^n (v_j^n - a_1)(v_j^n - 1) - v_j^n r_j^{n+1} + I_j^n
\end{aligned} \tag{3.16}$$

and the recovery variable r and electrical potential v on each node for each time step are updated by:

$$\begin{aligned}
r_j^{n+1} &= r_j^n + \Delta t \left(\epsilon + \frac{\alpha_1 r_j^n}{(v_j^n + \alpha_1)}\right)\left(-r_j^n - k_2 v_j^n (v_j^n - b_1 - 1)\right) \\
v_j^{n+1} &= v_j^n + \Delta t \left(D\frac{v_{j+1}^n - 2v_j^n + v_{j-1}^n}{\Delta z^2} - k_1 v_j^n (v_j^n - a_1)(v_j^n - 1) - v_j^n r_j^{n+1} + I_j^n\right)
\end{aligned} \tag{3.17}$$

3.3 Fourier pseudospectral method

To implement the model using the Fourier pseudospectral method, the space variable is discretised by expanding the series as a Fourier series in the longitudinal coordinate z (Dehghan and Fakhar-Izadi, 2011):

$$s_j = \sum_{m=-M}^{M-1} h_m e^{i\beta_m z_j} \tag{3.18}$$

where

$$h_m = \frac{1}{2M} \sum_{m=-M}^{M-1} s_j e^{-i\beta_m z_j} \tag{3.19}$$

in which

$$\beta_m = \frac{m\pi}{L} \tag{3.20}$$

and the m frequency sample indices are in bit-reversed order.

The second derivative s_j'' can be written as:

$$s_j'' = -\sum_{m=-M}^{M-1} \beta_m^2 h_m e^{i\beta_m z_j} \tag{3.21}$$

Here, defining $\mathbf{U} = (s_{-M}, ..., s_{M-1})^T$ and $\mathbf{w} = (h_{-M}, ..., h_{M-1})^T$ give:

$$\mathbf{U} = \mathbf{H}^{-1}\mathbf{w} \tag{3.22}$$

$$\mathbf{w} = \mathbf{H}\mathbf{U} \tag{3.23}$$

where $\mathbf{H}$ is the Fourier matrix, and $\mathbf{H}^{-1}$ is the inverse of $\mathbf{H}$, with entries:

$$H_{mj} = \frac{1}{2M} e^{-i\beta_m z_j} \tag{3.24}$$

$$H^{-1}_{jm} = e^{i\beta_m z_j} \tag{3.25}$$

The Fourier matrices $\mathbf{H}^{-1}$ and $\mathbf{H}$ can be given further as a multiplication of sparse matrices. For example, for a case with $2M = 8$, $\mathbf{H}^{-1}$ can be defined as $W^{jm} = \left(e^{i\frac{\pi}{L}\Delta z}\right)^{jm} = e^{i\beta_m z_j}$, and the sparse matrices can be written as shown in Equation (3.28), where "$\cdot$" in the matrices means 0. For $2M = 2^g$, the factorisation involves g matrices of size $2M \times 2M$, each with two non-zero entries in each row.

For s''_j in matrix notation, it is defined that:

$$\mathbf{E} = -diag(\beta^2_{-M}, ..., \beta^2_{M-1}) \tag{3.26}$$

giving

$$\mathbf{U}'' = \mathbf{H}^{-1}\mathbf{E}\mathbf{H}\mathbf{U} \tag{3.27}$$

$$\mathbf{H}^{-1} = \begin{bmatrix} 1 & \cdot & \cdot & \cdot & W^{-4} & \cdot & \cdot & \cdot \\ \cdot & 1 & \cdot & \cdot & \cdot & W^{-3} & \cdot & \cdot \\ \cdot & \cdot & 1 & \cdot & \cdot & \cdot & W^{-2} & \cdot \\ \cdot & \cdot & \cdot & 1 & \cdot & \cdot & \cdot & W^{-1} \\ 1 & \cdot & \cdot & \cdot & W^{0} & \cdot & \cdot & \cdot \\ \cdot & 1 & \cdot & \cdot & \cdot & W^{1} & \cdot & \cdot \\ \cdot & \cdot & 1 & \cdot & \cdot & \cdot & W^{2} & \cdot \\ \cdot & \cdot & \cdot & 1 & \cdot & \cdot & \cdot & W^{3} \end{bmatrix} \cdot \begin{bmatrix} 1 & \cdot & W^{-4} & \cdot & \cdot & \cdot & \cdot & \cdot \\ \cdot & 1 & \cdot & W^{-2} & \cdot & \cdot & \cdot & \cdot \\ 1 & \cdot & W^{0} & \cdot & \cdot & \cdot & \cdot & \cdot \\ \cdot & 1 & \cdot & W^{2} & \cdot & \cdot & \cdot & \cdot \\ \cdot & \cdot & \cdot & \cdot & 1 & \cdot & W^{-4} & \cdot \\ \cdot & \cdot & \cdot & \cdot & \cdot & 1 & \cdot & W^{-2} \\ \cdot & \cdot & \cdot & \cdot & 1 & \cdot & W^{0} & \cdot \\ \cdot & \cdot & \cdot & \cdot & \cdot & 1 & \cdot & W^{2} \end{bmatrix} \cdot \begin{bmatrix} 1 & W^{-4} & \cdot & \cdot & \cdot & \cdot & \cdot & \cdot \\ 1 & W^{0} & \cdot & \cdot & \cdot & \cdot & \cdot & \cdot \\ \cdot & \cdot & 1 & W^{-4} & \cdot & \cdot & \cdot & \cdot \\ \cdot & \cdot & 1 & W^{0} & \cdot & \cdot & \cdot & \cdot \\ \cdot & \cdot & \cdot & \cdot & 1 & W^{-4} & \cdot & \cdot \\ \cdot & \cdot & \cdot & \cdot & 1 & W^{0} & \cdot & \cdot \\ \cdot & \cdot & \cdot & \cdot & \cdot & \cdot & 1 & W^{-4} \\ \cdot & \cdot & \cdot & \cdot & \cdot & \cdot & 1 & W^{0} \end{bmatrix} \tag{3.28}$$

When using the Fourier pseudospectral method, the wave equation in Equation (3.1) can be written as (Dehghan and Fakhar-Izadi, 2011):

$$\frac{\partial^2 \mathbf{G}}{\partial t^2} = c^2 \mathbf{H}^{-1}\mathbf{E}\mathbf{H}\mathbf{G} \tag{3.29}$$

where

$$\mathbf{G} = (\delta_{z-M}, ...\delta_{zM-1})^T \tag{3.30}$$

and the displacement δ_z for each time step on all the nodes is updated using the explicit finite difference scheme to solve the temporal second derivative:

$$\mathbf{G}^{n+1} = 2\mathbf{G}^n - \mathbf{G}^{n-1} + \Delta t^2 c^2 \mathbf{H}^{-1}\mathbf{E}\mathbf{H}\mathbf{G}^n \tag{3.31}$$

The Aliev-Panfilov equation (Aliev and Panfilov, 1996) in Equation (3.9) is then written as:

$$\begin{aligned} \frac{\partial r}{\partial t} &= \left(\epsilon + \frac{\alpha_1 r}{(v+\alpha_1)}\right)(-r - k_2 v(v - b_1 - 1)) \\ \frac{\partial \mathbf{V}}{\partial t} &= D\mathbf{H}^{-1}\mathbf{E}\mathbf{H}\mathbf{V} - k_1 \mathbf{V}(\mathbf{V} - a_1)(\mathbf{V} - 1) - \mathbf{V}\mathbf{R} + \mathbf{I} \end{aligned} \tag{3.32}$$

where

$$\mathbf{R} = (r_{-M}, ..., r_{M-1})^T$$

$$\mathbf{V} = (v_{-M}, ..., v_{M-1})^T \tag{3.33}$$

$$\mathbf{I} = (I_{-M}, ..., I_{M-1})^T \tag{3.34}$$

Each time step on all the nodes can be updated using the explicit temporal derivative by:

$$r_j^{n+1} = r_j^n + \Delta t \left(\epsilon + \frac{\alpha_1 r_j^n}{(v_j^n + \alpha_1)}\right)\left(-r_j^n - k_2 v_j^n (v_j^n - b_1 - 1)\right)$$
$$\mathbf{V}^{n+1} = \mathbf{V}^n + \Delta t \left(D\mathbf{H}^{-1}\mathbf{E}\mathbf{H}\mathbf{V} - k_1\mathbf{K}^2\mathbf{V}^n + (1+a_1)k_1\mathbf{K}\mathbf{V}^n - k_1 a_1 \mathbf{R}^{n+1}\mathbf{V}^n + \mathbf{I}^n\right) \tag{3.35}$$

where

$$\mathbf{K} = diag(v_{-M}, ..., v_{M-1}) \tag{3.36}$$

Overall, the Aliev-Panfilov model is a two-variable model with a fast electric potential v and a recovery variable r. The recovery variable r summarises the concentration of all ionic currents in one single phenomenological variable. To account for the propagating nature of excitation waves, a phenomenological diffusion term is introduced for the electric potential v, while the recovery variable r is assumed to be strictly local (Kotikanyadanam et al., 2010). Current I is generated from the applied displacement δz on the axon through the direct flexoelectric effect, and is the term added to the Aliev-Panfilov model to induce the electric potential v.

3.4 Results and discussion

As discussed above, the H-H model of action potential (Hodgkin and Huxley, 1952) is limited in its description of a nerve impulse. It does not include the mechanical and thermodynamic aspects associated with nerve impulses (Mueller and Tyler, 2014; Appali et al., 2012). Therefore, many theories and hypotheses have been proposed to take account of this non-electrical phenomena. However, it is

still currently a great challenge to incorporate all of these observed phenomena in one theory. For example, the soliton theory (Heimburg and Jackson, 2005), in principle, is able to account for the thermodynamics of nerve impulses, but it cannot explain the role of voltage-gated ion channel proteins in nerve impulse generation and propagation phenomenologically captured by the H-H model (Hodgkin and Huxley, 1952).

Here, a dimensionless 1D electromechanical coupled axonal model has been developed with the purpose to establish a framework whereby current influx occur through deformation gradient rate. In particular, and a prelude to the upcoming chapter, a view is taken that membrane movement creates current in a fashion akin to flexoelectricity. Whether or not Petrov's underlying theory (Petrov, 2006) is exactly the mechanism occurring, the approach assumes that phenomenologically, Equations (3.6), (3.7) and (3.8) do apply to the axonal system, while potentially lumping together more than one mechanism. Doing so, the model can take account of the coupling between the mechanical aspect of a nerve impulse, and the role of the voltage-gated ion channel proteins in the generation of an action potential.

The 1D axonal model was calibrated so that the action potential would roughly have a resting state of -80 mV and a depolarised state of 20 mV (Aliev and Panfilov, 1996). Here, the FHN parameters used were a=0.05, b=35, k_1=10, k_2=52, ϵ=0.02, μ_1=0.1, μ_2=0.3, and D=0.1e-5. The FHN parameters have been chosen arbitrarily. A sinusoidal displacement with a peak value of 0.5 μm was applied to one end of the axon.

The model was numerically implemented in two ways: with the explicit finite difference method and with the Fourier pseudospectral method. The results of the implementations on the electromechanical coupling for a specific axon length are

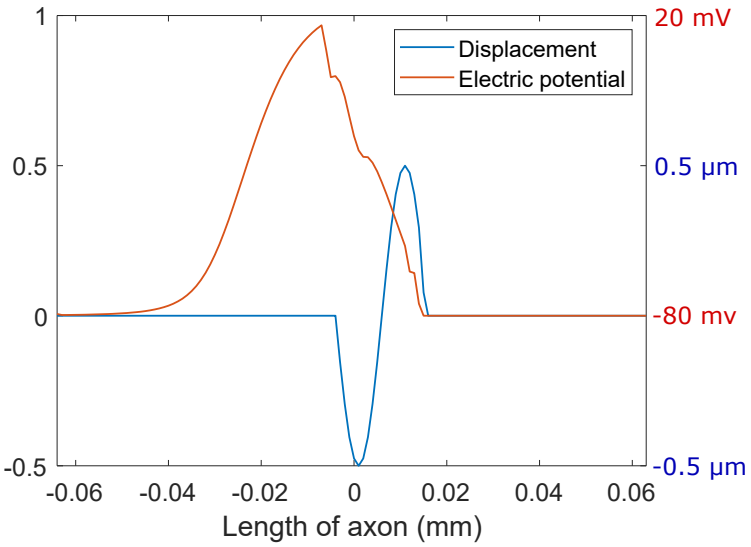


Figure 3.2: Finite difference method.

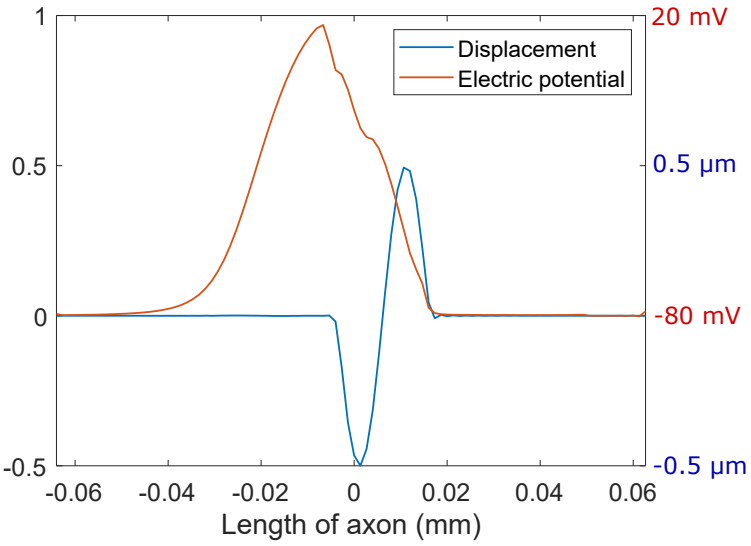


Figure 3.3: Fourier pseudospectral method.

given in Figure 3.2 for the explicit finite difference method and Figure 3.3 for the Fourier pseudospectral method. In both figures, the mechanical stimulus, e.g., the displacement is represented by the blue line while the induced action potential is illustrated in red. Both Figures 3.2 and 3.3 give almost identical results. The increase in electrical potential up to the value of 1 (corresponding to 20 mV) from the resting state with a value of 0 (corresponding to -80 mV) refers to the depolarisation phase of action potential. This is followed by a decrease in electrical potential referring to the repolarisation phase which then goes back to the resting state with a value of 0 (corresponding to -80 mV). Note however, that for simplification, the Aliev-Panfilov model which simulates the cardiac action potential was used here. This is why the action potential shown in Figures 3.2 and 3.3 do not show the undershoot typically observed in neuronal action potentials.

The displacement change along the length of the axon (with a peak value of 0.5 corresponding to 0.5 μm) has caused the axon to bulge, creating a mechanical strain gradient, which induces an electric polarisation through the direct flexoelectric effect, in turn triggering an action potential. The Fourier pseudospectral method is a more advantageous numerical method than the explicit finite difference method because for much larger simulations, it is able to perform faster computations. It can also be particularly convenient to use for time domain modelling of high-frequency waves, which can become cumbersome and slow when using other numerical methods such as finite difference method and/or finite element method (Demi et al., 2014).

A 1D membrane model for neuronal axons has previously been developed by Chen et al. (2019) to study the electromechanical coupling phenomenon in neuronal membranes with an application to TUS. The membrane model assumes that the axon is a revolution solid with an isotropic, homogeneous and axisymmetric membrane with a thin wall of constant thickness. Here, the proposed model

assumes the axon to be a symmetric, incompressible, isotropic and homogeneous cylinder. Furthermore, the membrane model's mechanical pulse is modelled using the beam theory under dynamic loading conditions. In contrast, the axon model's mechanical pulse is an applied longitudinal displacement using the wave equation, which causes the whole axon to bulge. Lastly, the membrane model's electrophysiological pulse is modelled using the H-H theory and cable theory, which is a four-variable model (Postnikov and Titkova, 2016). Whereas, the axonal model uses the Aliev-Panfilov model, which is a simpler two-variable model mainly used for cardiac excitation based on the FHN model for neuronal excitation (Aliev and Panfilov, 1996). Therefore, the action potential shown in Figures 3.2 and 3.3 do not show the typical undershoot characteristic of a neuronal action potential. The Aliev-Panfilov model has been chosen in this instance for simplification and to avoid the cyclic behaviour of the FHN model.

Although the axonal model cannot be directly extended into 2D and 3D and it only captures bulging as the main deformation mechanism, it gives a starting point on how the electromechanical coupling in neurons can be investigated at a macroscale level. In addition, the implementation of the axonal model using the Fourier pseudospectral method proves that the study of the electromechanical coupling phenomenon at the organ scale can be explored using *k*-Wave (Treeby and Cox, 2010).

4 | Theoretical framework

Building on the proof of concept of Chapter 3, this chapter extends the proposed model to 2D and 3D. To this end, a homogenised bulk flexoelectric model focussing on the continuum level formulations of bundles of flexoelectric cylinders is proposed. This provides the coupling between the electrophysiological and mechanical pulses of axonal bundle embedded within the white matter. This approach can be used directly at the macroscale for the description of strain-gradient induced electromechanical coupling without the need to account for the microstructural polarisation. Here, a mechanical pulse modelled using a wave equation from *k*-Wave (Treeby and Cox, 2010) can trigger the induction of an action potential modelled as an electrophysiological pulse using the FHN model (Fitzhugh, 1961). At the cellular level, a membrane deformation affects the action potential according to the direct flexoelectric effect, which in turn influences the membrane potential (Petrov, 2006, 2002). In this work, this effect is scaled up by the establishment of a volumetric polarisation which generates a current that induces the action potential within a tissue.

4.1 Density and orientation of axons

To estimate the density of the fibres or axons within a voxel ρ_a, diffusion tensor imaging (DTI) data can be used to get an approximation of the volume fraction through neurite orientation dispersion and density imaging (NODDI):

$$\rho_a = 1 - \sqrt{\frac{1}{2}\left(\frac{3\overline{\lambda}_h}{d} - 1\right)} \tag{4.1}$$

where d is the intrinsic free diffusivity given as $1.7 \times 10^{-3} \ \ mm^2 s^{-1}$ (Field et al., 2021; Edwards et al., 2017).

The heuristical corrected mean diffusivity, $\overline{\lambda}_h$ is:

$$\overline{\lambda}_h = \lambda + \frac{b}{6}\left(\sum_{i,j=1}^{3} \frac{1+2\delta_{ij}}{15}\lambda_i\lambda_j\right) \tag{4.2}$$

where b is the b-value (a factor that reflects the strength and timing of the gradients used to generate diffusion-weighted images), δ_{ij} is the Kronecker delta function, λ_1, λ_2 and λ_3 are the eigenvalues, and λ is the mean diffusivity given by (Field et al., 2021; Edwards et al., 2017; Soares et al., 2013):

$$\lambda = \frac{\lambda_1 + \lambda_2 + \lambda_3}{3} \tag{4.3}$$

The orientation of axons can be acquired from the principal eigenvector **V1**, which is a measure of the principal direction of diffusion within each voxel:

$$\begin{aligned} V1_1 &= cos\ \psi \\ V1_2 &= cos\ \phi \\ V1_3 &= cos\ \varphi \end{aligned} \tag{4.4}$$

where ψ, ϕ and φ are the angles with respect to the DTI x, y and z-directions, respectively (Minati and Weglarz, 2007).

4.2 Electrophysiological model

As seen in Chapter 3, the pioneering work of Hodgkin and Huxley (Hodgkin and Huxley, 1952) has established that a system of ordinary differential equations coupled to a diffusion equation can phenomenologically represent the conduction of nerve impulses along an axon. Fitzhugh (Fitzhugh, 1961) and Nagumo (Nagumo et al., 1962) proposed a simplified electrophysiological model describing the qualitative behaviour of axons. In the dimensionless FHN model, the action potential propagation in the axon is modelled using the following partial differential equations (Engelbrecht et al., 2018b):

$$\begin{aligned} \frac{\partial v}{\partial t} &= v(v-a_1)(1-v) - r + D_i\left(\frac{\partial^2 v}{\partial x_i^2}\right) + I \\ \frac{\partial r}{\partial t} &= \epsilon(-r + b_1 v) \end{aligned} \tag{4.5}$$

where v is the electrical potential, r is the recovery variable, I is the potential source current, a_1, b_1 and ϵ are constants, $\mathbf{D}$ is the diffusion tensor, t is the time, i is the Cartesian coordinate direction (1,2 in 2D and 1,2,3 in 3D) and x is the spatial dimension.

The FHN model conceptually separates the key mathematical properties of excitation and propagation from the electro-chemical properties of sodium and potassium ion flow defined in the H-H model. First of all, the model has a voltage-like variable with cubic non-linearity giving rise to a regenerative self-excitation through positive feedback (the sodium ion channel contribution). On the other hand, the recovery variable follows a linear dynamics, which gives a slower negative feedback (the potassium ion channel contribution) (Nagumo et al., 1962).

The diffusion tensor $\mathbf{D}$ in Equation (4.5) can be decomposed between the isotropic

and anisotropic contributions (Garcia-Gonzalez and Jérusalem, 2019):

$$\mathbf{D} = D_{iso}\mathbf{I} + D_{ani}\mathbf{A_{axon}} \tag{4.6}$$

where D_{iso} is the isotropic contribution of the material conductivity, D_{ani} is the anisotropic contribution, $\mathbf{I}$ is the identity tensor and $\mathbf{A_{axon}}$ is the axonal structural tensor. When only focussing on the anisotropic contribution of material conductivity, this can be given as (Garcia-Gonzalez and Jérusalem, 2019):

$$\mathbf{D} = D_{ani}\mathbf{A_{axon}} \tag{4.7}$$

To include the dispersion and orientation of axons in each voxel, the axonal structural tensor $\mathbf{A_{axon}}$ (Garcia-Gonzalez and Jérusalem, 2019; Gasser et al., 2006) can be written as:

$$\mathbf{A_{axon}} = \varepsilon\mathbf{I} + (1 - 3\varepsilon)\mathbf{a}_{axon} \otimes \mathbf{a}_{axon} \tag{4.8}$$

where $\mathbf{a}_{axon}$ is the preferred axonal orientation and ε is a single dispersion parameter (Garcia-Gonzalez and Jérusalem, 2019; Wright et al., 2013):

$$\varepsilon = \frac{1}{2}\frac{-6 + 4FA^2 + 2\sqrt{3FA^2 - 2FA^4}}{-9 + 6FA^2} \tag{4.9}$$

The fractional anisotropy FA in Equation (4.9) is a dimensionless representation of the degree of anisotropy in the axon orientation for each voxel from the eigenvalues λ_1, λ_2 and λ_3 (Garcia-Gonzalez and Jérusalem, 2019; Pierpaoli and Basser, 1996):

$$FA = \frac{\sqrt{3[(\lambda_1 - \lambda)^2 + (\lambda_2 - \lambda)^2 + (\lambda_3 - \lambda)^2]}}{\sqrt{2(\lambda_1^2 + \lambda_2^2 + \lambda_3^2)}} \tag{4.10}$$

where the mean diffusivity λ is given in Equation (4.3).

When it is assumed that the axons are ideally coaligned, the axonal tensor $\mathbf{A}_{\mathbf{axon}}$ in Equation (4.8) is given as (Garcia-Gonzalez et al., 2018):

$$\mathbf{A}_{\mathbf{axon}} = \mathbf{a}_{axon} \otimes \mathbf{a}_{axon} \tag{4.11}$$

where ε has a value of 0. The anisotropic unit vector $\mathbf{a}_{axon}$ can be expressed using the two spherical coordinates φ and ψ (Garcia-Gonzalez et al., 2018; Chatelin et al., 2012) (see Figure 4.1):

$$\mathbf{a}_{axon}(\varphi, \psi) = sin\ \varphi\ cos\ \psi\ \mathbf{e}_1 + sin\ \varphi\ sin\ \psi\ \mathbf{e}_2 + cos\ \varphi\ \mathbf{e}_3 \tag{4.12}$$

where $\mathbf{e}_{i=1,2,3}$ denote the Cartesian coordinate basis.

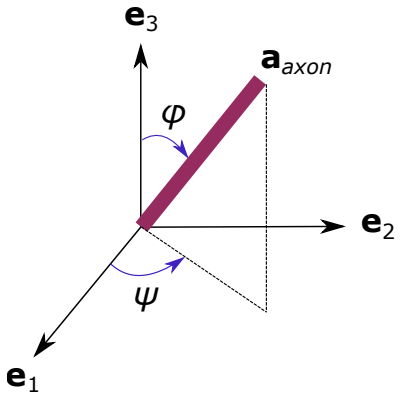


Figure 4.1: The unit fibre orientation vector $\mathbf{a}_{axon}$ using spherical coordinates.

4.3 Mechanical model

For the mechanical model, *k*-Wave (Treeby and Cox, 2010) simulates the ultrasound wave propagation, where a series of coupled first-order partial differential equations based on the conservation of mass, momentum, and energy within a compressible medium is used. For example, if the medium is a homogeneous and lossless fluid, and assumed to be quiescent and isotropic (Pierce, 1998), the first-order equations are:

$$\frac{\partial \mathbf{u}}{\partial t} = -\frac{1}{\rho_0}\nabla p \tag{4.13}$$

$$\frac{\partial \rho}{\partial t} = -\rho_0 \nabla \cdot \mathbf{u} \tag{4.14}$$

$$p = c_0^2 \rho \tag{4.15}$$

where $\mathbf{u}$ is the acoustic velocity, p is the acoustic pressure, ρ is the acoustic density, ρ_0 is ambient density, c_0 is the isentropic sound speed and t is the time. Equation (4.13) represents the conservation of momentum, Equation 4.14 is for the conservation of mass and Equation (4.15) is for the pressure-density relation. These equations can be combined together to give the second-order wave equation:

$$\frac{\partial^2 p}{\partial t^2} = c_0^2 \nabla^2 p \tag{4.16}$$

The first-order equations are used in *k*-Wave since the mass and force sources can be easily included in these equations compared to the second-order wave equation. It can also allow for a special anisotropic layer, called perfectly matched layer (PML) to be used to absorb the waves when they reach the edges of the computational domain (Treeby and Cox, 2010). This counteracts the periodic boundary condition assumed by the Fourier method for infinite domains, where

the waves are reflected back into the medium when reaching the boundaries. Thus, this means that the PML layer prevents the waves from being reflected back into the domain.

4.4 Flexoelectric coupling model

Flexoelectricity is defined as a local change in the electric polarisation of a membrane induced by strain gradient at the cellular scale (Petrov, 2006, 2002):

$$P_i = f_{ijkl}\frac{\partial \varepsilon_{jk}}{\partial x_l} \tag{4.17}$$

where **P** is the membrane polarisation, **f** is the membrane flexoelectricity tensor, $\boldsymbol{\varepsilon}$ is the membrane strain tensor, and $\boldsymbol{x}$ is the spatial coordinate vector. The electric polarisation generates an electrical field within the membrane, i.e., the charges within the molecules get displaced due to the alteration in the electronic distribution and nuclear position, thus producing small electric dipoles within the membrane (Azaroff and Brophy, 1963). From this, the resulting current passing across a patch of membrane of area S can be obtained from **P** by (Chen et al., 2019):

$$dI = \frac{\partial \iint_S \mathbf{P}\cdot\mathbf{n}\, dS}{\partial t} \tag{4.18}$$

where I is the induced current, and **n** is the normal vector to the membrane.

As a direct consequence of flexoelectricity, any deformation mode involving strain gradient, e.g., bending or local bulging, will induce current across the membrane. While the previous chapter and previous work considered localised bulging as the main deformation mechanism (Chen et al., 2019), here ultrasound is assumed to more likely cause local bending on axons. Hence, the focus is on this deformation. Specifically, bending a cylindrical axon would locally stretch the membrane on

one side of the axon and more so on its outer surface than on its inner surface, and the other way around on the diametrically opposed side of the axon. This leads to a current flowing in on one side, and flowing out on the other side, see Figure 4.2-a. When considering a representative volume element (RVE) of brain white matter, the net current contribution of each axon's current can be obtained using Equation (4.18), where, e.g., $S \in \{S_1, S_2, S_3\}$ for each one of the three axons in Figure 4.2.

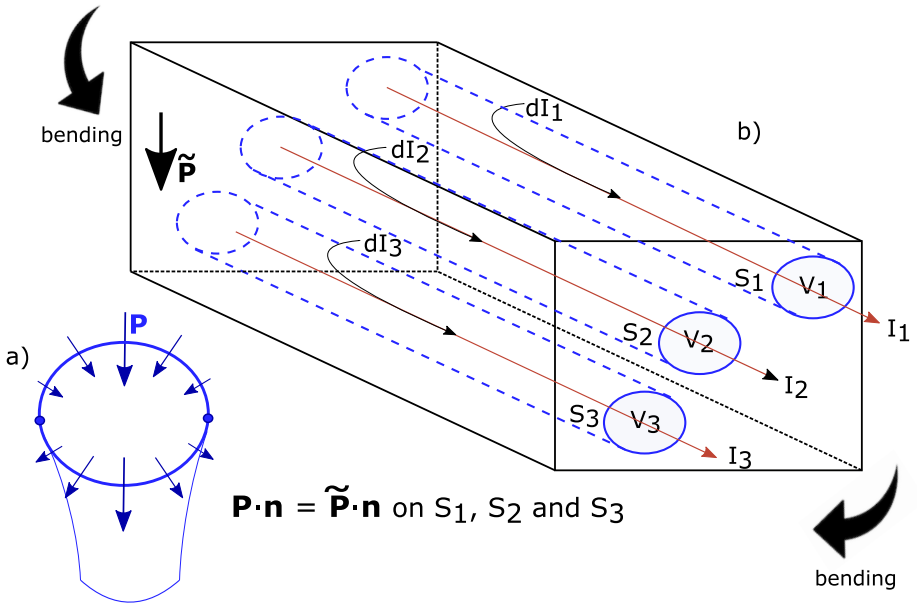


Figure 4.2: Continuum bulk flexoelectricity framework: a) membrane polarisation $\mathbf{P}$ (naturally orthogonal to the membrane) arises from bending of the axons; b) in the bulk, the homogenised bulk polarisation $\tilde{\mathbf{P}}$ is defined at the tissue level (here with three axons of volume V_1, V_2 and V_3 and surface S_1, S_2 and S_3) and coincides with its membrane counterpart when projected orthogonally to the membrane.

Noting that $dI = dI_1 + dI_2 + dI_3$, the total contribution of all three axons in the RVE calculated from all the membrane areas, contributes to a net current flowing in the axonal direction at the RVE level. This contribution can be rewritten as a bulk contribution by using a fictitious volumetric flexoelectric tensor $\tilde{\mathbf{f}}$. This $\tilde{\mathbf{f}}$ is

defined within the bulk of the fibrous tissue such that the current created through polarisation flows in the fibre direction. This however, is not the same as the **f** in Equation (4.17) as **f** is only defined in the membrane to quantify the current flowing through it. A volumetric polarisation $\tilde{\mathbf{P}}$ is defined as:

$$\tilde{P}_i = \tilde{f}_{ijkl} \frac{\partial \varepsilon_{jk}}{\partial x_l} \tag{4.19}$$

where $\boldsymbol{\varepsilon}$ is the strain tensor now defined in the bulk, and such that $\tilde{\mathbf{P}}$ coincides with **P** on the fibres' surface S:

$$\tilde{\mathbf{P}} \cdot \mathbf{n} = \mathbf{P} \cdot \mathbf{n} \text{ on } S \tag{4.20}$$

where, as in Equation (4.18), **n** is the normal vector to the membrane. Combining both equations and making use of the divergence theorem leads to a new definition for the overall current created in the RVE:

$$dI = \frac{\partial \iiint_V \nabla \cdot \tilde{\mathbf{P}} \, dV}{\partial t} \tag{4.21}$$

where V is the volume of all fibres enclosed in S within the RVE. Note that, **P** here is assumed to be defined and perpendicular to **n** at the cross-sections of the fibres on the boundaries of the RVE.

For this formulation, there is no need to explicitly account for the underlying microstructures. It can also be used in any problem involving strain-gradient-induced electrical activity, whether or not flexoelectricity is the mechanism dominating at the microscopic level. This is as long as it is phenomenologically so at the macroscale. Finally, as flexoelectricity is now defined as a bulk property related to the underlying fibre orientation, it is thus dependent on it and can be rotated

through (Le Quang and He, 2011):

$$\tilde{f}_{rmns} = Q_{ri}Q_{mj}Q_{nk}Q_{sl}\tilde{f}_{ijkl} \tag{4.22}$$

where $\tilde{f}_{rmns}$ are the rotated flexoelectric tensor coefficients, $\tilde{f}_{ijkl}$ are the unrotated flexoelectric tensor coefficients and $\mathbf{Q}$ is the rotation matrix.

In 2D, where fibres are parallel to the 2D plane, when the bulk strain coincides with the membrane strain on S, by virtue of Equations (4.17), (4.19) (4.20), and using the fact that:

$$\tilde{\mathbf{f}} = \mathbf{f} \text{ on } S, \tag{4.23}$$

for the whole 2D RVE, $\tilde{\mathbf{f}} = \mathbf{f}$ can be assumed. This is however, not as straightforward in 3D as $\mathbf{f}$ rotates with the curvature along the circular cross-section of the membrane while $\tilde{\mathbf{f}}$ remains fixed within the bulk for a constant fibre orientation. Although, it is assumed here as a first approximation without loss of generality.

4.5 The *k*-space pseudospectral method

Both the mechanical and electrophysiological models can be solved using the Fourier pseudospectral method. For a linear case in the mechanical model, the mass and momentum conservation equations in Equations (4.13) and (4.14) can be written as (Treeby and Cox, 2010):

$$\frac{\partial p^n}{\partial x_i} = \mathscr{F}^{-1}\{jk_i\kappa e^{jk_i\Delta x_i/2}\mathscr{F}\{p^n\}\} \tag{4.24}$$

$$u_i^{n+\frac{1}{2}} = u_i^{n-\frac{1}{2}} - \frac{\Delta t}{\rho_0}\frac{\partial p^n}{\partial x_i} \tag{4.25}$$

$$\frac{\partial u_{x_i}^{n+\frac{1}{2}}}{\partial x_i} = \mathscr{F}^{-1}\{jk_i\kappa e^{-jk_i\Delta x_i/2}\mathscr{F}\{u_i^{n+\frac{1}{2}}\}\} \tag{4.26}$$

$$\rho_i^{n+1} = \rho_i^n - \Delta t\rho_0\frac{\partial u_i^{n+\frac{1}{2}}}{\partial x_i} \tag{4.27}$$

The $\mathscr{F}$ and $\mathscr{F}^{-1}$ are the forward and inverse spatial Fourier transform, i is the Cartesian coordinate direction (1,2 in 2D and 1,2,3 in 3D), j is the unit imaginary number, Δx_i is the grid spacing, Δt is the time increment, n is the time step, and κ is the *k*-space operator, see Equation (4.30). k is the wavenumber in the i direction, and if the number of grid points N_i in the i-direction is even:

$$k_i = \left[-\frac{N_i}{2}, -\frac{N_i}{2}+1, ..., \frac{N_i}{2}-1\right]\frac{2\pi}{\Delta x_i N_i} \tag{4.28}$$

and if N_i is odd,

$$k_i = \left[-\frac{N_i-1}{2}, -\frac{N_i-1}{2}+1, ..., \frac{N_i-1}{2}-1\right]\frac{2\pi}{\Delta x_i N_i} \tag{4.29}$$

The Fourier spectral method spatial gradient evaluations are given in Equations (4.24) and (4.26), while the *k*-space finite difference update steps are given in Equations (4.25) and (4.27), which are repeated for each Cartesian i-direction. The approximation of the temporal derivative using the finite difference method in Equations (4.24) and (4.26) causes errors in the numerical solution. This can be controlled by limiting the size of the time step. But this can be also be relaxed by using the *k*-space method, which allows for larger time steps to be used without

compromising the accuracy of the solution. To do this, the Δt term from the temporal gradient is replaced with $\Delta t\kappa$, where κ is the k-space operator:

$$\kappa = sinc(c_0 k \Delta t/2) \tag{4.30}$$

and can be seen in the rearranged discrete form in Equations (4.24) and (4.26). The *sinc* term provides an exact solution when using larger time steps freeing it from numerical dispersion in linear cases, and can significantly decrease the numerical dispersion in non-linear and heterogeneous cases (Tabei et al., 2002; Cox et al., 2007).

To allow the waves to be absorbed at the edges of the computational domain, an anisotropic PML is used, where Berenger's split-field formulation of the PML (Berenger, 1996) is utilised. This requires the acoustic density to be artificially split into Cartesian components as seen in Equation (4.27). This counteracts the periodicity assumed by the Fourier method for infinite domains. From this, the relationship between the pressure and density is:

$$p^{n+1} = c_0^2(\rho^{n+1}) \tag{4.31}$$

where the total density is given by $\rho^{n+1} = \sum_i \rho_i^{n+1}$.

The exponential terms $e^{\pm jk_i\Delta x_i/2}$ within Equations (4.24) and (4.26) are the spatial shift operators. These translate the result of the gradient calculations by half the grid point spacing in the i-direction allowing the components of the velocity to be evaluated on a staggered grid. The use of staggered spatial and temporal grids provides additional accuracy and stability when computing odd-order derivatives (Fornberg, 1990). The staggered grid scheme is illustrated in Figure 4.3. In addition, the function values at the current and next time points are represented by the

superscripts n and $n+1$, and the function values at the time staggered points are represented by $n-\frac{1}{2}$ and $n+\frac{1}{2}$ (Treeby and Cox, 2010).

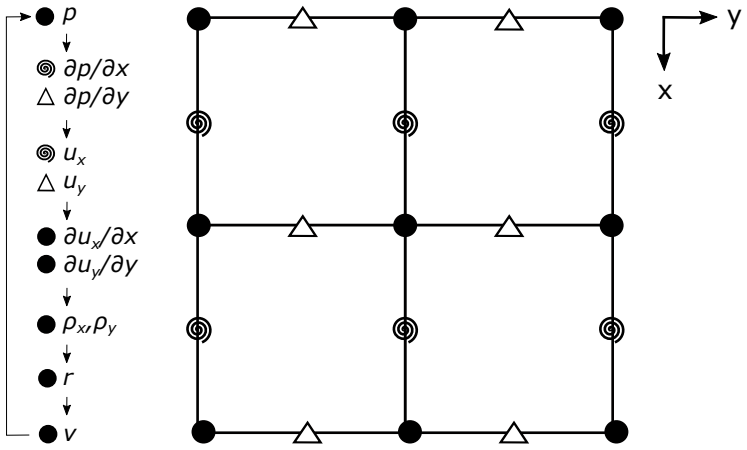


Figure 4.3: Schematic of the staggered grid.

The components of acoustic velocity **u** are integrated to obtain the components of displacement, which are used to calculate the induced current I from the bulk flexoelectric effect in Equation (4.21). Similar to the mechanical model, the FHN model in Equation (4.5) can be written in a discrete form as:

$$\frac{\partial^2 v^n}{\partial x_i^2} = \mathscr{F}^{-1}\{(jk_i)^2 \kappa \mathscr{F}\{v^n\}\} \tag{4.32}$$

$$v^{n+1} = v^n + \Delta t \left(v^n(v^n - a)(1 - v^n) - r^{n+1} + D\frac{\partial^2 v^n}{\partial x_i^2} + I^n \right) \tag{4.33}$$

$$r^{n+1} = r^n + \Delta t \left(\epsilon(-r^n + bv^n)\right) \tag{4.34}$$

4.6 Finite element formulation

The flexoelectric coupling model in Section 4.4 can be discretised using the finite element typical interpolation method (Huebner, 2001). The polarisation gradient in Equation (4.21) is obtained from:

$$\nabla \cdot \tilde{\mathbf{P}} = \nabla \cdot \left(\tilde{\mathbf{f}} \cdot \mathbf{B} \cdot \mathbf{d}^{e} \right) \tag{4.35}$$

where $\mathbf{B}$ is the second derivative shape function matrix and $\mathbf{d}^{e}$ is the displacement vector for a bulk element e. $\mathbf{B}$ is obtained by making use of the first and second order gradient matrices $\mathbf{L}_1$, $\mathbf{L}_2$, respectively, and the shape function matrix $\mathbf{N}$:

$$\mathbf{B} = \mathbf{L}_2 \cdot \mathbf{L}_1 \cdot \mathbf{N} \tag{4.36}$$

4.6.1 2D model

In 2D, here and subsequently, an 8-node elements is considered, see Figure 4.4.

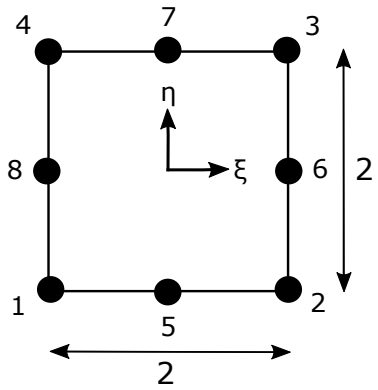


Figure 4.4: 8-node 2D quadrilateral element in the isoparametric reference frame (ξ, η).

The displacement vector $\mathbf{d}^e$ for one element is written as[1]:

$$\mathbf{d}^e = \begin{bmatrix} d_x^1 & d_y^1 & d_x^2 & d_y^2 & d_x^3 & d_y^3 & d_x^4 & d_y^4 & d_x^5 & d_y^5 & d_x^6 & d_y^6 & d_x^7 & d_y^7 & d_x^8 & d_y^8 \end{bmatrix}^T \tag{4.37}$$

The structure of the displacement vector is dependent on the dimension of the model e.g., 2D or 3D, and also on the number of nodes in the element.

Here and subsequently, some intermediary equations are provided in Appendix A and B for convenience. Making use of Equations (A.1), (A.2) and (A.3), $\mathbf{B}$ from Equation (4.36) becomes:

$$\mathbf{B} = \begin{bmatrix} \frac{\partial^2 N_1}{\partial x^2} & 0 & \frac{\partial^2 N_2}{\partial x^2} & 0 & \frac{\partial^2 N_3}{\partial x^2} & 0 & \frac{\partial^2 N_4}{\partial x^2} & 0 & \cdot & \cdot & \frac{\partial^2 N_8}{\partial x^2} & 0 \\ \frac{\partial^2 N_1}{\partial x \partial y} & 0 & \frac{\partial^2 N_2}{\partial x \partial y} & 0 & \frac{\partial^2 N_3}{\partial x \partial y} & 0 & \frac{\partial^2 N_4}{\partial x \partial y} & 0 & \cdot & \cdot & \frac{\partial^2 N_8}{\partial x \partial y} & 0 \\ 0 & \frac{\partial^2 N_1}{\partial x \partial y} & 0 & \frac{\partial^2 N_2}{\partial x \partial y} & 0 & \frac{\partial^2 N_3}{\partial x \partial y} & 0 & \frac{\partial^2 N_4}{\partial x \partial y} & \cdot & \cdot & 0 & \frac{\partial^2 N_8}{\partial x \partial y} \\ 0 & \frac{\partial^2 N_1}{\partial y^2} & 0 & \frac{\partial^2 N_2}{\partial y^2} & 0 & \frac{\partial^2 N_3}{\partial y^2} & 0 & \frac{\partial^2 N_4}{\partial y^2} & \cdot & \cdot & 0 & \frac{\partial^2 N_8}{\partial y^2} \\ \frac{\partial^2 N_1}{\partial x \partial y} & \frac{\partial^2 N_1}{\partial x^2} & \frac{\partial^2 N_2}{\partial x \partial y} & \frac{\partial^2 N_2}{\partial x^2} & \frac{\partial^2 N_3}{\partial x \partial y} & \frac{\partial^2 N_3}{\partial x^2} & \frac{\partial^2 N_4}{\partial x \partial y} & \frac{\partial^2 N_4}{\partial x^2} & \cdot & \cdot & \frac{\partial^2 N_8}{\partial x \partial y} & \frac{\partial^2 N_8}{\partial x^2} \\ \frac{\partial^2 N_1}{\partial y^2} & \frac{\partial^2 N_1}{\partial x \partial y} & \frac{\partial^2 N_2}{\partial y^2} & \frac{\partial^2 N_2}{\partial x \partial y} & \frac{\partial^2 N_3}{\partial y^2} & \frac{\partial^2 N_3}{\partial x \partial y} & \frac{\partial^2 N_4}{\partial y^2} & \frac{\partial^2 N_4}{\partial x \partial y} & \cdot & \cdot & \frac{\partial^2 N_8}{\partial y^2} & \frac{\partial^2 N_8}{\partial x \partial y} \end{bmatrix} \tag{4.38}$$

Similar to the displacement vector, the structure of $\mathbf{B}$ depends on the dimension of the model e.g., 2D or 3D, and the number of nodes in the element.

The transversely isotropic volumetric flexoelectric tensor $\tilde{\mathbf{f}}^T$ is following the same notation as its surface counterpart (Shu et al., 2011):

$$\tilde{\mathbf{f}}^T = \begin{bmatrix} \tilde{f}_{1111} & 0 & \tilde{f}_{1221} & 0 & 0 & \tilde{f}_{1122} \\ 0 & \tilde{f}_{2112} & 0 & \tilde{f}_{2222} & \tilde{f}_{2121} & 0 \end{bmatrix} \tag{4.39}$$

[1] In the following, the notation for the coordinate system (x_1, x_2, x_3) used earlier is replaced by (x, y, z) for convenience.

or, by a virtue of symmetry (Eliseev and Morozovska, 2018; Le Quang and He, 2011):

$$\tilde{\mathbf{f}}^T = \begin{bmatrix} \tilde{f}_{11} & 0 & \tilde{f}_{55} & 0 & 0 & \tilde{f}_{55} \\ 0 & \tilde{f}_{44} & 0 & \tilde{f}_{22} & \tilde{f}_{44} & 0 \end{bmatrix} \tag{4.40}$$

where $\tilde{f}_{11} = \tilde{f}_{1111}$, $\tilde{f}_{22} = \tilde{f}_{2222}$, $\tilde{f}_{44} = \tilde{f}_{2112} = \tilde{f}_{2121}$ and $\tilde{f}_{55} = \tilde{f}_{1221} = \tilde{f}_{1122}$.

Typically, the flexoelectric tensor is presented as a fourth rank tensor. The symmetry of the flexoelectric coefficients however, allows the tensor to be presented in 2×6 matrix form in 2D and 3×18 matrix form in 3D (Shu et al., 2011).

To change the orientation of the fibre using Equation (4.22), the 2D coordinate system rotation matrix used to rotate $\tilde{\mathbf{f}}^T$ through a clockwise angle ϑ is:

$$\mathbf{Q} = \begin{bmatrix} cos\ \vartheta & -sin\ \vartheta \\ sin\ \vartheta & cos\ \vartheta \end{bmatrix} \tag{4.41}$$

This rotation gives the resulting $\tilde{\mathbf{f}}$ (Shu et al., 2011):

$$\tilde{\mathbf{f}} = \begin{bmatrix} \tilde{f}_{1111} & \tilde{f}_{1112} & \tilde{f}_{1221} & \tilde{f}_{1222} & \tilde{f}_{1121} & \tilde{f}_{1122} \\ \tilde{f}_{2111} & \tilde{f}_{2112} & \tilde{f}_{2221} & \tilde{f}_{2222} & \tilde{f}_{2121} & \tilde{f}_{2122} \end{bmatrix} \tag{4.42}$$

Note that, while a compact form for the rotated flexoelectric tensor can still be used, the symmetry of Equation (4.40) cannot be assumed and the full compact tensor needs to be considered.

For a quadrilateral element of size $2a \times 2b$, the Jacobian matrix $\mathbf{J}$ between the original reference frame and the isoparametric reference frame, containing the information on the element size and shape is given by:

$$\mathbf{J} = \begin{bmatrix} \frac{\partial x}{\partial \xi} & \frac{\partial y}{\partial \xi} \\ \frac{\partial x}{\partial \eta} & \frac{\partial y}{\partial \eta} \end{bmatrix} = \begin{bmatrix} a & 0 \\ 0 & b \end{bmatrix} \tag{4.43}$$

To obtain the polarisation gradient in Equation (4.21), making use of Equations (4.43), (A.5) and (A.6) leads to Equation (4.46).

The calculation of the induced current dI given by Equation (4.21) is:

$$dI = \frac{\partial \iint \nabla \cdot \tilde{\mathbf{P}} dxdy}{\partial t} = \frac{\partial \iint \nabla \cdot \left(\tilde{\mathbf{f}} \cdot \mathbf{B} \cdot \mathbf{d}^e \right) dxdy}{\partial t} \tag{4.44}$$

The integrand is constant within the element because **B** is constant, so after time discretisation, dI becomes:

$$dI = v_e \rho_a \frac{\nabla \cdot \left(\tilde{\mathbf{f}} \cdot \mathbf{B} \cdot \mathbf{d}^e \right)^{n+1} - \nabla \cdot \left(\tilde{\mathbf{f}} \cdot \mathbf{B} \cdot \mathbf{d}^e \right)^{n}}{\Delta t} \tag{4.45}$$

where ρ_a is the density of fibres obtained from Equation (4.1), v_e is the total volume (area in 2D) of the element, and Δt is the time step.

$$
\begin{aligned}
\nabla \cdot \tilde{\mathbf{P}} = \tilde{f}_{1112} \Bigg[& \left(d_x^1\right) \frac{-1}{2a^2b} + \left(d_x^2\right) \frac{-1}{2a^2b} + \left(d_x^3\right) \frac{1}{2a^2b} + \left(d_x^4\right) \frac{1}{2a^2b} + \left(d_x^5\right) \frac{1}{a^2b} + \left(d_x^7\right) \frac{-1}{a^2b} \Bigg] + \\
\tilde{f}_{1221} \Bigg[& \left(d_y^1\right) \frac{-1}{2a^2b} + \left(d_y^2\right) \frac{-1}{2a^2b} + \left(d_y^3\right) \frac{1}{2a^2b} + \left(d_y^4\right) \frac{1}{2a^2b} + \left(d_y^5\right) \frac{1}{a^2b} + \left(d_y^7\right) \frac{-1}{a^2b} \Bigg] + \\
\tilde{f}_{1222} \Bigg[& \left(d_y^1\right) \frac{-1}{2ab^2} + \left(d_y^2\right) \frac{1}{2ab^2} + \left(d_y^3\right) \frac{1}{2ab^2} + \left(d_y^4\right) \frac{-1}{2ab^2} + \left(d_y^6\right) \frac{-1}{ab^2} + \left(d_y^8\right) \frac{1}{ab^2} \Bigg] + \\
\tilde{f}_{1121} \Bigg[& \left(d_x^1\right) \frac{-1}{2a^2b} + \left(d_x^2\right) \frac{-1}{2a^2b} + \left(d_x^3\right) \frac{1}{2a^2b} + \left(d_x^4\right) \frac{1}{2a^2b} + \left(d_x^5\right) \frac{1}{a^2b} + \left(d_x^7\right) \frac{-1}{a^2b} \Bigg] + \\
\tilde{f}_{1122} \Bigg[& \left(d_x^1\right) \frac{-1}{2ab^2} + \left(d_y^1\right) \frac{-1}{2a^2b} + \left(d_x^2\right) \frac{1}{2ab^2} + \left(d_y^2\right) \frac{-1}{2a^2b} + \left(d_x^3\right) \frac{1}{2ab^2} + \left(d_y^3\right) \frac{1}{2a^2b} + \\
& \left(d_x^4\right) \frac{-1}{2ab^2} + \left(d_y^4\right) \frac{1}{2a^2b} + \left(d_y^5\right) \frac{1}{a^2b} + \left(d_x^6\right) \frac{-1}{ab^2} + \left(d_y^7\right) \frac{-1}{a^2b} + \left(d_x^8\right) \frac{1}{ab^2} \Bigg] + \\
\tilde{f}_{2111} \Bigg[& \left(d_x^1\right) \frac{-1}{2a^2b} + \left(d_x^2\right) \frac{-1}{2a^2b} + \left(d_x^3\right) \frac{1}{2a^2b} + \left(d_x^4\right) \frac{1}{2a^2b} \left(d_x^5\right) \frac{1}{a^2b} + \left(d_x^7\right) \frac{-1}{a^2b} \Bigg] + \\
\tilde{f}_{2112} \Bigg[& \left(d_x^1\right) \frac{-1}{2ab^2} + \left(d_x^2\right) \frac{1}{2ab^2} + \left(d_x^3\right) \frac{1}{2ab^2} + \left(d_x^4\right) \frac{-1}{2ab^2} + \left(d_x^6\right) \frac{-1}{ab^2} + \left(d_x^8\right) \frac{1}{ab^2} \Bigg] + \\
\tilde{f}_{2221} \Bigg[& \left(d_y^1\right) \frac{-1}{2ab^2} + \left(d_y^2\right) \frac{1}{2ab^2} + \left(d_y^3\right) \frac{1}{2ab^2} + \left(d_y^4\right) \frac{-1}{2ab^2} + \left(d_y^6\right) \frac{-1}{ab^2} + \left(d_y^8\right) \frac{1}{ab^2} \Bigg] + \\
\tilde{f}_{2121} \Bigg[& \left(d_x^1\right) \frac{-1}{2ab^2} + \left(d_y^1\right) \frac{-1}{2a^2b} + \left(d_x^2\right) \frac{1}{2ab^2} + \left(d_y^2\right) \frac{-1}{2a^2b} + \left(d_x^3\right) \frac{1}{2ab^2} + \left(d_y^3\right) \frac{1}{2a^2b} + \\
& \left(d_x^4\right) \frac{-1}{2ab^2} + \left(d_y^4\right) \frac{1}{2a^2b} + \left(d_y^5\right) \frac{1}{a^2b} + \left(d_x^6\right) \frac{-1}{ab^2} + \left(d_y^7\right) \frac{-1}{a^2b} + \left(d_x^8\right) \frac{1}{ab^2} \Bigg] + \\
\tilde{f}_{2122} \Bigg[& \left(d_y^1\right) \frac{-1}{2ab^2} + \left(d_y^2\right) \frac{1}{2ab^2} + \left(d_y^3\right) \frac{1}{2ab^2} + \left(d_y^4\right) \frac{-1}{2ab^2} + \left(d_y^6\right) \frac{-1}{ab^2} + \left(d_y^8\right) \frac{1}{ab^2} \Bigg]
\end{aligned}
\tag{4.46}
$$

4.6.2 3D model

For the 3D model, 20-node brick elements are considered, see Figure 4.5.

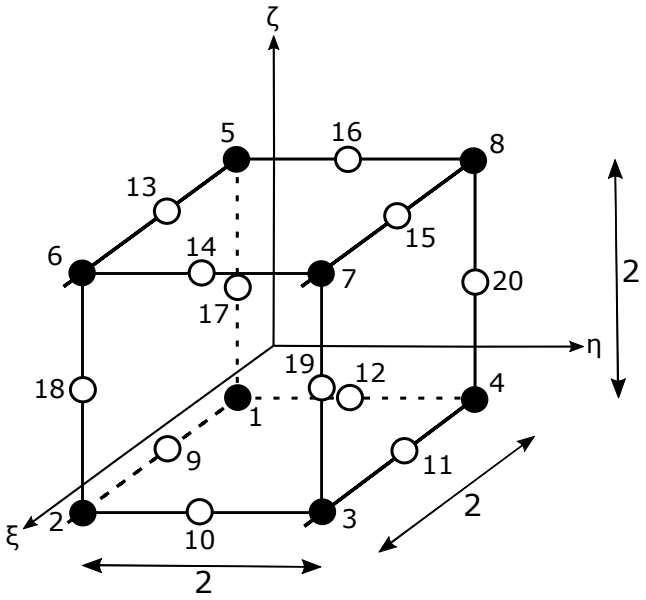


Figure 4.5: 20-node 3D brick element in the isoparametric reference frame (ξ, η, ζ).

The displacement vector $\mathbf{d}^e$ can be written as:

$$\mathbf{d}^e = \begin{bmatrix} d_x^1 & d_y^1 & d_z^1 & d_x^2 & d_y^2 & d_z^2 & d_x^3 & d_y^3 & d_z^3 & \cdot & \cdot & \cdot & d_x^{20} & d_y^{20} & d_z^{20} \end{bmatrix}^T \quad (4.47)$$

Making use of Equations (B.1), (B.2) and (B.3), **B** in Equation (4.36) becomes:

$$\mathbf{B} = \begin{bmatrix}
\frac{\partial^2 N_1}{\partial x^2} & 0 & 0 & \frac{\partial^2 N_2}{\partial x^2} & 0 & 0 & \cdots & \frac{\partial^2 N_{20}}{\partial x^2} & 0 & 0 \\
\frac{\partial^2 N_1}{\partial x \partial y} & 0 & 0 & \frac{\partial^2 N_2}{\partial x \partial y} & 0 & 0 & \cdots & \frac{\partial^2 N_{20}}{\partial x \partial y} & 0 & 0 \\
\frac{\partial^2 N_1}{\partial x \partial z} & 0 & 0 & \frac{\partial^2 N_2}{\partial x \partial z} & 0 & 0 & \cdots & \frac{\partial^2 N_{20}}{\partial x \partial z} & 0 & 0 \\
0 & \frac{\partial^2 N_1}{\partial x \partial y} & 0 & 0 & \frac{\partial^2 N_2}{\partial x \partial y} & 0 & \cdots & 0 & \frac{\partial^2 N_{20}}{\partial x \partial y} & 0 \\
0 & \frac{\partial^2 N_1}{\partial y^2} & 0 & 0 & \frac{\partial^2 N_2}{\partial y^2} & 0 & \cdots & 0 & \frac{\partial^2 N_{20}}{\partial y^2} & 0 \\
0 & \frac{\partial^2 N_1}{\partial y \partial z} & 0 & 0 & \frac{\partial^2 N_2}{\partial y \partial z} & 0 & \cdots & 0 & \frac{\partial^2 N_{20}}{\partial y \partial z} & 0 \\
0 & 0 & \frac{\partial^2 N_1}{\partial x \partial z} & 0 & 0 & \frac{\partial^2 N_2}{\partial x \partial z} & \cdots & 0 & 0 & \frac{\partial^2 N_{20}}{\partial x \partial z} \\
0 & 0 & \frac{\partial^2 N_1}{\partial y \partial z} & 0 & 0 & \frac{\partial^2 N_2}{\partial y \partial z} & \cdots & 0 & 0 & \frac{\partial^2 N_{20}}{\partial y \partial z} \\
0 & 0 & \frac{\partial^2 N_1}{\partial z^2} & 0 & 0 & \frac{\partial^2 N_2}{\partial z^2} & \cdots & 0 & 0 & \frac{\partial^2 N_{20}}{\partial z^2} \\
\frac{\partial^2 N_1}{\partial x \partial y} & \frac{\partial^2 N_1}{\partial x^2} & 0 & \frac{\partial^2 N_2}{\partial x \partial y} & \frac{\partial^2 N_2}{\partial x^2} & 0 & \cdots & \frac{\partial^2 N_{20}}{\partial x \partial y} & \frac{\partial^2 N_{20}}{\partial x^2} & 0 \\
\frac{\partial^2 N_1}{\partial y^2} & \frac{\partial^2 N_1}{\partial x \partial y} & 0 & \frac{\partial^2 N_2}{\partial y^2} & \frac{\partial^2 N_2}{\partial x \partial y} & 0 & \cdots & \frac{\partial^2 N_{20}}{\partial y^2} & \frac{\partial^2 N_{20}}{\partial x \partial y} & 0 \\
\frac{\partial^2 N_1}{\partial y \partial z} & \frac{\partial^2 N_1}{\partial x \partial z} & 0 & \frac{\partial^2 N_2}{\partial y \partial z} & \frac{\partial^2 N_2}{\partial x \partial z} & 0 & \cdots & \frac{\partial^2 N_{20}}{\partial y \partial z} & \frac{\partial^2 N_{20}}{\partial x \partial z} & 0 \\
\frac{\partial^2 N_1}{\partial x \partial z} & 0 & \frac{\partial^2 N_1}{\partial x^2} & \frac{\partial^2 N_2}{\partial x \partial z} & 0 & \frac{\partial^2 N_2}{\partial x^2} & \cdots & \frac{\partial^2 N_{20}}{\partial x \partial z} & 0 & \frac{\partial^2 N_{20}}{\partial x^2} \\
\frac{\partial^2 N_1}{\partial y \partial z} & 0 & \frac{\partial^2 N_1}{\partial x \partial y} & \frac{\partial^2 N_2}{\partial y \partial z} & 0 & \frac{\partial^2 N_2}{\partial x \partial y} & \cdots & \frac{\partial^2 N_{20}}{\partial y \partial z} & 0 & \frac{\partial^2 N_{20}}{\partial x \partial y} \\
\frac{\partial^2 N_1}{\partial z^2} & 0 & \frac{\partial^2 N_1}{\partial x \partial z} & \frac{\partial^2 N_2}{\partial z^2} & 0 & \frac{\partial^2 N_2}{\partial x \partial z} & \cdots & \frac{\partial^2 N_{20}}{\partial z^2} & 0 & \frac{\partial^2 N_{20}}{\partial x \partial z} \\
0 & \frac{\partial^2 N_1}{\partial x \partial z} & \frac{\partial^2 N_1}{\partial x \partial y} & 0 & \frac{\partial^2 N_2}{\partial x \partial z} & \frac{\partial^2 N_2}{\partial x \partial y} & \cdots & 0 & \frac{\partial^2 N_{20}}{\partial x \partial z} & \frac{\partial^2 N_{20}}{\partial x \partial y} \\
0 & \frac{\partial^2 N_1}{\partial y \partial z} & \frac{\partial^2 N_1}{\partial y^2} & 0 & \frac{\partial^2 N_2}{\partial y \partial z} & \frac{\partial^2 N_2}{\partial y^2} & \cdots & 0 & \frac{\partial^2 N_{20}}{\partial y \partial z} & \frac{\partial^2 N_{20}}{\partial y^2} \\
0 & \frac{\partial^2 N_1}{\partial z^2} & \frac{\partial^2 N_1}{\partial y \partial z} & 0 & \frac{\partial^2 N_2}{\partial z^2} & \frac{\partial^2 N_2}{\partial y \partial z} & \cdots & 0 & \frac{\partial^2 N_{20}}{\partial z^2} & \frac{\partial^2 N_{20}}{\partial y \partial z}
\end{bmatrix} \tag{4.48}$$

Similarly to the 2D case, the transversely isotropic volumetric flexoelectric tensor is given by (Shu et al., 2011):

$$\tilde{\mathbf{f}}^T = \begin{bmatrix} \tilde{f}_{1111} & 0 & 0 & \tilde{f}_{1221} & 0 & 0 & \tilde{f}_{1331} & 0 & 0 \\ 0 & \tilde{f}_{2112} & 0 & 0 & \tilde{f}_{2222} & 0 & 0 & \tilde{f}_{2332} & 0 \\ 0 & 0 & \tilde{f}_{3113} & 0 & 0 & \tilde{f}_{3223} & 0 & 0 & \tilde{f}_{3333} \end{bmatrix}$$
$$\begin{bmatrix} 0 & \tilde{f}_{1122} & 0 & 0 & 0 & \tilde{f}_{1133} & 0 & 0 & 0 \\ \tilde{f}_{2121} & 0 & 0 & 0 & 0 & 0 & 0 & 0 & \tilde{f}_{2233} \\ 0 & 0 & 0 & \tilde{f}_{3131} & 0 & 0 & 0 & \tilde{f}_{3232} & 0 \end{bmatrix} \tag{4.49}$$

or

$$\tilde{\mathbf{f}}^T = \begin{bmatrix} \tilde{f}_{11} & 0 & 0 & \tilde{f}_{55} & 0 & 0 & \tilde{f}_{55} & 0 & 0 & 0 & \tilde{f}_{55} & 0 & 0 & 0 & \tilde{f}_{55} & 0 & 0 & 0 \\ 0 & \tilde{f}_{44} & 0 & 0 & \tilde{f}_{22} & 0 & 0 & \tilde{f}_{33} & 0 & \tilde{f}_{44} & 0 & 0 & 0 & 0 & 0 & 0 & 0 & \tilde{f}_{33} \\ 0 & 0 & \tilde{f}_{44} & 0 & 0 & \tilde{f}_{33} & 0 & 0 & \tilde{f}_{22} & 0 & 0 & 0 & \tilde{f}_{44} & 0 & 0 & 0 & \tilde{f}_{33} & 0 \end{bmatrix} \tag{4.50}$$

where $\tilde{f}_{11} = \tilde{f}_{1111}$, $\tilde{f}_{22} = \tilde{f}_{2222} = \tilde{f}_{3333}$, $\tilde{f}_{33} = \tilde{f}_{2233} = \tilde{f}_{2332} = \tilde{f}_{3223} = \tilde{f}_{3232}$, $\tilde{f}_{44} = \tilde{f}_{2121} = \tilde{f}_{2112} = \tilde{f}_{3131} = \tilde{f}_{3113}$ and $\tilde{f}_{55} = \tilde{f}_{1122} = \tilde{f}_{1221} = \tilde{f}_{1133} = \tilde{f}_{1331}$ (Eliseev and Morozovska, 2018), with the equivalent symmetries to the 2D case.

To change the orientation of the fibre using Equation (4.22), a combination of 3D coordinate system rotation matrices is used to rotate $\tilde{\mathbf{f}}^T$ through a clockwise direction where:

$$\mathbf{Q} = \mathbf{R}_{y'} \cdot \mathbf{R}_z \tag{4.51}$$

The fibre is assumed to be originally oriented in the x-direction, rotated around the z-axis by an angle γ, then by β around the y'-axis, which is the y-axis rotated by $\mathbf{R}_z$.

The rotation matrices used are:

$$\mathbf{R}_{y'}(\beta) = \begin{bmatrix} cos\ \beta & 0 & sin\ \beta \\ 0 & 1 & 0 \\ -sin\ \beta & 0 & cos\ \beta \end{bmatrix}$$
$$\mathbf{R}_{z}(\gamma) = \begin{bmatrix} cos\ \gamma & -sin\ \gamma & 0 \\ sin\ \gamma & cos\ \gamma & 0 \\ 0 & 0 & 1 \end{bmatrix} \tag{4.52}$$

This rotation gives the resulting $\tilde{\mathbf{f}}$ (Shu et al., 2011):

$$\tilde{\mathbf{f}} = \begin{bmatrix} \tilde{f}_{1111} & \tilde{f}_{1112} & \tilde{f}_{1113} & \tilde{f}_{1221} & \tilde{f}_{1222} & \tilde{f}_{1223} & \tilde{f}_{1331} & \tilde{f}_{1332} & \tilde{f}_{1333} & \tilde{f}_{1121} & \tilde{f}_{1122} \\ \tilde{f}_{2111} & \tilde{f}_{2112} & \tilde{f}_{2113} & \tilde{f}_{2221} & \tilde{f}_{2222} & \tilde{f}_{2223} & \tilde{f}_{2331} & \tilde{f}_{2332} & \tilde{f}_{2333} & \tilde{f}_{2121} & \tilde{f}_{2122} \\ \tilde{f}_{3111} & \tilde{f}_{3112} & \tilde{f}_{3113} & \tilde{f}_{3221} & \tilde{f}_{3222} & \tilde{f}_{3223} & \tilde{f}_{3331} & \tilde{f}_{3332} & \tilde{f}_{3333} & \tilde{f}_{3121} & \tilde{f}_{3122} \\ & & & & & \tilde{f}_{1123} & \tilde{f}_{1131} & \tilde{f}_{1132} & \tilde{f}_{1133} & \tilde{f}_{1231} & \tilde{f}_{1232} & \tilde{f}_{1233} \\ & & & & & \tilde{f}_{2123} & \tilde{f}_{2131} & \tilde{f}_{2132} & \tilde{f}_{2133} & \tilde{f}_{2231} & \tilde{f}_{2232} & \tilde{f}_{2233} \\ & & & & & \tilde{f}_{3123} & \tilde{f}_{3131} & \tilde{f}_{3132} & \tilde{f}_{3133} & \tilde{f}_{3231} & \tilde{f}_{3232} & \tilde{f}_{3233} \end{bmatrix} \tag{4.53}$$

Again, after rotation, the symmetries of Equation (4.50) will not necessarily apply to the rotated flexoelectric tensor, and a full tensor will need to be considered.

For a brick element of size $2a \times 2b \times 2c$, the Jacobian matrix $\mathbf{J}$ between the original reference frame and the isoparametric reference frame is given by:

$$\mathbf{J} = \begin{bmatrix} \frac{\partial x}{\partial \xi} & \frac{\partial y}{\partial \xi} & \frac{\partial z}{\partial \xi} \\ \frac{\partial x}{\partial \eta} & \frac{\partial y}{\partial \eta} & \frac{\partial z}{\partial \eta} \\ \frac{\partial x}{\partial \zeta} & \frac{\partial y}{\partial \zeta} & \frac{\partial z}{\partial \zeta} \end{bmatrix} = \begin{bmatrix} a & 0 & 0 \\ 0 & b & 0 \\ 0 & 0 & c \end{bmatrix} \tag{4.54}$$

Note that, unlike the 2D case, **B** (see Equation (4.48)) in 3D is not constant within the element but linear in ξ, η and ζ. Therefore, to obtain the polarisation gradient in Equation (4.21), making use of Equations (4.54), (B.5) and (B.6) leads to Equation (B.7).

Assuming a homogeneous axonal distribution within the volume, the value of the integrand in the centre of the element i.e., at (ξ, η, ζ) = (0, 0, 0) can be taken. This changes Equation (B.7) to Equation (B.8).

The calculation of the induced current dI given by Equation (4.21) is:

$$dI = \frac{\partial \iiint \nabla \cdot \tilde{\mathbf{P}} \, dxdydz}{\partial t} = \frac{\partial \iiint \nabla \cdot \left(\tilde{\mathbf{f}} \cdot \mathbf{B} \cdot \mathbf{d}^e \right) dxdydz}{\partial t} \tag{4.55}$$

After time discretisation, dI is given by:

$$dI = v_e \rho_a \frac{\nabla \cdot \left(\tilde{\mathbf{f}} \cdot \mathbf{B} \cdot \mathbf{d}^e \right)_0^{n+1} - \nabla \cdot \left(\tilde{\mathbf{f}} \cdot \mathbf{B} \cdot \mathbf{d}^e \right)_0^{n}}{\Delta t} \tag{4.56}$$

which is similar to the induced current in 2D from Equation (4.45), but where the subscript 0 refers to the value at the centre of the element. Again, Equation (4.1) can be used to give the density of fibres ρ_a within each RVE from the DTI data.

4.7 Summary

In summary, the theoretical framework provides a scalable multi-physics numerical electromechanical coupled model that links TUS to current generation. It is able to capture the electromechanical coupling in neurons at the macroscale level without the need to account for cellular microstructures using continuum level formulations for bulk tissue flexoelectricity. Specifically, the adaption of

the framework in 3D can be used to further examine the effect of TUS on whole brain studies by capturing the activity coupling between a target region and other regions of the brain interconnected with it as discussed in the following Chapter 5.

In addition, the voxel size obtained from the MRI data of subjects such as monkeys or humans can be directly used as the element size in the 2D and 3D models discussed in Sections 4.6.1 and 4.6.2, respectively. This therefore, makes it easier to apply the information from experimental data to the computational model.

This work has the potential to contribute to the advancement of knowledge on the use of ultrasound as a neuromodulation tool as it may be able to help to establish TUS safety protocols by optimising the ultrasound parameters for a given application. This can be used for clinical and experimental applications to aid with the successful treatment of neurological and psychiatric disorders. Furthermore, this approach can be used for different applications in bulk flexoelectricity in biological and non-biological materials to investigate the electromechanical coupling phenomenon.

5 | Implementation and application to TUS

In this chapter, the 2D and 3D implementations of the homogenised bulk flexoelectric model described in Chapter 4 are first detailed. The model is then calibrated against a microscale formulation to ensure multi-scale compatibility. It is leveraged for the study of its application in TUS on a human head model for the illustration of the approach, and on a monkey head model to test against real experimental studies. Finally, a discussion on both sets of results is provided.

5.1 2D human model

This section details the implementation of a 2D human model and its calibration with a membrane model to study the validity of the approach, and provide a proof of concept for TUS application.

5.1.1 Validation

The proposed homogenised model from Section 4.6.1 was validated against a micromechanical model of one $250\ \mu m$-long axon. The micromechanical axonal model is a 2D plane-stress linear elastic single axon discretised with a finite element mesh of quadratic triangular $1\ \mu m$-long elements, see Figure 5.1-a. A sigmoid-shaped displacement load was applied at one end of the axon to avoid spurious oscillations, reaching 0.25 μm at 11.2 μs, and inducing a wave propagation along the axon by locally bending the outer surfaces (lines in 2D) of the axon. The other end of the axon was fixed in the x- and y-direction preventing the end of the axon from moving. The middle of the axon (middle horizontal line) was also fixed in the y-direction to ensure that the outer surfaces deformed symmetrically. While the material properties were chosen arbitrarily to: $E = 4800\ MPa$

for the Young's modulus and $\nu = 0.1$ for the Poisson's ratio, they resemble the literature value, e.g., giving $K = 2\ GPa$ for the bulk modulus (Ganpule et al., 2018). The simulation was run using ABAQUS Explicit (Dassault, 2017), and the x- and y-displacements from all the nodes were extracted and imported into MATLAB (MathWorks, 2017). The rectangular quadratic elements were created by combining each section of four triangular elements into one quadratic rectangular element, see Figure 5.1-b. New displacements values were given to the corresponding nodes by taking an average value for the displacement on the red nodes in Figure 5.1-a with their direct neighbouring nodes to smooth out the inherent noise in the nodal values. The current influx arising from the membrane bending was calculated using the two following methods.

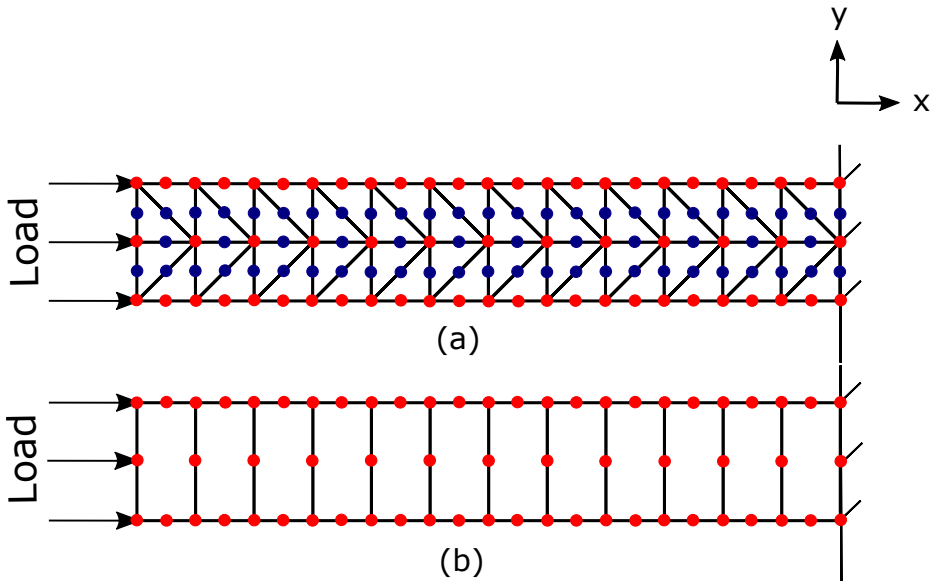


Figure 5.1: (a) 2D Abaqus model of one axon, and (b) 2D MATLAB homogenised model ($250\ \mu m$ length and number of elements in the x-direction not to scale).

The first method used the membrane nodal displacements and calculated the current induced by the membrane flexoelectric effect, e.g., through curvature-induced

membrane polarisation (Petrov, 2002):

$$P = fc_1 \tag{5.1}$$

where c_1 is the curvature of the membrane of the axon and $f = 2 \times 10^{-9}\ C/m$ is the flexoelectric coefficient (Chen et al., 2019).

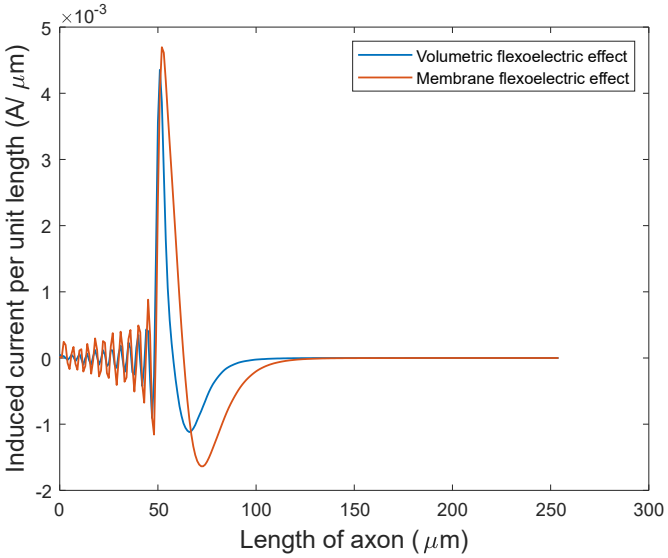


Figure 5.2: Induced current per unit length calculated by membrane flexoelectric effect and the proposed homogenised volumetric flexoelectric effect at 24.5 ns.

The second method used the 2D formulation proposed in Chapter 4.6.1 directly. $\tilde{\mathbf{f}}$ was assumed to be homogeneous throughout the axon ($\rho_a = 1$ corresponding to one axon) with transversely isotropic flexoelectric coefficients $\tilde{f}_{55} = 0\ C/m$, $\tilde{f}_{44} = 2 \times 10^{-9}\ C/m$, $\tilde{f}_{22} = 0\ C/m$ and $\tilde{f}_{11} = 0\ C/m$ (Chen et al., 2019), see Equation (4.39). The induced currents per unit length of both methods are shown at 24.5 ns in Figure 5.2. The discrepancies are attributed to the averaging of the nodes in the volumetric method. The results show that the homogenous model is able to capture and scale up the microscale phenomenon with good accuracy and without the need to track the membrane's displacement independently of the rest

of the axon.

5.1.2 Application to TUS

While flexoelectricity has been suggested as one of the possible mechanisms of TUS, the homogenised bulk flexoelectric model proposed here is aimed at phenomenologically simulating any electrical activity induction arising from time-dependent strain gradient deformation. As seen in Section 5.1.1, it can be calibrated and built from actual micromechanical flexoelectricity although this is not required. The only driving hypothesis is that, *at the organ scale*, it is the minute mechanical vibrations (thus leading to a time-varying gradient of strain in the tissue, i.e., the mechanical trigger of flexoelectricity), and not the mechanical deformation (the mechanical trigger of piezoelectricity), that lead to an electrical activity. A full understanding of the underlying microscopic mechanisms is not needed, as long as this condition is verified at the homogenised macroscale.

A 2D human head model was created from a slice of MRI-informed model in the sagittal plane ($1\ mm \times 1\ mm$ voxel size) proposed previously by Bing et al. (2020). This model is segmented into white matter, grey matter, ventricles, cerebellum, cerebral spinal fluid (CSF), skull, and flesh, which consists of muscle, fat and other tissues, see Figure 5.3. The material properties used here such as sound speed and density were taken from the literature (Hasgall et al., 2021; Mueller et al., 2016; Farrer et al., 2015; Firouzi and Saffari, 2015; Picardo et al., 2011; Tyler, 2011; Culjat et al., 2010; Goss et al., 1978; Mendez and Keys, 1960) and are listed in Table 5.1.

The material properties of each segmented region can vary. This is because each region can be made up of different structures. For example, the flesh includes skin, connective tissue, aponeurosis (intermediate fibrous sheet found over the vertex

Head model material properties		
Materials	Sound speed (m/s)	Density (kg/m^3)
White matter	1600 (Firouzi and Saffari, 2015)	1030 (Mueller et al., 2016; Firouzi and Saffari, 2015; Tyler, 2011)
Grey matter	1550 (Mueller et al., 2016; Firouzi and Saffari, 2015; Tyler, 2011)	1050 (Firouzi and Saffari, 2015)
Ventricles	1515 (Mueller et al., 2016; Goss et al., 1978)	1006 (Mueller et al., 2016)
Cerebellum	1537 (Hasgall et al., 2021)	1030 (Mueller et al., 2016)
CSF	1515 (Mueller et al., 2016; Goss et al., 1978)	1006 (Mueller et al., 2016)
Flesh	1540 (Farrer et al., 2015)	1059 (Culjat et al., 2010; Mendez and Keys, 1960)
Skull	3700 (Goss et al., 1978)	1912 (Mueller et al., 2016; Picardo et al., 2011)

Table 5.1: Sound speed and density of the brain regions included the human head model.

of the skull), loose connective tissue, and periosteum (Ellis, 2007). The skull is a multi-layered structure with a hard cortical shell and a blood- and fat-filled inner cancellous bone layer (Blackmore et al., 2019). The brain stem and cerebullum both include grey and white matter (Fernandez-Gil et al., 2010; Purves et al., 2001). The grey matter includes neuronal cell bodies, dendrites, unmyelinated axons, glial cells, synapses and capillaries. The white matter includes mainly myelinated axons surrounded by myelin sheath (Purves et al., 2001). In this model however, the segmented regions were assumed to have constant sound speed and density. Because of this limitation, the effects of the varying material properties in each segmented region cannot be observed using this head model.

The human head model was loaded into MATLAB (MathWorks, 2017), where a sinusoidal pressure of 250 kHz and 1.17 MPa (Folloni et al., 2019b; Verhagen et al., 2019) was applied to the target brain region using a 64 mm diameter and

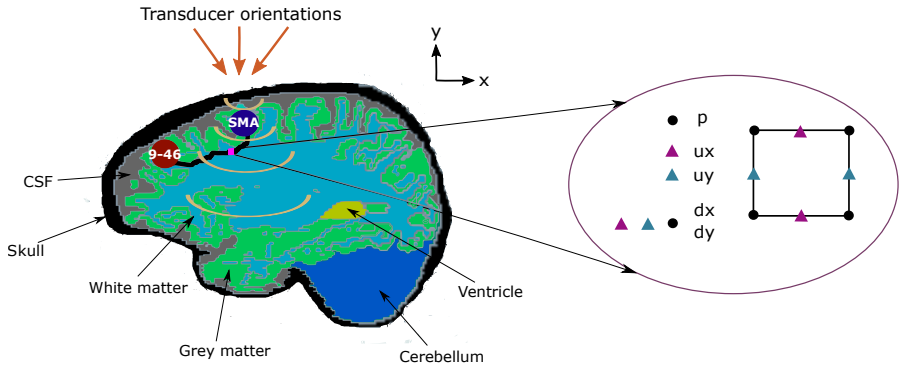


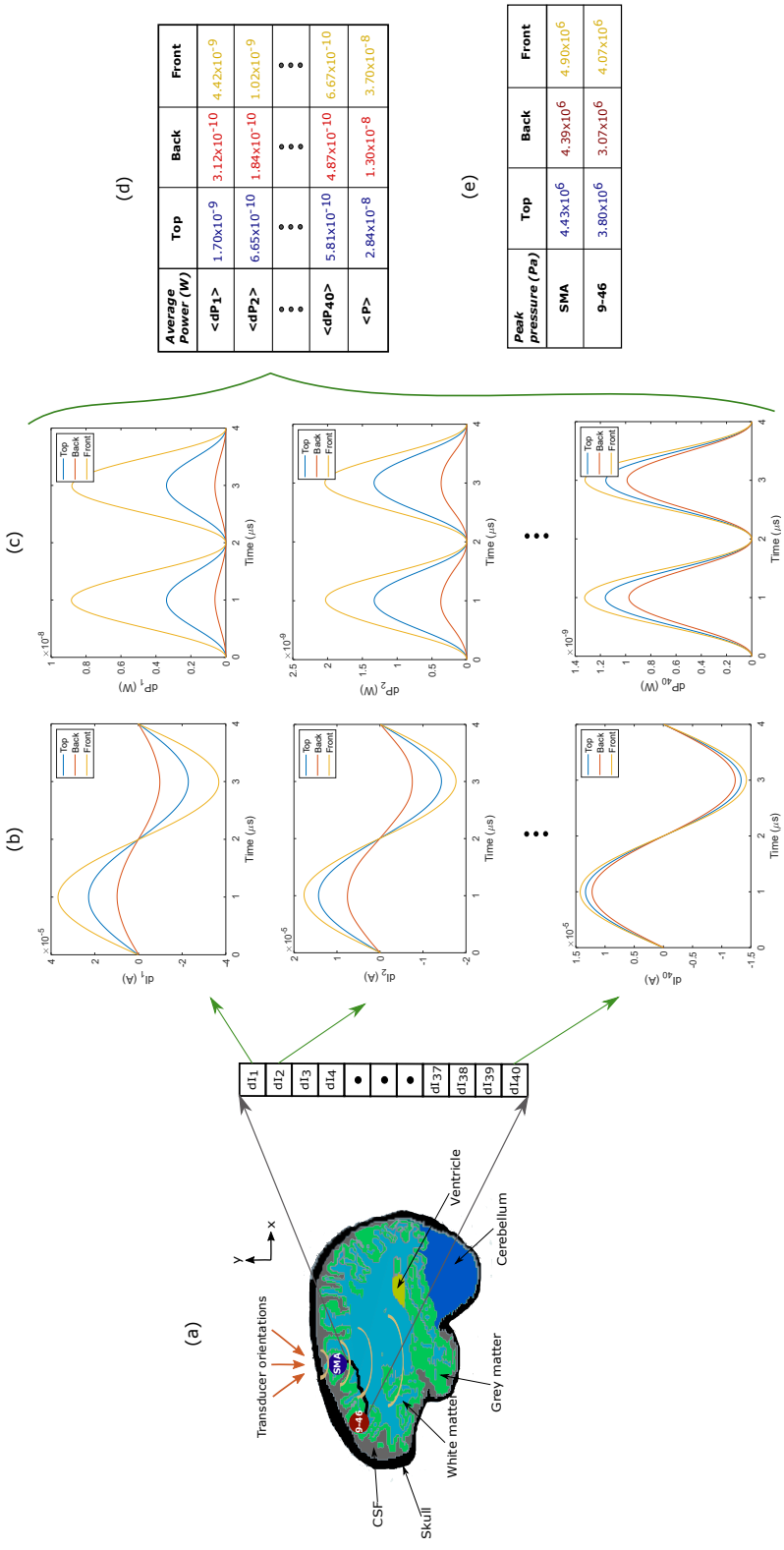
Figure 5.3: TUS in k-Wave with three transducer orientations, and the grid discretisation of the brain (blue and red dots correspond to the supplementary motor area (SMA) and Brodmann area 9-46, respectively; p, ux, uy, dx, dy are the pressure, velocities in x and y and displacements in x- and y-directions.

63 mm radius of curvature transducer for 12 ms. This was enough for a steady state to be reached using *k*-Wave (Treeby and Cox, 2010), see Figure 5.3. A layer of water, mimicking the coupling cone between the skull and the transducer in experiments, was used to ensure that the focus of ultrasound was on the target region. The material properties of water used were 1480 m/s for the sound speed and 1000 kg/m^3 for the density (Mueller et al., 2016). Three transducer orientations were considered: one inclined by 20° leaning towards the front ("Front") thus sending waves towards the back of the head, one sitting directly on top of the head ("Top"), and one inclined by 20° leaning towards the back ("Back") thus sending waves towards the front of the head. The thickness of the water was varied depending on the orientation of the transducer to ensure that the wave focus remain on the target region. This was approximately 42 mm, 40 mm, and 34 mm for the top, front and back transducers, respectively. Note that, in experimental studies on brain TUS, the only transducer position used is the one perpendicular to the skull or head. Any other transducer orientation can cause loss of acoustic coupling and therefore, loss of ultrasound focus from the air or gaps in between the head and water due to the shape of the coupling cone. Here however, an il-

lustrative ideal situation was taken such that all the transducer orientations have full acoustic coupling so that there is full contact between the water and head preventing air-induced loss of coupling in all three cases. The x- and y-velocity values obtained from *k*-Wave were integrated to obtain the displacement values at the nodes. The remaining x- and y-displacements on the staggered grid were obtained by taking the average between neighbouring non-staggered nodes, see Figure 5.3.

Here, supplementary motor area (SMA) TUS was conducted to examine the connection between the SMA, a part of the cerebral cortex that contributes to movement control (Tanji, 1994), and Brodmann area 9-46, an area located in the middle frontal gyrus (Hyder et al., 1997). The *in-silico* exploration of transducer orientation is particularly relevant to study how TUS can affect the current generation within the brain white matter tract between the two regions as different orientations mean different effects on neighbouring tracts. In this study, only one hemisphere was considered, where the tract was created on the left hemisphere by examining the white matter between the two regions on the head model with the help of atlases from FSL (Jenkinson et al., 2012). From this, a white matter tract of 40 voxels from the SMA to Brodmann area 9-46 was obtained, and the effects of transducer orientation was assessed. The density or volume fraction of axons within the tract was given as 0.6 (Easson et al., 2020). This was obtained from the average axonal density estimated through NODDI (Zhang et al., 2012), for the association tracts within the brain of young adults.

In k-Wave, the time increment used for this model was 1×10^{-8} s. The space increments were 1 mm for the x-direction and 1 mm for the y-direction. This matches the voxel size in the MRI structural data of the human head. The flexoelectric coefficients were given as $\tilde{f}_{55} = 0 \quad C/m$, $\tilde{f}_{44} = 2 \times 10^{-9}$ C/m, $\tilde{f}_{22} = 0 \quad C/m$ and $\tilde{f}_{11} = 0 \quad C/m$ (Chen et al., 2019) for the transversely isotropic



Average Power (W)	Top	Back	Front
<dP1>	1.70×10^{-9}	3.12×10^{-10}	4.42×10^{-9}
<dP2>	6.65×10^{-10}	1.84×10^{-10}	1.02×10^{-9}
⋮	⋮	⋮	⋮
<dP40>	5.81×10^{-10}	4.87×10^{-10}	6.67×10^{-10}
<P>	2.84×10^{-8}	1.30×10^{-8}	3.70×10^{-8}

(d)

Peak pressure (Pa)	Top	Back	Front
SMA	4.43×10^{6}	4.39×10^{6}	4.90×10^{6}
9-46	3.80×10^{6}	3.07×10^{6}	4.07×10^{6}

(e)

Figure 5.4: (a) White matter tract between the target region, SMA, and Broadmann area 9-46, (b) induced current for each element within the white matter tract for each transducer configuration after steady state is reached, (c) corresponding induced maximum power, (d) corresponding induced steady state average power, and total generated steady state average power for the whole tract for each transducer position, and (e) the peak pressure in the SMA and Broadmann area 9-46; three transducer configurations: leaning towards the front ("front") sending waves towards the back of the skull, sitting directly on top of the skull ("top"), and leaning towards the back ("back") thus sending waves towards the front of the skull.

flexoelectric tensor, see Equation (4.39). For each transducer configuration, the induced current in each voxel dI was calculated after steady state was reached ($\sim$ 10 ms), see Figure 5.4-b. The power dissipated or "absorbed" by one voxel dP can then be defined as:

$$dP = dI^2 R \tag{5.2}$$

where R is the electrical resistance of the brain white matter within the voxel:

$$R = \frac{\rho_R L}{A} \tag{5.3}$$

$\rho_R = 3.91\ \Omega m$ is the resistivity of white matter (Latikka et al., 2001), L is the length of the bundle of axons within the voxel which corresponds to the length of the element in the x-direction, and A is the cross-sectional area of the bundle of axons within the voxel taking into account their density which is obtained from Equation 4.1.

Noting that $< dI^2 >= \frac{{dI_{peak}}^2}{2}$ where dI_{peak} is the peak value of the sinusoidal induced current, the average power $< dP >$ per cycle for each voxel can be calculated from:

$$< dP > = \frac{{dI_{peak}}^2}{2} R \tag{5.4}$$

and is given for each voxel of the tract in Figure 5.4-c. The total average power $< P >$ was taken by summing the $< dP >$ of all the voxels within the white matter tract as given in Figure 5.4-d. Finally, the predicted peak pressure in the SMA and Broadmann area 9-46 are given in Figure 5.4-e.

5.2 3D macaque monkey model

This details the numerical implementation of the 3D model in *k*-Wave (Treeby and Cox, 2010) to further study the volumetric approach and test it against real TUS experimental studies on macaque monkeys.

A monkey head model was created from a full-head MRI of a healthy female macaque monkey with $0.5 \times 0.5 \times 0.5\ mm$ voxel resolution. The structures of the head were segmented using Amira (Zuse Institute Berlin and Thermo Fisher Scientific, 2019) into white matter, grey matter, brainstem, CSF, cerebellum, and ventricles. The skin, scalp, muscles and eyes were segmented as one material. Similar to the human head model, the sound speed and density of each segmented region in the monkey head model were assumed to be constant. Therefore, the same assumptions and limitations applies to the monkey head model. The material properties of the monkey head model were informed from a range of sources, sometimes involving the use of human data. They are listed in Table 5.2.

Probabilistic tractography (Folloni et al., 2019a) was used to reconstruct the projections or the white matter tracts from the ACC, which was the ultrasound target region, to other regions of interest (ROIs) that the ACC is interconnected with (Folloni et al., 2019b). Assuming that the macaque monkey brain is mostly symmetrical, only the tracts on the left hemisphere of the brain were reconstructed. A seed mask for the ACC was created by selecting a few voxels on the white matter next to the ACC grey matter region. For each of the ROIs, two different masks were created. The first one is the grey matter mask. This was created by selecting the voxels covering the ROI grey matter region. The second one is the white matter mask. This was created by selecting a few voxels in the white matter next to each ROI grey matter region. The seed mask and the white matter masks

Head model material properties		
Materials	Sound speed (m/s)	Density (kg/m^3)
White matter	1600 (Firouzi and Saffari, 2015)	1030 (Mueller et al., 2016; Firouzi and Saffari, 2015; Tyler, 2011)
Grey matter	1550 (Mueller et al., 2016; Firouzi and Saffari, 2015; Tyler, 2011)	1050 (Firouzi and Saffari, 2015)
Ventricles	1515 (Mueller et al., 2016; Goss et al., 1978)	1006 (Mueller et al., 2016)
CSF	1515 (Mueller et al., 2016; Goss et al., 1978)	1006 (Mueller et al., 2016)
Cerebellum	1537 (Hasgall et al., 2021)	1030 (Mueller et al., 2016)
Brain stem	1575	1030 (Mueller et al., 2016)
Skull	3700 (Goss et al., 1978)	1912 (Mueller et al., 2016; Picardo et al., 2011)
Flesh	1540 (Farrer et al., 2015)	1059 (Culjat et al., 2010; Mendez and Keys, 1960)

Table 5.2: Sound speed and density of the brain regions included the macaque monkey head model.

were the ones used in the probablistic tractography to recreate each of the tracts between the ACC and the ROIs (Folloni et al., 2019a). Subsequently, the resulting tractograms were transformed from the volumetric space into structural space to match the segmented monkey head model. The transformed tractograms were then thresholded to weaken the signal and reduce the width of the tracts to ease the selection of a single line of voxels that was used as the final white matter tract in the TUS simulations. All the final tracts started at the same voxel within the seed mask just next to the ACC grey matter region. The last voxel selected was the one closest to each ROI grey matter after extending the tract within the white matter mask to reach the edge of the ROI grey matter.

The DTI data of the monkey used here, however, had very low resolution. Therefore, the white matter tracts for all the brain regions that the ACC is interconnected with were not all recreated. The only tracts obtained were from the ACC to Brodmann areas 8m, 9mc, 24ab, 9-46v and 47-12o. These brain regions can be seen in Figure 5.5. The white matter tracts have difference lengths, where the tract for Brodmann area 24ab has 17 voxels, area 9-46v has 16 voxels, area 8m has 38 voxels, area 9m has 28 voxels, and area 47-12o has 28 voxels.

The space increments used for the model were 0.5 mm for the x-direction, 0.5 mm for the y-direction and 0.5 mm for the z-direction. This matches the voxel sizes in the MRI structural data of the monkey. The time increment used was 1×10^{-8} s. The flexoelectric coefficients were given as $\tilde{f}_{55} = 0 \quad C/m$, $\tilde{f}_{44} = 2 \times 10^{-9}$ C/m, $\tilde{f}_{33} = 0 \quad C/m$, $\tilde{f}_{22} = 0 \quad C/m$ and $\tilde{f}_{11} = 0 \quad C/m$ (Chen et al., 2019) for the transversely isotropic flexoelectric tensor, see Equation (4.49). The density of axons in each voxel within each of the tracts was obtained using Equation (4.1). For the orientation of the axons in each voxel, the DTI eigenvector **V1** from Equation (4.4) could not be used because of data corruption when transformed from the volumetric space to structural space due to the low resolution. As a

result, each voxel within each of the tracts was instead given a certain orientation to match the direction in which the tracts were heading to reach each of the ROIs. To clarify, the orientation of the axons in each voxel is provided in the model by rotating the flexoelectric tensor. The orientation of axons in each voxel is aligned with the model such that the model always follows the orientation of the axons for a specific white matter tract.

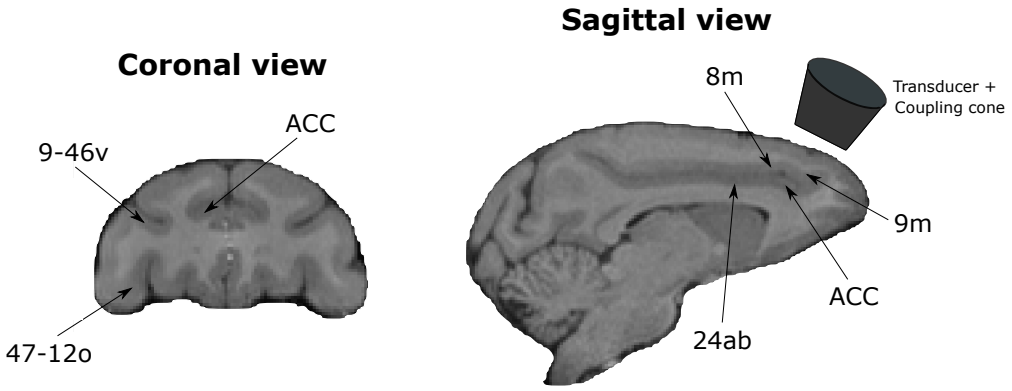


Figure 5.5: The different ROIs in the monkey brain, and the position of the transducer and coupling cone on the head.

Similar to the 2D k-Wave implementation, a train of continuous sinusoidal ultrasound wave of 250 kHz and 1.17 MPa (Folloni et al., 2019b) was applied to the target region (ACC) using a transducer with a 64 mm diameter and 63 mm radius of curvature. This was positioned towards the front of the head at an inclination of 30° to the ACC. Water acting as the coupling cone with material properties of 1480 m/s and 1000 kg/m^3 (Mueller et al., 2016) and a thickness of 47 mm was placed between the transducer and the monkey head to allow for full acoustic coupling or full contact between the transducer and the head or scalp. Figure 5.5 shows the position of the coupling cone and the transducer on the monkey head model, noting that this figure does not include the flesh and skull in the illustration. The x- and y-velocity values were again obtained from k-Wave and integrated to get

the displacement values on the nodes. The remaining x-, y-, and z-displacements on the staggered grid were obtained by taking the average between neighbouring non-staggered nodes. The simulation for each white matter tract was ran for 8 ms reaching the steady state at around 7 ms, which took $\sim$38 days to run using a single compute node providing 14 cores for processing.

After reaching the steady state, the power dissipated or "absorbed" by one voxel dP (given in Figure 5.6-e) was obtained from current dI (given in Figure 5.6-d) by using Equations (5.2) and (5.3). The total maximum current I and total maximum power P were obtained by summing dI and dP for all the voxels within the white matter tract and taking the peak value for one cycle as given in Figure 5.6-a and Figure 5.6-b, respectively. The average current $< dI >$ for each voxel is given by:

$$< dI > = \sqrt{\frac{{dI_{peak}}^2}{2}} \tag{5.5}$$

in Figure 5.6-d and the total average current $< I >$ is taken by summing all the voxels within the white matter tract as given in Figure 5.6-a. In addition, noting again that for each voxel, $< dI^2 >= \frac{{dI_{peak}}^2}{2}$, the corresponding average power was calculated using Equation (5.4) and is given in Figure 5.6-e. The total average power $< P >$ is taken by summing the $< dP >$ of all the voxels within the tract and is given in Figure 5.6-b.

For the full coupling with the electrophysiological model, as a first approximation, the dI generated within each voxel of the white matter tract for each ROI was added to a 1D dimensionless FHN model (see Section 4.2). This assumes that each tract creates a long line of axon between the ACC and each of the ROIs. To implement this, the implicit finite difference scheme (LeVeque, 2007) using the Newton-Raphson method was used. A linearised version of a residual equation of the FHN model ($R = 0$) was solved to find the correction to the initial guess

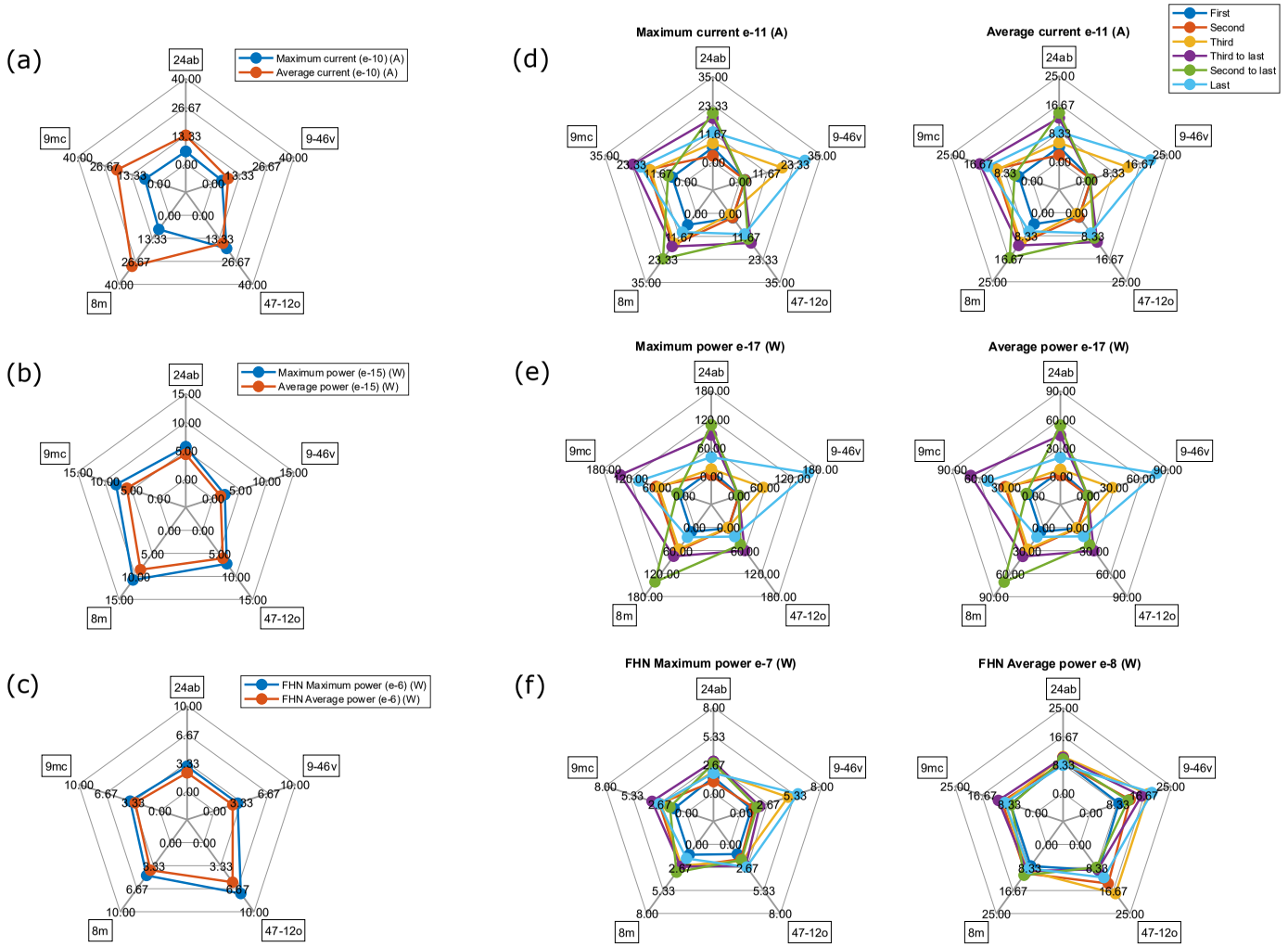


Figure 5.6: (a) Total steady state maximum and average current for the white matter tracts, (b) total steady state maximum and average power for the tracts, (c) total steady state maximum and average power for the tracts from the FHN model, (d) induced steady state maximum and average current for each voxel showing the first three voxels and last three voxels within each tract, (e) corresponding induced steady state maximum and average power for each voxel, and (f) corresponding induced steady state maximum and average power for each voxel from the FHN model.

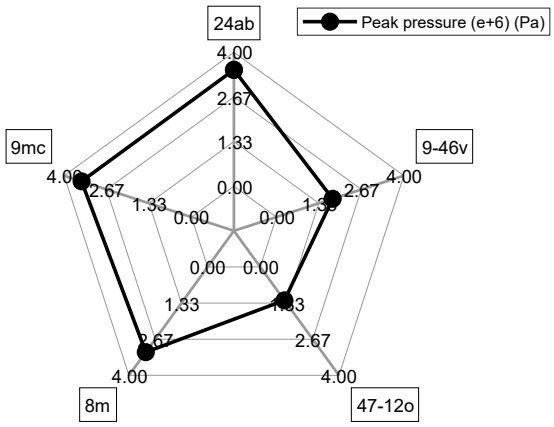


Figure 5.7: Peak pressure at each ROI.

for v^{n+1}. The current guess for v^{n+1} was defined as v^m where m indicates the sub-iteration in the Newton-Raphson method. To find the correction Δv where:

$$v^{m+1} = v^m + \Delta v \tag{5.6}$$

the non-linear residual equation was linearised and solved through:

$$\begin{aligned} R(v^{m+1}) &= 0 \\ R(v^m + \Delta v) &= 0 \\ R(v^m) + \frac{\partial R}{\partial v}|_{v^m} \Delta v &= 0 \\ \frac{\partial R}{\partial v}|_{v^m} \Delta v &= -R(v^m) \\ \Delta v = -\left[\frac{\partial R}{\partial v}|_{v^m}\right]^{-1} & R(v^m) \end{aligned} \tag{5.7}$$

The FHN model was calibrated so that an action potential would last for 1 ms, with a resting state of -65 mV and a depolarised state of -5 mV, which can be triggered with a 40 pA current (Tamayo Elizalde, 2020). In addition, the FHN constant parameters used were $a = 0.4$, $b = 0.4$, $\epsilon = 0.01$ (Garcia-Gonzalez

and Jérusalem, 2019; Engelbrecht et al., 2018a). The diffusion coefficient was given as $D = 2$ by calibrating the model to the cortical axons in monkeys with a conduction velocity of $\sim$30 m/s (Liewald et al., 2014). The continuous sinusoidal current had a time period of 4 μs and the grid spacing used was 0.5 mm to follow the size of the voxels.

The parameters in the FHN model (see Equation (4.5)) can be converted between real dimensions and their dimensionless form using conversion factors (Berberoglu et al., 2014):

$$\phi = \beta_\phi v - \gamma_\phi \tag{5.8}$$

where ϕ is the electrical potential (μV), v is the dimensionless electrical potential, and the electrical potential factors are $\beta_\phi = 62500\ \mu V$ and $\gamma_\phi = 55000\ \mu V$,

$$T = \gamma_T t \tag{5.9}$$

where T is the time (μs), t is the dimensionless time and the time factor is $\gamma_T = 4\ \mu s$,

$$X = \alpha_X x \tag{5.10}$$

where X is the length (μm), x is the dimensionless length and the length factor is $\alpha_X = 250\ \mu m$; and

$$I = \frac{\beta_I}{\gamma_T \beta_\phi} \overline{I} \tag{5.11}$$

where I is the current (μA), $\overline{I}$ is the dimensionless current and the energy factor is $\beta_I = 10\ \mu J$.

A continuous sinusoidal current calculated from Equation (4.21) at steady state was added to all the elements in the FHN model. Once the electrophysiological model had also reached a steady state, the electrical potential ϕ was obtained from the FHN electrical potential v using Equation (5.8), and the power dissipated or "absorbed" by one voxel dP is given by:

$$dP = \frac{d\phi^2}{R} \tag{5.12}$$

in Figure 5.6-f, where R is the electrical resistance of brain white matter obtained from Equation (5.3). The total maximum power P is obtained by summing all the voxels within the white matter tract and taking the peak power value as given in Figure 5.6-c. However, because the resulting electrical potential is not a symmetrical wave, the corresponding power for one cycle is also not symmetrical. Equation (5.4) cannot be used to calculate the average power $< dP >$ for each voxel. Instead, for one cycle, $< dP >$ is given by:

$$< dP >= \frac{1}{T} \int_0^T dP(t)\, dt \tag{5.13}$$

in Figure 5.6-f. The total average power $< P >$ is then again taken by summing the $< dP >$ of all the voxels within the tract as given in Figure 5.6-c. Lastly, the peak pressure at each of the five ROIs is shown in Figure 5.7.

5.3 Discussion

Building on the original observation of flexoelectricity in liquid crystals, Petrov hypothesised that phospholipid membranes could also exhibit flexoelectricity (Petrov, 1975). His work and others' have supported this by demonstrating that a change in the curvature of these membranes could modify the membrane polarisation

(Ahmadpoor et al., 2013; Petrov, 1999; Todorov et al., 1994a), but also that the application of an electrical field could create changes in the membrane curvature (Todorov et al., 1994b). It was found that flexoelectricity was likely to play a role in several biological membrane functions, which involves changes in the curvature of a membrane, e.g., exocytosis, endocytosis or even cell migration (Mueller and Tyler, 2014). However, whether in the context of liquid crystals or more specifically biological membranes, flexoelectricity inherently requires any model to focus on the deformation of the underlying microstructure. This thus naturally precludes a straightforward upscaling of the phenomenon, e.g., from axonal membrane to brain white matter tissue.

A theoretical framework for homogenised bulk flexoelectricity from Chapter 4, was proposed and validated by focussing on cylindrical representations of axons. The resulting formulation only requires the knowledge of axonal density and orientation. This can be obtained from DTI to compute the resulting current increment in the element of interest submitted to a given deformation. The current can then be inputted into any electrophysiological model such as the H-H model (Hodgkin and Huxley, 1952) or the FHN model (Fitzhugh, 1961) to induce an action potential. For the sake of providing a calibration strategy, the model was calibrated against a micromechanical model of flexoelectricity developed by Chen et al. (2019), where the local deformation of the membrane induces a membrane polarisation through flexoelectricity in a 2D problem (see Section 5.1.1). It is important to emphasise that the proposed approach does not require flexoelectricity to be the main driving phenomenon at the membrane level. Instead, it can be used as a phenomenological model for any system whose time-varying strain gradient deformation is observed to lead to current generation. This is in line with the electromechanical coupling observed in the context of action potential generation (Jérusalem et al., 2019). Whether mechanosensitive ion channels, membrane

movement through phase transition (Heimburg and Jackson, 2005) or flexoelectricity (Chen et al., 2019; Todorov et al., 1994b), among others, are at the origin of this coupling, all these hypotheses lead to the same observation at the mesoscale.

The proposed approach has important implication in the context of TUS. This method is very appealing to the healthcare community as it offers avenues for the treatment of neurological disorders, a category of disease currently presenting an increasing societal challenge in the ageing populations (GBD 2016 Neurology Collaborators, 2019; World Health Organisation, 2018). It also provides avenues for examining the neuronal mechanisms of cognitive, sensory, and motor functions in the brain (Fini and Tyler, 2017). Nevertheless, the mechanisms of ultrasound and its capability to modulate the brain are yet to be fully understood. Thus, it has been the subject of growing investigations in recent years to optimise sonication parameters and effect localisation. This however, requires further understanding of electromechanical coupling occurring in nerve impulses (Naor et al., 2016; Sassaroli and Vykhodtseva, 2016). Thus, the proposed theoretical framework can be valuable in providing some insight into this problem and to further study how ultrasound can affect the activities in the brain, while not necessarily postulating the exact nature of the underlying mechanism. This can eventually lead to the optimisation of sonication parameters for a given disease and subject.

5.3.1 TUS configuration effect

The results from the application of the theoretical framework in TUS using a 2D slice of a human head model (see Section 5.1.2) show that the transducer orientation on the head has an effect on the current and power generated within the white matter tract. In particular, as shown in Figure 5.4-d, the "Back" transducer generated the least power in the immediate neighbourhood of the SMA ($< dP_1 >$)

while the "Front" transducer maximised it, with an increase of 13%. As both transducers were focussed equally on the same region, with a target pressure difference of approximately 10%, the difference can be attributed to the change in pressure, which could be due to the topology and mechanical properties of the different regions of the brain or head potentially leading directly and indirectly (by essentially "bouncing" on other structures) to the focal region. On the other hand, at Broadmann area 9-46, the measured pressures were within 32% of each other and the calculated powers in the immediate neighbourhood ($< dP_{40} >$) were within 37% of each other for all three transducer configuration. Both the pressure and power were at maximum for the Front configuration, and minimum for the Back configuration. This shows that the percentage differences in both pressure and power around Brodmann area 9-46 seem to also be around a similar range. However, when accounting for the total power contribution for the entire tract ($< P >$), there was a larger change with a difference of 185% between the Back configuration and the Front configuration. Here, the topology could again be playing a role but it could also be due to the compound contributions of very complex non-linear mechanical interactions with the tracts through its trajectory.

Folloni and coworkers indicated that when applying 250 kHz ultrasound for 40 s with 30 ms pulse every 100 ms to investigate the offline effects of ultrasound on the brain, the target region (e.g., amygdala and/or ACC) was the main affected area. This was because the strongest neuromodulatory effect was observed there. There were some observed changes in the activity coupling in the areas between the target region and the transducer, but a possible explanation to these could be due to the anatomical connectivity shared between the target region and these other areas (Folloni et al., 2019b). Assuming that the brain tissue acts as a flexoelectric system, a full understanding of the effect of focussed ultrasound, when used in the context of a target region and its connected ROI, could benefit from

accounting for the tract between these regions.

While the 2D model needs further calibration and validation, it demonstrates that other factors other than the target region pressure level and the set-up limitations for achieving a full acoustic coupling may need be considered when studying TUS. The resulting electrical power along the tract of interest may also be expected to participate to the resulting functional alterations in some way.

5.3.2 TUS functional effect

The growing body of research in TUS aimed at optimising sonication parameters and effect localisation is pointing towards the need for better understanding on how the multi-physics properties of neurons can lead, or at the very least, is connected to the functional changes observed at the organ scale (Sassaroli and Vykhodtseva, 2016). This need is particularly important in light of recent experimental results where the sonication of the a target region i.e., amygdala and/or the ACC of macaque monkeys was observed to lead to changes in the activity coupling between the target region and a number of ROIs in the cortex of the brain (Folloni et al., 2019b). However, these changes were not of the same magnitude across the different ROIs, hinting that the sole characterisation of the sonicated target region is not enough to universally predict how its activity coupling with various ROIs is altered. With recent work demonstrating how white matter could also be modulated (Vion-Bailly et al., 2019; Duffau, 2015; Hamani et al., 2011; Lozano et al., 2008; Mayberg et al., 2005; Gavrilov, 1984), one explanation for this discrepancy could lie in the understanding of how the tracts leaving the sonicated target region are themselves sonicated in the neighbourhood of the target region. Doing so requires a thorough understanding of how white matter tract electrophysiology can be altered in the presence of a given pressure field. Here, the 3D model was leveraged to explore the possibility that ultrasound mediated

white matter tract stimulation could be responsible for the discrepancies observed in the connectivity fingerprint of the sonicated target region in macaque monkeys (Folloni et al., 2019b).

The implemented 3D model discussed in Section 5.2, was compared with an experiment conducted by Folloni et al. (2019b). In the experiment, both the ACC and amygdala of macaque monkeys were targeted with TUS. The measured BOLD signal activities from both the left and right hemispheres of the brain were obtained from 9 monkeys for the control, 4 monkeys post amygdala TUS and 3 monkeys post ACC TUS. The BOLD signal measurements were averaged and used to create the functional connectivity fingerprints of the ACC and amygdala (Folloni et al., 2019b). The connectivity fingerprint is defined as a pattern of activity coupling that reflects a unique constellation of projections and interactions of a specific brain region, e.g., ACC and/or amygdala (Passingham et al., 2002). These connectivity fingerprints were normalised, where a value of 0 was given to the weakest connection of a given ROI with the target region, and a value of 1 was given to the strongest connection with the target region (Mars et al., 2016). Note that it is only a relative measure of activity change in that specific region in regards to external activity or activity recorded from other brain regions. Therefore, it can only correlate the BOLD activity of a specific target region, e.g., ACC and/or amygdala with the BOLD activity in other regions, the ROIs (Folloni et al., 2019b; O'Reilly et al., 2013).

As mentioned previously, the monkey model used here had DTI data with very low resolution. Therefore, the white matter tracts for the amygdala could not be reliably recreated since the resolution around this region was not sufficient. Because of this, only the tracts from the ACC to Brodmann areas 8m, 9mc, 24ab, 9-46v and 47-12o for the left hemisphere were recreated. To compare the model to the experiment, a relative change (see Figure 5.8-a) and an absolute change

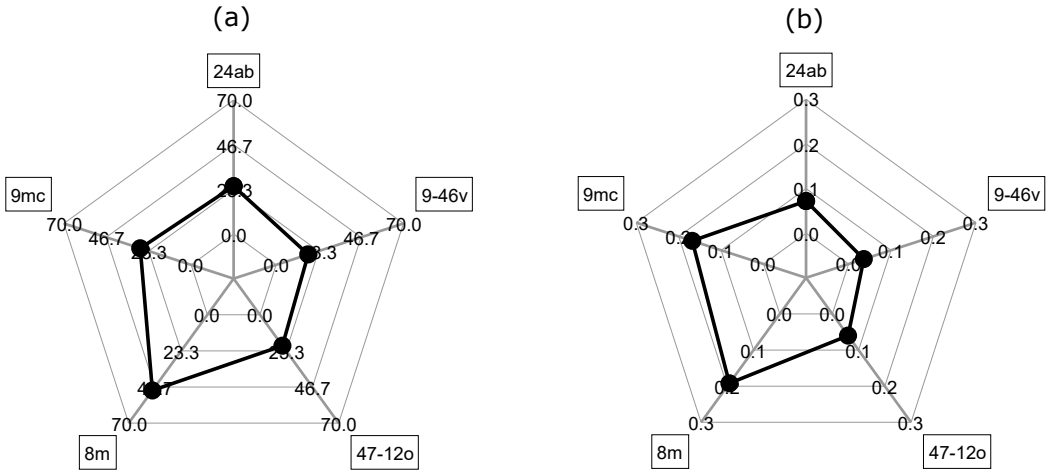


Figure 5.8: (a) Relative change between the experimental control and ACC TUS in the connectivity fingerprint of ACC, and (b) absolute change between the experimental control and ACC TUS in the connectivity fingerprint of ACC.

(see Figure 5.8-b) were obtained from the connectivity fingerprint of the ACC using the control and ACC TUS experimental results for Brodmann areas 8m, 9mc, 24ab, 9-46v and 47-12o. Figure 5.8 shows how much the activity coupling between the ACC and other brain regions have changed or decreased due to the loss of activity coupling after ACC TUS. The relative and absolute change both show a very similar trend. Brodmann area 8m had the highest relative and absolute change, followed by Brodmann area 9mc, 24ab, 47-12o and 9-46v, respectively. Specifically, from Figure 5.8-a, the relative change in activity coupling was 49% for area 8m, 28% for area 9mc, 25% for area 24ab, 20% for area 47-12o, and 18% for area 9-46v, respectively. From Figure 5.8-b, the absolute change in activity coupling was 0.16 for area 8m, 0.14 for area 9mc, 0.06 for area 24ab, 0.05 for area 47-12o, and 0.03 for area 9-46v, respectively. For the sake of clarity, these spider graphs quantify the degree of loss of correlation between the ACC and the five ROIs, between the sonicated and the non-sonicated regions. Note that the tracts for the regions that were observed to have an enhanced correlation were not recreated due to this resolution problem.

The loss of correlation between the ACC and the five ROIs after ACC TUS may potentially be related to the suppression of activity in these regions due to TUS. Therefore, the results may be relevant especially for the treatment of epilepsy where the suppression of seizures (over-activity of electrical impulses in the brain) is the desired effect. However, the loss of correlation may be determined by the TUS protocol, since TUS can cause either excitation or inhibition depending on the combination of ultrasound parameters used. Thus, further research is still required to fully understand the effects of TUS on the functional activity of the brain, and how TUS can be used to treat neurological disorders such as epilepsy where long-lasting suppression of brain activity is preferred.

When comparing the experimental results in Figure 5.8 and the model results in Figures 5.6-a and 5.6-b, higher mediated total current (I and $< I >$) and power (P and $< P >$) contributions correlate with a higher observed loss of activity coupling between the ACC and other ROIs. This correlation however, was lost with Brodmann area 47-12o particularly for Figure 5.6-c. A possible explanation for this is that a higher current generated within the tract heading towards a particular ROI may be causing a greater disruption in the electrical activity of that brain region. This could potentially cause a greater change in the BOLD signal activity coupling between the ACC and these regions.

Figures 5.6-d, 5.6-e, and 5.6-f on the other hand, show the individual current (dI and $< dI >$) and power (dP and $< dP >$) contributions of each voxel for the first three voxels of the tract nearest to the ACC and the last three voxels of the tract nearest to each ROI. These results do not show a similar pattern to the loss of activity coupling from the experiment in Figure 5.8. Whether focussing on the current or power (maximum or average), the model predicts very little current generation in the first voxel of the white matter tract immediately leaving the ACC, but some activity in the second voxel for the tracts going to Broadmann areas 9-46v, 8m

and 9mc, see Figures 5.6-d, and 5.6-e. This can be directly linked to the fibre orientation change from the first to the second voxel along with potential change in pressure level. More generally, these figures also show that there is no obvious relation between the level of induced current or power in a voxel and its distance to the target region or ROI, e.g., there are few occurrences of abrupt change of current or power between one voxel and its neighbour (e.g., second and third for Brodmann area 9-46v). The non-straightforward combination of rotation of the fibre when going from one voxel to another along with pressure level changes may be driving these trends or lack thereof. This further highlights the fact that outside of the targeted grey matter region, the level of white matter current generation cannot be straightforwardly estimated without numerical prediction, especially if it is fibre orientation dependent, such as proposed here. It is therefore proposed to focus on averaged or maximum cumulated values across the entire tract.

As can be seen in Figure 5.5, three ROIs (Broadmann areas 8m, 9mc and 24ab) are relatively close to the target region, the ACC, while Brodmann areas 9-46v and 47-12o are more distant. Because these three ROIs are closer to the focus of ultrasound, the peak pressure at Brodmann areas 8m, 9mc and 24ab are higher than the peak pressure at Brodmann areas 9-46v and 47-12o as shown in Figure 5.7. However, the differences in values are not that large. Furthermore, the fact that the pressure field is non-zero outside of the target region (because of e.g., tissue inhomogeneity or skull morphology) does not necessarily mean that white matter tracts around the distal ROIs should be largely less sonicated than around the closest ones. The additional effect of fibre orientation with respect to the pressure wave further impedes any straightforward prediction.

The lack of qualitative correlation with the fully coupled model (Figure 5.6-c) is not necessarily surprising in light of the binary behaviour of the FHN model. In other words, the FHN equations model the electrophysiological signal as firing or

not. The current input generated by the flexoelectric coupling model thus seems a more reliable measure of sonication effect than the resulting FHN signal.

Figures 5.6-a and 5.6-d show that the generated overall current I and the generated current in individual voxels dI within the white matter tract can reach the 40 pA current threshold required to induce action potentials in neurons. This means that TUS is able to generate enough currents within the white matter tracts to cause changes in the electrical activity of the brain. Furthermore, Figure 5.6-b shows that more generated power corresponds with more generated current within the white matter tract (see Figure 5.6-a). This correlation between generated current and power suggests that power may also be a useful metric to utilise when studying TUS and its effects on the functional activity of the brain.

The most important property of white matter may be its intrinsic anisotropy, i.e., the fibre orientation. This has electrophysiological implications such that the current is mainly flowing in this direction but also mechanical implications where the tissue's stiffness differs depending on the loading direction (Feng et al., 2013). This duality means that any attempt at coupling electrophysiology and mechanics in the white matter needs to take account of this anisotropy (Garcia-Gonzalez and Jérusalem, 2019). Accordingly, the proposed methodology discussed in Chapter 4 assumes that current generation solely occurs when there is a strain gradient which is time-varying (strain gradient phenomenologically polarises the tissue, but current is only generated when the polarisation is changing with time). This leads to the observation that a pressure wave in the direction of the fibre is less likely to generate current than when at an angle with it, where the axon can thus vibrate in bending mode.

Neuromodulation studies on treatment-resistant depression have shown that DBS can stimulate the white matter tracts adjacent to the subcallosal cingulate (SCC)

region, leading to antidepressant effects (Wu et al., 2021; Lozano et al., 2008; Mayberg et al., 2005) similar to when targeting the immediate adjacent grey matter (Hamani et al., 2011; Lozano et al., 2008). In particular, SCC DBS can normalise the activity abnormalities at the SCC and other brain regions connected to the SCC (Mayberg et al., 2005). This suggests that DBS drives focal activity at the SCC, which then leads to the inhibition or excitation of the connected adjacent and remote regions (Wu et al., 2021). This, in turn, disrupts the pathological activity in limbic-cortical circuits, which underlies depression, thus allowing for more normal cerebral function and behaviour (Hamani et al., 2011). It was also demonstrated that the response to SCC DBS could be mediated by the direct impact in three specific distinct fibre bundles on the SCC white matter (the bilateral forceps minor of the anterior corpus callosum, the bilateral cingulum bundles, and the medial branch of the uncinate fasciculus) (Riva-Posse et al., 2014; Lehman et al., 2011). Taken together, such results point towards a more important role for white matter sonication than generally considered in TUS. These results on the DBS neuromodulation of the SCC and adjacent white matter (Mayberg et al., 2005) also confirm that the differences observed here in the magnitude of loss of activity coupling between the ROIs and the sonicated ACC may indeed arise from the *spill-out* sonication of the neighbouring white matter tracts adjacent to the target region. This means that white matter density and orientation for the different ROI tracts leaving the ACC need to be accounted for when sonicating the ACC. This cannot be straightforwardly accounted for when only focussing on grey matter model simulations. The complexity of the head morphology, material properties of the different brain regions and TUS set-up thus require the use of *in silico* predictions, such as proposed here.

Moreover, despite the limited number of ROIs used, the results show a strong correlation between the induced maximum current in the entire tracts leaving the

sonicated region, the ACC, and the change in activity coupling with the corresponding ROIs, where more current leads to a stronger loss of activity coupling. The model is however, not without limitations. Its validation would benefit from additional experiments which include other measurements of activity rather than just BOLD MRI measurements. Other sonicated regions and other ROIs would also be required to be investigated. Validation on different brain or skull morphologies would ensure that these changes can acquire a patient-specific dimension. But overall, the adaption of the theoretical framework in 3D can be further used to study TUS to examine the activity coupling within the brain as well as the important role of white matter tracts in disrupting brain activity within circuits.

6 | Conclusion

6.1 Summary

The increase in life expectancy and population growth is causing neurological disorders to be more prevalent and increasingly causing a substantial burden on society and posing serious threats to public health. Hence, it is important for the health community to focus on its prevention, treatment and management. Many experimental studies have investigated the effects of low-intensity TUS as a possible treatment of neurological disorders as it has been shown to non-invasively alter the behaviour, cognition and sensory processes of small animals, primates and more recently, humans with high spatial precision. However, due to the many different effects observed when using different combinations of ultrasound parameters, the mechanisms of ultrasound are still not fully understood. A few cellular scale numerical models have been developed to attempt to explain the mechanisms of ultrasound, but none of these have delved into extending these models to tissue level which would be more useful when comparing with whole brain neuromodulation experiments. Current modelling approaches are also mostly based on the sonication effects through the skull and do not predict how ultrasound effects translate into brain electrical activity. Therefore, the aim of this research is to gain more understanding on how ultrasound affects the electrical activity in brain tissues through electromechanical coupling.

The main contribution of this research is to provide a scalable multiphysics numerical electromechanical coupled model linking TUS to current generation. This framework defines a continuum level formulation for bulk tissue flexoelectricity without the need to account for cellular microstructures. This approach was successfully validated in 2D and therefore, has the potential to be used for differ-

ent applications in bulk flexoelectricity in biological and non-biological materials to investigate the electromechanical coupling phenomenon. The adaption of the framework in 3D also showed that the model can be used to further examine the effect of TUS on the functional connectivity of the brain. Specifically, the 3D results showed that the model is able to capture the activity coupling between a target region, i.e., ACC and other areas of the brain interconnected with it. In particular, higher total current and/or power contributions result in higher loss of activity coupling between the ACC and other ROIs. This is attributed to the disruptions caused by the induction of currents within the tracts, which affects the electrical signal activity between the two regions.

6.2 Limitations and future work

A full calibration and validation of the 3D model with experimental results was hindered by the very low resolution of experimental data available to this study. Therefore, the probabilistic tractography was only able to recreate a subset of the white matter tracts experimentally studied in the brain due to the low signal in the data. Another limitation was that segmenting the monkey head model took a significant amount of time ($\sim$ 4-5 months). Therefore, only one 3D monkey head model was segmented for this work and the effects of different brain geometries for a sensitivity study was not investigated. Furthermore, the 3D model simulations for the white matter tracts each took approximately 38 days to run so the effects of varying the material properties of the brain was also not studied.

For the future work, an intermediate point of validation would be useful to allow for a more direct biophysical measurement for example, using slice preparations before conducting the full validation for whole brain models. This allows an initial step to be able to translate the results observed at cellular level before scaling up

into whole brain level. Furthermore, slice preparations can also allow for a more detailed study into the effects of axonal dispersion, orientation and density.

Continuation on the work on whole brain models can then be conducted. The DTI data of a macaque monkey with a higher resolution can be obtained to allow for better probabilistic tractography, allowing for the recreation of more tracts between different brain regions. This would then allow for more model results to be obtained and compared to the experimental study thereby, fully calibrating and validating the model. Additionally, it would allow for TUS of a different brain region to see the effects on its functional connectivity fingerprint and/or its effect on another area's functional connectivity fingerprint similar to the experiment in Folloni et al. (2019b)'s study. The high resolution DTI data will allow white matter tracts from both left and right hemispheres to be recreated and compared to see if there are any significant differences between the two hemispheres. Furthermore, rather than just taking the fingerprint connectivity values in a manual fashion, the experimental BOLD signal data for these fingerprint connectivities should be obtained automatically.

Sensitivity studies can be conducted to vary the material properties of the brain used in modelling, as well as varying the flexoelectric coefficients used. This may require conducting experiments to measure the flexoelectricity in brain tissues. In addition, multiple head models can be created so that the variation in the geometry of the brain for individual monkeys can be taken into account. By doing this, a group data can be collected to match the results obtained in experiments more, including accounting for both the left and right hemispheres.

The effect of targeting the white matter instead of the grey matter can also be investigated. Furthermore, the soma of the neuron can be modelled in addition to the axon. This could involve needing to adapt the theoretical framework formula-

tion in Chapter 4 to also model a spherical shape for the soma. This means that the model would require an isotropic diffusion to allow for the electrical activity propagation within the soma.

Lastly, the full implementation of the 3D model using the Fourier pseudospectral method can be considered, where the electrophysiological model is also implemented in 3D. This however, would require a vast amount of computational time making the simulations extremely long.

A | 2D model

The shape function tensor **N** is:

$$\mathbf{N} = \begin{bmatrix} N_1 & 0 & N_2 & 0 & N_3 & 0 & N_4 & 0 & N_5 & 0 & N_6 & 0 & N_7 & 0 & N_8 & 0 \\ 0 & N_1 & 0 & N_2 & 0 & N_3 & 0 & N_4 & 0 & N_5 & 0 & N_6 & 0 & N_7 & 0 & N_8 \end{bmatrix} \tag{A.1}$$

The first derivative gradient tensor $\mathbf{L}_1$ is:

$$\mathbf{L}_1 = \begin{bmatrix} \frac{\partial}{\partial x} & 0 \\ 0 & \frac{\partial}{\partial y} \\ \frac{\partial}{\partial y} & \frac{\partial}{\partial x} \end{bmatrix} \tag{A.2}$$

The second derivative gradient tensor $\mathbf{L}_2$ is:

$$\mathbf{L}_2 = \begin{bmatrix} \frac{\partial}{\partial x} & 0 & 0 \\ \frac{\partial}{\partial y} & 0 & 0 \\ 0 & \frac{\partial}{\partial x} & 0 \\ 0 & \frac{\partial}{\partial y} & 0 \\ 0 & 0 & \frac{\partial}{\partial x} \\ 0 & 0 & \frac{\partial}{\partial y} \end{bmatrix} \tag{A.3}$$

The shape functions of the 8-node quadratic element expressed in the local natural coordinates are (see Figure 4.4):

$$
\begin{aligned}
N_1 &= \frac{1}{4}(1-\xi)(1-\eta)(-1-\xi-\eta) \\
N_2 &= \frac{1}{4}(1+\xi)(1-\eta)(-1+\xi-\eta) \\
N_3 &= \frac{1}{4}(1+\xi)(1+\eta)(-1+\xi+\eta) \\
N_4 &= \frac{1}{4}(1-\xi)(1+\eta)(-1-\xi+\eta) \\
N_5 &= \frac{1}{2}(1-\xi^2)(1-\eta) \\
N_6 &= \frac{1}{2}(1+\xi)(1-\eta^2) \\
N_7 &= \frac{1}{2}(1-\xi^2)(1+\eta) \\
N_8 &= \frac{1}{2}(1-\xi)(1-\eta^2)
\end{aligned}
\tag{A.4}
$$

From Equation (A.4), the third derivatives of the shape functions are:

$$
\begin{array}{llll}
\dfrac{\partial^3 N_1}{\partial \xi^3} = 0 & \dfrac{\partial^3 N_1}{\partial \eta^3} = 0 & \dfrac{\partial^3 N_1}{\partial \xi^2 \partial \eta} = -\dfrac{1}{2} & \dfrac{\partial^3 N_1}{\partial \xi \partial \eta^2} = -\dfrac{1}{2} \\
\dfrac{\partial^3 N_2}{\partial \xi^3} = 0 & \dfrac{\partial^3 N_2}{\partial \eta^3} = 0 & \dfrac{\partial^3 N_2}{\partial \xi^2 \partial \eta} = -\dfrac{1}{2} & \dfrac{\partial^3 N_2}{\partial \xi \partial \eta^2} = \dfrac{1}{2} \\
\dfrac{\partial^3 N_3}{\partial \xi^3} = 0 & \dfrac{\partial^3 N_3}{\partial \eta^3} = 0 & \dfrac{\partial^3 N_3}{\partial \xi^2 \partial \eta} = \dfrac{1}{2} & \dfrac{\partial^3 N_3}{\partial \xi \partial \eta^2} = \dfrac{1}{2} \\
\dfrac{\partial^3 N_4}{\partial \xi^3} = 0 & \dfrac{\partial^3 N_4}{\partial \eta^3} = 0 & \dfrac{\partial^3 N_4}{\partial \xi^2 \partial \eta} = \dfrac{1}{2} & \dfrac{\partial^3 N_4}{\partial \xi \partial \eta^2} = -\dfrac{1}{2} \\
\dfrac{\partial^3 N_5}{\partial \xi^3} = 0 & \dfrac{\partial^3 N_5}{\partial \eta^3} = 0 & \dfrac{\partial^3 N_5}{\partial \xi^2 \partial \eta} = 1 & \dfrac{\partial^3 N_5}{\partial \xi \partial \eta^2} = 0 \\
\dfrac{\partial^3 N_6}{\partial \xi^3} = 0 & \dfrac{\partial^3 N_6}{\partial \eta^3} = 0 & \dfrac{\partial^3 N_6}{\partial \xi^2 \partial \eta} = 0 & \dfrac{\partial^3 N_6}{\partial \xi \partial \eta^2} = -1 \\
\dfrac{\partial^3 N_7}{\partial \xi^3} = 0 & \dfrac{\partial^3 N_7}{\partial \eta^3} = 0 & \dfrac{\partial^3 N_7}{\partial \xi^2 \partial \eta} = -1 & \dfrac{\partial^3 N_7}{\partial \xi \partial \eta^2} = 0 \\
\dfrac{\partial^3 N_8}{\partial \xi^3} = 0 & \dfrac{\partial^3 N_8}{\partial \eta^3} = 0 & \dfrac{\partial^3 N_8}{\partial \xi^2 \partial \eta} = 0 & \dfrac{\partial^3 N_8}{\partial \xi \partial \eta^2} = 1
\end{array}
\tag{A.5}
$$

The polarisation gradient in Equation (4.35) can be obtained by multiplying Equations (4.42) (A.3), (A.2), (A.1), and (4.37) together, and taking its divergence:

$$
\begin{aligned}
\nabla \cdot \tilde{\mathbf{P}} = \tilde{f}_{1111} \Bigg[& \left(d_x^1\right) \frac{\partial^3 N_1}{\partial x^3} + \left(d_x^2\right) \frac{\partial^3 N_2}{\partial x^3} + \left(d_x^3\right) \frac{\partial^3 N_3}{\partial x^3} + \left(d_x^4\right) \frac{\partial^3 N_4}{\partial x^3} + \\
& \left(d_x^5\right) \frac{\partial^3 N_5}{\partial x^3} + \left(d_x^6\right) \frac{\partial^3 N_6}{\partial x^3} + \left(d_x^7\right) \frac{\partial^3 N_7}{\partial x^3} + \left(d_x^8\right) \frac{\partial^3 N_8}{\partial x^3} \Bigg] + \\
\tilde{f}_{1112} \Bigg[& \left(d_x^1\right) \frac{\partial^3 N_1}{\partial x^2 \partial y} + \left(d_x^2\right) \frac{\partial^3 N_2}{\partial x^2 \partial y} + \left(d_x^3\right) \frac{\partial^3 N_3}{\partial x^2 \partial y} + \left(d_x^4\right) \frac{\partial^3 N_4}{\partial x^2 \partial y} + \\
& \left(d_x^5\right) \frac{\partial^3 N_5}{\partial x^2 \partial y} + \left(d_x^6\right) \frac{\partial^3 N_6}{\partial x^2 \partial y} + \left(d_x^7\right) \frac{\partial^3 N_7}{\partial x^2 \partial y} + \left(d_x^8\right) \frac{\partial^3 N_8}{\partial x^2 \partial y} \Bigg] + \\
\tilde{f}_{1221} \Bigg[& \left(d_y^1\right) \frac{\partial^3 N_1}{\partial x^2 \partial y} + \left(d_y^2\right) \frac{\partial^3 N_2}{\partial x^2 \partial y} + \left(d_y^3\right) \frac{\partial^3 N_3}{\partial x^2 \partial y} + \left(d_y^4\right) \frac{\partial^3 N_4}{\partial x^2 \partial y} + \\
& \left(d_y^5\right) \frac{\partial^3 N_5}{\partial x^2 \partial y} + \left(d_y^6\right) \frac{\partial^3 N_6}{\partial x^2 \partial y} + \left(d_y^7\right) \frac{\partial^3 N_7}{\partial x^2 \partial y} + \left(d_y^8\right) \frac{\partial^3 N_8}{\partial x^2 \partial y} \Bigg] + \\
\tilde{f}_{1222} \Bigg[& \left(d_y^1\right) \frac{\partial^3 N_1}{\partial x \partial y^2} + \left(d_y^2\right) \frac{\partial^3 N_2}{\partial x \partial y^2} + \left(d_y^3\right) \frac{\partial^3 N_3}{\partial x \partial y^2} + \left(d_y^4\right) \frac{\partial^3 N_4}{\partial x \partial y^2} + \\
& \left(d_y^5\right) \frac{\partial^3 N_5}{\partial x \partial y^2} + \left(d_y^6\right) \frac{\partial^3 N_6}{\partial x \partial y^2} + \left(d_y^7\right) \frac{\partial^3 N_7}{\partial x \partial y^2} + \left(d_y^8\right) \frac{\partial^3 N_8}{\partial x \partial y^2} \Bigg] + \\
\tilde{f}_{1121} \Bigg[& \left(d_x^1\right) \frac{\partial^3 N_1}{\partial x^2 \partial y} + \left(d_y^1\right) \frac{\partial^3 N_1}{\partial x^3} + \left(d_x^2\right) \frac{\partial^3 N_2}{\partial x^2 \partial y} + \left(d_y^2\right) \frac{\partial^3 N_2}{\partial x^3} + \\
& \left(d_x^3\right) \frac{\partial^3 N_3}{\partial x^2 \partial y} + \left(d_y^3\right) \frac{\partial^3 N_3}{\partial x^3} + \left(d_x^4\right) \frac{\partial^3 N_4}{\partial x^2 \partial y} + \left(d_y^4\right) \frac{\partial^3 N_4}{\partial x^3} + \\
& \left(d_x^5\right) \frac{\partial^3 N_5}{\partial x^2 \partial y} + \left(d_y^5\right) \frac{\partial^3 N_5}{\partial x^3} + \left(d_x^6\right) \frac{\partial^3 N_6}{\partial x^2 \partial y} + \left(d_y^6\right) \frac{\partial^3 N_6}{\partial x^3} + \\
& \left(d_x^7\right) \frac{\partial^3 N_7}{\partial x^2 \partial y} + \left(d_y^7\right) \frac{\partial^3 N_7}{\partial x^3} + \left(d_x^8\right) \frac{\partial^3 N_8}{\partial x^2 \partial y} + \left(d_y^8\right) \frac{\partial^3 N_8}{\partial x^3} \Bigg] + \\
\end{aligned}
$$

$$
\begin{aligned}
\tilde{f}_{1122}\Bigg[& \left(d_x^1\right)\frac{\partial^3 N_1}{\partial x\partial y^2}+\left(d_y^1\right)\frac{\partial^3 N_1}{\partial x^2\partial y}+\left(d_x^2\right)\frac{\partial^3 N_2}{\partial x\partial y^2}+\left(d_y^2\right)\frac{\partial^3 N_2}{\partial x^2\partial y}+\\
& \left(d_x^3\right)\frac{\partial^3 N_3}{\partial x\partial y^2}+\left(d_y^3\right)\frac{\partial^3 N_3}{\partial x^2\partial y}+\left(d_x^4\right)\frac{\partial^3 N_4}{\partial x\partial y^2}+\left(d_y^4\right)\frac{\partial^3 N_4}{\partial x^2\partial y}+\\
& \left(d_x^5\right)\frac{\partial^3 N_5}{\partial x\partial y^2}+\left(d_y^5\right)\frac{\partial^3 N_5}{\partial x^2\partial y}+\left(d_x^6\right)\frac{\partial^3 N_6}{\partial x\partial y^2}+\left(d_y^6\right)\frac{\partial^3 N_6}{\partial x^2\partial y}+\\
& \left(d_x^7\right)\frac{\partial^3 N_7}{\partial x\partial y^2}+\left(d_y^7\right)\frac{\partial^3 N_7}{\partial x^2\partial y}+\left(d_x^8\right)\frac{\partial^3 N_8}{\partial x\partial y^2}+\left(d_y^8\right)\frac{\partial^3 N_8}{\partial x^2\partial y}\Bigg]+\\
\tilde{f}_{2111}\Bigg[& \left(d_x^1\right)\frac{\partial^3 N_1}{\partial x^2\partial y}+\left(d_x^2\right)\frac{\partial^3 N_2}{\partial x^2\partial y}+\left(d_x^3\right)\frac{\partial^3 N_3}{\partial x^2\partial y}+\left(d_x^4\right)\frac{\partial^3 N_4}{\partial x^2\partial y}+\\
& \left(d_x^5\right)\frac{\partial^3 N_5}{\partial x^2\partial y}+\left(d_x^6\right)\frac{\partial^3 N_6}{\partial x^2\partial y}+\left(d_x^7\right)\frac{\partial^3 N_7}{\partial x^2\partial y}+\left(d_x^8\right)\frac{\partial^3 N_8}{\partial x^2\partial y}\Bigg]+\\
\tilde{f}_{2112}\Bigg[& \left(d_x^1\right)\frac{\partial^3 N_1}{\partial x\partial y^2}+\left(d_x^2\right)\frac{\partial^3 N_2}{\partial x\partial y^2}+\left(d_x^3\right)\frac{\partial^3 N_3}{\partial x\partial y^2}+\left(d_x^4\right)\frac{\partial^3 N_4}{\partial x\partial y^2}+\\
& \left(d_x^5\right)\frac{\partial^3 N_5}{\partial x\partial y^2}+\left(d_x^6\right)\frac{\partial^3 N_6}{\partial x\partial y^2}+\left(d_x^7\right)\frac{\partial^3 N_7}{\partial x\partial y^2}+\left(d_x^8\right)\frac{\partial^3 N_8}{\partial x\partial y^2}\Bigg]+\\
\tilde{f}_{2221}\Bigg[& \left(d_y^1\right)\frac{\partial^3 N_1}{\partial x\partial y^2}+\left(d_y^2\right)\frac{\partial^3 N_2}{\partial x\partial y^2}+\left(d_y^3\right)\frac{\partial^3 N_3}{\partial x\partial y^2}+\left(d_y^4\right)\frac{\partial^3 N_4}{\partial x\partial y^2}+\\
& \left(d_y^5\right)\frac{\partial^3 N_5}{\partial x\partial y^2}+\left(d_y^6\right)\frac{\partial^3 N_6}{\partial x\partial y^2}+\left(d_y^7\right)\frac{\partial^3 N_7}{\partial x\partial y^2}+\left(d_y^8\right)\frac{\partial^3 N_8}{\partial x\partial y^2}\Bigg]+\\
\tilde{f}_{2222}\Bigg[& \left(d_y^1\right)\frac{\partial^3 N_1}{\partial y^3}+\left(d_y^2\right)\frac{\partial^3 N_2}{\partial y^3}+\left(d_y^3\right)\frac{\partial^3 N_3}{\partial y^3}+\left(d_y^4\right)\frac{\partial^3 N_4}{\partial y^3}+\\
& \left(d_y^5\right)\frac{\partial^3 N_5}{\partial y^3}+\left(d_y^6\right)\frac{\partial^3 N_6}{\partial y^3}+\left(d_y^7\right)\frac{\partial^3 N_7}{\partial y^3}+\left(d_y^8\right)\frac{\partial^3 N_8}{\partial y^3}\Bigg]+
\end{aligned}
$$

$$
\begin{aligned}
\tilde{f}_{2121}\Bigg[& \left(d_x^1\right)\frac{\partial^3 N_1}{\partial x\partial y^2}+\left(d_y^1\right)\frac{\partial^3 N_1}{\partial x^2\partial y}+\left(d_x^2\right)\frac{\partial^3 N_2}{\partial x\partial y^2}+\left(d_y^2\right)\frac{\partial^3 N_2}{\partial x^2\partial y}+\\
& \left(d_x^3\right)\frac{\partial^3 N_3}{\partial x\partial y^2}+\left(d_y^3\right)\frac{\partial^3 N_3}{\partial x^2\partial y}+\left(d_x^4\right)\frac{\partial^3 N_4}{\partial x\partial y^2}+\left(d_y^4\right)\frac{\partial^3 N_4}{\partial x^2\partial y}+\\
& \left(d_x^5\right)\frac{\partial^3 N_5}{\partial x\partial y^2}+\left(d_y^5\right)\frac{\partial^3 N_5}{\partial x^2\partial y}+\left(d_x^6\right)\frac{\partial^3 N_6}{\partial x\partial y^2}+\left(d_y^6\right)\frac{\partial^3 N_6}{\partial x^2\partial y}+\\
& \left(d_x^7\right)\frac{\partial^3 N_7}{\partial x\partial y^2}+\left(d_y^7\right)\frac{\partial^3 N_7}{\partial x^2\partial y}+\left(d_x^8\right)\frac{\partial^3 N_8}{\partial x\partial y^2}+\left(d_y^8\right)\frac{\partial^3 N_8}{\partial x^2\partial y}\Bigg]+\\
\tilde{f}_{2122}\Bigg[& \left(d_x^1\right)\frac{\partial^3 N_1}{\partial y^3}+\left(d_y^1\right)\frac{\partial^3 N_1}{\partial x\partial y^2}+\left(d_x^2\right)\frac{\partial^3 N_2}{\partial y^3}+\left(d_y^2\right)\frac{\partial^3 N_2}{\partial x\partial y^2}+\\
& \left(d_x^3\right)\frac{\partial^3 N_3}{\partial y^3}+\left(d_y^3\right)\frac{\partial^3 N_3}{\partial x\partial y^2}+\left(d_x^4\right)\frac{\partial^3 N_4}{\partial y^3}+\left(d_y^4\right)\frac{\partial^3 N_4}{\partial x\partial y^2}+\\
& \left(d_x^5\right)\frac{\partial^3 N_5}{\partial y^3}+\left(d_y^5\right)\frac{\partial^3 N_5}{\partial x\partial y^2}+\left(d_x^6\right)\frac{\partial^3 N_6}{\partial y^3}+\left(d_y^6\right)\frac{\partial^3 N_6}{\partial x\partial y^2}+\\
& \left(d_x^7\right)\frac{\partial^3 N_7}{\partial y^3}+\left(d_y^7\right)\frac{\partial^3 N_7}{\partial x\partial y^2}+\left(d_x^8\right)\frac{\partial^3 N_8}{\partial y^3}+\left(d_y^8\right)\frac{\partial^3 N_8}{\partial x\partial y^2}\Bigg]
\end{aligned}
\tag{A.6}
$$

B | 3D model

The shape function tensor **N** is:

$$\mathbf{N} = \begin{bmatrix} N_1 & 0 & 0 & N_2 & 0 & 0 & N_3 & 0 & 0 & \cdot & \cdot & \cdot & N_{20} & 0 & 0 \\ 0 & N_1 & 0 & 0 & N_2 & 0 & 0 & N_3 & 0 & \cdot & \cdot & \cdot & 0 & N_{20} & 0 \\ 0 & 0 & N_1 & 0 & 0 & N_2 & 0 & 0 & N_3 & \cdot & \cdot & \cdot & 0 & 0 & N_{20} \end{bmatrix} \tag{B.1}$$

The first derivative gradient tensor is given by:

$$\mathbf{L}_1 = \begin{bmatrix} \frac{\partial}{\partial x} & 0 & 0 \\ 0 & \frac{\partial}{\partial y} & 0 \\ 0 & 0 & \frac{\partial}{\partial z} \\ \frac{\partial}{\partial y} & \frac{\partial}{\partial x} & 0 \\ \frac{\partial}{\partial z} & 0 & \frac{\partial}{\partial x} \\ 0 & \frac{\partial}{\partial z} & \frac{\partial}{\partial y} \end{bmatrix} \tag{B.2}$$

The second derivative gradient tensor is given by:

$$\mathbf{L}_2 = \begin{bmatrix} \frac{\partial}{\partial x} & 0 & 0 & 0 & 0 & 0 \\ \frac{\partial}{\partial y} & 0 & 0 & 0 & 0 & 0 \\ \frac{\partial}{\partial z} & 0 & 0 & 0 & 0 & 0 \\ 0 & \frac{\partial}{\partial x} & 0 & 0 & 0 & 0 \\ 0 & \frac{\partial}{\partial y} & 0 & 0 & 0 & 0 \\ 0 & \frac{\partial}{\partial z} & 0 & 0 & 0 & 0 \\ 0 & 0 & \frac{\partial}{\partial x} & 0 & 0 & 0 \\ 0 & 0 & \frac{\partial}{\partial y} & 0 & 0 & 0 \\ 0 & 0 & \frac{\partial}{\partial z} & 0 & 0 & 0 \\ 0 & 0 & 0 & \frac{\partial}{\partial x} & 0 & 0 \\ 0 & 0 & 0 & \frac{\partial}{\partial y} & 0 & 0 \\ 0 & 0 & 0 & \frac{\partial}{\partial z} & 0 & 0 \\ 0 & 0 & 0 & 0 & \frac{\partial}{\partial x} & 0 \\ 0 & 0 & 0 & 0 & \frac{\partial}{\partial y} & 0 \\ 0 & 0 & 0 & 0 & \frac{\partial}{\partial z} & 0 \\ 0 & 0 & 0 & 0 & 0 & \frac{\partial}{\partial x} \\ 0 & 0 & 0 & 0 & 0 & \frac{\partial}{\partial y} \\ 0 & 0 & 0 & 0 & 0 & \frac{\partial}{\partial z} \end{bmatrix} \tag{B.3}$$

The shape functions of the 20-node quadratic element expressed in the local nat-

ural coordinates are (see Figure 4.5):

$$
\begin{aligned}
N_1 &= \frac{1}{8}(1-\xi)(1-\eta)(1-\zeta)(-2-\xi-\eta-\zeta) \\
N_2 &= \frac{1}{8}(1+\xi)(1-\eta)(1-\zeta)(-2+\xi-\eta-\zeta) \\
N_3 &= \frac{1}{8}(1+\xi)(1+\eta)(1-\zeta)(-2+\xi+\eta-\zeta) \\
N_4 &= \frac{1}{8}(1-\xi)(1+\eta)(1-\zeta)(-2-\xi+\eta-\zeta) \\
N_5 &= \frac{1}{8}(1-\xi)(1-\eta)(1+\zeta)(-2-\xi-\eta+\zeta) \\
N_6 &= \frac{1}{8}(1+\xi)(1-\eta)(1+\zeta)(-2+\xi-\eta+\zeta) \\
N_7 &= \frac{1}{8}(1+\xi)(1+\eta)(1+\zeta)(-2+\xi+\eta+\zeta) \\
N_8 &= \frac{1}{8}(1-\xi)(1+\eta)(1+\zeta)(-2-\xi+\eta+\zeta) \\
N_9 &= \frac{1}{4}(1-\xi^2)(1-\eta)(1-\zeta) \\
N_{10} &= \frac{1}{4}(1+\xi)(1-\eta^2)(1-\zeta) \\
N_{11} &= \frac{1}{4}(1-\xi^2)(1+\eta)(1-\zeta) \\
N_{12} &= \frac{1}{4}(1-\xi)(1-\eta^2)(1-\zeta) \\
N_{13} &= \frac{1}{4}(1-\xi^2)(1-\eta)(1+\zeta) \\
N_{14} &= \frac{1}{4}(1+\xi)(1-\eta^2)(1+\zeta) \\
N_{15} &= \frac{1}{4}(1-\xi^2)(1+\eta)(1+\zeta) \\
N_{16} &= \frac{1}{4}(1-\xi)(1-\eta^2)(1+\zeta) \\
N_{17} &= \frac{1}{4}(1-\xi)(1-\eta)(1-\zeta^2) \\
N_{18} &= \frac{1}{4}(1+\xi)(1-\eta)(1-\zeta^2) \\
N_{19} &= \frac{1}{4}(1+\xi)(1+\eta)(1-\zeta^2) \\
N_{20} &= \frac{1}{4}(1-\xi)(1+\eta)(1-\zeta^2)
\end{aligned}
\tag{B.4}
$$

The third derivative of the shape functions are:

$$\frac{\partial^3 N_1}{\partial \xi^3} = 0 \qquad \frac{\partial^3 N_{11}}{\partial \xi^3} = 0 \qquad \frac{\partial^3 N_1}{\partial \eta^3} = 0$$
$$\frac{\partial^3 N_2}{\partial \xi^3} = 0 \qquad \frac{\partial^3 N_{12}}{\partial \xi^3} = 0 \qquad \frac{\partial^3 N_2}{\partial \eta^3} = 0$$
$$\frac{\partial^3 N_3}{\partial \xi^3} = 0 \qquad \frac{\partial^3 N_{13}}{\partial \xi^3} = 0 \qquad \frac{\partial^3 N_3}{\partial \eta^3} = 0$$
$$\frac{\partial^3 N_4}{\partial \xi^3} = 0 \qquad \frac{\partial^3 N_{14}}{\partial \xi^3} = 0 \qquad \frac{\partial^3 N_4}{\partial \eta^3} = 0$$
$$\frac{\partial^3 N_5}{\partial \xi^3} = 0 \qquad \frac{\partial^3 N_{15}}{\partial \xi^3} = 0 \qquad \frac{\partial^3 N_5}{\partial \eta^3} = 0$$
$$\frac{\partial^3 N_6}{\partial \xi^3} = 0 \qquad \frac{\partial^3 N_{16}}{\partial \xi^3} = 0 \qquad \frac{\partial^3 N_6}{\partial \eta^3} = 0$$
$$\frac{\partial^3 N_7}{\partial \xi^3} = 0 \qquad \frac{\partial^3 N_{17}}{\partial \xi^3} = 0 \qquad \frac{\partial^3 N_7}{\partial \eta^3} = 0$$
$$\frac{\partial^3 N_8}{\partial \xi^3} = 0 \qquad \frac{\partial^3 N_{18}}{\partial \xi^3} = 0 \qquad \frac{\partial^3 N_8}{\partial \eta^3} = 0$$
$$\frac{\partial^3 N_9}{\partial \xi^3} = 0 \qquad \frac{\partial^3 N_{19}}{\partial \xi^3} = 0 \qquad \frac{\partial^3 N_9}{\partial \eta^3} = 0$$
$$\frac{\partial^3 N_{10}}{\partial \xi^3} = 0 \qquad \frac{\partial^3 N_{20}}{\partial \xi^3} = 0 \qquad \frac{\partial^3 N_{10}}{\partial \eta^3} = 0$$

$$\frac{\partial^3 N_{11}}{\partial \eta^3} = 0 \qquad \frac{\partial^3 N_1}{\partial \zeta^3} = 0 \qquad \frac{\partial^3 N_{11}}{\partial \zeta^3} = 0$$
$$\frac{\partial^3 N_{12}}{\partial \eta^3} = 0 \qquad \frac{\partial^3 N_2}{\partial \zeta^3} = 0 \qquad \frac{\partial^3 N_{12}}{\partial \zeta^3} = 0$$
$$\frac{\partial^3 N_{13}}{\partial \eta^3} = 0 \qquad \frac{\partial^3 N_3}{\partial \zeta^3} = 0 \qquad \frac{\partial^3 N_{13}}{\partial \zeta^3} = 0$$
$$\frac{\partial^3 N_{14}}{\partial \eta^3} = 0 \qquad \frac{\partial^3 N_4}{\partial \zeta^3} = 0 \qquad \frac{\partial^3 N_{14}}{\partial \zeta^3} = 0$$
$$\frac{\partial^3 N_{15}}{\partial \eta^3} = 0 \qquad \frac{\partial^3 N_5}{\partial \zeta^3} = 0 \qquad \frac{\partial^3 N_{15}}{\partial \zeta^3} = 0$$
$$\frac{\partial^3 N_{16}}{\partial \eta^3} = 0 \qquad \frac{\partial^3 N_6}{\partial \zeta^3} = 0 \qquad \frac{\partial^3 N_{16}}{\partial \zeta^3} = 0$$
$$\frac{\partial^3 N_{17}}{\partial \eta^3} = 0 \qquad \frac{\partial^3 N_7}{\partial \zeta^3} = 0 \qquad \frac{\partial^3 N_{17}}{\partial \zeta^3} = 0$$
$$\frac{\partial^3 N_{18}}{\partial \eta^3} = 0 \qquad \frac{\partial^3 N_8}{\partial \zeta^3} = 0 \qquad \frac{\partial^3 N_{18}}{\partial \zeta^3} = 0$$
$$\frac{\partial^3 N_{19}}{\partial \eta^3} = 0 \qquad \frac{\partial^3 N_9}{\partial \zeta^3} = 0 \qquad \frac{\partial^3 N_{19}}{\partial \zeta^3} = 0$$
$$\frac{\partial^3 N_{20}}{\partial \eta^3} = 0 \qquad \frac{\partial^3 N_{10}}{\partial \zeta^3} = 0 \qquad \frac{\partial^3 N_{20}}{\partial \zeta^3} = 0$$

$$\frac{\partial^3 N_1}{\partial\xi^2\partial\eta} = \frac{1}{4}(-1+\zeta) \qquad \frac{\partial^3 N_{11}}{\partial\xi^2\partial\eta} = \frac{1}{2}(-1+\zeta) \qquad \frac{\partial^3 N_1}{\partial\xi^2\partial\zeta} = \frac{1}{4}(-1+\eta)$$
$$\frac{\partial^3 N_2}{\partial\xi^2\partial\eta} = \frac{1}{4}(-1+\zeta) \qquad \frac{\partial^3 N_{12}}{\partial\xi^2\partial\eta} = 0 \qquad \frac{\partial^3 N_2}{\partial\xi^2\partial\zeta} = \frac{1}{4}(-1+\eta)$$
$$\frac{\partial^3 N_3}{\partial\xi^2\partial\eta} = \frac{1}{4}(1-\zeta) \qquad \frac{\partial^3 N_{13}}{\partial\xi^2\partial\eta} = \frac{1}{2}(1+\zeta) \qquad \frac{\partial^3 N_3}{\partial\xi^2\partial\zeta} = \frac{1}{4}(-1-\eta)$$
$$\frac{\partial^3 N_4}{\partial\xi^2\partial\eta} = \frac{1}{4}(1-\zeta) \qquad \frac{\partial^3 N_{14}}{\partial\xi^2\partial\eta} = 0 \qquad \frac{\partial^3 N_4}{\partial\xi^2\partial\zeta} = \frac{1}{4}(-1-\eta)$$
$$\frac{\partial^3 N_5}{\partial\xi^2\partial\eta} = \frac{1}{4}(-1-\zeta) \qquad \frac{\partial^3 N_{15}}{\partial\xi^2\partial\eta} = \frac{1}{2}(-1-\zeta) \qquad \frac{\partial^3 N_5}{\partial\xi^2\partial\zeta} = \frac{1}{4}(1-\eta)$$
$$\frac{\partial^3 N_6}{\partial\xi^2\partial\eta} = \frac{1}{4}(-1-\zeta) \qquad \frac{\partial^3 N_{16}}{\partial\xi^2\partial\eta} = 0 \qquad \frac{\partial^3 N_6}{\partial\xi^2\partial\zeta} = \frac{1}{4}(1-\eta)$$
$$\frac{\partial^3 N_7}{\partial\xi^2\partial\eta} = \frac{1}{4}(1+\zeta) \qquad \frac{\partial^3 N_{17}}{\partial\xi^2\partial\eta} = 0 \qquad \frac{\partial^3 N_7}{\partial\xi^2\partial\zeta} = \frac{1}{4}(1+\eta)$$
$$\frac{\partial^3 N_8}{\partial\xi^2\partial\eta} = \frac{1}{4}(1+\zeta) \qquad \frac{\partial^3 N_{18}}{\partial\xi^2\partial\eta} = 0 \qquad \frac{\partial^3 N_8}{\partial\xi^2\partial\zeta} = \frac{1}{4}(1+\eta)$$
$$\frac{\partial^3 N_9}{\partial\xi^2\partial\eta} = \frac{1}{2}(1-\zeta) \qquad \frac{\partial^3 N_{19}}{\partial\xi^2\partial\eta} = 0 \qquad \frac{\partial^3 N_9}{\partial\xi^2\partial\zeta} = \frac{1}{2}(1-\eta)$$
$$\frac{\partial^3 N_{10}}{\partial\xi^2\partial\eta} = 0 \qquad \frac{\partial^3 N_{20}}{\partial\xi^2\partial\eta} = 0 \qquad \frac{\partial^3 N_{10}}{\partial\xi^2\partial\zeta} = 0$$

$$\frac{\partial^3 N_{11}}{\partial\xi^2\partial\zeta} = \frac{1}{2}(1+\eta) \qquad \frac{\partial^3 N_{1}}{\partial\eta^2\partial\xi} = \frac{1}{4}(-1+\zeta) \qquad \frac{\partial^3 N_{11}}{\partial\eta^2\partial\xi} = 0$$
$$\frac{\partial^3 N_{12}}{\partial\xi^2\partial\zeta} = 0 \qquad \frac{\partial^3 N_{2}}{\partial\eta^2\partial\xi} = \frac{1}{4}(1-\zeta) \qquad \frac{\partial^3 N_{12}}{\partial\eta^2\partial\xi} = \frac{1}{2}(1-\zeta)$$
$$\frac{\partial^3 N_{13}}{\partial\xi^2\partial\zeta} = \frac{1}{2}(-1+\eta) \qquad \frac{\partial^3 N_{3}}{\partial\eta^2\partial\xi} = \frac{1}{4}(1-\zeta) \qquad \frac{\partial^3 N_{13}}{\partial\eta^2\partial\xi} = 0$$
$$\frac{\partial^3 N_{14}}{\partial\xi^2\partial\zeta} = 0 \qquad \frac{\partial^3 N_{4}}{\partial\eta^2\partial\xi} = \frac{1}{4}(-1+\zeta) \qquad \frac{\partial^3 N_{14}}{\partial\eta^2\partial\xi} = \frac{1}{2}(-1-\zeta)$$
$$\frac{\partial^3 N_{15}}{\partial\xi^2\partial\zeta} = \frac{1}{2}(-1-\eta) \qquad \frac{\partial^3 N_{5}}{\partial\eta^2\partial\xi} = \frac{1}{4}(-1-\zeta) \qquad \frac{\partial^3 N_{15}}{\partial\eta^2\partial\xi} = 0$$
$$\frac{\partial^3 N_{16}}{\partial\xi^2\partial\zeta} = 0 \qquad \frac{\partial^3 N_{6}}{\partial\eta^2\partial\xi} = \frac{1}{4}(1+\zeta) \qquad \frac{\partial^3 N_{16}}{\partial\eta^2\partial\xi} = \frac{1}{2}(1+\zeta)$$
$$\frac{\partial^3 N_{17}}{\partial\xi^2\partial\zeta} = 0 \qquad \frac{\partial^3 N_{7}}{\partial\eta^2\partial\xi} = \frac{1}{4}(1+\zeta) \qquad \frac{\partial^3 N_{17}}{\partial\eta^2\partial\xi} = 0$$
$$\frac{\partial^3 N_{18}}{\partial\xi^2\partial\zeta} = 0 \qquad \frac{\partial^3 N_{8}}{\partial\eta^2\partial\xi} = \frac{1}{4}(-1-\zeta) \qquad \frac{\partial^3 N_{18}}{\partial\eta^2\partial\xi} = 0$$
$$\frac{\partial^3 N_{19}}{\partial\xi^2\partial\zeta} = 0 \qquad \frac{\partial^3 N_{9}}{\partial\eta^2\partial\xi} = 0 \qquad \frac{\partial^3 N_{19}}{\partial\eta^2\partial\xi} = 0$$
$$\frac{\partial^3 N_{20}}{\partial\xi^2\partial\zeta} = 0 \qquad \frac{\partial^3 N_{10}}{\partial\eta^2\partial\xi} = \frac{1}{2}(-1+\zeta) \qquad \frac{\partial^3 N_{20}}{\partial\eta^2\partial\xi} = 0$$

$$\frac{\partial^3 N_1}{\partial\eta^2\partial\zeta} = \frac{1}{4}(-1+\xi) \qquad \frac{\partial^3 N_{11}}{\partial\eta^2\partial\zeta} = 0 \qquad \frac{\partial^3 N_1}{\partial\zeta^2\partial\xi} = \frac{1}{4}(-1+\eta)$$
$$\frac{\partial^3 N_2}{\partial\eta^2\partial\zeta} = \frac{1}{4}(-1-\xi) \qquad \frac{\partial^3 N_{12}}{\partial\eta^2\partial\zeta} = \frac{1}{2}(1-\xi) \qquad \frac{\partial^3 N_2}{\partial\zeta^2\partial\xi} = \frac{1}{4}(1-\eta)$$
$$\frac{\partial^3 N_3}{\partial\eta^2\partial\zeta} = \frac{1}{4}(-1-\xi) \qquad \frac{\partial^3 N_{13}}{\partial\eta^2\partial\zeta} = 0 \qquad \frac{\partial^3 N_3}{\partial\zeta^2\partial\xi} = \frac{1}{4}(1+\eta)$$
$$\frac{\partial^3 N_4}{\partial\eta^2\partial\zeta} = \frac{1}{4}(-1+\xi) \qquad \frac{\partial^3 N_{14}}{\partial\eta^2\partial\zeta} = \frac{1}{2}(-1-\xi) \qquad \frac{\partial^3 N_4}{\partial\zeta^2\partial\xi} = \frac{1}{4}(-1-\eta)$$
$$\frac{\partial^3 N_5}{\partial\eta^2\partial\zeta} = \frac{1}{4}(1-\xi) \qquad \frac{\partial^3 N_{15}}{\partial\eta^2\partial\zeta} = 0 \qquad \frac{\partial^3 N_5}{\partial\zeta^2\partial\xi} = \frac{1}{4}(-1+\eta)$$
$$\frac{\partial^3 N_6}{\partial\eta^2\partial\zeta} = \frac{1}{4}(1+\xi) \qquad \frac{\partial^3 N_{16}}{\partial\eta^2\partial\zeta} = \frac{1}{2}(-1+\xi) \qquad \frac{\partial^3 N_6}{\partial\zeta^2\partial\xi} = \frac{1}{4}(1-\eta)$$
$$\frac{\partial^3 N_7}{\partial\eta^2\partial\zeta} = \frac{1}{4}(1+\xi) \qquad \frac{\partial^3 N_{17}}{\partial\eta^2\partial\zeta} = 0 \qquad \frac{\partial^3 N_7}{\partial\zeta^2\partial\xi} = \frac{1}{4}(1+\eta)$$
$$\frac{\partial^3 N_8}{\partial\eta^2\partial\zeta} = \frac{1}{4}(1-\xi) \qquad \frac{\partial^3 N_{18}}{\partial\eta^2\partial\zeta} = 0 \qquad \frac{\partial^3 N_8}{\partial\zeta^2\partial\xi} = \frac{1}{4}(-1-\eta)$$
$$\frac{\partial^3 N_9}{\partial\eta^2\partial\zeta} = 0 \qquad \frac{\partial^3 N_{19}}{\partial\eta^2\partial\zeta} = 0 \qquad \frac{\partial^3 N_9}{\partial\zeta^2\partial\xi} = 0$$
$$\frac{\partial^3 N_{10}}{\partial\eta^2\partial\zeta} = \frac{1}{2}(1+\xi) \qquad \frac{\partial^3 N_{20}}{\partial\eta^2\partial\zeta} = 0 \qquad \frac{\partial^3 N_{10}}{\partial\zeta^2\partial\xi} = 0$$

$$\frac{\partial^3 N_{11}}{\partial\zeta^2\partial\xi} = 0 \qquad \frac{\partial^3 N_1}{\partial\zeta^2\partial\eta} = \frac{1}{4}(-1+\xi) \qquad \frac{\partial^3 N_{11}}{\partial\zeta^2\partial\eta} = 0$$
$$\frac{\partial^3 N_{12}}{\partial\zeta^2\partial\xi} = 0 \qquad \frac{\partial^3 N_2}{\partial\zeta^2\partial\eta} = \frac{1}{4}(-1-\xi) \qquad \frac{\partial^3 N_{12}}{\partial\zeta^2\partial\eta} = 0$$
$$\frac{\partial^3 N_{13}}{\partial\zeta^2\partial\xi} = 0 \qquad \frac{\partial^3 N_3}{\partial\zeta^2\partial\eta} = \frac{1}{4}(1+\xi) \qquad \frac{\partial^3 N_{13}}{\partial\zeta^2\partial\eta} = 0$$
$$\frac{\partial^3 N_{14}}{\partial\zeta^2\partial\xi} = 0 \qquad \frac{\partial^3 N_4}{\partial\zeta^2\partial\eta} = \frac{1}{4}(1-\xi) \qquad \frac{\partial^3 N_{14}}{\partial\zeta^2\partial\eta} = 0$$
$$\frac{\partial^3 N_{15}}{\partial\zeta^2\partial\xi} = 0 \qquad \frac{\partial^3 N_5}{\partial\zeta^2\partial\eta} = \frac{1}{4}(-1+\xi) \qquad \frac{\partial^3 N_{15}}{\partial\zeta^2\partial\eta} = 0$$
$$\frac{\partial^3 N_{16}}{\partial\zeta^2\partial\xi} = 0 \qquad \frac{\partial^3 N_6}{\partial\zeta^2\partial\eta} = \frac{1}{4}(-1-\xi) \qquad \frac{\partial^3 N_{16}}{\partial\zeta^2\partial\eta} = 0$$
$$\frac{\partial^3 N_{17}}{\partial\zeta^2\partial\xi} = \frac{1}{2}(1-\eta) \qquad \frac{\partial^3 N_7}{\partial\zeta^2\partial\eta} = \frac{1}{4}(1+\xi) \qquad \frac{\partial^3 N_{17}}{\partial\zeta^2\partial\eta} = \frac{1}{2}(1-\xi)$$
$$\frac{\partial^3 N_{18}}{\partial\zeta^2\partial\xi} = \frac{1}{2}(-1+\eta) \qquad \frac{\partial^3 N_8}{\partial\zeta^2\partial\eta} = \frac{1}{4}(1-\xi) \qquad \frac{\partial^3 N_{18}}{\partial\zeta^2\partial\eta} = \frac{1}{2}(1+\xi)$$
$$\frac{\partial^3 N_{19}}{\partial\zeta^2\partial\xi} = \frac{1}{2}(-1-\eta) \qquad \frac{\partial^3 N_9}{\partial\zeta^2\partial\eta} = 0 \qquad \frac{\partial^3 N_{19}}{\partial\zeta^2\partial\eta} = \frac{1}{2}(-1-\xi)$$
$$\frac{\partial^3 N_{20}}{\partial\zeta^2\partial\xi} = \frac{1}{2}(1+\eta) \qquad \frac{\partial^3 N_{10}}{\partial\zeta^2\partial\eta} = 0 \qquad \frac{\partial^3 N_{20}}{\partial\zeta^2\partial\eta} = \frac{1}{2}(-1+\xi)$$

$$
\begin{aligned}
\frac{\partial^3 N_1}{\partial\xi\partial\eta\partial\zeta} &= \frac{1}{8}(-1+2\xi+2\eta+2\zeta) & \frac{\partial^3 N_{11}}{\partial\xi\partial\eta\partial\zeta} &= \frac{1}{2}(\xi)\\
\frac{\partial^3 N_2}{\partial\xi\partial\eta\partial\zeta} &= \frac{1}{8}(1+2\xi-2\eta-2\zeta) & \frac{\partial^3 N_{12}}{\partial\xi\partial\eta\partial\zeta} &= \frac{1}{2}(-\eta)\\
\frac{\partial^3 N_3}{\partial\xi\partial\eta\partial\zeta} &= \frac{1}{8}(-1-2\xi-2\eta+2\zeta) & \frac{\partial^3 N_{13}}{\partial\xi\partial\eta\partial\zeta} &= \frac{1}{2}(\xi)\\
\frac{\partial^3 N_4}{\partial\xi\partial\eta\partial\zeta} &= \frac{1}{8}(1-2\xi+2\eta-2\zeta) & \frac{\partial^3 N_{14}}{\partial\xi\partial\eta\partial\zeta} &= \frac{1}{2}(-\eta)\\
\frac{\partial^3 N_5}{\partial\xi\partial\eta\partial\zeta} &= \frac{1}{8}(1-2\xi-2\eta+2\zeta) & \frac{\partial^3 N_{15}}{\partial\xi\partial\eta\partial\zeta} &= \frac{1}{2}(-\xi)\\
\frac{\partial^3 N_6}{\partial\xi\partial\eta\partial\zeta} &= \frac{1}{8}(-1-2\xi+2\eta-2\zeta) & \frac{\partial^3 N_{16}}{\partial\xi\partial\eta\partial\zeta} &= \frac{1}{2}(\eta)\\
\frac{\partial^3 N_7}{\partial\xi\partial\eta\partial\zeta} &= \frac{1}{8}(1+2\xi+2\eta+2\zeta) & \frac{\partial^3 N_{17}}{\partial\xi\partial\eta\partial\zeta} &= \frac{1}{2}(-\zeta)\\
\frac{\partial^3 N_8}{\partial\xi\partial\eta\partial\zeta} &= \frac{1}{8}(-1+2\xi-2\eta-2\zeta) & \frac{\partial^3 N_{18}}{\partial\xi\partial\eta\partial\zeta} &= \frac{1}{2}(\zeta)\\
\frac{\partial^3 N_9}{\partial\xi\partial\eta\partial\zeta} &= \frac{1}{2}(-\xi) & \frac{\partial^3 N_{19}}{\partial\xi\partial\eta\partial\zeta} &= \frac{1}{2}(-\zeta)\\
\frac{\partial^3 N_{10}}{\partial\xi\partial\eta\partial\zeta} &= \frac{1}{2}(\eta) & \frac{\partial^3 N_{20}}{\partial\xi\partial\eta\partial\zeta} &= \frac{1}{2}(\zeta)
\end{aligned}
\tag{B.5}
$$

The polarisation gradient in Equation (4.35) can be obtained by multiplying Equations (4.53) (B.3), (B.2), (B.1), and (4.47) together, and taking its divergence:

$$
\begin{aligned}
\nabla \cdot \tilde{\mathbf{P}} = \tilde{f}_{1111} \Bigg[& \left(d_x^1\right) \frac{\partial^3 N_1}{\partial x^3} + \left(d_x^2\right) \frac{\partial^3 N_2}{\partial x^3} + \left(d_x^3\right) \frac{\partial^3 N_3}{\partial x^3} + \left(d_x^4\right) \frac{\partial^3 N_4}{\partial x^3} + \left(d_x^5\right) \frac{\partial^3 N_5}{\partial x^3} + \\
& \left(d_x^6\right) \frac{\partial^3 N_6}{\partial x^3} + \left(d_x^7\right) \frac{\partial^3 N_7}{\partial x^3} + \left(d_x^8\right) \frac{\partial^3 N_8}{\partial x^3} + \left(d_x^9\right) \frac{\partial^3 N_9}{\partial x^3} + \left(d_x^{10}\right) \frac{\partial^3 N_{10}}{\partial x^3} + \\
& \left(d_x^{11}\right) \frac{\partial^3 N_{11}}{\partial x^3} + \left(d_x^{12}\right) \frac{\partial^3 N_{12}}{\partial x^3} + \left(d_x^{13}\right) \frac{\partial^3 N_{13}}{\partial x^3} + \left(d_x^{14}\right) \frac{\partial^3 N_{14}}{\partial x^3} + \left(d_x^{15}\right) \frac{\partial^3 N_{15}}{\partial x^3} + \\
& \left(d_x^{16}\right) \frac{\partial^3 N_{16}}{\partial x^3} + \left(d_x^{17}\right) \frac{\partial^3 N_{17}}{\partial x^3} + \left(d_x^{18}\right) \frac{\partial^3 N_{18}}{\partial x^3} + \left(d_x^{19}\right) \frac{\partial^3 N_{19}}{\partial x^3} + \left(d_x^{20}\right) \frac{\partial^3 N_{20}}{\partial x^3} \Bigg] + \\
\tilde{f}_{1112} \Bigg[& \left(d_x^1\right) \frac{\partial^3 N_1}{\partial x^2 \partial y} + \left(d_x^2\right) \frac{\partial^3 N_2}{\partial x^2 \partial y} + \left(d_x^3\right) \frac{\partial^3 N_3}{\partial x^2 \partial y} + \left(d_x^4\right) \frac{\partial^3 N_4}{\partial x^2 \partial y} + \left(d_x^5\right) \frac{\partial^3 N_5}{\partial x^2 \partial y} + \\
& \left(d_x^6\right) \frac{\partial^3 N_6}{\partial x^2 \partial y} + \left(d_x^7\right) \frac{\partial^3 N_7}{\partial x^2 \partial y} + \left(d_x^8\right) \frac{\partial^3 N_8}{\partial x^2 \partial y} + \left(d_x^9\right) \frac{\partial^3 N_9}{\partial x^2 \partial y} + \left(d_x^{10}\right) \frac{\partial^3 N_{10}}{\partial x^2 \partial y} + \\
& \left(d_x^{11}\right) \frac{\partial^3 N_{11}}{\partial x^2 \partial y} + \left(d_x^{12}\right) \frac{\partial^3 N_{12}}{\partial x^2 \partial y} + \left(d_x^{13}\right) \frac{\partial^3 N_{13}}{\partial x^2 \partial y} + \left(d_x^{14}\right) \frac{\partial^3 N_{14}}{\partial x^2 \partial y} + \left(d_x^{15}\right) \frac{\partial^3 N_{15}}{\partial x^2 \partial y} + \\
& \left(d_x^{16}\right) \frac{\partial^3 N_{16}}{\partial x^2 \partial y} + \left(d_x^{17}\right) \frac{\partial^3 N_{17}}{\partial x^2 \partial y} + \left(d_x^{18}\right) \frac{\partial^3 N_{18}}{\partial x^2 \partial y} + \left(d_x^{19}\right) \frac{\partial^3 N_{19}}{\partial x^2 \partial y} + \left(d_x^{20}\right) \frac{\partial^3 N_{20}}{\partial x^2 \partial y} \Bigg] + \\
\tilde{f}_{1113} \Bigg[& \left(d_x^1\right) \frac{\partial^3 N_1}{\partial x^2 \partial z} + \left(d_x^2\right) \frac{\partial^3 N_2}{\partial x^2 \partial z} + \left(d_x^3\right) \frac{\partial^3 N_3}{\partial x^2 \partial z} + \left(d_x^4\right) \frac{\partial^3 N_4}{\partial x^2 \partial z} + \left(d_x^5\right) \frac{\partial^3 N_5}{\partial x^2 \partial z} + \\
& \left(d_x^6\right) \frac{\partial^3 N_6}{\partial x^2 \partial z} + \left(d_x^7\right) \frac{\partial^3 N_7}{\partial x^2 \partial z} + \left(d_x^8\right) \frac{\partial^3 N_8}{\partial x^2 \partial z} + \left(d_x^9\right) \frac{\partial^3 N_9}{\partial x^2 \partial z} + \left(d_x^{10}\right) \frac{\partial^3 N_{10}}{\partial x^2 \partial z} + \\
& \left(d_x^{11}\right) \frac{\partial^3 N_{11}}{\partial x^2 \partial z} + \left(d_x^{12}\right) \frac{\partial^3 N_{12}}{\partial x^2 \partial z} + \left(d_x^{13}\right) \frac{\partial^3 N_{13}}{\partial x^2 \partial z} + \left(d_x^{14}\right) \frac{\partial^3 N_{14}}{\partial x^2 \partial z} + \left(d_x^{15}\right) \frac{\partial^3 N_{15}}{\partial x^2 \partial z} + \\
& \left(d_x^{16}\right) \frac{\partial^3 N_{16}}{\partial x^2 \partial z} + \left(d_x^{17}\right) \frac{\partial^3 N_{17}}{\partial x^2 \partial z} + \left(d_x^{18}\right) \frac{\partial^3 N_{18}}{\partial x^2 \partial z} + \left(d_x^{19}\right) \frac{\partial^3 N_{19}}{\partial x^2 \partial z} + \left(d_x^{20}\right) \frac{\partial^3 N_{20}}{\partial x^2 \partial z} \Bigg] + \\
\end{aligned}
$$

$$
\begin{aligned}
\tilde{f}_{1221}\Bigg[& \left(d_y^1\right)\frac{\partial^3 N_1}{\partial x^2\partial y}+\left(d_y^2\right)\frac{\partial^3 N_2}{\partial x^2\partial y}+\left(d_y^3\right)\frac{\partial^3 N_3}{\partial x^2\partial y}+\left(d_y^4\right)\frac{\partial^3 N_4}{\partial x^2\partial y}+\left(d_y^5\right)\frac{\partial^3 N_5}{\partial x^2\partial y}+\\
& \left(d_y^6\right)\frac{\partial^3 N_6}{\partial x^2\partial y}+\left(d_y^7\right)\frac{\partial^3 N_7}{\partial x^2\partial y}+\left(d_y^8\right)\frac{\partial^3 N_8}{\partial x^2\partial y}+\left(d_y^9\right)\frac{\partial^3 N_9}{\partial x^2\partial y}+\left(d_y^{10}\right)\frac{\partial^3 N_{10}}{\partial x^2\partial y}+\\
& \left(d_y^{11}\right)\frac{\partial^3 N_{11}}{\partial x^2\partial y}+\left(d_y^{12}\right)\frac{\partial^3 N_{12}}{\partial x^2\partial y}+\left(d_y^{13}\right)\frac{\partial^3 N_{13}}{\partial x^2\partial y}+\left(d_y^{14}\right)\frac{\partial^3 N_{14}}{\partial x^2\partial y}+\left(d_y^{15}\right)\frac{\partial^3 N_{15}}{\partial x^2\partial y}+\\
& \left(d_y^{16}\right)\frac{\partial^3 N_{16}}{\partial x^2\partial y}+\left(d_y^{17}\right)\frac{\partial^3 N_{17}}{\partial x^2\partial y}+\left(d_y^{18}\right)\frac{\partial^3 N_{18}}{\partial x^2\partial y}+\left(d_y^{19}\right)\frac{\partial^3 N_{19}}{\partial x^2\partial y}+\left(d_y^{20}\right)\frac{\partial^3 N_{20}}{\partial x^2\partial y}\Bigg]+\\
\tilde{f}_{1222}\Bigg[& \left(d_y^1\right)\frac{\partial^3 N_1}{\partial x\partial y^2}+\left(d_y^2\right)\frac{\partial^3 N_2}{\partial x\partial y^2}+\left(d_y^3\right)\frac{\partial^3 N_3}{\partial x\partial y^2}+\left(d_y^4\right)\frac{\partial^3 N_4}{\partial x\partial y^2}+\left(d_y^5\right)\frac{\partial^3 N_5}{\partial x\partial y^2}+\\
& \left(d_y^6\right)\frac{\partial^3 N_6}{\partial x\partial y^2}+\left(d_y^7\right)\frac{\partial^3 N_7}{\partial x\partial y^2}+\left(d_y^8\right)\frac{\partial^3 N_8}{\partial x\partial y^2}+\left(d_y^9\right)\frac{\partial^3 N_9}{\partial x\partial y^2}+\left(d_y^{10}\right)\frac{\partial^3 N_{10}}{\partial x\partial y^2}+\\
& \left(d_y^{11}\right)\frac{\partial^3 N_{11}}{\partial x\partial y^2}+\left(d_y^{12}\right)\frac{\partial^3 N_{12}}{\partial x\partial y^2}+\left(d_y^{13}\right)\frac{\partial^3 N_{13}}{\partial x\partial y^2}+\left(d_y^{14}\right)\frac{\partial^3 N_{14}}{\partial x\partial y^2}+\left(d_y^{15}\right)\frac{\partial^3 N_{15}}{\partial x\partial y^2}+\\
& \left(d_y^{16}\right)\frac{\partial^3 N_{16}}{\partial x\partial y^2}+\left(d_y^{17}\right)\frac{\partial^3 N_{17}}{\partial x\partial y^2}+\left(d_y^{18}\right)\frac{\partial^3 N_{18}}{\partial x\partial y^2}+\left(d_y^{19}\right)\frac{\partial^3 N_{19}}{\partial x\partial y^2}+\left(d_y^{20}\right)\frac{\partial^3 N_{20}}{\partial x\partial y^2}\Bigg]+\\
\tilde{f}_{1223}\Bigg[& \left(d_y^1\right)\frac{\partial^3 N_1}{\partial x\partial y\partial z}+\left(d_y^2\right)\frac{\partial^3 N_2}{\partial x\partial y\partial z}+\left(d_y^3\right)\frac{\partial^3 N_3}{\partial x\partial y\partial z}+\left(d_y^4\right)\frac{\partial^3 N_4}{\partial x\partial y\partial z}+\left(d_y^5\right)\frac{\partial^3 N_5}{\partial x\partial y\partial z}+\\
& \left(d_y^6\right)\frac{\partial^3 N_6}{\partial x\partial y\partial z}+\left(d_y^7\right)\frac{\partial^3 N_7}{\partial x\partial y\partial z}+\left(d_y^8\right)\frac{\partial^3 N_8}{\partial x\partial y\partial z}+\left(d_y^9\right)\frac{\partial^3 N_9}{\partial x\partial y\partial z}+\left(d_y^{10}\right)\frac{\partial^3 N_{10}}{\partial x\partial y\partial z}+\\
& \left(d_y^{11}\right)\frac{\partial^3 N_{11}}{\partial x\partial y\partial z}+\left(d_y^{12}\right)\frac{\partial^3 N_{12}}{\partial x\partial y\partial z}+\left(d_y^{13}\right)\frac{\partial^3 N_{13}}{\partial x\partial y\partial z}+\left(d_y^{14}\right)\frac{\partial^3 N_{14}}{\partial x\partial y\partial z}+\left(d_y^{15}\right)\frac{\partial^3 N_{15}}{\partial x\partial y\partial z}+\\
& \left(d_y^{16}\right)\frac{\partial^3 N_{16}}{\partial x\partial y\partial z}+\left(d_y^{17}\right)\frac{\partial^3 N_{17}}{\partial x\partial y\partial z}+\left(d_y^{18}\right)\frac{\partial^3 N_{18}}{\partial x\partial y\partial z}+\left(d_y^{19}\right)\frac{\partial^3 N_{19}}{\partial x\partial y\partial z}+\left(d_y^{20}\right)\frac{\partial^3 N_{20}}{\partial x\partial y\partial z}\Bigg]+
\end{aligned}
$$

$$
\begin{aligned}
\tilde{f}_{1331}\Bigg[& \left(d_z^1\right)\frac{\partial^3 N_1}{\partial x^2\partial z}+\left(d_z^2\right)\frac{\partial^3 N_2}{\partial x^2\partial z}+\left(d_z^3\right)\frac{\partial^3 N_3}{\partial x^2\partial z}+\left(d_z^4\right)\frac{\partial^3 N_4}{\partial x^2\partial z}+\left(d_z^5\right)\frac{\partial^3 N_5}{\partial x^2\partial z}+\\
& \left(d_z^6\right)\frac{\partial^3 N_6}{\partial x^2\partial z}+\left(d_z^7\right)\frac{\partial^3 N_7}{\partial x^2\partial z}+\left(d_z^8\right)\frac{\partial^3 N_8}{\partial x^2\partial z}+\left(d_z^9\right)\frac{\partial^3 N_9}{\partial x^2\partial z}+\left(d_z^{10}\right)\frac{\partial^3 N_{10}}{\partial x^2\partial z}+\\
& \left(d_z^{11}\right)\frac{\partial^3 N_{11}}{\partial x^2\partial z}+\left(d_z^{12}\right)\frac{\partial^3 N_{12}}{\partial x^2\partial z}+\left(d_z^{13}\right)\frac{\partial^3 N_{13}}{\partial x^2\partial z}+\left(d_z^{14}\right)\frac{\partial^3 N_{14}}{\partial x^2\partial z}+\left(d_z^{15}\right)\frac{\partial^3 N_{15}}{\partial x^2\partial z}+\\
& \left(d_z^{16}\right)\frac{\partial^3 N_{16}}{\partial x^2\partial z}+\left(d_z^{17}\right)\frac{\partial^3 N_{17}}{\partial x^2\partial z}+\left(d_z^{18}\right)\frac{\partial^3 N_{18}}{\partial x^2\partial z}+\left(d_z^{19}\right)\frac{\partial^3 N_{19}}{\partial x^2\partial z}+\left(d_z^{20}\right)\frac{\partial^3 N_{20}}{\partial x^2\partial z}\Bigg]+\\
\tilde{f}_{1332}\Bigg[& \left(d_z^1\right)\frac{\partial^3 N_1}{\partial x\partial y\partial z}+\left(d_z^2\right)\frac{\partial^3 N_2}{\partial x\partial y\partial z}+\left(d_z^3\right)\frac{\partial^3 N_3}{\partial x\partial y\partial z}+\left(d_z^4\right)\frac{\partial^3 N_4}{\partial x\partial y\partial z}+\left(d_z^5\right)\frac{\partial^3 N_5}{\partial x\partial y\partial z}+\\
& \left(d_z^6\right)\frac{\partial^3 N_6}{\partial x\partial y\partial z}+\left(d_z^7\right)\frac{\partial^3 N_7}{\partial x\partial y\partial z}+\left(d_z^8\right)\frac{\partial^3 N_8}{\partial x\partial y\partial z}+\left(d_z^9\right)\frac{\partial^3 N_9}{\partial x\partial y\partial z}+\left(d_z^{10}\right)\frac{\partial^3 N_{10}}{\partial x\partial y\partial z}+\\
& \left(d_z^{11}\right)\frac{\partial^3 N_{11}}{\partial x\partial y\partial z}+\left(d_z^{12}\right)\frac{\partial^3 N_{12}}{\partial x\partial y\partial z}+\left(d_z^{13}\right)\frac{\partial^3 N_{13}}{\partial x\partial y\partial z}+\left(d_z^{14}\right)\frac{\partial^3 N_{14}}{\partial x\partial y\partial z}+\left(d_z^{15}\right)\frac{\partial^3 N_{15}}{\partial x\partial y\partial z}+\\
& \left(d_z^{16}\right)\frac{\partial^3 N_{16}}{\partial x\partial y\partial z}+\left(d_z^{17}\right)\frac{\partial^3 N_{17}}{\partial x\partial y\partial z}+\left(d_z^{18}\right)\frac{\partial^3 N_{18}}{\partial x\partial y\partial z}+\left(d_z^{19}\right)\frac{\partial^3 N_{19}}{\partial x\partial y\partial z}+\left(d_z^{20}\right)\frac{\partial^3 N_{20}}{\partial x\partial y\partial z}\Bigg]+\\
\tilde{f}_{1333}\Bigg[& \left(d_z^1\right)\frac{\partial^3 N_1}{\partial x\partial z^2}+\left(d_z^2\right)\frac{\partial^3 N_2}{\partial x\partial z^2}+\left(d_z^3\right)\frac{\partial^3 N_3}{\partial x\partial z^2}+\left(d_z^4\right)\frac{\partial^3 N_4}{\partial x\partial z^2}+\left(d_z^5\right)\frac{\partial^3 N_5}{\partial x\partial z^2}+\\
& \left(d_z^6\right)\frac{\partial^3 N_6}{\partial x\partial z^2}+\left(d_z^7\right)\frac{\partial^3 N_7}{\partial x\partial z^2}+\left(d_z^8\right)\frac{\partial^3 N_8}{\partial x\partial z^2}+\left(d_z^9\right)\frac{\partial^3 N_9}{\partial x\partial z^2}+\left(d_z^{10}\right)\frac{\partial^3 N_{10}}{\partial x\partial z^2}+\\
& \left(d_z^{11}\right)\frac{\partial^3 N_{11}}{\partial x\partial z^2}+\left(d_z^{12}\right)\frac{\partial^3 N_{12}}{\partial x\partial z^2}+\left(d_z^{13}\right)\frac{\partial^3 N_{13}}{\partial x\partial z^2}+\left(d_z^{14}\right)\frac{\partial^3 N_{14}}{\partial x\partial z^2}+\left(d_z^{15}\right)\frac{\partial^3 N_{15}}{\partial x\partial z^2}+\\
& \left(d_z^{16}\right)\frac{\partial^3 N_{16}}{\partial x\partial z^2}+\left(d_z^{17}\right)\frac{\partial^3 N_{17}}{\partial x\partial z^2}+\left(d_z^{18}\right)\frac{\partial^3 N_{18}}{\partial x\partial z^2}+\left(d_z^{19}\right)\frac{\partial^3 N_{19}}{\partial x\partial z^2}+\left(d_z^{20}\right)\frac{\partial^3 N_{20}}{\partial x\partial z^2}\Bigg]+
\end{aligned}
$$

$$
\begin{aligned}
\tilde{f}_{1121}\Bigg[& \left(d_x^1\right)\frac{\partial^3 N_1}{\partial x^2\partial y}+\left(d_y^1\right)\frac{\partial^3 N_1}{\partial x^3}+\left(d_x^2\right)\frac{\partial^3 N_2}{\partial x^2\partial y}+\left(d_y^2\right)\frac{\partial^2 N_2}{\partial x^3}+\left(d_x^3\right)\frac{\partial^3 N_3}{\partial x^2\partial y}+\\
& \left(d_y^3\right)\frac{\partial^3 N_3}{\partial x^3}+\left(d_x^4\right)\frac{\partial^3 N_4}{\partial x^2\partial y}+\left(d_y^4\right)\frac{\partial^3 N_4}{\partial x^3}+\left(d_x^5\right)\frac{\partial^3 N_5}{\partial x^2\partial y}+\left(d_y^5\right)\frac{\partial^3 N_5}{\partial x^3}+\\
& \left(d_x^6\right)\frac{\partial^3 N_6}{\partial x^2\partial y}+\left(d_y^6\right)\frac{\partial^3 N_6}{\partial x^3}+\left(d_x^7\right)\frac{\partial^3 N_7}{\partial x^2\partial y}+\left(d_y^7\right)\frac{\partial^3 N_7}{\partial x^3}+\left(d_x^8\right)\frac{\partial^3 N_8}{\partial x^2\partial y}+\\
& \left(d_y^8\right)\frac{\partial^3 N_8}{\partial x^3}+\left(d_x^9\right)\frac{\partial^3 N_9}{\partial x^2\partial y}+\left(d_y^9\right)\frac{\partial^3 N_9}{\partial x^3}+\left(d_x^{10}\right)\frac{\partial^3 N_{10}}{\partial x^2\partial y}+\left(d_y^{10}\right)\frac{\partial^3 N_{10}}{\partial x^3}+\\
& \left(d_x^{11}\right)\frac{\partial^3 N_{11}}{\partial x^2\partial y}+\left(d_y^{11}\right)\frac{\partial^3 N_{11}}{\partial x^3}+\left(d_x^{12}\right)\frac{\partial^3 N_{12}}{\partial x^2\partial y}+\left(d_y^{12}\right)\frac{\partial^3 N_{12}}{\partial x^3}+\left(d_x^{13}\right)\frac{\partial^3 N_{13}}{\partial x^2\partial y}+\\
& \left(d_y^{13}\right)\frac{\partial^3 N_{13}}{\partial x^3}+\left(d_x^{14}\right)\frac{\partial^3 N_{14}}{\partial x^2\partial y}+\left(d_y^{14}\right)\frac{\partial^3 N_{14}}{\partial x^3}+\left(d_x^{15}\right)\frac{\partial^3 N_{15}}{\partial x^2\partial y}+\left(d_y^{15}\right)\frac{\partial^3 N_{15}}{\partial x^3}+\\
& \left(d_x^{16}\right)\frac{\partial^3 N_{16}}{\partial x^2\partial y}+\left(d_y^{16}\right)\frac{\partial^3 N_{16}}{\partial x^3}+\left(d_x^{17}\right)\frac{\partial^3 N_{17}}{\partial x^2\partial y}+\left(d_y^{17}\right)\frac{\partial^3 N_{17}}{\partial x^3}+\left(d_x^{18}\right)\frac{\partial^3 N_{18}}{\partial x^2\partial y}+\\
& \left(d_y^{18}\right)\frac{\partial^3 N_{18}}{\partial x^3}+\left(d_x^{19}\right)\frac{\partial^3 N_{19}}{\partial x^2\partial y}+\left(d_y^{19}\right)\frac{\partial^3 N_{19}}{\partial x^3}+\left(d_x^{20}\right)\frac{\partial^3 N_{20}}{\partial x^2\partial y}+\left(d_y^{20}\right)\frac{\partial^3 N_{20}}{\partial x^3}\Bigg]+\\
\tilde{f}_{1122}\Bigg[& \left(d_x^1\right)\frac{\partial^3 N_1}{\partial x\partial y^2}+\left(d_y^1\right)\frac{\partial^3 N_1}{\partial x^2\partial y}+\left(d_x^2\right)\frac{\partial^3 N_2}{\partial x\partial y^2}+\left(d_y^2\right)\frac{\partial^3 N_2}{\partial x^2\partial y}+\left(d_x^3\right)\frac{\partial^3 N_3}{\partial x\partial y^2}+\\
& \left(d_y^3\right)\frac{\partial^3 N_3}{\partial x^2\partial y}+\left(d_x^4\right)\frac{\partial^2 N_4}{\partial x\partial y^2}+\left(d_y^4\right)\frac{\partial^3 N_4}{\partial x^2\partial y}+\left(d_x^5\right)\frac{\partial^3 N_5}{\partial x\partial y^2}+\left(d_y^5\right)\frac{\partial^3 N_5}{\partial x^2\partial y}+\\
& \left(d_x^6\right)\frac{\partial^3 N_6}{\partial x\partial y^2}+\left(d_y^6\right)\frac{\partial^3 N_6}{\partial x^2\partial y}+\left(d_x^7\right)\frac{\partial^3 N_7}{\partial x\partial y^2}+\left(d_y^7\right)\frac{\partial^3 N_7}{\partial x^2\partial y}+\left(d_x^8\right)\frac{\partial^3 N_8}{\partial x\partial y^2}+\\
& \left(d_y^8\right)\frac{\partial^3 N_8}{\partial x^2\partial y}+\left(d_x^9\right)\frac{\partial^3 N_9}{\partial x\partial y^2}+\left(d_y^9\right)\frac{\partial^3 N_9}{\partial x^2\partial y}+\left(d_x^{10}\right)\frac{\partial^3 N_{10}}{\partial x\partial y^2}+\left(d_y^{10}\right)\frac{\partial^3 N_{10}}{\partial x^2\partial y}+\\
& \left(d_x^{11}\right)\frac{\partial^3 N_{11}}{\partial x\partial y^2}+\left(d_y^{11}\right)\frac{\partial^3 N_{11}}{\partial x^2\partial y}+\left(d_x^{12}\right)\frac{\partial^3 N_{12}}{\partial x\partial y^2}+\left(d_y^{12}\right)\frac{\partial^3 N_{12}}{\partial x^2\partial y}+\left(d_x^{13}\right)\frac{\partial^3 N_{13}}{\partial x\partial y^2}+\\
& \left(d_y^{13}\right)\frac{\partial^3 N_{13}}{\partial x^2\partial y}+\left(d_x^{14}\right)\frac{\partial^3 N_{14}}{\partial x\partial y^2}+\left(d_y^{14}\right)\frac{\partial^3 N_{14}}{\partial x^2\partial y}+\left(d_x^{15}\right)\frac{\partial^3 N_{15}}{\partial x\partial y^2}+\left(d_y^{15}\right)\frac{\partial^3 N_{15}}{\partial x^2\partial y}+\\
& \left(d_x^{16}\right)\frac{\partial^3 N_{16}}{\partial x\partial y^2}+\left(d_y^{16}\right)\frac{\partial^3 N_{16}}{\partial x^2\partial y}+\left(d_x^{17}\right)\frac{\partial^3 N_{17}}{\partial x\partial y^2}+\left(d_y^{17}\right)\frac{\partial^3 N_{17}}{\partial x^2\partial y}+\left(d_x^{18}\right)\frac{\partial^3 N_{18}}{\partial x\partial y^2}+\\
& \left(d_y^{18}\right)\frac{\partial^3 N_{18}}{\partial x^2\partial y}+\left(d_x^{19}\right)\frac{\partial^3 N_{19}}{\partial x\partial y^2}+\left(d_y^{19}\right)\frac{\partial^3 N_{19}}{\partial x^2\partial y}+\left(d_x^{20}\right)\frac{\partial^3 N_{20}}{\partial x\partial y^2}+\left(d_y^{20}\right)\frac{\partial^3 N_{20}}{\partial x^2\partial y}\Bigg]+
\end{aligned}
$$

$$
\begin{aligned}
\tilde{f}_{1123}\Bigg[& \left(d_x^1\right)\frac{\partial^3 N_1}{\partial x\partial y\partial z}+\left(d_y^1\right)\frac{\partial^3 N_1}{\partial x^2\partial z}+\left(d_x^2\right)\frac{\partial^3 N_2}{\partial x\partial y\partial z}+\left(d_y^2\right)\frac{\partial^3 N_2}{\partial x^2\partial z}+\left(d_x^3\right)\frac{\partial^3 N_3}{\partial x\partial y\partial z}+\\
& \left(d_y^3\right)\frac{\partial^3 N_3}{\partial x^2\partial z}+\left(d_x^4\right)\frac{\partial^3 N_4}{\partial x\partial y\partial z}+\left(d_y^4\right)\frac{\partial^3 N_4}{\partial x^2\partial z}+\left(d_x^5\right)\frac{\partial^3 N_5}{\partial x\partial y\partial z}+\left(d_y^5\right)\frac{\partial^3 N_5}{\partial x^2\partial z}+\\
& \left(d_x^6\right)\frac{\partial^3 N_6}{\partial x\partial y\partial z}+\left(d_y^6\right)\frac{\partial^3 N_6}{\partial x^2\partial z}+\left(d_x^7\right)\frac{\partial^3 N_7}{\partial x\partial y\partial z}+\left(d_y^7\right)\frac{\partial^3 N_7}{\partial x^2\partial z}+\left(d_x^8\right)\frac{\partial^3 N_8}{\partial x\partial y\partial z}+\\
& \left(d_y^8\right)\frac{\partial^3 N_8}{\partial x^2\partial z}+\left(d_x^9\right)\frac{\partial^3 N_9}{\partial x\partial y\partial z}+\left(d_y^9\right)\frac{\partial^3 N_9}{\partial x^2\partial z}+\left(d_x^{10}\right)\frac{\partial^3 N_{10}}{\partial x\partial y\partial z}+\left(d_y^{10}\right)\frac{\partial^3 N_{10}}{\partial x^2\partial z}+\\
& \left(d_x^{11}\right)\frac{\partial^3 N_{11}}{\partial x\partial y\partial z}+\left(d_y^{11}\right)\frac{\partial^3 N_{11}}{\partial x^2\partial z}+\left(d_x^{12}\right)\frac{\partial^3 N_{12}}{\partial x\partial y\partial z}+\left(d_y^{12}\right)\frac{\partial^3 N_{12}}{\partial x^2\partial z}+\left(d_x^{13}\right)\frac{\partial^3 N_{13}}{\partial x\partial y\partial z}+\\
& \left(d_y^{13}\right)\frac{\partial^3 N_{13}}{\partial x^2\partial z}+\left(d_x^{14}\right)\frac{\partial^3 N_{14}}{\partial x\partial y\partial z}+\left(d_y^{14}\right)\frac{\partial^3 N_{14}}{\partial x^2\partial z}+\left(d_x^{15}\right)\frac{\partial^3 N_{15}}{\partial x\partial y\partial z}+\left(d_y^{15}\right)\frac{\partial^3 N_{15}}{\partial x^2\partial z}+\\
& \left(d_x^{16}\right)\frac{\partial^3 N_{16}}{\partial x\partial y\partial z}+\left(d_y^{16}\right)\frac{\partial^3 N_{16}}{\partial x^2\partial z}+\left(d_x^{17}\right)\frac{\partial^3 N_{17}}{\partial x\partial y\partial z}+\left(d_y^{17}\right)\frac{\partial^3 N_{17}}{\partial x^2\partial z}+\left(d_x^{18}\right)\frac{\partial^3 N_{18}}{\partial x\partial y\partial z}+\\
& \left(d_y^{18}\right)\frac{\partial^3 N_{18}}{\partial x^2\partial z}+\left(d_x^{19}\right)\frac{\partial^3 N_{19}}{\partial x\partial y\partial z}+\left(d_y^{19}\right)\frac{\partial^3 N_{19}}{\partial x^2\partial z}+\left(d_x^{20}\right)\frac{\partial^3 N_{20}}{\partial x\partial y\partial z}+\left(d_y^{20}\right)\frac{\partial^3 N_{20}}{\partial x^2\partial z}\Bigg]+\\
\tilde{f}_{1131}\Bigg[& \left(d_x^1\right)\frac{\partial^3 N_1}{\partial x^2\partial z}+\left(d_z^1\right)\frac{\partial^3 N_1}{\partial x^3}+\left(d_x^2\right)\frac{\partial^3 N_2}{\partial x^2\partial z}+\left(d_z^2\right)\frac{\partial^3 N_2}{\partial x^3}+\left(d_x^3\right)\frac{\partial^3 N_3}{\partial x^2\partial z}+\\
& \left(d_z^3\right)\frac{\partial^3 N_3}{\partial x^3}+\left(d_x^4\right)\frac{\partial^3 N_4}{\partial x^2\partial z}+\left(d_z^4\right)\frac{\partial^3 N_4}{\partial x^3}+\left(d_x^5\right)\frac{\partial^3 N_5}{\partial x^2\partial z}+\left(d_z^5\right)\frac{\partial^3 N_5}{\partial x^3}+\\
& \left(d_x^6\right)\frac{\partial^3 N_6}{\partial x^2\partial z}+\left(d_z^6\right)\frac{\partial^3 N_6}{\partial x^3}+\left(d_x^7\right)\frac{\partial^3 N_7}{\partial x^2\partial z}+\left(d_z^7\right)\frac{\partial^3 N_7}{\partial x^3}+\left(d_x^8\right)\frac{\partial^3 N_8}{\partial x^2\partial z}+\\
& \left(d_z^8\right)\frac{\partial^3 N_8}{\partial x^3}+\left(d_x^9\right)\frac{\partial^3 N_9}{\partial x^2\partial z}+\left(d_z^9\right)\frac{\partial^3 N_9}{\partial x^3}+\left(d_x^{10}\right)\frac{\partial^3 N_{10}}{\partial x^2\partial z}+\left(d_z^{10}\right)\frac{\partial^3 N_{10}}{\partial x^3}+\\
& \left(d_x^{11}\right)\frac{\partial^3 N_{11}}{\partial x^2\partial z}+\left(d_z^{11}\right)\frac{\partial^3 N_{11}}{\partial x^3}+\left(d_x^{12}\right)\frac{\partial^3 N_{12}}{\partial x^2\partial z}+\left(d_z^{12}\right)\frac{\partial^3 N_{12}}{\partial x^3}+\left(d_x^{13}\right)\frac{\partial^3 N_{13}}{\partial x^2\partial z}+\\
& \left(d_z^{13}\right)\frac{\partial^3 N_{13}}{\partial x^3}+\left(d_x^{14}\right)\frac{\partial^3 N_{14}}{\partial x^2\partial z}+\left(d_z^{14}\right)\frac{\partial^3 N_{14}}{\partial x^3}+\left(d_x^{15}\right)\frac{\partial^3 N_{15}}{\partial x^2\partial z}+\left(d_z^{15}\right)\frac{\partial^3 N_{15}}{\partial x^3}+\\
& \left(d_x^{16}\right)\frac{\partial^3 N_{16}}{\partial x^2\partial z}+\left(d_z^{16}\right)\frac{\partial^3 N_{16}}{\partial x^3}+\left(d_x^{17}\right)\frac{\partial^3 N_{17}}{\partial x^2\partial z}+\left(d_z^{17}\right)\frac{\partial^3 N_{17}}{\partial x^3}+\left(d_x^{18}\right)\frac{\partial^3 N_{18}}{\partial x^2\partial z}+\\
& \left(d_z^{18}\right)\frac{\partial^3 N_{18}}{\partial x^3}+\left(d_x^{19}\right)\frac{\partial^3 N_{19}}{\partial x^2\partial z}+\left(d_z^{19}\right)\frac{\partial^3 N_{19}}{\partial x^3}+\left(d_x^{20}\right)\frac{\partial^3 N_{20}}{\partial x^2\partial z}+\left(d_z^{20}\right)\frac{\partial^3 N_{20}}{\partial x^3}\Bigg]+
\end{aligned}
$$

$$
\begin{aligned}
\tilde{f}_{1132}\Bigg[& \left(d_x^1\right)\frac{\partial^3 N_1}{\partial x\partial y\partial z}+\left(d_z^1\right)\frac{\partial^3 N_1}{\partial x^2\partial y}+\left(d_x^2\right)\frac{\partial^3 N_2}{\partial x\partial y\partial z}+\left(d_z^2\right)\frac{\partial^3 N_2}{\partial x^2\partial y}+\left(d_x^3\right)\frac{\partial^3 N_3}{\partial x\partial y\partial z}+\\
& \left(d_z^3\right)\frac{\partial^3 N_3}{\partial x^2\partial y}+\left(d_x^4\right)\frac{\partial^3 N_4}{\partial x\partial y\partial z}+\left(d_z^4\right)\frac{\partial^3 N_4}{\partial x^2\partial y}+\left(d_x^5\right)\frac{\partial^3 N_5}{\partial x\partial y\partial z}+\left(d_z^5\right)\frac{\partial^3 N_5}{\partial x^2\partial y}+\\
& \left(d_x^6\right)\frac{\partial^3 N_6}{\partial x\partial y\partial z}+\left(d_z^6\right)\frac{\partial^3 N_6}{\partial x^2\partial y}+\left(d_x^7\right)\frac{\partial^3 N_7}{\partial x\partial y\partial z}+\left(d_z^7\right)\frac{\partial^3 N_7}{\partial x^2\partial y}+\left(d_x^8\right)\frac{\partial^3 N_8}{\partial x\partial y\partial z}+\\
& \left(d_z^8\right)\frac{\partial^3 N_8}{\partial x^2\partial y}+\left(d_x^9\right)\frac{\partial^3 N_9}{\partial x\partial y\partial z}+\left(d_z^9\right)\frac{\partial^3 N_9}{\partial x^2\partial y}+\left(d_x^{10}\right)\frac{\partial^3 N_{10}}{\partial x\partial y\partial z}+\left(d_z^{10}\right)\frac{\partial^3 N_{10}}{\partial x^2\partial y}+\\
& \left(d_x^{11}\right)\frac{\partial^3 N_{11}}{\partial x\partial y\partial z}+\left(d_z^{11}\right)\frac{\partial^3 N_{11}}{\partial x^2\partial y}+\left(d_x^{12}\right)\frac{\partial^3 N_{12}}{\partial x\partial y\partial z}+\left(d_z^{12}\right)\frac{\partial^3 N_{12}}{\partial x^2\partial y}+\left(d_x^{13}\right)\frac{\partial^3 N_{13}}{\partial x\partial y\partial z}+\\
& \left(d_z^{13}\right)\frac{\partial^3 N_{13}}{\partial x^2\partial y}+\left(d_x^{14}\right)\frac{\partial^3 N_{14}}{\partial x\partial y\partial z}+\left(d_z^{14}\right)\frac{\partial^3 N_{14}}{\partial x^2\partial y}+\left(d_x^{15}\right)\frac{\partial^3 N_{15}}{\partial x\partial y\partial z}+\left(d_z^{15}\right)\frac{\partial^3 N_{15}}{\partial x^2\partial y}+\\
& \left(d_x^{16}\right)\frac{\partial^3 N_{16}}{\partial x\partial y\partial z}+\left(d_z^{16}\right)\frac{\partial^3 N_{16}}{\partial x^2\partial y}+\left(d_x^{17}\right)\frac{\partial^3 N_{17}}{\partial x\partial y\partial z}+\left(d_z^{17}\right)\frac{\partial^3 N_{17}}{\partial x^2\partial y}+\left(d_x^{18}\right)\frac{\partial^3 N_{18}}{\partial x\partial y\partial z}+\\
& \left(d_z^{18}\right)\frac{\partial^3 N_{18}}{\partial x^2\partial y}+\left(d_x^{19}\right)\frac{\partial^3 N_{19}}{\partial x\partial y\partial z}+\left(d_z^{19}\right)\frac{\partial^3 N_{19}}{\partial x^2\partial y}+\left(d_x^{20}\right)\frac{\partial^3 N_{20}}{\partial x\partial y\partial z}+\left(d_z^{20}\right)\frac{\partial^3 N_{20}}{\partial x^2\partial y}\Bigg]+\\
\tilde{f}_{1133}\Bigg[& \left(d_x^1\right)\frac{\partial^3 N_1}{\partial x\partial z^2}+\left(d_z^1\right)\frac{\partial^3 N_1}{\partial x^2\partial z}+\left(d_x^2\right)\frac{\partial^3 N_2}{\partial x\partial z^2}+\left(d_z^2\right)\frac{\partial^3 N_2}{\partial x^2\partial z}+\left(d_x^3\right)\frac{\partial^3 N_3}{\partial x\partial z^2}+\\
& \left(d_z^3\right)\frac{\partial^3 N_3}{\partial x^2\partial z}+\left(d_x^4\right)\frac{\partial^3 N_4}{\partial x\partial z^2}+\left(d_z^4\right)\frac{\partial^3 N_4}{\partial x^2\partial z}+\left(d_x^5\right)\frac{\partial^3 N_5}{\partial x\partial z^2}+\left(d_z^5\right)\frac{\partial^3 N_5}{\partial x^2\partial z}+\\
& \left(d_x^6\right)\frac{\partial^3 N_6}{\partial x\partial z^2}+\left(d_z^6\right)\frac{\partial^3 N_6}{\partial x^2\partial z}+\left(d_x^7\right)\frac{\partial^3 N_7}{\partial x\partial z^2}+\left(d_z^7\right)\frac{\partial^3 N_7}{\partial x^2\partial z}+\left(d_x^8\right)\frac{\partial^3 N_8}{\partial x\partial z^2}+\\
& \left(d_z^8\right)\frac{\partial^3 N_8}{\partial x^2\partial z}+\left(d_x^9\right)\frac{\partial^3 N_9}{\partial x\partial z^2}+\left(d_z^9\right)\frac{\partial^3 N_9}{\partial x^2\partial z}+\left(d_x^{10}\right)\frac{\partial^3 N_{10}}{\partial x\partial z^2}+\left(d_z^{10}\right)\frac{\partial^3 N_{10}}{\partial x^2\partial z}+\\
& \left(d_x^{11}\right)\frac{\partial^3 N_{11}}{\partial x\partial z^2}+\left(d_z^{11}\right)\frac{\partial^3 N_{11}}{\partial x^2\partial z}+\left(d_x^{12}\right)\frac{\partial^3 N_{12}}{\partial x\partial z^2}+\left(d_z^{12}\right)\frac{\partial^3 N_{12}}{\partial x^2\partial z}+\left(d_x^{13}\right)\frac{\partial^3 N_{13}}{\partial x\partial z^2}+\\
& \left(d_z^{13}\right)\frac{\partial^3 N_{13}}{\partial x^2\partial z}+\left(d_x^{14}\right)\frac{\partial^3 N_{14}}{\partial x\partial z^2}+\left(d_z^{14}\right)\frac{\partial^3 N_{14}}{\partial x^2\partial z}+\left(d_x^{15}\right)\frac{\partial^3 N_{15}}{\partial x\partial z^2}+\left(d_z^{15}\right)\frac{\partial^3 N_{15}}{\partial x^2\partial z}+\\
& \left(d_x^{16}\right)\frac{\partial^3 N_{16}}{\partial x\partial z^2}+\left(d_z^{16}\right)\frac{\partial^3 N_{16}}{\partial x^2\partial z}+\left(d_x^{17}\right)\frac{\partial^3 N_{17}}{\partial x\partial z^2}+\left(d_z^{17}\right)\frac{\partial^3 N_{17}}{\partial x^2\partial z}+\left(d_x^{18}\right)\frac{\partial^3 N_{18}}{\partial x\partial z^2}+\\
& \left(d_z^{18}\right)\frac{\partial^3 N_{18}}{\partial x^2\partial z}+\left(d_x^{19}\right)\frac{\partial^3 N_{19}}{\partial x\partial z^2}+\left(d_z^{19}\right)\frac{\partial^3 N_{19}}{\partial x^2\partial z}+\left(d_x^{20}\right)\frac{\partial^3 N_{20}}{\partial x\partial z^2}+\left(d_z^{20}\right)\frac{\partial^3 N_{20}}{\partial x^2\partial z}\Bigg]+
\end{aligned}
$$

$$
\begin{aligned}
\tilde{f}_{1231}\Bigg[& \left(d_y^1\right)\frac{\partial^3 N_1}{\partial x^2\partial z}+\left(d_z^1\right)\frac{\partial^3 N_1}{\partial x^2\partial y}+\left(d_y^2\right)\frac{\partial^3 N_2}{\partial x^2\partial z}+\left(d_z^2\right)\frac{\partial^3 N_2}{\partial x^2\partial y}+\left(d_y^3\right)\frac{\partial^3 N_3}{\partial x^2\partial z}+\\
& \left(d_z^3\right)\frac{\partial^3 N_3}{\partial x^2\partial y}+\left(d_y^4\right)\frac{\partial^3 N_4}{\partial x^2\partial z}+\left(d_z^4\right)\frac{\partial^3 N_4}{\partial x^2\partial y}+\left(d_y^5\right)\frac{\partial^3 N_5}{\partial x^2\partial z}+\left(d_z^5\right)\frac{\partial^3 N_5}{\partial x^2\partial y}+\\
& \left(d_y^6\right)\frac{\partial^3 N_6}{\partial x^2\partial z}+\left(d_z^6\right)\frac{\partial^3 N_6}{\partial x^2\partial y}+\left(d_y^7\right)\frac{\partial^3 N_7}{\partial x^2\partial z}+\left(d_z^7\right)\frac{\partial^3 N_7}{\partial x^2\partial y}+\left(d_y^8\right)\frac{\partial^3 N_8}{\partial x^2\partial z}+\\
& \left(d_z^8\right)\frac{\partial^3 N_8}{\partial x^2\partial y}+\left(d_y^9\right)\frac{\partial^3 N_9}{\partial x^2\partial z}+\left(d_z^9\right)\frac{\partial^3 N_9}{\partial x^2\partial y}+\left(d_y^{10}\right)\frac{\partial^3 N_{10}}{\partial x^2\partial z}+\left(d_z^{10}\right)\frac{\partial^3 N_{10}}{\partial x^2\partial y}+\\
& \left(d_y^{11}\right)\frac{\partial^3 N_{11}}{\partial x^2\partial z}+\left(d_z^{11}\right)\frac{\partial^3 N_{11}}{\partial x^2\partial y}+\left(d_y^{12}\right)\frac{\partial^3 N_{12}}{\partial x^2\partial z}+\left(d_z^{12}\right)\frac{\partial^3 N_{12}}{\partial x^2\partial y}+\left(d_y^{13}\right)\frac{\partial^3 N_{13}}{\partial x^2\partial z}+\\
& \left(d_z^{13}\right)\frac{\partial^3 N_{13}}{\partial x^2\partial y}+\left(d_y^{14}\right)\frac{\partial^3 N_{14}}{\partial x^2\partial z}+\left(d_z^{14}\right)\frac{\partial^3 N_{14}}{\partial x^2\partial y}+\left(d_y^{15}\right)\frac{\partial^3 N_{15}}{\partial x^2\partial z}+\left(d_z^{15}\right)\frac{\partial^3 N_{15}}{\partial x^2\partial y}+\\
& \left(d_y^{16}\right)\frac{\partial^3 N_{16}}{\partial x^2\partial z}+\left(d_z^{16}\right)\frac{\partial^3 N_{16}}{\partial x^2\partial y}+\left(d_y^{17}\right)\frac{\partial^3 N_{17}}{\partial x^2\partial z}+\left(d_z^{17}\right)\frac{\partial^3 N_{17}}{\partial x^2\partial y}+\left(d_y^{18}\right)\frac{\partial^3 N_{18}}{\partial x^2\partial z}+\\
& \left(d_z^{18}\right)\frac{\partial^3 N_{18}}{\partial x^2\partial y}+\left(d_y^{19}\right)\frac{\partial^3 N_{19}}{\partial x^2\partial z}+\left(d_z^{19}\right)\frac{\partial^3 N_{19}}{\partial x^2\partial y}+\left(d_y^{20}\right)\frac{\partial^3 N_{20}}{\partial x^2\partial z}+\left(d_z^{20}\right)\frac{\partial^3 N_{20}}{\partial x^2\partial y}\Bigg]+\\
\tilde{f}_{1232}\Bigg[& \left(d_y^1\right)\frac{\partial^3 N_1}{\partial x\partial y\partial z}+\left(d_z^1\right)\frac{\partial^3 N_1}{\partial x\partial y^2}+\left(d_y^2\right)\frac{\partial^3 N_2}{\partial x\partial y\partial z}+\left(d_z^2\right)\frac{\partial^3 N_2}{\partial x\partial y^2}+\left(d_y^3\right)\frac{\partial^3 N_3}{\partial x\partial y\partial z}+\\
& \left(d_z^3\right)\frac{\partial^3 N_3}{\partial x\partial y^2}+\left(d_y^4\right)\frac{\partial^3 N_4}{\partial x\partial y\partial z}+\left(d_z^4\right)\frac{\partial^3 N_4}{\partial x\partial y^2}+\left(d_y^5\right)\frac{\partial^3 N_5}{\partial x\partial y\partial z}+\left(d_z^5\right)\frac{\partial^3 N_5}{\partial x\partial y^2}+\\
& \left(d_y^6\right)\frac{\partial^3 N_6}{\partial x\partial y\partial z}+\left(d_z^6\right)\frac{\partial^3 N_6}{\partial x\partial y^2}+\left(d_y^7\right)\frac{\partial^3 N_7}{\partial x\partial y\partial z}+\left(d_z^7\right)\frac{\partial^3 N_7}{\partial x\partial y^2}+\left(d_y^8\right)\frac{\partial^3 N_8}{\partial x\partial y\partial z}+\\
& \left(d_z^8\right)\frac{\partial^3 N_8}{\partial x\partial y^2}+\left(d_y^9\right)\frac{\partial^3 N_9}{\partial x\partial y\partial z}+\left(d_z^9\right)\frac{\partial^3 N_9}{\partial x\partial y^2}+\left(d_y^{10}\right)\frac{\partial^3 N_{10}}{\partial x\partial y\partial z}+\left(d_z^{10}\right)\frac{\partial^3 N_{10}}{\partial x\partial y^2}+\\
& \left(d_y^{11}\right)\frac{\partial^3 N_{11}}{\partial x\partial y\partial z}+\left(d_z^{11}\right)\frac{\partial^3 N_{11}}{\partial x\partial y^2}+\left(d_y^{12}\right)\frac{\partial^3 N_{12}}{\partial x\partial y\partial z}+\left(d_z^{12}\right)\frac{\partial^3 N_{12}}{\partial x\partial y^2}+\left(d_y^{13}\right)\frac{\partial^3 N_{13}}{\partial x\partial y\partial z}+\\
& \left(d_z^{13}\right)\frac{\partial^3 N_{13}}{\partial x\partial y^2}+\left(d_y^{14}\right)\frac{\partial^3 N_{14}}{\partial x\partial y\partial z}+\left(d_z^{14}\right)\frac{\partial^3 N_{14}}{\partial x\partial y^2}+\left(d_y^{15}\right)\frac{\partial^3 N_{15}}{\partial x\partial y\partial z}+\left(d_z^{15}\right)\frac{\partial^3 N_{15}}{\partial x\partial y^2}+\\
& \left(d_y^{16}\right)\frac{\partial^3 N_{16}}{\partial x\partial y\partial z}+\left(d_z^{16}\right)\frac{\partial^3 N_{16}}{\partial x\partial y^2}+\left(d_y^{17}\right)\frac{\partial^3 N_{17}}{\partial x\partial y\partial z}+\left(d_z^{17}\right)\frac{\partial^3 N_{17}}{\partial x\partial y^2}+\left(d_y^{18}\right)\frac{\partial^3 N_{18}}{\partial x\partial y\partial z}+\\
& \left(d_z^{18}\right)\frac{\partial^3 N_{18}}{\partial x\partial y^2}+\left(d_y^{19}\right)\frac{\partial^3 N_{19}}{\partial x\partial y\partial z}+\left(d_z^{19}\right)\frac{\partial^3 N_{19}}{\partial x\partial y^2}+\left(d_y^{20}\right)\frac{\partial^3 N_{20}}{\partial x\partial y\partial z}+\left(d_z^{20}\right)\frac{\partial^3 N_{20}}{\partial x\partial y^2}\Bigg]+
\end{aligned}
$$

$$
\begin{aligned}
\tilde{f}_{1233}\Bigg[& \left(d_y^1\right)\frac{\partial^3 N_1}{\partial x\partial z^2}+\left(d_z^1\right)\frac{\partial^3 N_1}{\partial x\partial y\partial z}+\left(d_y^2\right)\frac{\partial^3 N_2}{\partial x\partial z^2}+\left(d_z^2\right)\frac{\partial^3 N_2}{\partial x\partial y\partial z}+\left(d_y^3\right)\frac{\partial^3 N_3}{\partial x\partial z^2}+\\
& \left(d_z^3\right)\frac{\partial^3 N_3}{\partial x\partial y\partial z}+\left(d_y^4\right)\frac{\partial^3 N_4}{\partial x\partial z^2}+\left(d_z^4\right)\frac{\partial^3 N_4}{\partial x\partial y\partial z}+\left(d_y^5\right)\frac{\partial^3 N_5}{\partial x\partial z^2}+\left(d_z^5\right)\frac{\partial^3 N_5}{\partial x\partial y\partial z}+\\
& \left(d_y^6\right)\frac{\partial^3 N_6}{\partial x\partial z^2}+\left(d_z^6\right)\frac{\partial^3 N_6}{\partial x\partial y\partial z}+\left(d_y^7\right)\frac{\partial^3 N_7}{\partial x\partial z^2}+\left(d_z^7\right)\frac{\partial^3 N_7}{\partial x\partial y\partial z}+\left(d_y^8\right)\frac{\partial^3 N_8}{\partial x\partial z^2}+\\
& \left(d_z^8\right)\frac{\partial^3 N_8}{\partial x\partial y\partial z}+\left(d_y^9\right)\frac{\partial^3 N_9}{\partial x\partial z^2}+\left(d_z^9\right)\frac{\partial^3 N_9}{\partial x\partial y\partial z}+\left(d_y^{10}\right)\frac{\partial^3 N_{10}}{\partial x\partial z^2}+\left(d_z^{10}\right)\frac{\partial^3 N_{10}}{\partial x\partial y\partial z}+\\
& \left(d_y^{11}\right)\frac{\partial^3 N_{11}}{\partial x\partial z^2}+\left(d_z^{11}\right)\frac{\partial^3 N_{11}}{\partial x\partial y\partial z}+\left(d_y^{12}\right)\frac{\partial^3 N_{12}}{\partial x\partial z^2}+\left(d_z^{12}\right)\frac{\partial^3 N_{12}}{\partial x\partial y\partial z}+\left(d_y^{13}\right)\frac{\partial^3 N_{13}}{\partial z^2}+\\
& \left(d_z^{13}\right)\frac{\partial^3 N_{13}}{\partial x\partial y\partial z}+\left(d_y^{14}\right)\frac{\partial^3 N_{14}}{\partial x\partial z^2}+\left(d_z^{14}\right)\frac{\partial^3 N_{14}}{\partial x\partial y\partial z}+\left(d_y^{15}\right)\frac{\partial^3 N_{15}}{\partial x\partial z^2}+\left(d_z^{15}\right)\frac{\partial^3 N_{15}}{\partial x\partial y\partial z}+\\
& \left(d_y^{16}\right)\frac{\partial^3 N_{16}}{\partial x\partial z^2}+\left(d_z^{16}\right)\frac{\partial^3 N_{16}}{\partial x\partial y\partial z}+\left(d_y^{17}\right)\frac{\partial^3 N_{17}}{\partial x\partial z^2}+\left(d_z^{17}\right)\frac{\partial^3 N_{17}}{\partial x\partial y\partial z}+\left(d_y^{18}\right)\frac{\partial^3 N_{18}}{\partial x\partial z^2}+\\
& \left(d_z^{18}\right)\frac{\partial^3 N_{18}}{\partial x\partial y\partial z}+\left(d_y^{19}\right)\frac{\partial^3 N_{19}}{\partial x\partial z^2}+\left(d_z^{19}\right)\frac{\partial^3 N_{19}}{\partial x\partial y\partial z}+\left(d_y^{20}\right)\frac{\partial^3 N_{20}}{\partial x\partial z^2}+\left(d_z^{20}\right)\frac{\partial^3 N_{20}}{\partial x\partial y\partial z}\Bigg]+\\
\tilde{f}_{2111}\Bigg[& \left(d_x^1\right)\frac{\partial^3 N_1}{\partial x^2\partial y}+\left(d_x^2\right)\frac{\partial^3 N_2}{\partial x^2\partial y}+\left(d_x^3\right)\frac{\partial^3 N_3}{\partial x^2\partial y}+\left(d_x^4\right)\frac{\partial^3 N_4}{\partial x^2\partial y}+\left(d_x^5\right)\frac{\partial^3 N_5}{\partial x^2\partial y}+\\
& \left(d_x^6\right)\frac{\partial^3 N_6}{\partial x^2\partial y}+\left(d_x^7\right)\frac{\partial^3 N_7}{\partial x^2\partial y}+\left(d_x^8\right)\frac{\partial^3 N_8}{\partial x^2\partial y}+\left(d_x^9\right)\frac{\partial^3 N_9}{\partial x^2\partial y}+\left(d_x^{10}\right)\frac{\partial^3 N_{10}}{\partial x^2\partial y}+\\
& \left(d_x^{11}\right)\frac{\partial^3 N_{11}}{\partial x^2\partial y}+\left(d_x^{12}\right)\frac{\partial^3 N_{12}}{\partial x^2\partial y}+\left(d_x^{13}\right)\frac{\partial^3 N_{13}}{\partial x^2\partial y}+\left(d_x^{14}\right)\frac{\partial^3 N_{14}}{\partial x^2\partial y}+\left(d_x^{15}\right)\frac{\partial^3 N_{15}}{\partial x^2\partial y}+\\
& \left(d_x^{16}\right)\frac{\partial^3 N_{16}}{\partial x^2\partial y}+\left(d_x^{17}\right)\frac{\partial^3 N_{17}}{\partial x^2\partial y}+\left(d_x^{18}\right)\frac{\partial^3 N_{18}}{\partial x^2\partial y}+\left(d_x^{19}\right)\frac{\partial^3 N_{19}}{\partial x^2\partial y}+\left(d_x^{20}\right)\frac{\partial^3 N_{20}}{\partial x^2\partial y}\Bigg]+\\
\tilde{f}_{2112}\Bigg[& \left(d_x^1\right)\frac{\partial^3 N_1}{\partial x\partial y^2}+\left(d_x^2\right)\frac{\partial^3 N_2}{\partial x\partial y^2}+\left(d_x^3\right)\frac{\partial^3 N_3}{\partial x\partial y^2}+\left(d_x^4\right)\frac{\partial^3 N_4}{\partial x\partial y^2}+\left(d_x^5\right)\frac{\partial^3 N_5}{\partial x\partial y^2}+\\
& \left(d_x^6\right)\frac{\partial^3 N_6}{\partial x\partial y^2}+\left(d_x^7\right)\frac{\partial^3 N_7}{\partial x\partial y^2}+\left(d_x^8\right)\frac{\partial^3 N_8}{\partial x\partial y^2}+\left(d_x^9\right)\frac{\partial^3 N_9}{\partial x\partial y^2}+\left(d_x^{10}\right)\frac{\partial^3 N_{10}}{\partial x\partial y^2}+\\
& \left(d_x^{11}\right)\frac{\partial^3 N_{11}}{\partial x\partial y^2}+\left(d_x^{12}\right)\frac{\partial^3 N_{12}}{\partial x\partial y^2}+\left(d_x^{13}\right)\frac{\partial^3 N_{13}}{\partial x\partial y^2}+\left(d_x^{14}\right)\frac{\partial^3 N_{14}}{\partial x\partial y^2}+\left(d_x^{15}\right)\frac{\partial^3 N_{15}}{\partial x\partial y^2}+\\
& \left(d_x^{16}\right)\frac{\partial^3 N_{16}}{\partial x\partial y^2}+\left(d_x^{17}\right)\frac{\partial^3 N_{17}}{\partial x\partial y^2}+\left(d_x^{18}\right)\frac{\partial^3 N_{18}}{\partial x\partial y^2}+\left(d_x^{19}\right)\frac{\partial^3 N_{19}}{\partial x\partial y^2}+\left(d_x^{20}\right)\frac{\partial^3 N_{20}}{\partial x\partial y^2}\Bigg]+
\end{aligned}
$$

$$
\begin{aligned}
\tilde{f}_{2113}\Bigg[& \left(d_x^1\right)\frac{\partial^3 N_1}{\partial x\partial y\partial z}+\left(d_x^2\right)\frac{\partial^3 N_2}{\partial x\partial y\partial z}+\left(d_x^3\right)\frac{\partial^3 N_3}{\partial x\partial y\partial z}+\left(d_x^4\right)\frac{\partial^3 N_4}{\partial x\partial y\partial z}+\left(d_x^5\right)\frac{\partial^3 N_5}{\partial x\partial y\partial z}+\\
& \left(d_x^6\right)\frac{\partial^3 N_6}{\partial x\partial y\partial z}+\left(d_x^7\right)\frac{\partial^3 N_7}{\partial x\partial y\partial z}+\left(d_x^8\right)\frac{\partial^3 N_8}{\partial x\partial y\partial z}+\left(d_x^9\right)\frac{\partial^3 N_9}{\partial x\partial y\partial z}+\left(d_x^{10}\right)\frac{\partial^3 N_{10}}{\partial x\partial y\partial z}+\\
& \left(d_x^{11}\right)\frac{\partial^3 N_{11}}{\partial x\partial y\partial z}+\left(d_x^{12}\right)\frac{\partial^3 N_{12}}{\partial x\partial y\partial z}+\left(d_x^{13}\right)\frac{\partial^3 N_{13}}{\partial x\partial y\partial z}+\left(d_x^{14}\right)\frac{\partial^3 N_{14}}{\partial x\partial y\partial z}+\left(d_x^{15}\right)\frac{\partial^3 N_{15}}{\partial x\partial y\partial z}+\\
& \left(d_x^{16}\right)\frac{\partial^3 N_{16}}{\partial x\partial y\partial z}+\left(d_x^{17}\right)\frac{\partial^3 N_{17}}{\partial x\partial y\partial z}+\left(d_x^{18}\right)\frac{\partial^3 N_{18}}{\partial x\partial y\partial z}+\left(d_x^{19}\right)\frac{\partial^3 N_{19}}{\partial x\partial y\partial z}+\left(d_x^{20}\right)\frac{\partial^3 N_{20}}{\partial x\partial y\partial z}\Bigg]+\\
\tilde{f}_{2221}\Bigg[& \left(d_y^1\right)\frac{\partial^3 N_1}{\partial x\partial y^2}+\left(d_y^2\right)\frac{\partial^3 N_2}{\partial x\partial y^2}+\left(d_y^3\right)\frac{\partial^3 N_3}{\partial x\partial y^2}+\left(d_y^4\right)\frac{\partial^3 N_4}{\partial x\partial y^2}+\left(d_y^5\right)\frac{\partial^3 N_5}{\partial x\partial y^2}+\\
& \left(d_y^6\right)\frac{\partial^3 N_6}{\partial x\partial y^2}+\left(d_y^7\right)\frac{\partial^3 N_7}{\partial x\partial y^2}+\left(d_y^8\right)\frac{\partial^3 N_8}{\partial x\partial y^2}+\left(d_y^9\right)\frac{\partial^3 N_9}{\partial x\partial y^2}+\left(d_y^{10}\right)\frac{\partial^3 N_{10}}{\partial x\partial y^2}+\\
& \left(d_y^{11}\right)\frac{\partial^3 N_{11}}{\partial x\partial y^2}+\left(d_y^{12}\right)\frac{\partial^3 N_{12}}{\partial x\partial y^2}+\left(d_y^{13}\right)\frac{\partial^3 N_{13}}{\partial x\partial y^2}+\left(d_y^{14}\right)\frac{\partial^3 N_{14}}{\partial x\partial y^2}+\left(d_y^{15}\right)\frac{\partial^3 N_{15}}{\partial x\partial y^2}+\\
& \left(d_y^{16}\right)\frac{\partial^3 N_{16}}{\partial x\partial y^2}+\left(d_y^{17}\right)\frac{\partial^3 N_{17}}{\partial x\partial y^2}+\left(d_y^{18}\right)\frac{\partial^3 N_{18}}{\partial x\partial y^2}+\left(d_y^{19}\right)\frac{\partial^3 N_{19}}{\partial x\partial y^2}+\left(d_y^{20}\right)\frac{\partial^3 N_{20}}{\partial x\partial y^2}\Bigg]+\\
\tilde{f}_{2222}\Bigg[& \left(d_y^1\right)\frac{\partial^3 N_1}{\partial y^3}+\left(d_y^2\right)\frac{\partial^3 N_2}{\partial y^3}+\left(d_y^3\right)\frac{\partial^3 N_3}{\partial y^3}+\left(d_y^4\right)\frac{\partial^3 N_4}{\partial y^3}+\left(d_y^5\right)\frac{\partial^3 N_5}{\partial y^3}+\\
& \left(d_y^6\right)\frac{\partial^3 N_6}{\partial y^3}+\left(d_y^7\right)\frac{\partial^3 N_7}{\partial y^3}+\left(d_y^8\right)\frac{\partial^3 N_8}{\partial y^3}+\left(d_y^9\right)\frac{\partial^3 N_9}{\partial y^3}+\left(d_y^{10}\right)\frac{\partial^3 N_{10}}{\partial y^3}+\\
& \left(d_y^{11}\right)\frac{\partial^3 N_{11}}{\partial y^3}+\left(d_y^{12}\right)\frac{\partial^3 N_{12}}{\partial y^3}+\left(d_y^{13}\right)\frac{\partial^3 N_{13}}{\partial y^3}+\left(d_y^{14}\right)\frac{\partial^3 N_{14}}{\partial y^3}+\left(d_y^{15}\right)\frac{\partial^3 N_{15}}{\partial y^3}+\\
& \left(d_y^{16}\right)\frac{\partial^3 N_{16}}{\partial y^3}+\left(d_y^{17}\right)\frac{\partial^3 N_{17}}{\partial y^3}+\left(d_y^{18}\right)\frac{\partial^3 N_{18}}{\partial y^3}+\left(d_y^{19}\right)\frac{\partial^3 N_{19}}{\partial y^3}+\left(d_y^{20}\right)\frac{\partial^3 N_{20}}{\partial y^3}\Bigg]+\\
\tilde{f}_{2223}\Bigg[& \left(d_y^1\right)\frac{\partial^3 N_1}{\partial y^2\partial z}+\left(d_y^2\right)\frac{\partial^3 N_2}{\partial y^2\partial z}+\left(d_y^3\right)\frac{\partial^3 N_3}{\partial y^2\partial z}+\left(d_y^4\right)\frac{\partial^3 N_4}{\partial y^2\partial z}+\left(d_y^5\right)\frac{\partial^3 N_5}{\partial y^2\partial z}+\\
& \left(d_y^6\right)\frac{\partial^3 N_6}{\partial y^2\partial z}+\left(d_y^7\right)\frac{\partial^3 N_7}{\partial y^2\partial z}+\left(d_y^8\right)\frac{\partial^3 N_8}{\partial y^2\partial z}+\left(d_y^9\right)\frac{\partial^3 N_9}{\partial y^2\partial z}+\left(d_y^{10}\right)\frac{\partial^3 N_{10}}{\partial y^2\partial z}+\\
& \left(d_y^{11}\right)\frac{\partial^3 N_{11}}{\partial y^2\partial z}+\left(d_y^{12}\right)\frac{\partial^3 N_{12}}{\partial y^2\partial z}+\left(d_y^{13}\right)\frac{\partial^3 N_{13}}{\partial y^2\partial z}+\left(d_y^{14}\right)\frac{\partial^3 N_{14}}{\partial y^2\partial z}+\left(d_y^{15}\right)\frac{\partial^3 N_{15}}{\partial y^2\partial z}+\\
& \left(d_y^{16}\right)\frac{\partial^3 N_{16}}{\partial y^2\partial z}+\left(d_y^{17}\right)\frac{\partial^3 N_{17}}{\partial y^2\partial z}+\left(d_y^{18}\right)\frac{\partial^3 N_{18}}{\partial y^2\partial z}+\left(d_y^{19}\right)\frac{\partial^3 N_{19}}{\partial y^2\partial z}+\left(d_y^{20}\right)\frac{\partial^3 N_{20}}{\partial y^2\partial z}\Bigg]+
\end{aligned}
$$

$$
\begin{aligned}
\tilde{f}_{2331}\Bigg[& \left(d_z^1\right)\frac{\partial^3 N_1}{\partial x\partial y\partial z}+\left(d_z^2\right)\frac{\partial^3 N_2}{\partial x\partial y\partial z}+\left(d_z^3\right)\frac{\partial^3 N_3}{\partial x\partial y\partial z}+\left(d_z^4\right)\frac{\partial^3 N_4}{\partial x\partial y\partial z}+\left(d_z^5\right)\frac{\partial^3 N_5}{\partial x\partial y\partial z}+\\
& \left(d_z^6\right)\frac{\partial^3 N_6}{\partial x\partial y\partial z}+\left(d_z^7\right)\frac{\partial^3 N_7}{\partial x\partial y\partial z}+\left(d_z^8\right)\frac{\partial^3 N_8}{\partial x\partial y\partial z}+\left(d_z^9\right)\frac{\partial^3 N_9}{\partial x\partial y\partial z}+\left(d_z^{10}\right)\frac{\partial^3 N_{10}}{\partial x\partial y\partial z}+\\
& \left(d_z^{11}\right)\frac{\partial^3 N_{11}}{\partial x\partial y\partial z}+\left(d_z^{12}\right)\frac{\partial^3 N_{12}}{\partial x\partial y\partial z}+\left(d_z^{13}\right)\frac{\partial^3 N_{13}}{\partial x\partial y\partial z}+\left(d_z^{14}\right)\frac{\partial^3 N_{14}}{\partial x\partial y\partial z}+\left(d_z^{15}\right)\frac{\partial^3 N_{15}}{\partial x\partial y\partial z}+\\
& \left(d_z^{16}\right)\frac{\partial^3 N_{16}}{\partial x\partial y\partial z}+\left(d_z^{17}\right)\frac{\partial^3 N_{17}}{\partial x\partial y\partial z}+\left(d_z^{18}\right)\frac{\partial^3 N_{18}}{\partial x\partial y\partial z}+\left(d_z^{19}\right)\frac{\partial^3 N_{19}}{\partial x\partial y\partial z}+\left(d_z^{20}\right)\frac{\partial^3 N_{20}}{\partial x\partial y\partial z}\Bigg]+\\
\tilde{f}_{2332}\Bigg[& \left(d_z^1\right)\frac{\partial^3 N_1}{\partial y^2\partial z}+\left(d_z^2\right)\frac{\partial^3 N_2}{\partial y^2\partial z}+\left(d_z^3\right)\frac{\partial^3 N_3}{\partial y^2\partial z}+\left(d_z^4\right)\frac{\partial^3 N_4}{\partial y^2\partial z}+\left(d_z^5\right)\frac{\partial^3 N_5}{\partial y^2\partial z}+\\
& \left(d_z^6\right)\frac{\partial^3 N_6}{\partial y^2\partial z}+\left(d_z^7\right)\frac{\partial^3 N_7}{\partial y^2\partial z}+\left(d_z^8\right)\frac{\partial^3 N_8}{\partial y^2\partial z}+\left(d_z^9\right)\frac{\partial^3 N_9}{\partial y^2\partial z}+\left(d_z^{10}\right)\frac{\partial^3 N_{10}}{\partial y^2\partial z}+\\
& \left(d_z^{11}\right)\frac{\partial^3 N_{11}}{\partial y^2\partial z}+\left(d_z^{12}\right)\frac{\partial^3 N_{12}}{\partial y^2\partial z}+\left(d_z^{13}\right)\frac{\partial^3 N_{13}}{\partial y^2\partial z}+\left(d_z^{14}\right)\frac{\partial^3 N_{14}}{\partial y^2\partial z}+\left(d_z^{15}\right)\frac{\partial^3 N_{15}}{\partial y^2\partial z}+\\
& \left(d_z^{16}\right)\frac{\partial^3 N_{16}}{\partial y^2\partial z}+\left(d_z^{17}\right)\frac{\partial^3 N_{17}}{\partial y^2\partial z}+\left(d_z^{18}\right)\frac{\partial^3 N_{18}}{\partial y^2\partial z}+\left(d_z^{19}\right)\frac{\partial^3 N_{19}}{\partial y^2\partial z}+\left(d_z^{20}\right)\frac{\partial^3 N_{20}}{\partial y^2\partial z}\Bigg]+\\
\tilde{f}_{2333}\Bigg[& \left(d_z^1\right)\frac{\partial^3 N_1}{\partial y\partial z^2}+\left(d_z^2\right)\frac{\partial^3 N_2}{\partial y\partial z^2}+\left(d_z^3\right)\frac{\partial^3 N_3}{\partial y\partial z^2}+\left(d_z^4\right)\frac{\partial^3 N_4}{\partial y\partial z^2}+\left(d_z^5\right)\frac{\partial^3 N_5}{\partial y\partial z^2}+\\
& \left(d_z^6\right)\frac{\partial^3 N_6}{\partial y\partial z^2}+\left(d_z^7\right)\frac{\partial^3 N_7}{\partial y\partial z^2}+\left(d_z^8\right)\frac{\partial^3 N_8}{\partial y\partial z^2}+\left(d_z^9\right)\frac{\partial^3 N_9}{\partial y\partial z^2}+\left(d_z^{10}\right)\frac{\partial^3 N_{10}}{\partial y\partial z^2}+\\
& \left(d_z^{11}\right)\frac{\partial^3 N_{11}}{\partial y\partial z^2}+\left(d_z^{12}\right)\frac{\partial^3 N_{12}}{\partial y\partial z^2}+\left(d_z^{13}\right)\frac{\partial^3 N_{13}}{\partial y\partial z^2}+\left(d_z^{14}\right)\frac{\partial^3 N_{14}}{\partial y\partial z^2}+\left(d_z^{15}\right)\frac{\partial^3 N_{15}}{\partial y\partial z^2}+\\
& \left(d_z^{16}\right)\frac{\partial^3 N_{16}}{\partial y\partial z^2}+\left(d_z^{17}\right)\frac{\partial^3 N_{17}}{\partial y\partial z^2}+\left(d_z^{18}\right)\frac{\partial^3 N_{18}}{\partial y\partial z^2}+\left(d_z^{19}\right)\frac{\partial^3 N_{19}}{\partial y\partial z^2}+\left(d_z^{20}\right)\frac{\partial^3 N_{20}}{\partial y\partial z^2}\Bigg]+
\end{aligned}
$$

$$
\begin{aligned}
\tilde{f}_{2121}\Bigg[& \left(d_x^1\right)\frac{\partial^3 N_1}{\partial x\partial y^2}+\left(d_y^1\right)\frac{\partial^3 N_1}{\partial x^2\partial y}+\left(d_x^2\right)\frac{\partial^3 N_2}{\partial x\partial y^2}+\left(d_y^2\right)\frac{\partial^3 N_2}{\partial x^2\partial y}+\left(d_x^3\right)\frac{\partial^3 N_3}{\partial x\partial y^2}+\\
& \left(d_y^3\right)\frac{\partial^3 N_3}{\partial x^2\partial y}+\left(d_x^4\right)\frac{\partial^3 N_4}{\partial x\partial y^2}+\left(d_y^4\right)\frac{\partial^3 N_4}{\partial x^2\partial y}+\left(d_x^5\right)\frac{\partial^3 N_5}{\partial x\partial y^2}+\left(d_y^5\right)\frac{\partial^3 N_5}{\partial x^2\partial y}+\\
& \left(d_x^6\right)\frac{\partial^3 N_6}{\partial x\partial y^2}+\left(d_y^6\right)\frac{\partial^3 N_6}{\partial x^2\partial y}+\left(d_x^7\right)\frac{\partial^3 N_7}{\partial x\partial y^2}+\left(d_y^7\right)\frac{\partial^3 N_7}{\partial x^2\partial y}+\left(d_x^8\right)\frac{\partial^3 N_8}{\partial x\partial y^2}+\\
& \left(d_y^8\right)\frac{\partial^3 N_8}{\partial x^2\partial y}+\left(d_x^9\right)\frac{\partial^3 N_9}{\partial x\partial y^2}+\left(d_y^9\right)\frac{\partial^3 N_9}{\partial x^2\partial y}+\left(d_x^{10}\right)\frac{\partial^3 N_{10}}{\partial x\partial y^2}+\left(d_y^{10}\right)\frac{\partial^3 N_{10}}{\partial x^2\partial y}+\\
& \left(d_x^{11}\right)\frac{\partial^3 N_{11}}{\partial x\partial y^2}+\left(d_y^{11}\right)\frac{\partial^3 N_{11}}{\partial x^2\partial y}+\left(d_x^{12}\right)\frac{\partial^3 N_{12}}{\partial x\partial y^2}+\left(d_y^{12}\right)\frac{\partial^3 N_{12}}{\partial x^2\partial y}+\left(d_x^{13}\right)\frac{\partial^3 N_{13}}{\partial x\partial y^2}+\\
& \left(d_y^{13}\right)\frac{\partial^3 N_{13}}{\partial x^2\partial y}+\left(d_x^{14}\right)\frac{\partial^3 N_{14}}{\partial x\partial y^2}+\left(d_y^{14}\right)\frac{\partial^3 N_{14}}{\partial x^2\partial y}+\left(d_x^{15}\right)\frac{\partial^3 N_{15}}{\partial x\partial y^2}+\left(d_y^{15}\right)\frac{\partial^3 N_{15}}{\partial x^2\partial y}+\\
& \left(d_x^{16}\right)\frac{\partial^3 N_{16}}{\partial x\partial y^2}+\left(d_y^{16}\right)\frac{\partial^3 N_{16}}{\partial x^2\partial y}+\left(d_x^{17}\right)\frac{\partial^3 N_{17}}{\partial x\partial y^2}+\left(d_y^{17}\right)\frac{\partial^3 N_{17}}{\partial x^2\partial y}+\left(d_x^{18}\right)\frac{\partial^3 N_{18}}{\partial x\partial y^2}+\\
& \left(d_y^{18}\right)\frac{\partial^3 N_{18}}{\partial x^2\partial y}+\left(d_x^{19}\right)\frac{\partial^3 N_{19}}{\partial x\partial y^2}+\left(d_y^{19}\right)\frac{\partial^3 N_{19}}{\partial x^2\partial y}+\left(d_x^{20}\right)\frac{\partial^3 N_{20}}{\partial x\partial y^2}+\left(d_y^{20}\right)\frac{\partial^3 N_{20}}{\partial x^2\partial y}\Bigg]+\\
\tilde{f}_{2122}\Bigg[& \left(d_x^1\right)\frac{\partial^3 N_1}{\partial y^3}+\left(d_y^1\right)\frac{\partial^3 N_1}{\partial x\partial y^2}+\left(d_x^2\right)\frac{\partial^3 N_2}{\partial y^3}+\left(d_y^2\right)\frac{\partial^3 N_2}{\partial x\partial y^2}+\left(d_x^3\right)\frac{\partial^3 N_3}{\partial y^3}+\\
& \left(d_y^3\right)\frac{\partial^3 N_3}{\partial x\partial y^2}+\left(d_x^4\right)\frac{\partial^3 N_4}{\partial y^3}+\left(d_y^4\right)\frac{\partial^3 N_4}{\partial x\partial y^2}+\left(d_x^5\right)\frac{\partial^3 N_5}{\partial y^3}+\left(d_y^5\right)\frac{\partial^3 N_5}{\partial x\partial y^2}+\\
& \left(d_x^6\right)\frac{\partial^3 N_6}{\partial y^3}+\left(d_y^6\right)\frac{\partial^3 N_6}{\partial x\partial y^2}+\left(d_x^7\right)\frac{\partial^3 N_7}{\partial y^3}+\left(d_y^7\right)\frac{\partial^3 N_7}{\partial x\partial y^2}+\left(d_x^8\right)\frac{\partial^3 N_8}{\partial y^3}+\\
& \left(d_y^8\right)\frac{\partial^3 N_8}{\partial x\partial y^2}+\left(d_x^9\right)\frac{\partial^3 N_9}{\partial y^3}+\left(d_y^9\right)\frac{\partial^3 N_9}{\partial x\partial y^2}+\left(d_x^{10}\right)\frac{\partial^3 N_{10}}{\partial y^3}+\left(d_y^{10}\right)\frac{\partial^3 N_{10}}{\partial x\partial y^2}+\\
& \left(d_x^{11}\right)\frac{\partial^3 N_{11}}{\partial y^3}+\left(d_y^{11}\right)\frac{\partial^3 N_{11}}{\partial x\partial y^2}+\left(d_x^{12}\right)\frac{\partial^3 N_{12}}{\partial y^3}+\left(d_y^{12}\right)\frac{\partial^3 N_{12}}{\partial x\partial y^2}+\left(d_x^{13}\right)\frac{\partial^3 N_{13}}{\partial y^3}+\\
& \left(d_y^{13}\right)\frac{\partial^3 N_{13}}{\partial x\partial y^2}+\left(d_x^{14}\right)\frac{\partial^3 N_{14}}{\partial y^3}+\left(d_y^{14}\right)\frac{\partial^3 N_{14}}{\partial x\partial y^2}+\left(d_x^{15}\right)\frac{\partial^3 N_{15}}{\partial y^3}+\left(d_y^{15}\right)\frac{\partial^3 N_{15}}{\partial x\partial y^2}+\\
& \left(d_x^{16}\right)\frac{\partial^3 N_{16}}{\partial y^3}+\left(d_y^{16}\right)\frac{\partial^3 N_{16}}{\partial x\partial y^2}+\left(d_x^{17}\right)\frac{\partial^3 N_{17}}{\partial y^3}+\left(d_y^{17}\right)\frac{\partial^3 N_{17}}{\partial x\partial y^2}+\left(d_x^{18}\right)\frac{\partial^3 N_{18}}{\partial y^3}+\\
& \left(d_y^{18}\right)\frac{\partial^3 N_{18}}{\partial x\partial y^2}+\left(d_x^{19}\right)\frac{\partial^3 N_{19}}{\partial y^3}+\left(d_y^{19}\right)\frac{\partial^3 N_{19}}{\partial x\partial y^2}+\left(d_x^{20}\right)\frac{\partial^3 N_{20}}{\partial y^3}+\left(d_y^{20}\right)\frac{\partial^3 N_{20}}{\partial x\partial y^2}\Bigg]+
\end{aligned}
$$

$$
\begin{aligned}
\tilde{f}_{2123}\Bigg[& \left(d_x^1\right)\frac{\partial^3 N_1}{\partial y^2\partial z}+\left(d_y^1\right)\frac{\partial^3 N_1}{\partial x\partial y\partial z}+\left(d_x^2\right)\frac{\partial^3 N_2}{\partial y^2\partial z}+\left(d_y^2\right)\frac{\partial^3 N_2}{\partial x\partial y\partial z}+\left(d_x^3\right)\frac{\partial^3 N_3}{\partial y^2\partial z}+\\
& \left(d_y^3\right)\frac{\partial^3 N_3}{\partial x\partial y\partial z}+\left(d_x^4\right)\frac{\partial^3 N_4}{\partial y^2\partial z}+\left(d_y^4\right)\frac{\partial^3 N_4}{\partial x\partial y\partial z}+\left(d_x^5\right)\frac{\partial^3 N_5}{\partial y^2\partial z}+\left(d_y^5\right)\frac{\partial^3 N_5}{\partial x\partial y\partial z}+\\
& \left(d_x^6\right)\frac{\partial^3 N_6}{\partial y^2\partial z}+\left(d_y^6\right)\frac{\partial^3 N_6}{\partial x\partial y\partial z}+\left(d_x^7\right)\frac{\partial^3 N_7}{\partial y^2\partial z}+\left(d_y^7\right)\frac{\partial^3 N_7}{\partial x\partial y\partial z}+\left(d_x^8\right)\frac{\partial^3 N_8}{\partial y^2\partial z}+\\
& \left(d_y^8\right)\frac{\partial^3 N_8}{\partial x\partial y\partial z}+\left(d_x^9\right)\frac{\partial^3 N_9}{\partial y^2\partial z}+\left(d_y^9\right)\frac{\partial^3 N_9}{\partial x\partial y\partial z}+\left(d_x^{10}\right)\frac{\partial^3 N_{10}}{\partial y^2\partial z}+\left(d_y^{10}\right)\frac{\partial^3 N_{10}}{\partial x\partial y\partial z}+\\
& \left(d_x^{11}\right)\frac{\partial^3 N_{11}}{\partial y^2\partial z}+\left(d_y^{11}\right)\frac{\partial^3 N_{11}}{\partial x\partial y\partial z}+\left(d_x^{12}\right)\frac{\partial^3 N_{12}}{\partial y^2\partial z}+\left(d_y^{12}\right)\frac{\partial^3 N_{12}}{\partial x\partial y\partial z}+\left(d_x^{13}\right)\frac{\partial^3 N_{13}}{\partial y^2\partial z}+\\
& \left(d_y^{13}\right)\frac{\partial^3 N_{13}}{\partial x\partial y\partial z}+\left(d_x^{14}\right)\frac{\partial^3 N_{14}}{\partial y^2\partial z}+\left(d_y^{14}\right)\frac{\partial^3 N_{14}}{\partial x\partial y\partial z}+\left(d_x^{15}\right)\frac{\partial^3 N_{15}}{\partial y^2\partial z}+\left(d_y^{15}\right)\frac{\partial^3 N_{15}}{\partial x\partial y\partial z}+\\
& \left(d_x^{16}\right)\frac{\partial^3 N_{16}}{\partial y^2\partial z}+\left(d_y^{16}\right)\frac{\partial^3 N_{16}}{\partial x\partial y\partial z}+\left(d_x^{17}\right)\frac{\partial^3 N_{17}}{\partial y^2\partial z}+\left(d_y^{17}\right)\frac{\partial^3 N_{17}}{\partial x\partial y\partial z}+\left(d_x^{18}\right)\frac{\partial^3 N_{18}}{\partial y^2\partial z}+\\
& \left(d_y^{18}\right)\frac{\partial^3 N_{18}}{\partial x\partial y\partial z}+\left(d_x^{19}\right)\frac{\partial^3 N_{19}}{\partial y^2\partial z}+\left(d_y^{19}\right)\frac{\partial^3 N_{19}}{\partial x\partial y\partial z}+\left(d_x^{20}\right)\frac{\partial^3 N_{20}}{\partial y^2\partial z}+\left(d_y^{20}\right)\frac{\partial^3 N_{20}}{\partial x\partial y\partial z}\Bigg]+\\
\tilde{f}_{2131}\Bigg[& \left(d_x^1\right)\frac{\partial^3 N_1}{\partial x\partial y\partial z}+\left(d_z^1\right)\frac{\partial^3 N_1}{\partial x^2\partial y}+\left(d_x^2\right)\frac{\partial^3 N_2}{\partial x\partial y\partial z}+\left(d_z^2\right)\frac{\partial^3 N_2}{\partial x^2\partial y}+\left(d_x^3\right)\frac{\partial^3 N_3}{\partial x\partial y\partial z}+\\
& \left(d_z^3\right)\frac{\partial^3 N_3}{\partial x^2\partial y}+\left(d_x^4\right)\frac{\partial^3 N_4}{\partial x\partial y\partial z}+\left(d_z^4\right)\frac{\partial^3 N_4}{\partial x^2\partial y}+\left(d_x^5\right)\frac{\partial^3 N_5}{\partial x\partial y\partial z}+\left(d_z^5\right)\frac{\partial^3 N_5}{\partial x^2\partial y}+\\
& \left(d_x^6\right)\frac{\partial^3 N_6}{\partial x\partial y\partial z}+\left(d_z^6\right)\frac{\partial^3 N_6}{\partial x^2\partial y}+\left(d_x^7\right)\frac{\partial^3 N_7}{\partial x\partial y\partial z}+\left(d_z^7\right)\frac{\partial^3 N_7}{\partial x^2\partial y}+\left(d_x^8\right)\frac{\partial^3 N_8}{\partial x\partial y\partial z}+\\
& \left(d_z^8\right)\frac{\partial^3 N_8}{\partial x^2\partial y}+\left(d_x^9\right)\frac{\partial^3 N_9}{\partial x\partial y\partial z}+\left(d_z^9\right)\frac{\partial^3 N_9}{\partial x^2\partial y}+\left(d_x^{10}\right)\frac{\partial^3 N_{10}}{\partial x\partial y\partial z}+\left(d_z^{10}\right)\frac{\partial^3 N_{10}}{\partial x^2\partial y}+\\
& \left(d_x^{11}\right)\frac{\partial^3 N_{11}}{\partial x\partial y\partial z}+\left(d_z^{11}\right)\frac{\partial^3 N_{11}}{\partial x^2\partial y}+\left(d_x^{12}\right)\frac{\partial^3 N_{12}}{\partial x\partial y\partial z}+\left(d_z^{12}\right)\frac{\partial^3 N_{12}}{\partial x^2\partial y}+\left(d_x^{13}\right)\frac{\partial^3 N_{13}}{\partial x\partial y\partial z}+\\
& \left(d_z^{13}\right)\frac{\partial^3 N_{13}}{\partial x^2\partial y}+\left(d_x^{14}\right)\frac{\partial^3 N_{14}}{\partial x\partial y\partial z}+\left(d_z^{14}\right)\frac{\partial^3 N_{14}}{\partial x^2\partial y}+\left(d_x^{15}\right)\frac{\partial^3 N_{15}}{\partial x\partial y\partial z}+\left(d_z^{15}\right)\frac{\partial^3 N_{15}}{\partial x^2\partial y}+\\
& \left(d_x^{16}\right)\frac{\partial^3 N_{16}}{\partial x\partial y\partial z}+\left(d_z^{16}\right)\frac{\partial^3 N_{16}}{\partial x^2\partial y}+\left(d_x^{17}\right)\frac{\partial^3 N_{17}}{\partial x\partial y\partial z}+\left(d_z^{17}\right)\frac{\partial^3 N_{17}}{\partial x^2\partial y}+\left(d_x^{18}\right)\frac{\partial^3 N_{18}}{\partial x\partial y\partial z}+\\
& \left(d_z^{18}\right)\frac{\partial^3 N_{18}}{\partial x^2\partial y}+\left(d_x^{19}\right)\frac{\partial^3 N_{19}}{\partial x\partial y\partial z}+\left(d_z^{19}\right)\frac{\partial^3 N_{19}}{\partial x^2\partial y}+\left(d_x^{20}\right)\frac{\partial^3 N_{20}}{\partial x\partial y\partial z}+\left(d_z^{20}\right)\frac{\partial^3 N_{20}}{\partial x^2\partial y}\Bigg]+
\end{aligned}
$$

$$
\begin{aligned}
\tilde{f}_{2132}\Bigg[& \left(d_x^1\right)\frac{\partial^3 N_1}{\partial y^2\partial z}+\left(d_z^1\right)\frac{\partial^3 N_1}{\partial x\partial y^2}+\left(d_x^2\right)\frac{\partial^3 N_2}{\partial y^2\partial z}+\left(d_z^2\right)\frac{\partial^3 N_2}{\partial x\partial y^2}+\left(d_x^3\right)\frac{\partial^3 N_3}{\partial y^2\partial z}+\\
& \left(d_z^3\right)\frac{\partial^3 N_3}{\partial x\partial y^2}+\left(d_x^4\right)\frac{\partial^3 N_4}{\partial y^2\partial z}+\left(d_z^4\right)\frac{\partial^3 N_4}{\partial x\partial y^2}+\left(d_x^5\right)\frac{\partial^3 N_5}{\partial y^2\partial z}+\left(d_z^5\right)\frac{\partial^3 N_5}{\partial x\partial y^2}+\\
& \left(d_x^6\right)\frac{\partial^3 N_6}{\partial y^2\partial z}+\left(d_z^6\right)\frac{\partial^3 N_6}{\partial x\partial y^2}+\left(d_x^7\right)\frac{\partial^3 N_7}{\partial y^2\partial z}+\left(d_z^7\right)\frac{\partial^3 N_7}{\partial x\partial y^2}+\left(d_x^8\right)\frac{\partial^3 N_8}{\partial y^2\partial z}+\\
& \left(d_z^8\right)\frac{\partial^3 N_8}{\partial x\partial y^2}+\left(d_x^9\right)\frac{\partial^3 N_9}{\partial y^2\partial z}+\left(d_z^9\right)\frac{\partial^3 N_9}{\partial x\partial y^2}+\left(d_x^{10}\right)\frac{\partial^3 N_{10}}{\partial y^2\partial z}+\left(d_z^{10}\right)\frac{\partial^3 N_{10}}{\partial x\partial y^2}+\\
& \left(d_x^{11}\right)\frac{\partial^3 N_{11}}{\partial y^2\partial z}+\left(d_z^{11}\right)\frac{\partial^3 N_{11}}{\partial x\partial y^2}+\left(d_x^{12}\right)\frac{\partial^3 N_{12}}{\partial y^2\partial z}+\left(d_z^{12}\right)\frac{\partial^3 N_{12}}{\partial x\partial y^2}+\left(d_x^{13}\right)\frac{\partial^3 N_{13}}{\partial y^2\partial z}+\\
& \left(d_z^{13}\right)\frac{\partial^3 N_{13}}{\partial x\partial y^2}+\left(d_x^{14}\right)\frac{\partial^3 N_{14}}{\partial y^2\partial z}+\left(d_z^{14}\right)\frac{\partial^3 N_{14}}{\partial x\partial y^2}+\left(d_x^{15}\right)\frac{\partial^3 N_{15}}{\partial y^2\partial z}+\left(d_z^{15}\right)\frac{\partial^3 N_{15}}{\partial x\partial y^2}+\\
& \left(d_x^{16}\right)\frac{\partial^3 N_{16}}{\partial y^2\partial z}+\left(d_z^{16}\right)\frac{\partial^3 N_{16}}{\partial x\partial y^2}+\left(d_x^{17}\right)\frac{\partial^3 N_{17}}{\partial y^2\partial z}+\left(d_z^{17}\right)\frac{\partial^3 N_{17}}{\partial x\partial y^2}+\left(d_x^{18}\right)\frac{\partial^3 N_{18}}{\partial y^2\partial z}+\\
& \left(d_z^{18}\right)\frac{\partial^3 N_{18}}{\partial x\partial y^2}+\left(d_x^{19}\right)\frac{\partial^3 N_{19}}{\partial y^2\partial z}+\left(d_z^{19}\right)\frac{\partial^3 N_{19}}{\partial x\partial y^2}+\left(d_x^{20}\right)\frac{\partial^3 N_{20}}{\partial y^2\partial z}+\left(d_z^{20}\right)\frac{\partial^3 N_{20}}{\partial x\partial y^2}\Bigg]+\\
\tilde{f}_{2133}\Bigg[& \left(d_x^1\right)\frac{\partial^3 N_1}{\partial y\partial z^2}+\left(d_z^1\right)\frac{\partial^3 N_1}{\partial x\partial y\partial z}+\left(d_x^2\right)\frac{\partial^3 N_2}{\partial y\partial z^2}+\left(d_z^2\right)\frac{\partial^3 N_2}{\partial x\partial y\partial z}+\left(d_x^3\right)\frac{\partial^3 N_3}{\partial y\partial z^2}+\\
& \left(d_z^3\right)\frac{\partial^3 N_3}{\partial x\partial y\partial z}+\left(d_x^4\right)\frac{\partial^3 N_4}{\partial y\partial z^2}+\left(d_z^4\right)\frac{\partial^3 N_4}{\partial x\partial y\partial z}+\left(d_x^5\right)\frac{\partial^3 N_5}{\partial y\partial z^2}+\left(d_z^5\right)\frac{\partial^3 N_5}{\partial x\partial y\partial z}+\\
& \left(d_x^6\right)\frac{\partial^3 N_6}{\partial y\partial z^2}+\left(d_z^6\right)\frac{\partial^3 N_6}{\partial x\partial y\partial z}+\left(d_x^7\right)\frac{\partial^3 N_7}{\partial y\partial z^2}+\left(d_z^7\right)\frac{\partial^3 N_7}{\partial x\partial y\partial z}+\left(d_x^8\right)\frac{\partial^3 N_8}{\partial y\partial z^2}+\\
& \left(d_z^8\right)\frac{\partial^3 N_8}{\partial x\partial y\partial z}+\left(d_x^9\right)\frac{\partial^3 N_9}{\partial y\partial z^2}+\left(d_z^9\right)\frac{\partial^3 N_9}{\partial x\partial y\partial z}+\left(d_x^{10}\right)\frac{\partial^3 N_{10}}{\partial y\partial z^2}+\left(d_z^{10}\right)\frac{\partial^3 N_{10}}{\partial x\partial y\partial z}+\\
& \left(d_x^{11}\right)\frac{\partial^3 N_{11}}{\partial y\partial z^2}+\left(d_z^{11}\right)\frac{\partial^3 N_{11}}{\partial x\partial y\partial z}+\left(d_x^{12}\right)\frac{\partial^3 N_{12}}{\partial y\partial z^2}+\left(d_z^{12}\right)\frac{\partial^3 N_{12}}{\partial x\partial y\partial z}+\left(d_x^{13}\right)\frac{\partial^3 N_{13}}{\partial y\partial z^2}+\\
& \left(d_z^{13}\right)\frac{\partial^3 N_{13}}{\partial x\partial y\partial z}+\left(d_x^{14}\right)\frac{\partial^3 N_{14}}{\partial y\partial z^2}+\left(d_z^{14}\right)\frac{\partial^3 N_{14}}{\partial x\partial y\partial z}+\left(d_x^{15}\right)\frac{\partial^3 N_{15}}{\partial y\partial z^2}+\left(d_z^{15}\right)\frac{\partial^3 N_{15}}{\partial x\partial y\partial z}+\\
& \left(d_x^{16}\right)\frac{\partial^3 N_{16}}{\partial y\partial z^2}+\left(d_z^{16}\right)\frac{\partial^3 N_{16}}{\partial x\partial y\partial z}+\left(d_x^{17}\right)\frac{\partial^3 N_{17}}{\partial y\partial z^2}+\left(d_z^{17}\right)\frac{\partial^3 N_{17}}{\partial x\partial y\partial z}+\left(d_x^{18}\right)\frac{\partial^3 N_{18}}{\partial y\partial z^2}+\\
& \left(d_z^{18}\right)\frac{\partial^3 N_{18}}{\partial x\partial y\partial z}+\left(d_x^{19}\right)\frac{\partial^3 N_{19}}{\partial y\partial z^2}+\left(d_z^{19}\right)\frac{\partial^3 N_{19}}{\partial x\partial y\partial z}+\left(d_x^{20}\right)\frac{\partial^3 N_{20}}{\partial y\partial z^2}+\left(d_z^{20}\right)\frac{\partial^3 N_{20}}{\partial x\partial y\partial z}\Bigg]+
\end{aligned}
$$

$$
\begin{aligned}
\tilde{f}_{2231}\Bigg[& \left(d_y^1\right)\frac{\partial^3 N_1}{\partial x\partial y\partial z}+\left(d_z^1\right)\frac{\partial^3 N_1}{\partial x\partial y^2}+\left(d_y^2\right)\frac{\partial^3 N_2}{\partial x\partial y\partial z}+\left(d_z^2\right)\frac{\partial^3 N_2}{\partial x\partial y^2}+\left(d_y^3\right)\frac{\partial^3 N_3}{\partial x\partial y\partial z}+\\
& \left(d_z^3\right)\frac{\partial^3 N_3}{\partial x\partial y^2}+\left(d_y^4\right)\frac{\partial^3 N_4}{\partial x\partial y\partial z}+\left(d_z^4\right)\frac{\partial^3 N_4}{\partial x\partial y^2}+\left(d_y^5\right)\frac{\partial^3 N_5}{\partial x\partial y\partial z}+\left(d_z^5\right)\frac{\partial^3 N_5}{\partial x\partial y^2}+\\
& \left(d_y^6\right)\frac{\partial^3 N_6}{\partial x\partial y\partial z}+\left(d_z^6\right)\frac{\partial^3 N_6}{\partial x\partial y^2}+\left(d_y^7\right)\frac{\partial^3 N_7}{\partial x\partial y\partial z}+\left(d_z^7\right)\frac{\partial^3 N_7}{\partial x\partial y^2}+\left(d_y^8\right)\frac{\partial^3 N_8}{\partial x\partial y\partial z}+\\
& \left(d_z^8\right)\frac{\partial^3 N_8}{\partial x\partial y^2}+\left(d_y^9\right)\frac{\partial^3 N_9}{\partial x\partial y\partial z}+\left(d_z^9\right)\frac{\partial^3 N_9}{\partial x\partial y^2}+\left(d_y^{10}\right)\frac{\partial^3 N_{10}}{\partial x\partial y\partial z}+\left(d_z^{10}\right)\frac{\partial^3 N_{10}}{\partial x\partial y^2}+\\
& \left(d_y^{11}\right)\frac{\partial^3 N_{11}}{\partial x\partial y\partial z}+\left(d_z^{11}\right)\frac{\partial^3 N_{11}}{\partial x\partial y^2}+\left(d_y^{12}\right)\frac{\partial^3 N_{12}}{\partial x\partial y\partial z}+\left(d_z^{12}\right)\frac{\partial^3 N_{12}}{\partial x\partial y^2}+\left(d_y^{13}\right)\frac{\partial^3 N_{13}}{\partial x\partial y\partial z}+\\
& \left(d_z^{13}\right)\frac{\partial^3 N_{13}}{\partial x\partial y^2}+\left(d_y^{14}\right)\frac{\partial^3 N_{14}}{\partial x\partial y\partial z}+\left(d_z^{14}\right)\frac{\partial^3 N_{14}}{\partial x\partial y^2}+\left(d_y^{15}\right)\frac{\partial^3 N_{15}}{\partial x\partial y\partial z}+\left(d_z^{15}\right)\frac{\partial^3 N_{15}}{\partial x\partial y^2}+\\
& \left(d_y^{16}\right)\frac{\partial^3 N_{16}}{\partial x\partial y\partial z}+\left(d_z^{16}\right)\frac{\partial^3 N_{16}}{\partial x\partial y^2}+\left(d_y^{17}\right)\frac{\partial^3 N_{17}}{\partial x\partial y\partial z}+\left(d_z^{17}\right)\frac{\partial^3 N_{17}}{\partial x\partial y^2}+\left(d_y^{18}\right)\frac{\partial^3 N_{18}}{\partial x\partial y\partial z}+\\
& \left(d_z^{18}\right)\frac{\partial^3 N_{18}}{\partial x\partial y^2}+\left(d_y^{19}\right)\frac{\partial^3 N_{19}}{\partial x\partial y\partial z}+\left(d_z^{19}\right)\frac{\partial^3 N_{19}}{\partial x\partial y^2}+\left(d_y^{20}\right)\frac{\partial^3 N_{20}}{\partial x\partial y\partial z}+\left(d_z^{20}\right)\frac{\partial^3 N_{20}}{\partial x\partial y^2}\Bigg]+\\
\tilde{f}_{2232}\Bigg[& \left(d_y^1\right)\frac{\partial^3 N_1}{\partial y^2\partial z}+\left(d_z^1\right)\frac{\partial^3 N_1}{\partial y^3}+\left(d_y^2\right)\frac{\partial^3 N_2}{\partial y^2\partial z}+\left(d_z^2\right)\frac{\partial^3 N_2}{\partial y^3}+\left(d_y^3\right)\frac{\partial^3 N_3}{\partial y^2\partial z}+\\
& \left(d_z^3\right)\frac{\partial^3 N_3}{\partial y^3}+\left(d_y^4\right)\frac{\partial^3 N_4}{\partial y^2\partial z}+\left(d_z^4\right)\frac{\partial^3 N_4}{\partial y^3}+\left(d_y^5\right)\frac{\partial^3 N_5}{\partial y^2\partial z}+\left(d_z^5\right)\frac{\partial^3 N_5}{\partial y^3}+\\
& \left(d_y^6\right)\frac{\partial^3 N_6}{\partial y^2\partial z}+\left(d_z^6\right)\frac{\partial^3 N_6}{\partial y^3}+\left(d_y^7\right)\frac{\partial^3 N_7}{\partial y^2\partial z}+\left(d_z^7\right)\frac{\partial^3 N_7}{\partial y^3}+\left(d_y^8\right)\frac{\partial^3 N_8}{\partial y^2\partial z}+\\
& \left(d_z^8\right)\frac{\partial^3 N_8}{\partial y^3}+\left(d_y^9\right)\frac{\partial^3 N_9}{\partial y^2\partial z}+\left(d_z^9\right)\frac{\partial^3 N_9}{\partial y^3}+\left(d_y^{10}\right)\frac{\partial^3 N_{10}}{\partial y^2\partial z}+\left(d_z^{10}\right)\frac{\partial^3 N_{10}}{\partial y^3}+\\
& \left(d_y^{11}\right)\frac{\partial^3 N_{11}}{\partial y^2\partial z}+\left(d_z^{11}\right)\frac{\partial^3 N_{11}}{\partial y^3}+\left(d_y^{12}\right)\frac{\partial^3 N_{12}}{\partial y^2\partial z}+\left(d_z^{12}\right)\frac{\partial^3 N_{12}}{\partial y^3}+\left(d_y^{13}\right)\frac{\partial^3 N_{13}}{\partial y^2\partial z}+\\
& \left(d_z^{13}\right)\frac{\partial^3 N_{13}}{\partial y^3}+\left(d_y^{14}\right)\frac{\partial^3 N_{14}}{\partial y^2\partial z}+\left(d_z^{14}\right)\frac{\partial^3 N_{14}}{\partial y^3}+\left(d_y^{15}\right)\frac{\partial^3 N_{15}}{\partial y^2\partial z}+\left(d_z^{15}\right)\frac{\partial^3 N_{15}}{\partial y^3}+\\
& \left(d_y^{16}\right)\frac{\partial^3 N_{16}}{\partial y^2\partial z}+\left(d_z^{16}\right)\frac{\partial^3 N_{16}}{\partial y^3}+\left(d_y^{17}\right)\frac{\partial^3 N_{17}}{\partial y^2\partial z}+\left(d_z^{17}\right)\frac{\partial^3 N_{17}}{\partial y^3}+\left(d_y^{18}\right)\frac{\partial^3 N_{18}}{\partial y^2\partial z}+\\
& \left(d_z^{18}\right)\frac{\partial^3 N_{18}}{\partial y^3}+\left(d_y^{19}\right)\frac{\partial^3 N_{19}}{\partial y^2\partial z}+\left(d_z^{19}\right)\frac{\partial^3 N_{19}}{\partial y^3}+\left(d_y^{20}\right)\frac{\partial^3 N_{20}}{\partial y^2\partial z}+\left(d_z^{20}\right)\frac{\partial^3 N_{20}}{\partial y^3}\Bigg]+
\end{aligned}
$$

$$
\begin{aligned}
\tilde{f}_{2233}\Bigg[& \left(d_y^1\right)\frac{\partial^3 N_1}{\partial y\partial z^2}+\left(d_z^1\right)\frac{\partial^3 N_1}{\partial y^2\partial z}+\left(d_y^2\right)\frac{\partial^3 N_2}{\partial y\partial z^2}+\left(d_z^2\right)\frac{\partial^3 N_2}{\partial y^2\partial z}+\left(d_y^3\right)\frac{\partial^3 N_3}{\partial y\partial z^2}+\\
& \left(d_z^3\right)\frac{\partial^3 N_3}{\partial y^2\partial z}+\left(d_y^4\right)\frac{\partial^3 N_4}{\partial y\partial z^2}+\left(d_z^4\right)\frac{\partial^3 N_4}{\partial y^2\partial z}+\left(d_y^5\right)\frac{\partial^3 N_5}{\partial y\partial z^2}+\left(d_z^5\right)\frac{\partial^3 N_5}{\partial y^2\partial z}+\\
& \left(d_y^6\right)\frac{\partial^3 N_6}{\partial y\partial z^2}+\left(d_z^6\right)\frac{\partial^3 N_6}{\partial y^2\partial z}+\left(d_y^7\right)\frac{\partial^3 N_7}{\partial y\partial z^2}+\left(d_z^7\right)\frac{\partial^3 N_7}{\partial y^2\partial z}+\left(d_y^8\right)\frac{\partial^3 N_8}{\partial y\partial z^2}+\\
& \left(d_z^8\right)\frac{\partial^3 N_8}{\partial y^2\partial z}+\left(d_y^9\right)\frac{\partial^3 N_9}{\partial y\partial z^2}+\left(d_z^9\right)\frac{\partial^3 N_9}{\partial y^2\partial z}+\left(d_y^{10}\right)\frac{\partial^3 N_{10}}{\partial y\partial z^2}+\left(d_z^{10}\right)\frac{\partial^3 N_{10}}{\partial y^2\partial z}+\\
& \left(d_y^{11}\right)\frac{\partial^3 N_{11}}{\partial y\partial z^2}+\left(d_z^{11}\right)\frac{\partial^3 N_{11}}{\partial y^2\partial z}+\left(d_y^{12}\right)\frac{\partial^3 N_{12}}{\partial y\partial z^2}+\left(d_z^{12}\right)\frac{\partial^3 N_{12}}{\partial y^2\partial z}+\left(d_y^{13}\right)\frac{\partial^3 N_{13}}{\partial y\partial z^2}+\\
& \left(d_z^{13}\right)\frac{\partial^3 N_{13}}{\partial y^2\partial z}+\left(d_y^{14}\right)\frac{\partial^3 N_{14}}{\partial y\partial z^2}+\left(d_z^{14}\right)\frac{\partial^3 N_{14}}{\partial y^2\partial z}+\left(d_y^{15}\right)\frac{\partial^3 N_{15}}{\partial y\partial z^2}+\left(d_z^{15}\right)\frac{\partial^3 N_{15}}{\partial y^2\partial z}+\\
& \left(d_y^{16}\right)\frac{\partial^3 N_{16}}{\partial y\partial z^2}+\left(d_z^{16}\right)\frac{\partial^3 N_{16}}{\partial y^2\partial z}+\left(d_y^{17}\right)\frac{\partial^3 N_{17}}{\partial y\partial z^2}+\left(d_z^{17}\right)\frac{\partial^3 N_{17}}{\partial y^2\partial z}+\left(d_y^{18}\right)\frac{\partial^3 N_{18}}{\partial y\partial z^2}+\\
& \left(d_z^{18}\right)\frac{\partial^3 N_{18}}{\partial y^2\partial z}+\left(d_y^{19}\right)\frac{\partial^3 N_{19}}{\partial y\partial z^2}+\left(d_z^{19}\right)\frac{\partial^3 N_{19}}{\partial y^2\partial z}+\left(d_y^{20}\right)\frac{\partial^3 N_{20}}{\partial y\partial z^2}+\left(d_z^{20}\right)\frac{\partial^3 N_{20}}{\partial y^2\partial z}\Bigg]+\\
\tilde{f}_{3111}\Bigg[& \left(d_x^1\right)\frac{\partial^3 N_1}{\partial x^2\partial z}+\left(d_x^2\right)\frac{\partial^3 N_2}{\partial x^2\partial z}+\left(d_x^3\right)\frac{\partial^3 N_3}{\partial x^2\partial z}+\left(d_x^4\right)\frac{\partial^3 N_4}{\partial x^2\partial z}+\left(d_x^5\right)\frac{\partial^3 N_5}{\partial x^2\partial z}+\\
& \left(d_x^6\right)\frac{\partial^3 N_6}{\partial x^2\partial z}+\left(d_x^7\right)\frac{\partial^3 N_7}{\partial x^2\partial z}+\left(d_x^8\right)\frac{\partial^3 N_8}{\partial x^2\partial z}+\left(d_x^9\right)\frac{\partial^3 N_9}{\partial x^2\partial z}+\left(d_x^{10}\right)\frac{\partial^3 N_{10}}{\partial x^2\partial z}+\\
& \left(d_x^{11}\right)\frac{\partial^3 N_{11}}{\partial x^2\partial z}+\left(d_x^{12}\right)\frac{\partial^3 N_{12}}{\partial x^2\partial z}+\left(d_x^{13}\right)\frac{\partial^3 N_{13}}{\partial x^2\partial z}+\left(d_x^{14}\right)\frac{\partial^3 N_{14}}{\partial x^2\partial z}+\left(d_x^{15}\right)\frac{\partial^3 N_{15}}{\partial x^2\partial z}+\\
& \left(d_x^{16}\right)\frac{\partial^3 N_{16}}{\partial x^2\partial z}+\left(d_x^{17}\right)\frac{\partial^3 N_{17}}{\partial x^2\partial z}+\left(d_x^{18}\right)\frac{\partial^3 N_{18}}{\partial x^2\partial z}+\left(d_x^{19}\right)\frac{\partial^3 N_{19}}{\partial x^2\partial z}+\left(d_x^{20}\right)\frac{\partial^3 N_{20}}{\partial x^2\partial z}\Bigg]+\\
\tilde{f}_{3112}\Bigg[& \left(d_x^1\right)\frac{\partial^3 N_1}{\partial x\partial y\partial z}+\left(d_x^2\right)\frac{\partial^3 N_2}{\partial x\partial y\partial z}+\left(d_x^3\right)\frac{\partial^3 N_3}{\partial x\partial y\partial z}+\left(d_x^4\right)\frac{\partial^3 N_4}{\partial x\partial y\partial z}+\left(d_x^5\right)\frac{\partial^3 N_5}{\partial x\partial y\partial z}+\\
& \left(d_x^6\right)\frac{\partial^3 N_6}{\partial x\partial y\partial z}+\left(d_x^7\right)\frac{\partial^3 N_7}{\partial x\partial y\partial z}+\left(d_x^8\right)\frac{\partial^3 N_8}{\partial x\partial y\partial z}+\left(d_x^9\right)\frac{\partial^3 N_9}{\partial x\partial y\partial z}+\left(d_x^{10}\right)\frac{\partial^3 N_{10}}{\partial x\partial y\partial z}+\\
& \left(d_x^{11}\right)\frac{\partial^3 N_{11}}{\partial x\partial y\partial z}+\left(d_x^{12}\right)\frac{\partial^3 N_{12}}{\partial x\partial y\partial z}+\left(d_x^{13}\right)\frac{\partial^3 N_{13}}{\partial x\partial y\partial z}+\left(d_x^{14}\right)\frac{\partial^3 N_{14}}{\partial x\partial y\partial z}+\left(d_x^{15}\right)\frac{\partial^3 N_{15}}{\partial x\partial y\partial z}+\\
& \left(d_x^{16}\right)\frac{\partial^3 N_{16}}{\partial x\partial y\partial z}+\left(d_x^{17}\right)\frac{\partial^3 N_{17}}{\partial x\partial y\partial z}+\left(d_x^{18}\right)\frac{\partial^3 N_{18}}{\partial x\partial y\partial z}+\left(d_x^{19}\right)\frac{\partial^3 N_{19}}{\partial x\partial y\partial z}+\left(d_x^{20}\right)\frac{\partial^3 N_{20}}{\partial x\partial y\partial z}\Bigg]+
\end{aligned}
$$

$$
\begin{aligned}
\tilde{f}_{3113}\Bigg[& \left(d_x^1\right)\frac{\partial^3 N_1}{\partial x\partial z^2}+\left(d_x^2\right)\frac{\partial^3 N_2}{\partial x\partial z^2}+\left(d_x^3\right)\frac{\partial^3 N_3}{\partial x\partial z^2}+\left(d_x^4\right)\frac{\partial^3 N_4}{\partial x\partial z^2}+\left(d_x^5\right)\frac{\partial^3 N_5}{\partial x\partial z^2}+\\
& \left(d_x^6\right)\frac{\partial^3 N_6}{\partial x\partial z^2}+\left(d_x^7\right)\frac{\partial^3 N_7}{\partial x\partial z^2}+\left(d_x^8\right)\frac{\partial^3 N_8}{\partial x\partial z^2}+\left(d_x^9\right)\frac{\partial^3 N_9}{\partial x\partial z^2}+\left(d_x^{10}\right)\frac{\partial^3 N_{10}}{\partial x\partial z^2}+\\
& \left(d_x^{11}\right)\frac{\partial^3 N_{11}}{\partial x\partial z^2}+\left(d_x^{12}\right)\frac{\partial^3 N_{12}}{\partial x\partial z^2}+\left(d_x^{13}\right)\frac{\partial^3 N_{13}}{\partial x\partial z^2}+\left(d_x^{14}\right)\frac{\partial^3 N_{14}}{\partial x\partial z^2}+\left(d_x^{15}\right)\frac{\partial^3 N_{15}}{\partial x\partial z^2}+\\
& \left(d_x^{16}\right)\frac{\partial^3 N_{16}}{\partial x\partial z^2}+\left(d_x^{17}\right)\frac{\partial^3 N_{17}}{\partial x\partial z^2}+\left(d_x^{18}\right)\frac{\partial^3 N_{18}}{\partial x\partial z^2}+\left(d_x^{19}\right)\frac{\partial^3 N_{19}}{\partial x\partial z^2}+\left(d_x^{20}\right)\frac{\partial^3 N_{20}}{\partial x\partial z^2}\Bigg]+\\
\tilde{f}_{3221}\Bigg[& \left(d_y^1\right)\frac{\partial^3 N_1}{\partial x\partial y\partial z}+\left(d_y^2\right)\frac{\partial^3 N_2}{\partial x\partial y\partial z}+\left(d_y^3\right)\frac{\partial^3 N_3}{\partial x\partial y\partial z}+\left(d_y^4\right)\frac{\partial^3 N_4}{\partial x\partial y\partial z}+\left(d_y^5\right)\frac{\partial^3 N_5}{\partial x\partial y\partial z}+\\
& \left(d_y^6\right)\frac{\partial^3 N_6}{\partial x\partial y\partial z}+\left(d_y^7\right)\frac{\partial^3 N_7}{\partial x\partial y\partial z}+\left(d_y^8\right)\frac{\partial^3 N_8}{\partial x\partial y\partial z}+\left(d_y^9\right)\frac{\partial^3 N_9}{\partial x\partial y\partial z}+\left(d_y^{10}\right)\frac{\partial^3 N_{10}}{\partial x\partial y\partial z}+\\
& \left(d_y^{11}\right)\frac{\partial^3 N_{11}}{\partial x\partial y\partial z}+\left(d_y^{12}\right)\frac{\partial^3 N_{12}}{\partial x\partial y\partial z}+\left(d_y^{13}\right)\frac{\partial^3 N_{13}}{\partial x\partial y\partial z}+\left(d_y^{14}\right)\frac{\partial^3 N_{14}}{\partial x\partial y\partial z}+\left(d_y^{15}\right)\frac{\partial^3 N_{15}}{\partial x\partial y\partial z}+\\
& \left(d_y^{16}\right)\frac{\partial^3 N_{16}}{\partial x\partial y\partial z}+\left(d_y^{17}\right)\frac{\partial^3 N_{17}}{\partial x\partial y\partial z}+\left(d_y^{18}\right)\frac{\partial^3 N_{18}}{\partial x\partial y\partial z}+\left(d_y^{19}\right)\frac{\partial^3 N_{19}}{\partial x\partial y\partial z}+\left(d_y^{20}\right)\frac{\partial^3 N_{20}}{\partial x\partial y\partial z}\Bigg]+\\
\tilde{f}_{3222}\Bigg[& \left(d_y^1\right)\frac{\partial^3 N_1}{\partial y^2\partial z}+\left(d_y^2\right)\frac{\partial^3 N_2}{\partial y^2\partial z}+\left(d_y^3\right)\frac{\partial^3 N_3}{\partial y^2\partial z}+\left(d_y^4\right)\frac{\partial^3 N_4}{\partial y^2\partial z}+\left(d_y^5\right)\frac{\partial^3 N_5}{\partial y^2\partial z}+\\
& \left(d_y^6\right)\frac{\partial^3 N_6}{\partial y^2\partial z}+\left(d_y^7\right)\frac{\partial^3 N_7}{\partial y^2\partial z}+\left(d_y^8\right)\frac{\partial^3 N_8}{\partial y^2\partial z}+\left(d_y^9\right)\frac{\partial^3 N_9}{\partial y^2\partial z}+\left(d_y^{10}\right)\frac{\partial^3 N_{10}}{\partial y^2\partial z}+\\
& \left(d_y^{11}\right)\frac{\partial^3 N_{11}}{\partial y^2\partial z}+\left(d_y^{12}\right)\frac{\partial^3 N_{12}}{\partial y^2\partial z}+\left(d_y^{13}\right)\frac{\partial^3 N_{13}}{\partial y^2\partial z}+\left(d_y^{14}\right)\frac{\partial^3 N_{14}}{\partial y^2\partial z}+\left(d_y^{15}\right)\frac{\partial^3 N_{15}}{\partial y^2\partial z}+\\
& \left(d_y^{16}\right)\frac{\partial^3 N_{16}}{\partial y^2\partial z}+\left(d_y^{17}\right)\frac{\partial^3 N_{17}}{\partial y^2\partial z}+\left(d_y^{18}\right)\frac{\partial^3 N_{18}}{\partial y^2\partial z}+\left(d_y^{19}\right)\frac{\partial^3 N_{19}}{\partial y^2\partial z}+\left(d_y^{20}\right)\frac{\partial^3 N_{20}}{\partial y^2\partial z}\Bigg]+\\
\tilde{f}_{3223}\Bigg[& \left(d_y^1\right)\frac{\partial^3 N_1}{\partial y\partial z^2}+\left(d_y^2\right)\frac{\partial^3 N_2}{\partial y\partial z^2}+\left(d_y^3\right)\frac{\partial^3 N_3}{\partial y\partial z^2}+\left(d_y^4\right)\frac{\partial^3 N_4}{\partial y\partial z^2}+\left(d_y^5\right)\frac{\partial^3 N_5}{\partial y\partial z^2}+\\
& \left(d_y^6\right)\frac{\partial^3 N_6}{\partial y\partial z^2}+\left(d_y^7\right)\frac{\partial^3 N_7}{\partial y\partial z^2}+\left(d_y^8\right)\frac{\partial^3 N_8}{\partial y\partial z^2}+\left(d_y^9\right)\frac{\partial^3 N_9}{\partial y\partial z^2}+\left(d_y^{10}\right)\frac{\partial^3 N_{10}}{\partial y\partial z^2}+\\
& \left(d_y^{11}\right)\frac{\partial^3 N_{11}}{\partial y\partial z^2}+\left(d_y^{12}\right)\frac{\partial^3 N_{12}}{\partial y\partial z^2}+\left(d_y^{13}\right)\frac{\partial^3 N_{13}}{\partial y\partial z^2}+\left(d_y^{14}\right)\frac{\partial^3 N_{14}}{\partial y\partial z^2}+\left(d_y^{15}\right)\frac{\partial^3 N_{15}}{\partial y\partial z^2}+\\
& \left(d_y^{16}\right)\frac{\partial^3 N_{16}}{\partial y\partial z^2}+\left(d_y^{17}\right)\frac{\partial^3 N_{17}}{\partial y\partial z^2}+\left(d_y^{18}\right)\frac{\partial^3 N_{18}}{\partial y\partial z^2}+\left(d_y^{19}\right)\frac{\partial^3 N_{19}}{\partial y\partial z^2}+\left(d_y^{20}\right)\frac{\partial^3 N_{20}}{\partial y\partial z^2}\Bigg]+
\end{aligned}
$$

$$
\begin{aligned}
\tilde{f}_{3331}\Bigg[& \left(d_z^1\right)\frac{\partial^3 N_1}{\partial x\partial z^2}+\left(d_z^2\right)\frac{\partial^3 N_2}{\partial x\partial z^2}+\left(d_z^3\right)\frac{\partial^3 N_3}{\partial x\partial z^2}+\left(d_z^4\right)\frac{\partial^3 N_4}{\partial x\partial z^2}+\left(d_z^5\right)\frac{\partial^3 N_5}{\partial x\partial z^2}+\\
& \left(d_z^6\right)\frac{\partial^3 N_6}{\partial x\partial z^2}+\left(d_z^7\right)\frac{\partial^3 N_7}{\partial x\partial z^2}+\left(d_z^8\right)\frac{\partial^3 N_8}{\partial x\partial z^2}+\left(d_z^9\right)\frac{\partial^3 N_9}{\partial x\partial z^2}+\left(d_z^{10}\right)\frac{\partial^3 N_{10}}{\partial x\partial z^2}+\\
& \left(d_z^{11}\right)\frac{\partial^3 N_{11}}{\partial x\partial z^2}+\left(d_z^{12}\right)\frac{\partial^3 N_{12}}{\partial x\partial z^2}+\left(d_z^{13}\right)\frac{\partial^3 N_{13}}{\partial x\partial z^2}+\left(d_z^{14}\right)\frac{\partial^3 N_{14}}{\partial x\partial z^2}+\left(d_z^{15}\right)\frac{\partial^3 N_{15}}{\partial x\partial z^2}+\\
& \left(d_z^{16}\right)\frac{\partial^3 N_{16}}{\partial x\partial z^2}+\left(d_z^{17}\right)\frac{\partial^3 N_{17}}{\partial x\partial z^2}+\left(d_z^{18}\right)\frac{\partial^3 N_{18}}{\partial x\partial z^2}+\left(d_z^{19}\right)\frac{\partial^3 N_{19}}{\partial x\partial z^2}+\left(d_z^{20}\right)\frac{\partial^3 N_{20}}{\partial x\partial z^2}\Bigg]+\\
\tilde{f}_{3332}\Bigg[& \left(d_z^1\right)\frac{\partial^3 N_1}{\partial y\partial z^2}+\left(d_z^2\right)\frac{\partial^3 N_2}{\partial y\partial z^2}+\left(d_z^3\right)\frac{\partial^3 N_3}{\partial y\partial z^2}+\left(d_z^4\right)\frac{\partial^3 N_4}{\partial y\partial z^2}+\left(d_z^5\right)\frac{\partial^3 N_5}{\partial y\partial z^2}+\\
& \left(d_z^6\right)\frac{\partial^3 N_6}{\partial y\partial z^2}+\left(d_z^7\right)\frac{\partial^3 N_7}{\partial y\partial z^2}+\left(d_z^8\right)\frac{\partial^3 N_8}{\partial y\partial z^2}+\left(d_z^9\right)\frac{\partial^3 N_9}{\partial y\partial z^2}+\left(d_z^{10}\right)\frac{\partial^3 N_{10}}{\partial y\partial z^2}+\\
& \left(d_z^{11}\right)\frac{\partial^3 N_{11}}{\partial y\partial z^2}+\left(d_z^{12}\right)\frac{\partial^3 N_{12}}{\partial y\partial z^2}+\left(d_z^{13}\right)\frac{\partial^3 N_{13}}{\partial y\partial z^2}+\left(d_z^{14}\right)\frac{\partial^3 N_{14}}{\partial y\partial z^2}+\left(d_z^{15}\right)\frac{\partial^3 N_{15}}{\partial y\partial z^2}+\\
& \left(d_z^{16}\right)\frac{\partial^3 N_{16}}{\partial y\partial z^2}+\left(d_z^{17}\right)\frac{\partial^3 N_{17}}{\partial y\partial z^2}+\left(d_z^{18}\right)\frac{\partial^3 N_{18}}{\partial y\partial z^2}+\left(d_z^{19}\right)\frac{\partial^3 N_{19}}{\partial y\partial z^2}+\left(d_z^{20}\right)\frac{\partial^3 N_{20}}{\partial y\partial z^2}\Bigg]+\\
\tilde{f}_{3333}\Bigg[& \left(d_z^1\right)\frac{\partial^3 N_1}{\partial z^3}+\left(d_z^2\right)\frac{\partial^3 N_2}{\partial z^3}+\left(d_z^3\right)\frac{\partial^3 N_3}{\partial z^3}+\left(d_z^4\right)\frac{\partial^3 N_4}{\partial z^3}+\left(d_z^5\right)\frac{\partial^3 N_5}{\partial z^3}+\\
& \left(d_z^6\right)\frac{\partial^3 N_6}{\partial z^3}+\left(d_z^7\right)\frac{\partial^3 N_7}{\partial z^3}+\left(d_z^8\right)\frac{\partial^3 N_8}{\partial z^3}+\left(d_z^9\right)\frac{\partial^3 N_9}{\partial z^3}+\left(d_z^{10}\right)\frac{\partial^3 N_{10}}{\partial z^3}+\\
& \left(d_z^{11}\right)\frac{\partial^3 N_{11}}{\partial z^3}+\left(d_z^{12}\right)\frac{\partial^3 N_{12}}{\partial z^3}+\left(d_z^{13}\right)\frac{\partial^3 N_{13}}{\partial z^3}+\left(d_z^{14}\right)\frac{\partial^3 N_{14}}{\partial z^3}+\left(d_z^{15}\right)\frac{\partial^3 N_{15}}{\partial z^3}+\\
& \left(d_z^{16}\right)\frac{\partial^3 N_{16}}{\partial z^3}+\left(d_z^{17}\right)\frac{\partial^3 N_{17}}{\partial z^3}+\left(d_z^{18}\right)\frac{\partial^3 N_{18}}{\partial z^3}+\left(d_z^{19}\right)\frac{\partial^3 N_{19}}{\partial z^3}+\left(d_z^{20}\right)\frac{\partial^3 N_{20}}{\partial z^3}\Bigg]+
\end{aligned}
$$

$$
\begin{aligned}
\tilde{f}_{3121}\Bigg[& \left(d_x^1\right)\frac{\partial^3 N_1}{\partial x\partial y\partial z}+\left(d_y^1\right)\frac{\partial^3 N_1}{\partial x^2\partial z}+\left(d_x^2\right)\frac{\partial^3 N_2}{\partial x\partial y\partial z}+\left(d_y^2\right)\frac{\partial^3 N_2}{\partial x^2 partial z}+\left(d_x^3\right)\frac{\partial^3 N_3}{\partial x\partial y\partial z}+\\
& \left(d_y^3\right)\frac{\partial^3 N_3}{\partial x^2\partial z}+\left(d_x^4\right)\frac{\partial^3 N_4}{\partial x\partial y\partial z}+\left(d_y^4\right)\frac{\partial^3 N_4}{\partial x^2\partial z}+\left(d_x^5\right)\frac{\partial^3 N_5}{\partial x\partial y\partial z}+\left(d_y^5\right)\frac{\partial^3 N_5}{\partial x^2\partial z}+\\
& \left(d_x^6\right)\frac{\partial^3 N_6}{\partial x\partial y\partial z}+\left(d_y^6\right)\frac{\partial^3 N_6}{\partial x^2\partial z}+\left(d_x^7\right)\frac{\partial^3 N_7}{\partial x\partial y\partial z}+\left(d_y^7\right)\frac{\partial^3 N_7}{\partial x^2\partial z}+\left(d_x^8\right)\frac{\partial^3 N_8}{\partial x\partial y\partial z}+\\
& \left(d_y^8\right)\frac{\partial^3 N_8}{\partial x^2\partial z}+\left(d_x^9\right)\frac{\partial^3 N_9}{\partial x\partial y\partial z}+\left(d_y^9\right)\frac{\partial^3 N_9}{\partial x^2\partial z}+\left(d_x^{10}\right)\frac{\partial^3 N_{10}}{\partial x\partial y\partial z}+\left(d_y^{10}\right)\frac{\partial^3 N_{10}}{\partial x^2\partial z}+\\
& \left(d_x^{11}\right)\frac{\partial^3 N_{11}}{\partial x\partial y\partial z}+\left(d_y^{11}\right)\frac{\partial^3 N_{11}}{\partial x^2\partial z}+\left(d_x^{12}\right)\frac{\partial^3 N_{12}}{\partial x\partial y\partial z}+\left(d_y^{12}\right)\frac{\partial^3 N_{12}}{\partial x^2\partial z}+\left(d_x^{13}\right)\frac{\partial^3 N_{13}}{\partial x\partial y\partial z}+\\
& \left(d_y^{13}\right)\frac{\partial^3 N_{13}}{\partial x^2\partial z}+\left(d_x^{14}\right)\frac{\partial^3 N_{14}}{\partial x\partial y\partial z}+\left(d_y^{14}\right)\frac{\partial^3 N_{14}}{\partial x^2\partial z}+\left(d_x^{15}\right)\frac{\partial^3 N_{15}}{\partial x\partial y\partial z}+\left(d_y^{15}\right)\frac{\partial^3 N_{15}}{\partial x^2\partial z}+\\
& \left(d_x^{16}\right)\frac{\partial^3 N_{16}}{\partial x\partial y\partial z}+\left(d_y^{16}\right)\frac{\partial^3 N_{16}}{\partial x^2\partial z}+\left(d_x^{17}\right)\frac{\partial^3 N_{17}}{\partial x\partial y\partial z}+\left(d_y^{17}\right)\frac{\partial^3 N_{17}}{\partial x^2\partial z}+\left(d_x^{18}\right)\frac{\partial^3 N_{18}}{\partial x\partial y\partial z}+\\
& \left(d_y^{18}\right)\frac{\partial^3 N_{18}}{\partial x^2\partial z}+\left(d_x^{19}\right)\frac{\partial^3 N_{19}}{\partial x\partial y\partial z}+\left(d_y^{19}\right)\frac{\partial^3 N_{19}}{\partial x^2\partial z}+\left(d_x^{20}\right)\frac{\partial^3 N_{20}}{\partial x\partial y\partial z}+\left(d_y^{20}\right)\frac{\partial^3 N_{20}}{\partial x^2\partial z}\Bigg]+\\
\tilde{f}_{3122}\Bigg[& \left(d_x^1\right)\frac{\partial^3 N_1}{\partial y^2\partial z}+\left(d_y^1\right)\frac{\partial^3 N_1}{\partial x\partial y\partial z}+\left(d_x^2\right)\frac{\partial^3 N_2}{\partial y^2\partial z}+\left(d_y^2\right)\frac{\partial^3 N_2}{\partial x\partial y\partial z}+\left(d_x^3\right)\frac{\partial^3 N_3}{\partial y^2\partial z}+\\
& \left(d_y^3\right)\frac{\partial^3 N_3}{\partial x\partial y\partial z}+\left(d_x^4\right)\frac{\partial^3 N_4}{\partial y^2\partial z}+\left(d_y^4\right)\frac{\partial^3 N_4}{\partial x\partial y\partial z}+\left(d_x^5\right)\frac{\partial^3 N_5}{\partial y^2\partial z}+\left(d_y^5\right)\frac{\partial^3 N_5}{\partial x\partial y\partial z}+\\
& \left(d_x^6\right)\frac{\partial^3 N_6}{\partial y^2\partial z}+\left(d_y^6\right)\frac{\partial^3 N_6}{\partial x\partial y\partial z}+\left(d_x^7\right)\frac{\partial^3 N_7}{\partial y^2\partial z}+\left(d_y^7\right)\frac{\partial^3 N_7}{\partial x\partial y\partial z}+\left(d_x^8\right)\frac{\partial^3 N_8}{\partial y^2\partial z}+\\
& \left(d_y^8\right)\frac{\partial^3 N_8}{\partial x\partial y\partial z}+\left(d_x^9\right)\frac{\partial^3 N_9}{\partial y^2\partial z}+\left(d_y^9\right)\frac{\partial^3 N_9}{\partial x\partial y\partial z}+\left(d_x^{10}\right)\frac{\partial^3 N_{10}}{\partial y^2\partial z}+\left(d_y^{10}\right)\frac{\partial^3 N_{10}}{\partial x\partial y\partial z}+\\
& \left(d_x^{11}\right)\frac{\partial^3 N_{11}}{\partial y^2\partial z}+\left(d_y^{11}\right)\frac{\partial^3 N_{11}}{\partial x\partial y\partial z}+\left(d_x^{12}\right)\frac{\partial^3 N_{12}}{\partial y^2\partial z}+\left(d_y^{12}\right)\frac{\partial^3 N_{12}}{\partial x\partial y\partial z}+\left(d_x^{13}\right)\frac{\partial^3 N_{13}}{\partial y^2\partial z}+\\
& \left(d_y^{13}\right)\frac{\partial^3 N_{13}}{\partial x\partial y\partial z}+\left(d_x^{14}\right)\frac{\partial^3 N_{14}}{\partial y^2\partial z}+\left(d_y^{14}\right)\frac{\partial^3 N_{14}}{\partial x\partial y\partial z}+\left(d_x^{15}\right)\frac{\partial^3 N_{15}}{\partial y^2\partial z}+\left(d_y^{15}\right)\frac{\partial^3 N_{15}}{\partial x\partial y\partial z}+\\
& \left(d_x^{16}\right)\frac{\partial^3 N_{16}}{\partial y^2\partial z}+\left(d_y^{16}\right)\frac{\partial^3 N_{16}}{\partial x\partial y\partial z}+\left(d_x^{17}\right)\frac{\partial^3 N_{17}}{\partial y^2\partial z}+\left(d_y^{17}\right)\frac{\partial^3 N_{17}}{\partial x\partial y\partial z}+\left(d_x^{18}\right)\frac{\partial^3 N_{18}}{\partial y^2\partial z}+\\
& \left(d_y^{18}\right)\frac{\partial^3 N_{18}}{\partial x\partial y\partial z}+\left(d_x^{19}\right)\frac{\partial^3 N_{19}}{\partial y^2\partial z}+\left(d_y^{19}\right)\frac{\partial^3 N_{19}}{\partial x\partial y\partial z}+\left(d_x^{20}\right)\frac{\partial^3 N_{20}}{\partial y^2\partial z}+\left(d_y^{20}\right)\frac{\partial^3 N_{20}}{\partial x\partial y\partial z}\Bigg]+
\end{aligned}
$$

$$
\begin{aligned}
\tilde{f}_{3123}\Bigg[& \left(d_x^1\right)\frac{\partial^3 N_1}{\partial y\partial z^2}+\left(d_y^1\right)\frac{\partial^3 N_1}{\partial x\partial z^2}+\left(d_x^2\right)\frac{\partial^3 N_2}{\partial y\partial z^2}+\left(d_y^2\right)\frac{\partial^3 N_2}{\partial x\partial z^2}+\left(d_x^3\right)\frac{\partial^3 N_3}{\partial y\partial z^2}+\\
& \left(d_y^3\right)\frac{\partial^3 N_3}{\partial x\partial z^2}+\left(d_x^4\right)\frac{\partial^3 N_4}{\partial y\partial z^2}+\left(d_y^4\right)\frac{\partial^3 N_4}{\partial x\partial z^2}+\left(d_x^5\right)\frac{\partial^3 N_5}{\partial y\partial z^2}+\left(d_y^5\right)\frac{\partial^3 N_5}{\partial x\partial z^2}+\\
& \left(d_x^6\right)\frac{\partial^3 N_6}{\partial y\partial z^2}+\left(d_y^6\right)\frac{\partial^3 N_6}{\partial x\partial z^2}+\left(d_x^7\right)\frac{\partial^3 N_7}{\partial y\partial z^2}+\left(d_y^7\right)\frac{\partial^3 N_7}{\partial x\partial z^2}+\left(d_x^8\right)\frac{\partial^3 N_8}{\partial y\partial z^2}+\\
& \left(d_y^8\right)\frac{\partial^3 N_8}{\partial x\partial z^2}+\left(d_x^9\right)\frac{\partial^3 N_9}{\partial y\partial z^2}+\left(d_y^9\right)\frac{\partial^3 N_9}{\partial x\partial z^2}+\left(d_x^{10}\right)\frac{\partial^3 N_{10}}{\partial y\partial z^2}+\left(d_y^{10}\right)\frac{\partial^3 N_{10}}{\partial x\partial z^2}+\\
& \left(d_x^{11}\right)\frac{\partial^3 N_{11}}{\partial y\partial z^2}+\left(d_y^{11}\right)\frac{\partial^3 N_{11}}{\partial x\partial z^2}+\left(d_x^{12}\right)\frac{\partial^3 N_{12}}{\partial y\partial z^2}+\left(d_y^{12}\right)\frac{\partial^3 N_{12}}{\partial x\partial z^2}+\left(d_x^{13}\right)\frac{\partial^3 N_{13}}{\partial y\partial z^2}+\\
& \left(d_y^{13}\right)\frac{\partial^3 N_{13}}{\partial x\partial z^2}+\left(d_x^{14}\right)\frac{\partial^3 N_{14}}{\partial y\partial z^2}+\left(d_y^{14}\right)\frac{\partial^3 N_{14}}{\partial x\partial z^2}+\left(d_x^{15}\right)\frac{\partial^3 N_{15}}{\partial y\partial z^2}+\left(d_y^{15}\right)\frac{\partial^3 N_{15}}{\partial x\partial z^2}+\\
& \left(d_x^{16}\right)\frac{\partial^3 N_{16}}{\partial y\partial z^2}+\left(d_y^{16}\right)\frac{\partial^3 N_{16}}{\partial x\partial z^2}+\left(d_x^{17}\right)\frac{\partial^3 N_{17}}{\partial y\partial z^2}+\left(d_y^{17}\right)\frac{\partial^3 N_{17}}{\partial x\partial z^2}+\left(d_x^{18}\right)\frac{\partial^3 N_{18}}{\partial y\partial z^2}+\\
& \left(d_y^{18}\right)\frac{\partial^3 N_{18}}{\partial x\partial z^2}+\left(d_x^{19}\right)\frac{\partial^3 N_{19}}{\partial y\partial z^2}+\left(d_y^{19}\right)\frac{\partial^3 N_{19}}{\partial x\partial z^2}+\left(d_x^{20}\right)\frac{\partial^3 N_{20}}{\partial y\partial z^2}+\left(d_y^{20}\right)\frac{\partial^3 N_{20}}{\partial x\partial z^2}\Bigg]+\\
\tilde{f}_{3131}\Bigg[& \left(d_x^1\right)\frac{\partial^3 N_1}{\partial x\partial z^2}+\left(d_z^1\right)\frac{\partial^3 N_1}{\partial x^2\partial z}+\left(d_x^2\right)\frac{\partial^3 N_2}{\partial x\partial z^2}+\left(d_z^2\right)\frac{\partial^3 N_2}{\partial x^2\partial z}+\left(d_x^3\right)\frac{\partial^3 N_3}{\partial x\partial z^2}+\\
& \left(d_z^3\right)\frac{\partial^3 N_3}{\partial x^2\partial z}+\left(d_x^4\right)\frac{\partial^3 N_4}{\partial x\partial z^2}+\left(d_z^4\right)\frac{\partial^3 N_4}{\partial x^2\partial z}+\left(d_x^5\right)\frac{\partial^3 N_5}{\partial x\partial z^2}+\left(d_z^5\right)\frac{\partial^3 N_5}{\partial x^2\partial z}+\\
& \left(d_x^6\right)\frac{\partial^3 N_6}{\partial x\partial z^2}+\left(d_z^6\right)\frac{\partial^3 N_6}{\partial x^2\partial z}+\left(d_x^7\right)\frac{\partial^3 N_7}{\partial x\partial z^2}+\left(d_z^7\right)\frac{\partial^3 N_7}{\partial x^2\partial z}+\left(d_x^8\right)\frac{\partial^3 N_8}{\partial x\partial z^2}+\\
& \left(d_z^8\right)\frac{\partial^3 N_8}{\partial x^2\partial z}+\left(d_x^9\right)\frac{\partial^3 N_9}{\partial x\partial z^2}+\left(d_z^9\right)\frac{\partial^3 N_9}{\partial x^2\partial z}+\left(d_x^{10}\right)\frac{\partial^3 N_{10}}{\partial x\partial z^2}+\left(d_z^{10}\right)\frac{\partial^3 N_{10}}{\partial x^2\partial z}+\\
& \left(d_x^{11}\right)\frac{\partial^3 N_{11}}{\partial x\partial z^2}+\left(d_z^{11}\right)\frac{\partial^3 N_{11}}{\partial x^2\partial z}+\left(d_x^{12}\right)\frac{\partial^3 N_{12}}{\partial x\partial z^2}+\left(d_z^{12}\right)\frac{\partial^3 N_{12}}{\partial x^2\partial z}+\left(d_x^{13}\right)\frac{\partial^3 N_{13}}{\partial x\partial z^2}+\\
& \left(d_z^{13}\right)\frac{\partial^3 N_{13}}{\partial x^2\partial z}+\left(d_x^{14}\right)\frac{\partial^3 N_{14}}{\partial x\partial z^2}+\left(d_z^{14}\right)\frac{\partial^3 N_{14}}{\partial x^2\partial z}+\left(d_x^{15}\right)\frac{\partial^3 N_{15}}{\partial x\partial z^2}+\left(d_z^{15}\right)\frac{\partial^3 N_{15}}{\partial x^2\partial z}+\\
& \left(d_x^{16}\right)\frac{\partial^3 N_{16}}{\partial x\partial z^2}+\left(d_z^{16}\right)\frac{\partial^3 N_{16}}{\partial x^2\partial z}+\left(d_x^{17}\right)\frac{\partial^3 N_{17}}{\partial x\partial z^2}+\left(d_z^{17}\right)\frac{\partial^3 N_{17}}{\partial x^2\partial z}+\left(d_x^{18}\right)\frac{\partial^3 N_{18}}{\partial x\partial z^2}+\\
& \left(d_z^{18}\right)\frac{\partial^3 N_{18}}{\partial x^2\partial z}+\left(d_x^{19}\right)\frac{\partial^3 N_{19}}{\partial x\partial z^2}+\left(d_z^{19}\right)\frac{\partial^3 N_{19}}{\partial x^2\partial z}+\left(d_x^{20}\right)\frac{\partial^3 N_{20}}{\partial x\partial z^2}+\left(d_z^{20}\right)\frac{\partial^3 N_{20}}{\partial x^2\partial z}\Bigg]+
\end{aligned}
$$

$$
\begin{aligned}
\tilde{f}_{3132}\Bigg[& \left(d_x^1\right)\frac{\partial^3 N_1}{\partial y\partial z^2}+\left(d_z^1\right)\frac{\partial^3 N_1}{\partial x\partial y\partial z}+\left(d_x^2\right)\frac{\partial^3 N_2}{\partial y\partial z^2}+\left(d_z^2\right)\frac{\partial^3 N_2}{\partial x\partial y\partial z}+\left(d_x^3\right)\frac{\partial^3 N_3}{\partial y\partial z^2}+\\
& \left(d_z^3\right)\frac{\partial^3 N_3}{\partial x\partial y\partial z}+\left(d_x^4\right)\frac{\partial^3 N_4}{\partial y\partial z^2}+\left(d_z^4\right)\frac{\partial^3 N_4}{\partial x\partial y\partial z}+\left(d_x^5\right)\frac{\partial^3 N_5}{\partial y\partial z^2}+\left(d_z^5\right)\frac{\partial^3 N_5}{\partial x\partial y\partial z}+\\
& \left(d_x^6\right)\frac{\partial^3 N_6}{\partial y\partial z^2}+\left(d_z^6\right)\frac{\partial^3 N_6}{\partial x\partial y\partial z}+\left(d_x^7\right)\frac{\partial^3 N_7}{\partial y\partial z^2}+\left(d_z^7\right)\frac{\partial^3 N_7}{\partial x\partial y\partial z}+\left(d_x^8\right)\frac{\partial^3 N_8}{\partial y\partial z^2}+\\
& \left(d_z^8\right)\frac{\partial^3 N_8}{\partial x\partial y\partial z}+\left(d_x^9\right)\frac{\partial^3 N_9}{\partial y\partial z^2}+\left(d_z^9\right)\frac{\partial^3 N_9}{\partial x\partial y\partial z}+\left(d_x^{10}\right)\frac{\partial^3 N_{10}}{\partial y\partial z^2}+\left(d_z^{10}\right)\frac{\partial^3 N_{10}}{\partial x\partial y\partial z}+\\
& \left(d_x^{11}\right)\frac{\partial^3 N_{11}}{\partial y\partial z^2}+\left(d_z^{11}\right)\frac{\partial^3 N_{11}}{\partial x\partial y\partial z}+\left(d_x^{12}\right)\frac{\partial^3 N_{12}}{\partial y\partial z^2}+\left(d_z^{12}\right)\frac{\partial^3 N_{12}}{\partial x\partial y\partial z}+\left(d_x^{13}\right)\frac{\partial^3 N_{13}}{\partial y\partial z^2}+\\
& \left(d_z^{13}\right)\frac{\partial^3 N_{13}}{\partial x\partial y\partial z}+\left(d_x^{14}\right)\frac{\partial^3 N_{14}}{\partial y\partial z^2}+\left(d_z^{14}\right)\frac{\partial^3 N_{14}}{\partial x\partial y\partial z}+\left(d_x^{15}\right)\frac{\partial^3 N_{15}}{\partial y\partial z^2}+\left(d_z^{15}\right)\frac{\partial^3 N_{15}}{\partial x\partial y\partial z}+\\
& \left(d_x^{16}\right)\frac{\partial^3 N_{16}}{\partial y\partial z^2}+\left(d_z^{16}\right)\frac{\partial^3 N_{16}}{\partial x\partial y\partial z}+\left(d_x^{17}\right)\frac{\partial^3 N_{17}}{\partial y\partial z^2}+\left(d_z^{17}\right)\frac{\partial^3 N_{17}}{\partial x\partial y\partial z}+\left(d_x^{18}\right)\frac{\partial^3 N_{18}}{\partial y\partial z^2}+\\
& \left(d_z^{18}\right)\frac{\partial^3 N_{18}}{\partial x\partial y\partial z}+\left(d_x^{19}\right)\frac{\partial^3 N_{19}}{\partial y\partial z^2}+\left(d_z^{19}\right)\frac{\partial^3 N_{19}}{\partial x\partial y\partial z}+\left(d_x^{20}\right)\frac{\partial^3 N_{20}}{\partial y\partial z^2}+\left(d_z^{20}\right)\frac{\partial^3 N_{20}}{\partial x\partial y\partial z}\Bigg]+\\
\tilde{f}_{3133}\Bigg[& \left(d_x^1\right)\frac{\partial^3 N_1}{\partial z^3}+\left(d_z^1\right)\frac{\partial^3 N_1}{\partial x\partial z^2}+\left(d_x^2\right)\frac{\partial^3 N_2}{\partial z^3}+\left(d_z^2\right)\frac{\partial^3 N_2}{\partial x\partial z^2}+\left(d_x^3\right)\frac{\partial^3 N_3}{\partial z^3}+\\
& \left(d_z^3\right)\frac{\partial^3 N_3}{\partial x\partial z^2}+\left(d_x^4\right)\frac{\partial^3 N_4}{\partial z^3}+\left(d_z^4\right)\frac{\partial^3 N_4}{\partial x\partial z^2}+\left(d_x^5\right)\frac{\partial^3 N_5}{\partial z^3}+\left(d_z^5\right)\frac{\partial^3 N_5}{\partial x\partial z^2}+\\
& \left(d_x^6\right)\frac{\partial^3 N_6}{\partial z^3}+\left(d_z^6\right)\frac{\partial^3 N_6}{\partial x\partial z^2}+\left(d_x^7\right)\frac{\partial^3 N_7}{\partial z^3}+\left(d_z^7\right)\frac{\partial^3 N_7}{\partial x\partial z^2}+\left(d_x^8\right)\frac{\partial^3 N_8}{\partial z^3}+\\
& \left(d_z^8\right)\frac{\partial^3 N_8}{\partial x\partial z^2}+\left(d_x^9\right)\frac{\partial^3 N_9}{\partial z^3}+\left(d_z^9\right)\frac{\partial^3 N_9}{\partial x\partial z^2}+\left(d_x^{10}\right)\frac{\partial^3 N_{10}}{\partial z^3}+\left(d_z^{10}\right)\frac{\partial^3 N_{10}}{\partial x\partial z^2}+\\
& \left(d_x^{11}\right)\frac{\partial^3 N_{11}}{\partial z^3}+\left(d_z^{11}\right)\frac{\partial^3 N_{11}}{\partial x\partial z^2}+\left(d_x^{12}\right)\frac{\partial^3 N_{12}}{\partial z^3}+\left(d_z^{12}\right)\frac{\partial^3 N_{12}}{\partial x\partial z^2}+\left(d_x^{13}\right)\frac{\partial^3 N_{13}}{\partial z^3}+\\
& \left(d_z^{13}\right)\frac{\partial^3 N_{13}}{\partial x\partial z^2}+\left(d_x^{14}\right)\frac{\partial^3 N_{14}}{\partial z^3}+\left(d_z^{14}\right)\frac{\partial^3 N_{14}}{\partial x\partial z^2}+\left(d_x^{15}\right)\frac{\partial^3 N_{15}}{\partial z^3}+\left(d_z^{15}\right)\frac{\partial^3 N_{15}}{\partial x\partial z^2}+\\
& \left(d_x^{16}\right)\frac{\partial^3 N_{16}}{\partial z^3}+\left(d_z^{16}\right)\frac{\partial^3 N_{16}}{\partial x\partial z^2}+\left(d_x^{17}\right)\frac{\partial^3 N_{17}}{\partial z^3}+\left(d_z^{17}\right)\frac{\partial^3 N_{17}}{\partial x\partial z^2}+\left(d_x^{18}\right)\frac{\partial^3 N_{18}}{\partial z^3}+\\
& \left(d_z^{18}\right)\frac{\partial^3 N_{18}}{\partial x\partial z^2}+\left(d_x^{19}\right)\frac{\partial^3 N_{19}}{\partial z^3}+\left(d_z^{19}\right)\frac{\partial^3 N_{19}}{\partial x\partial z^2}+\left(d_x^{20}\right)\frac{\partial^3 N_{20}}{\partial z^3}+\left(d_z^{20}\right)\frac{\partial^3 N_{20}}{\partial x\partial z^2}\Bigg]+
\end{aligned}
$$

$$
\begin{aligned}
\tilde{f}_{3231}\Bigg[& \left(d_y^1\right)\frac{\partial^3 N_1}{\partial x\partial z^2}+\left(d_z^1\right)\frac{\partial^3 N_1}{\partial x\partial y\partial z}+\left(d_y^2\right)\frac{\partial^3 N_2}{\partial x\partial z^2}+\left(d_z^2\right)\frac{\partial^3 N_2}{\partial x\partial y\partial z}+\left(d_y^3\right)\frac{\partial^3 N_3}{\partial x\partial z^2}+\\
& \left(d_z^3\right)\frac{\partial^3 N_3}{\partial x\partial y\partial z}+\left(d_y^4\right)\frac{\partial^3 N_4}{\partial x\partial z^2}+\left(d_z^4\right)\frac{\partial^3 N_4}{\partial x\partial y\partial z}+\left(d_y^5\right)\frac{\partial^3 N_5}{\partial x\partial z^2}+\left(d_z^5\right)\frac{\partial^3 N_5}{\partial x\partial y\partial z}+\\
& \left(d_y^6\right)\frac{\partial^3 N_6}{\partial x\partial z^2}+\left(d_z^6\right)\frac{\partial^3 N_6}{\partial x\partial y\partial z}+\left(d_y^7\right)\frac{\partial^3 N_7}{\partial x\partial z^2}+\left(d_z^7\right)\frac{\partial^3 N_7}{\partial x\partial y\partial z}+\left(d_y^8\right)\frac{\partial^3 N_8}{\partial x\partial z^2}+\\
& \left(d_z^8\right)\frac{\partial^3 N_8}{\partial x\partial y\partial z}+\left(d_y^9\right)\frac{\partial^3 N_9}{\partial x\partial z^2}+\left(d_z^9\right)\frac{\partial^3 N_9}{\partial x\partial y\partial z}+\left(d_y^{10}\right)\frac{\partial^3 N_{10}}{\partial x\partial z^2}+\left(d_z^{10}\right)\frac{\partial^3 N_{10}}{\partial x\partial y\partial z}+\\
& \left(d_y^{11}\right)\frac{\partial^3 N_{11}}{\partial x\partial z^2}+\left(d_z^{11}\right)\frac{\partial^3 N_{11}}{\partial x\partial y\partial z}+\left(d_y^{12}\right)\frac{\partial^3 N_{12}}{\partial x\partial z^2}+\left(d_z^{12}\right)\frac{\partial^3 N_{12}}{\partial x\partial y\partial z}+\left(d_y^{13}\right)\frac{\partial^3 N_{13}}{\partial x\partial z^2}+\\
& \left(d_z^{13}\right)\frac{\partial^3 N_{13}}{\partial x\partial y\partial z}+\left(d_y^{14}\right)\frac{\partial^3 N_{14}}{\partial x\partial z^2}+\left(d_z^{14}\right)\frac{\partial^3 N_{14}}{\partial x\partial y\partial z}+\left(d_y^{15}\right)\frac{\partial^3 N_{15}}{\partial x\partial z^2}+\left(d_z^{15}\right)\frac{\partial^3 N_{15}}{\partial x\partial y\partial z}+\\
& \left(d_y^{16}\right)\frac{\partial^3 N_{16}}{\partial x\partial z^2}+\left(d_z^{16}\right)\frac{\partial^3 N_{16}}{\partial x\partial y\partial z}+\left(d_y^{17}\right)\frac{\partial^3 N_{17}}{\partial x\partial z^2}+\left(d_z^{17}\right)\frac{\partial^3 N_{17}}{\partial x\partial y\partial z}+\left(d_y^{18}\right)\frac{\partial^3 N_{18}}{\partial x\partial z^2}+\\
& \left(d_z^{18}\right)\frac{\partial^3 N_{18}}{\partial x\partial y\partial z}+\left(d_y^{19}\right)\frac{\partial^3 N_{19}}{\partial x\partial z^2}+\left(d_z^{19}\right)\frac{\partial^3 N_{19}}{\partial x\partial y\partial z}+\left(d_y^{20}\right)\frac{\partial^3 N_{20}}{\partial x\partial z^2}+\left(d_z^{20}\right)\frac{\partial^3 N_{20}}{\partial x\partial y\partial z}\Bigg]+\\
\tilde{f}_{3232}\Bigg[& \left(d_y^1\right)\frac{\partial^3 N_1}{\partial y\partial z^2}+\left(d_z^1\right)\frac{\partial^3 N_1}{\partial y^2\partial z}+\left(d_y^2\right)\frac{\partial^3 N_2}{\partial y\partial z^2}+\left(d_z^2\right)\frac{\partial^3 N_2}{\partial y^2\partial z}+\left(d_y^3\right)\frac{\partial^3 N_3}{\partial y\partial z^2}+\\
& \left(d_z^3\right)\frac{\partial^3 N_3}{\partial y^2\partial z}+\left(d_y^4\right)\frac{\partial^3 N_4}{\partial y\partial z^2}+\left(d_z^4\right)\frac{\partial^3 N_4}{\partial y^2\partial z}+\left(d_y^5\right)\frac{\partial^3 N_5}{\partial y\partial z^2}+\left(d_z^5\right)\frac{\partial^3 N_5}{\partial y^2\partial z}+\\
& \left(d_y^6\right)\frac{\partial^3 N_6}{\partial y\partial z^2}+\left(d_z^6\right)\frac{\partial^3 N_6}{\partial y^2\partial z}+\left(d_y^7\right)\frac{\partial^3 N_7}{\partial y\partial z^2}+\left(d_z^7\right)\frac{\partial^3 N_7}{\partial y^2\partial z}+\left(d_y^8\right)\frac{\partial^3 N_8}{\partial y\partial z^2}+\\
& \left(d_z^8\right)\frac{\partial^3 N_8}{\partial y^2\partial z}+\left(d_y^9\right)\frac{\partial^3 N_9}{\partial y\partial z^2}+\left(d_z^9\right)\frac{\partial^3 N_9}{\partial y^2\partial z}+\left(d_y^{10}\right)\frac{\partial^3 N_{10}}{\partial y\partial z^2}+\left(d_z^{10}\right)\frac{\partial^3 N_{10}}{\partial y^2\partial z}+\\
& \left(d_y^{11}\right)\frac{\partial^3 N_{11}}{\partial y\partial z^2}+\left(d_z^{11}\right)\frac{\partial^3 N_{11}}{\partial y^2\partial z}+\left(d_y^{12}\right)\frac{\partial^3 N_{12}}{\partial y\partial z^2}+\left(d_z^{12}\right)\frac{\partial^3 N_{12}}{\partial y^2\partial z}+\left(d_y^{13}\right)\frac{\partial^3 N_{13}}{\partial y\partial z^2}+\\
& \left(d_z^{13}\right)\frac{\partial^3 N_{13}}{\partial y^2\partial z}+\left(d_y^{14}\right)\frac{\partial^3 N_{14}}{\partial y\partial z^2}+\left(d_z^{14}\right)\frac{\partial^3 N_{14}}{\partial y^2\partial z}+\left(d_y^{15}\right)\frac{\partial^3 N_{15}}{\partial y\partial z^2}+\left(d_z^{15}\right)\frac{\partial^3 N_{15}}{\partial y^2\partial z}+\\
& \left(d_y^{16}\right)\frac{\partial^3 N_{16}}{\partial y\partial z^2}+\left(d_z^{16}\right)\frac{\partial^3 N_{16}}{\partial y^2\partial z}+\left(d_y^{17}\right)\frac{\partial^3 N_{17}}{\partial y\partial z^2}+\left(d_z^{17}\right)\frac{\partial^3 N_{17}}{\partial y^2\partial z}+\left(d_y^{18}\right)\frac{\partial^3 N_{18}}{\partial y\partial z^2}+\\
& \left(d_z^{18}\right)\frac{\partial^3 N_{18}}{\partial y^2\partial z}+\left(d_y^{19}\right)\frac{\partial^3 N_{19}}{\partial y\partial z^2}+\left(d_z^{19}\right)\frac{\partial^3 N_{19}}{\partial y^2\partial z}+\left(d_y^{20}\right)\frac{\partial^3 N_{20}}{\partial y\partial z^2}+\left(d_z^{20}\right)\frac{\partial^3 N_{20}}{\partial y^2\partial z}\Bigg]+
\end{aligned}
$$

$$\tilde{f}_{3233}\Bigg[\left(d_y^1\right)\frac{\partial^3 N_1}{\partial z^3}+\left(d_z^1\right)\frac{\partial^3 N_1}{\partial y\partial z^2}+\left(d_y^2\right)\frac{\partial^3 N_2}{\partial z^3}+\left(d_z^2\right)\frac{\partial^3 N_2}{\partial y\partial z^2}+\left(d_y^3\right)\frac{\partial^3 N_3}{\partial z^3}+$$
$$\left(d_z^3\right)\frac{\partial^3 N_3}{\partial y\partial z^2}+\left(d_y^4\right)\frac{\partial^3 N_4}{\partial z^3}+\left(d_z^4\right)\frac{\partial^3 N_4}{\partial y\partial z^2}+\left(d_y^5\right)\frac{\partial^3 N_5}{\partial z^3}+\left(d_z^5\right)\frac{\partial^3 N_5}{\partial y\partial z^2}+$$
$$\left(d_y^6\right)\frac{\partial^3 N_6}{\partial z^3}+\left(d_z^6\right)\frac{\partial^3 N_6}{\partial y\partial z^2}+\left(d_y^7\right)\frac{\partial^3 N_7}{\partial z^3}+\left(d_z^7\right)\frac{\partial^3 N_7}{\partial y\partial z^2}+\left(d_y^8\right)\frac{\partial^3 N_8}{\partial z^3}+$$
$$\left(d_z^8\right)\frac{\partial^3 N_8}{\partial y\partial z^2}+\left(d_y^9\right)\frac{\partial^3 N_9}{\partial z^3}+\left(d_z^9\right)\frac{\partial^3 N_9}{\partial y\partial z^2}+\left(d_y^{10}\right)\frac{\partial^3 N_{10}}{\partial z^3}+\left(d_z^{10}\right)\frac{\partial^3 N_{10}}{\partial y\partial z^2}+$$
$$\left(d_y^{11}\right)\frac{\partial^3 N_{11}}{\partial z^3}+\left(d_z^{11}\right)\frac{\partial^3 N_{11}}{\partial y\partial z^2}+\left(d_y^{12}\right)\frac{\partial^3 N_{12}}{\partial z^3}+\left(d_z^{12}\right)\frac{\partial^3 N_{12}}{\partial y\partial z^2}+\left(d_y^{13}\right)\frac{\partial^3 N_{13}}{\partial z^3}+$$
$$\left(d_z^{13}\right)\frac{\partial^3 N_{13}}{\partial y\partial z^2}+\left(d_y^{14}\right)\frac{\partial^3 N_{14}}{\partial z^3}+\left(d_z^{14}\right)\frac{\partial^3 N_{14}}{\partial y\partial z^2}+\left(d_y^{15}\right)\frac{\partial^3 N_{15}}{\partial z^3}+\left(d_z^{15}\right)\frac{\partial^3 N_{15}}{\partial y\partial z^2}+$$
$$\left(d_y^{16}\right)\frac{\partial^3 N_{16}}{\partial z^3}+\left(d_z^{16}\right)\frac{\partial^3 N_{16}}{\partial y\partial z^2}+\left(d_y^{17}\right)\frac{\partial^3 N_{17}}{\partial z^3}+\left(d_z^{17}\right)\frac{\partial^3 N_{17}}{\partial y\partial z^2}+\left(d_y^{18}\right)\frac{\partial^3 N_{18}}{\partial z^3}+$$
$$\left(d_z^{18}\right)\frac{\partial^3 N_{18}}{\partial y\partial z^2}+\left(d_y^{19}\right)\frac{\partial^3 N_{19}}{\partial z^3}+\left(d_z^{19}\right)\frac{\partial^3 N_{19}}{\partial y\partial z^2}+\left(d_y^{20}\right)\frac{\partial^3 N_{20}}{\partial z^3}+\left(d_z^{20}\right)\frac{\partial^3 N_{20}}{\partial y\partial z^2}\Bigg] \tag{B.6}$$

Furthermore, making use of Equations (4.54), (B.5) and (B.6) leads to:

$$
\begin{aligned}
\nabla \cdot \tilde{\mathbf{P}} = \tilde{f}_{1112} \Bigg[& \left(d_x^1\right) \frac{-1+\zeta}{4a^2b} + \left(d_x^2\right) \frac{-1+\zeta}{4a^2b} + \left(d_x^3\right) \frac{1-\zeta}{4a^2b} + \left(d_x^4\right) \frac{1-\zeta}{4a^2b} + \\
& \left(d_x^5\right) \frac{-1-\zeta}{4a^2b} + \left(d_x^6\right) \frac{-1-\zeta}{4a^2b} + \left(d_x^7\right) \frac{1+\zeta}{4a^2b} + \left(d_x^8\right) \frac{1+\zeta}{4a^2b} + \\
& \left(d_x^9\right) \frac{1-\zeta}{2a^2b} + \left(d_x^{11}\right) \frac{-1+\zeta}{2a^2b} + \left(d_x^{13}\right) \frac{1+\zeta}{2a^2b} + \left(d_x^{15}\right) \frac{-1-\zeta}{2a^2b} \Bigg] + \\
\tilde{f}_{1113} \Bigg[& \left(d_x^1\right) \frac{-1+\eta}{4a^2c} + \left(d_x^2\right) \frac{-1+\eta}{4a^2c} + \left(d_x^3\right) \frac{-1-\eta}{4a^2c} + \left(d_x^4\right) \frac{-1-\eta}{4a^2c} + \\
& \left(d_x^5\right) \frac{1-\eta}{4a^2c} + \left(d_x^6\right) \frac{1-\eta}{4a^2c} + \left(d_x^7\right) \frac{1+\eta}{4a^2c} + \left(d_x^8\right) \frac{1+\eta}{4a^2c} + \\
& \left(d_x^9\right) \frac{1-\eta}{2a^2c} + \left(d_x^{11}\right) \frac{1+\eta}{2a^2c} + \left(d_x^{13}\right) \frac{-1+\eta}{2a^2c} + \left(d_x^{15}\right) \frac{-1-\eta}{2a^2c} \Bigg] + \\
\tilde{f}_{1221} \Bigg[& \left(d_y^1\right) \frac{-1+\zeta}{4a^2b} + \left(d_y^2\right) \frac{-1+\zeta}{4a^2b} + \left(d_y^3\right) \frac{1-\zeta}{4a^2b} + \left(d_y^4\right) \frac{1-\zeta}{4a^2b} + \\
& \left(d_y^5\right) \frac{-1-\zeta}{4a^2b} + \left(d_y^6\right) \frac{-1-\zeta}{4a^2b} + \left(d_y^7\right) \frac{1+\zeta}{4a^2b} + \left(d_y^8\right) \frac{1+\zeta}{4a^2b} + \\
& \left(d_y^9\right) \frac{1-\zeta}{2a^2b} + \left(d_y^{11}\right) \frac{-1+\zeta}{2a^2b} + \left(d_y^{13}\right) \frac{1+\zeta}{2a^2b} + \left(d_y^{15}\right) \frac{-1-\zeta}{2a^2b} \Bigg] + \\
\tilde{f}_{1222} \Bigg[& \left(d_y^1\right) \frac{-1+\zeta}{4ab^2} + \left(d_y^2\right) \frac{1-\zeta}{4ab^2} + \left(d_y^3\right) \frac{1-\zeta}{4ab^2} + \left(d_y^4\right) \frac{-1+\zeta}{4ab^2} + \\
& \left(d_y^5\right) \frac{-1-\zeta}{4ab^2} + \left(d_y^6\right) \frac{1+\zeta}{4ab^2} + \left(d_y^7\right) \frac{1+\zeta}{4ab^2} + \left(d_y^8\right) \frac{-1-\zeta}{4ab^2} + \\
& \left(d_y^{10}\right) \frac{-1+\zeta}{2ab^2} + \left(d_y^{12}\right) \frac{1-\zeta}{2ab^2} + \left(d_y^{14}\right) \frac{-1-\zeta}{2ab^2} + \left(d_y^{16}\right) \frac{1+\zeta}{2ab^2} \Bigg] + \\
\end{aligned}
$$

$$
\begin{aligned}
\tilde{f}_{1223}\Bigg[& \left(d_y^1\right)\frac{-1+2\xi+2\eta+2\zeta}{8abc}+\left(d_y^2\right)\frac{1+2\xi-2\eta-2\zeta}{8abc}+\\
& \left(d_y^3\right)\frac{-1-2\xi-2\eta+2\zeta}{8abc}+\left(d_y^4\right)\frac{1-2\xi+2\eta-2\zeta}{8abc}+\\
& \left(d_y^5\right)\frac{1-2\xi-2\eta+2\zeta}{8abc}+\left(d_y^6\right)\frac{-1-2\xi+2\eta-2\zeta}{8abc}+\\
& \left(d_y^7\right)\frac{1+2\xi+2\eta+2\zeta}{8abc}+\left(d_y^8\right)\frac{-1+2\xi-2\eta-2\zeta}{8abc}+\\
& \left(d_y^9\right)\frac{-\xi}{2abc}+\left(d_y^{10}\right)\frac{\eta}{2abc}+\left(d_y^{11}\right)\frac{\xi}{2abc}+\left(d_y^{12}\right)\frac{-\eta}{2abc}+\\
& \left(d_y^{13}\right)\frac{\xi}{2abc}+\left(d_y^{14}\right)\frac{-\eta}{2abc}+\left(d_y^{15}\right)\frac{-\xi}{2abc}+\left(d_y^{16}\right)\frac{\eta}{2abc}+\\
& \left(d_y^{17}\right)\frac{-\zeta}{2abc}+\left(d_y^{18}\right)\frac{\zeta}{2abc}+\left(d_y^{19}\right)\frac{-\zeta}{2abc}+\left(d_y^{20}\right)\frac{\zeta}{2abc}\Bigg]+\\
\tilde{f}_{1331}\Bigg[& \left(d_z^1\right)\frac{-1+\eta}{4a^2c}+\left(d_z^2\right)\frac{-1+\eta}{4a^2c}+\left(d_z^3\right)\frac{-1-\eta}{4a^2c}+\left(d_z^4\right)\frac{-1-\eta}{4a^2c}+\\
& \left(d_z^5\right)\frac{1-\eta}{4a^2c}+\left(d_z^6\right)\frac{1-\eta}{4a^2c}+\left(d_z^7\right)\frac{1+\eta}{4a^2c}+\left(d_z^8\right)\frac{1+\eta}{4a^2c}+\\
& \left(d_z^9\right)\frac{1-\eta}{2a^2c}+\left(d_z^{11}\right)\frac{1+\eta}{2a^2c}+\left(d_z^{13}\right)\frac{-1+\eta}{2a^2c}+\left(d_z^{15}\right)\frac{-1-\eta}{2a^2c}\Bigg]+\\
\tilde{f}_{1332}\Bigg[& \left(d_z^1\right)\frac{-1+2\xi+2\eta+2\zeta}{8abc}+\left(d_z^2\right)\frac{1+2\xi-2\eta-2\zeta}{8abc}+\\
& \left(d_z^3\right)\frac{-1-2\xi-2\eta+2\zeta}{8abc}+\left(d_z^4\right)\frac{1-2\xi+2\eta-2\zeta}{8abc}+\\
& \left(d_z^5\right)\frac{1-2\xi-2\eta+2\zeta}{8abc}+\left(d_z^6\right)\frac{-1-2\xi+2\eta-2\zeta}{8abc}+\\
& \left(d_z^7\right)\frac{1+2\xi+2\eta+2\zeta}{8abc}+\left(d_z^8\right)\frac{-1+2\xi-2\eta-2\zeta}{8abc}+\\
& \left(d_z^9\right)\frac{-\xi}{2abc}+\left(d_z^{10}\right)\frac{\eta}{2abc}+\left(d_z^{11}\right)\frac{\xi}{2abc}+\left(d_z^{12}\right)\frac{-\eta}{2abc}+\\
& \left(d_z^{13}\right)\frac{\xi}{2abc}+\left(d_z^{14}\right)\frac{-\eta}{2abc}+\left(d_z^{15}\right)\frac{-\xi}{2abc}+\left(d_z^{16}\right)\frac{\eta}{2abc}+\\
& \left(d_z^{17}\right)\frac{-\zeta}{2abc}+\left(d_z^{18}\right)\frac{\zeta}{2abc}+\left(d_z^{19}\right)\frac{-\zeta}{2abc}+\left(d_z^{20}\right)\frac{\zeta}{2abc}\Bigg]+
\end{aligned}
$$

$$
\begin{aligned}
\tilde{f}_{1333}\Bigg[& \left(d_z^1\right)\frac{-1+\eta}{4ac^2}+\left(d_z^2\right)\frac{1-\eta}{4ac^2}+\left(d_z^3\right)\frac{1+\eta}{4ac^2}+\left(d_z^4\right)\frac{-1-\eta}{4ac^2}+\\
& \left(d_z^5\right)\frac{-1+\eta}{4ac^2}+\left(d_z^6\right)\frac{1-\eta}{4ac^2}+\left(d_z^7\right)\frac{1+\eta}{4ac^2}+\left(d_z^8\right)\frac{-1-\eta}{4ac^2}+\\
& \left(d_z^{17}\right)\frac{1-\eta}{2ac^2}+\left(d_z^{18}\right)\frac{-1+\eta}{2ac^2}+\left(d_z^{19}\right)\frac{-1-\eta}{2ac^2}+\left(d_z^{20}\right)\frac{1+\eta}{2ac^2}\Bigg]+\\
\tilde{f}_{1121}\Bigg[& \left(d_x^1\right)\frac{-1+\zeta}{4a^2b}+\left(d_x^2\right)\frac{-1+\zeta}{4a^2b}+\left(d_x^3\right)\frac{1-\zeta}{4a^2b}+\left(d_x^4\right)\frac{1-\zeta}{4a^2b}+\\
& \left(d_x^5\right)\frac{-1-\zeta}{4a^2b}+\left(d_x^6\right)\frac{-1-\zeta}{4a^2b}+\left(d_x^7\right)\frac{1+\zeta}{4a^2b}+\left(d_x^8\right)\frac{1+\zeta}{4a^2b}+\\
& \left(d_x^9\right)\frac{1-\zeta}{2a^2b}+\left(d_x^{11}\right)\frac{-1+\zeta}{2a^2b}+\left(d_x^{13}\right)\frac{1+\zeta}{2a^2b}+\left(d_x^{15}\right)\frac{-1-\zeta}{2a^2b}\Bigg]+\\
\tilde{f}_{1122}\Bigg[& \left(d_x^1\right)\frac{-1+\zeta}{4ab^2}+\left(d_y^1\right)\frac{-1+\zeta}{4a^2b}+\left(d_x^2\right)\frac{1-\zeta}{4ab^2}+\left(d_y^2\right)\frac{-1+\zeta}{4a^2b}+\\
& \left(d_x^3\right)\frac{1-\zeta}{4ab^2}+\left(d_y^3\right)\frac{1-\zeta}{4a^2b}+\left(d_x^4\right)\frac{-1+\zeta}{4ab^2}+\left(d_y^4\right)\frac{1-\zeta}{4a^2b}+\\
& \left(d_x^5\right)\frac{-1-\zeta}{4ab^2}+\left(d_y^5\right)\frac{-1-\zeta}{4a^2b}+\left(d_x^6\right)\frac{1+\zeta}{4ab^2}+\left(d_y^6\right)\frac{-1-\zeta}{4a^2b}+\\
& \left(d_x^7\right)\frac{1+\zeta}{4ab^2}+\left(d_y^7\right)\frac{1+\zeta}{4a^2b}+\left(d_x^8\right)\frac{-1-\zeta}{4ab^2}+\left(d_y^8\right)\frac{1+\zeta}{4a^2b}+\\
& \left(d_y^9\right)\frac{1-\zeta}{2a^2b}+\left(d_x^{10}\right)\frac{-1+\zeta}{2ab^2}+\left(d_y^{11}\right)\frac{-1+\zeta}{2a^2b}+\left(d_x^{12}\right)\frac{1-\zeta}{2ab^2}+\\
& \left(d_y^{13}\right)\frac{1+\zeta}{2a^2b}+\left(d_x^{14}\right)\frac{-1-\zeta}{2ab^2}+\left(d_y^{15}\right)\frac{-1-\zeta}{2a^2b}+\left(d_x^{16}\right)\frac{1+\zeta}{2ab^2}\Bigg]+
\end{aligned}
$$

$$
\begin{aligned}
\tilde{f}_{1123}\Bigg[& \left(d_x^1\right)\frac{-1+2\xi+2\eta+2\zeta}{8abc}+\left(d_y^1\right)\frac{-1+\eta}{4a^2c}+\left(d_x^2\right)\frac{1+2\xi-2\eta-2\zeta}{8abc}+\\
& \left(d_y^2\right)\frac{-1+\eta}{4a^2c}+\left(d_x^3\right)\frac{-1-2\xi-2\eta+2\zeta}{8abc}+\left(d_y^3\right)\frac{-1-\eta}{4a^2c}+\\
& \left(d_x^4\right)\frac{1-2\xi+2\eta-2\zeta}{8abc}+\left(d_y^4\right)\frac{-1-\eta}{4a^2c}+\left(d_x^5\right)\frac{1-2\xi-2\eta+2\zeta}{8abc}+\\
& \left(d_y^5\right)\frac{1-\eta}{4a^2c}+\left(d_x^6\right)\frac{-1-2\xi+2\eta-2\zeta}{8abc}+\left(d_y^6\right)\frac{1-\eta}{4a^2c}+\\
& \left(d_x^7\right)\frac{1+2\xi+2\eta+2\zeta}{8abc}+\left(d_y^7\right)\frac{1+\eta}{4a^2c}+\left(d_x^8\right)\frac{-1+2\xi-2\eta-2\zeta}{8abc}+\\
& \left(d_y^8\right)\frac{1+\eta}{4a^2c}+\left(d_x^9\right)\frac{-\xi}{2abc}+\left(d_y^9\right)\frac{1-\eta}{2a^2c}+\left(d_x^{10}\right)\frac{\eta}{2abc}+\\
& \left(d_x^{11}\right)\frac{\xi}{2abc}+\left(d_y^{11}\right)\frac{1+\eta}{2a^2c}+\left(d_x^{12}\right)\frac{-\eta}{2abc}+\left(d_x^{13}\right)\frac{\xi}{2abc}+\\
& \left(d_y^{13}\right)\frac{-1+\eta}{2a^2c}+\left(d_x^{14}\right)\frac{-\eta}{2abc}+\left(d_x^{15}\right)\frac{-\xi}{2abc}+\left(d_y^{15}\right)\frac{-1-\eta}{2a^2c}+\\
& \left(d_x^{16}\right)\frac{\eta}{2abc}+\left(d_x^{17}\right)\frac{-\zeta}{2abc}+\left(d_x^{18}\right)\frac{\zeta}{2abc}+\left(d_x^{19}\right)\frac{-\zeta}{2abc}+\left(d_x^{20}\right)\frac{\zeta}{2abc}\Bigg]+\\
\tilde{f}_{1131}\Bigg[& \left(d_x^1\right)\frac{-1+\eta}{4a^2c}+\left(d_x^2\right)\frac{-1+\eta}{4a^2c}+\left(d_x^3\right)\frac{-1-\eta}{4a^2c}+\left(d_x^4\right)\frac{-1-\eta}{4a^2c}+\\
& \left(d_x^5\right)\frac{1-\eta}{4a^2c}+\left(d_x^6\right)\frac{1-\eta}{4a^2c}+\left(d_x^7\right)\frac{1+\eta}{4a^2c}+\left(d_x^8\right)\frac{1+\eta}{4a^2c}+\\
& \left(d_x^9\right)\frac{1-\eta}{2a^2c}+\left(d_x^{11}\right)\frac{1+\eta}{2a^2c}+\left(d_x^{13}\right)\frac{-1+\eta}{2a^2c}+\left(d_x^{15}\right)\frac{-1-\eta}{2a^2c}\Bigg]+
\end{aligned}
$$

$$
\begin{aligned}
\tilde{f}_{1132}\Bigg[& \left(d_x^1\right)\frac{-1+2\xi+2\eta+2\zeta}{8abc}+\left(d_z^1\right)\frac{-1+\zeta}{4a^2b}+\left(d_x^2\right)\frac{1+2\xi-2\eta-2\zeta}{8abc}+\\
& \left(d_z^2\right)\frac{-1+\zeta}{4a^b}+\left(d_x^3\right)\frac{-1-2\xi-2\eta+2\zeta}{8abc}+\left(d_z^3\right)\frac{1-\zeta}{4a^2b}+\\
& \left(d_x^4\right)\frac{1-2\xi+2\eta-2\zeta}{8abc}+\left(d_z^4\right)\frac{1-\zeta}{4a^2b}+\left(d_x^5\right)\frac{1-2\xi-2\eta+2\zeta}{8abc}+\\
& \left(d_z^5\right)\frac{-1-\zeta}{4a^2b}+\left(d_x^6\right)\frac{-1-2\xi+2\eta-2\zeta}{8abc}+\left(d_z^6\right)\frac{-1-\zeta}{4a^2b}+\\
& \left(d_x^7\right)\frac{1+2\xi+2\eta+2\zeta}{8abc}+\left(d_z^7\right)\frac{1+\zeta}{4a^2b}+\left(d_x^8\right)\frac{-1+2\xi-2\eta-2\zeta}{8abc}+\\
& \left(d_z^8\right)\frac{1+\zeta}{4a^2b}+\left(d_x^9\right)\frac{-\xi}{2abc}+\left(d_z^9\right)\frac{1-\zeta}{2a^2b}+\left(d_x^{10}\right)\frac{\eta}{2abc}+\\
& \left(d_x^{11}\right)\frac{\xi}{2abc}+\left(d_z^{11}\right)\frac{-1+\zeta}{2a^2b}+\left(d_x^{12}\right)\frac{-\eta}{2abc}+\left(d_x^{13}\right)\frac{\xi}{2abc}+\\
& \left(d_z^{13}\right)\frac{1+\zeta}{2a^2b}+\left(d_x^{14}\right)\frac{-\eta}{2abc}+\left(d_x^{15}\right)\frac{-\xi}{2abc}+\left(d_z^{15}\right)\frac{-1-\zeta}{2a^2b}+\\
& \left(d_x^{16}\right)\frac{\eta}{2abc}+\left(d_x^{17}\right)\frac{-\zeta}{2abc}+\left(d_x^{18}\right)\frac{\zeta}{2abc}+\left(d_x^{19}\right)\frac{-\zeta}{2abc}+\left(d_x^{20}\right)\frac{\zeta}{2abc}\Bigg]+\\
\tilde{f}_{1133}\Bigg[& \left(d_x^1\right)\frac{-1+\eta}{4ac^2}+\left(d_z^1\right)\frac{-1+\eta}{4a^2c}+\left(d_x^2\right)\frac{1-\eta}{4ac^2}+\left(d_z^2\right)\frac{-1+\eta}{4a^2c}+\\
& \left(d_x^3\right)\frac{1+\eta}{4ac^2}+\left(d_z^3\right)\frac{-1-\eta}{4a^2c}+\left(d_x^4\right)\frac{-1-\eta}{4ac^2}+\left(d_z^4\right)\frac{-1-\eta}{4a^2c}+\\
& \left(d_x^5\right)\frac{-1+\eta}{4ac^2}+\left(d_z^5\right)\frac{1-\eta}{4a^2c}+\left(d_x^6\right)\frac{1-\eta}{4ac^2}+\left(d_z^6\right)\frac{1-\eta}{4a^2c}+\\
& \left(d_x^7\right)\frac{1+\eta}{4ac^2}+\left(d_z^7\right)\frac{1+\eta}{4a^2c}+\left(d_x^8\right)\frac{-1-\eta}{4ac^2}+\left(d_z^8\right)\frac{1+\eta}{4a^2c}+\\
& \left(d_z^9\right)\frac{1-\eta}{2a^2c}+\left(d_z^{11}\right)\frac{1+\eta}{2a^2c}+\left(d_z^{13}\right)\frac{-1+\eta}{2a^2c}+\left(d_z^{15}\right)\frac{-1-\eta}{2a^2c}+\\
& \left(d_x^{17}\right)\frac{1-\eta}{2ac^2}+\left(d_x^{18}\right)\frac{-1+\eta}{2ac^2}+\left(d_x^{19}\right)\frac{-1-\eta}{2ac^2}+\left(d_x^{20}\right)\frac{1+\eta}{2ac^2}\Bigg]+
\end{aligned}
$$

$$
\begin{aligned}
\tilde{f}_{1231}\Bigg[& \left(d_y^1\right)\frac{-1+\eta}{4a^2c}+\left(d_z^1\right)\frac{-1+\zeta}{4a^2b}+\left(d_y^2\right)\frac{-1+\eta}{4a^2c}+\left(d_z^2\right)\frac{-1+\zeta}{4a^2b}+\\
& \left(d_y^3\right)\frac{-1-\eta}{4a^2c}+\left(d_z^3\right)\frac{1-\zeta}{4a^2b}+\left(d_y^4\right)\frac{-1-\eta}{4a^2c}+\left(d_z^4\right)\frac{1-\zeta}{4a^2b}+\\
& \left(d_y^5\right)\frac{1-\eta}{4a^2c}+\left(d_z^5\right)\frac{-1-\zeta}{4a^2b}+\left(d_y^6\right)\frac{1-\eta}{4a^2c}+\left(d_z^6\right)\frac{-1-\zeta}{4a^2b}+\\
& \left(d_y^7\right)\frac{1+\eta}{4a^2c}+\left(d_z^7\right)\frac{1+\zeta}{4a^2b}+\left(d_y^8\right)\frac{1+\eta}{4a^2c}+\left(d_z^8\right)\frac{1+\zeta}{4a^2b}+\\
& \left(d_y^9\right)\frac{1-\eta}{2a^2c}+\left(d_z^9\right)\frac{1-\zeta}{2a^2b}+\left(d_y^{11}\right)\frac{1+\eta}{2a^2c}+\left(d_z^{11}\right)\frac{-1+\zeta}{2a^2b}+\\
& \left(d_y^{13}\right)\frac{-1+\eta}{2a^2c}+\left(d_z^{13}\right)\frac{1+\zeta}{2a^2b}+\left(d_y^{15}\right)\frac{-1-\eta}{2a^2c}+\left(d_z^{15}\right)\frac{-1-\zeta}{2a^2b}\Bigg]+\\
\tilde{f}_{1232}\Bigg[& \left(d_y^1\right)\frac{-1+2\xi+2\eta+2\zeta}{8abc}+\left(d_z^1\right)\frac{-1+\zeta}{4ab^2}+\left(d_y^2\right)\frac{1+2\xi-2\eta-2\zeta}{8abc}+\\
& \left(d_z^2\right)\frac{1-\zeta}{4ab^2}+\left(d_y^3\right)\frac{-1-2\xi-2\eta+2\zeta}{8abc}+\left(d_z^3\right)\frac{1-\zeta}{4ab^2}+\\
& \left(d_y^4\right)\frac{1-2\xi+2\eta-2\zeta}{8abc}+\left(d_z^4\right)\frac{-1+\zeta}{4ab^2}+\left(d_y^5\right)\frac{1-2\xi-2\eta+2\zeta}{8abc}+\\
& \left(d_z^5\right)\frac{-1-\zeta}{4ab^2}+\left(d_y^6\right)\frac{-1-2\xi+2\eta-2\zeta}{8abc}+\left(d_z^6\right)\frac{1+\zeta}{4ab^2}+\\
& \left(d_y^7\right)\frac{1+2\xi+2\eta+2\zeta}{8abc}+\left(d_z^7\right)\frac{1+\zeta}{4ab^2}+\left(d_y^8\right)\frac{-1+2\xi-2\eta-2\zeta}{8abc}+\\
& \left(d_z^8\right)\frac{-1-\zeta}{4ab^2}+\left(d_y^9\right)\frac{-\xi}{2abc}+\left(d_y^{10}\right)\frac{\eta}{2abc}+\left(d_z^{10}\right)\frac{-1+\zeta}{2ab^2}+\\
& \left(d_y^{11}\right)\frac{\xi}{2abc}+\left(d_y^{12}\right)\frac{-\eta}{2abc}+\left(d_z^{12}\right)\frac{1-\zeta}{2ab^2}+\left(d_y^{13}\right)\frac{\xi}{2abc}+\\
& \left(d_y^{14}\right)\frac{-\eta}{2abc}+\left(d_z^{14}\right)\frac{-1-\zeta}{2ab^2}+\left(d_y^{15}\right)\frac{-\xi}{2abc}+\left(d_y^{16}\right)\frac{\eta}{2abc}+\\
& \left(d_z^{16}\right)\frac{1+\zeta}{2ab^2}+\left(d_y^{17}\right)\frac{-\zeta}{2abc}+\left(d_y^{18}\right)\frac{\zeta}{2abc}+\left(d_y^{19}\right)\frac{-\zeta}{2abc}+\left(d_y^{20}\right)\frac{\zeta}{2abc}\Bigg]+
\end{aligned}
$$

$$
\begin{aligned}
\tilde{f}_{1233}\Bigg[& \left(d_y^1\right)\frac{-1+\eta}{4ac^2}+\left(d_z^1\right)\frac{-1+2\xi+2\eta+2\zeta}{8abc}+\left(d_y^2\right)\frac{1-\eta}{4ac^2}+\\
& \left(d_z^2\right)\frac{1+2\xi-2\eta-2\zeta}{8abc}+\left(d_y^3\right)\frac{1+\eta}{4ac^2}+\left(d_z^3\right)\frac{-1-2\xi-2\eta+2\zeta}{8abc}+\\
& \left(d_y^4\right)\frac{-1-\eta}{4ac^2}+\left(d_z^4\right)\frac{1-2\xi+2\eta-2\zeta}{8abc}+\left(d_y^5\right)\frac{-1+\eta}{4ac^2}+\\
& \left(d_z^5\right)\frac{1-2\xi-2\eta+2\zeta}{8abc}+\left(d_y^6\right)\frac{1-\eta}{4ac^2}+\left(d_z^6\right)\frac{-1-2\xi+2\eta-2\zeta}{8abc}+\\
& \left(d_y^7\right)\frac{1+\eta}{4ac^2}+\left(d_z^7\right)\frac{1+2\xi+2\eta+2\zeta}{8abc}+\left(d_y^8\right)\frac{-1-\eta}{4ac^2}+\\
& \left(d_z^8\right)\frac{-1+2\xi-2\eta-2\zeta}{8abc}+\left(d_z^9\right)\frac{-\xi}{2abc}+\left(d_z^{10}\right)\frac{\eta}{2abc}+\left(d_z^{11}\right)\frac{\xi}{2abc}+\\
& \left(d_z^{12}\right)\frac{-\eta}{2abc}+\left(d_z^{13}\right)\frac{\xi}{2abc}+\left(d_z^{14}\right)\frac{-\eta}{2abc}+\left(d_z^{15}\right)\frac{-\xi}{2abc}+\\
& \left(d_z^{16}\right)\frac{\eta}{2abc}+\left(d_y^{17}\right)\frac{1-\eta}{2ac^2}+\left(d_z^{17}\right)\frac{-\zeta}{2abc}+\left(d_y^{18}\right)\frac{-1+\eta}{2ac^2}+\\
& \left(d_z^{18}\right)\frac{\zeta}{2abc}+\left(d_y^{19}\right)\frac{-1-\eta}{2ac^2}+\left(d_z^{19}\right)\frac{-\zeta}{2abc}+\left(d_y^{20}\right)\frac{1+\eta}{2ac^2}+\left(d_z^{20}\right)\frac{\zeta}{2abc}\Bigg]+\\
\tilde{f}_{2111}\Bigg[& \left(d_x^1\right)\frac{-1+\zeta}{4a^2b}+\left(d_x^2\right)\frac{-1+\zeta}{4a^2b}+\left(d_x^3\right)\frac{1-\zeta}{4a^2b}+\left(d_x^4\right)\frac{1-\zeta}{4a^2b}+\\
& \left(d_x^5\right)\frac{-1-\zeta}{4a^2b}+\left(d_x^6\right)\frac{-1-\zeta}{4a^2b}+\left(d_x^7\right)\frac{1+\zeta}{4a^2b}+\left(d_x^8\right)\frac{1+\zeta}{4a^2b}+\\
& \left(d_x^9\right)\frac{1-\zeta}{2a^2b}+\left(d_x^{11}\right)\frac{-1+\zeta}{2a^2b}+\left(d_x^{13}\right)\frac{1+\zeta}{2a^2b}+\left(d_x^{15}\right)\frac{-1-\zeta}{2a^2b}\Bigg]+\\
\tilde{f}_{2112}\Bigg[& \left(d_x^1\right)\frac{-1+\zeta}{4ab^2}+\left(d_x^2\right)\frac{1-\zeta}{4ab^2}+\left(d_x^3\right)\frac{1-\zeta}{4ab^2}+\left(d_x^4\right)\frac{-1+\zeta}{4ab^2}+\\
& \left(d_x^5\right)\frac{-1-\zeta}{4ab^2}+\left(d_x^6\right)\frac{1+\zeta}{4ab^2}+\left(d_x^7\right)\frac{1+\zeta}{4ab^2}+\left(d_x^8\right)\frac{-1-\zeta}{4ab^2}+\\
& \left(d_x^{10}\right)\frac{-1+\zeta}{2ab^2}+\left(d_x^{12}\right)\frac{1-\zeta}{2ab^2}+\left(d_x^{14}\right)\frac{-1-\zeta}{2ab^2}+\left(d_x^{16}\right)\frac{1+\zeta}{2ab^2}\Bigg]+
\end{aligned}
$$

$$
\begin{aligned}
\tilde{f}_{2113}\Bigg[& \left(d_x^1\right)\frac{-1+2\xi+2\eta+2\zeta}{8abc}+\left(d_x^2\right)\frac{1+2\xi-2\eta-2\zeta}{8abc}+\\
& \left(d_x^3\right)\frac{-1-2\xi-2\eta+2\zeta}{8abc}+\left(d_x^4\right)\frac{1-2\xi+2\eta-2\zeta}{8abc}+\\
& \left(d_x^5\right)\frac{1-2\xi-2\eta+2\zeta}{8abc}+\left(d_x^6\right)\frac{-1-2\xi+2\eta-2\zeta}{8abc}+\\
& \left(d_x^7\right)\frac{1+2\xi+2\eta+2\zeta}{8abc}+\left(d_x^8\right)\frac{-1+2\xi-2\eta-2\zeta}{8abc}+\\
& \left(d_x^9\right)\frac{-\xi}{2abc}+\left(d_x^{10}\right)\frac{\eta}{2abc}+\left(d_x^{11}\right)\frac{\xi}{2abc}+\left(d_x^{12}\right)\frac{-\eta}{2abc}+\\
& \left(d_x^{13}\right)\frac{\xi}{2abc}+\left(d_x^{14}\right)\frac{-\eta}{2abc}+\left(d_x^{15}\right)\frac{-\xi}{2abc}+\left(d_x^{16}\right)\frac{\eta}{2abc}+\\
& \left(d_x^{17}\right)\frac{-\zeta}{2abc}+\left(d_x^{18}\right)\frac{\zeta}{2abc}+\left(d_x^{19}\right)\frac{-\zeta}{2abc}+\left(d_x^{20}\right)\frac{\zeta}{2abc}\Bigg]+\\
\tilde{f}_{2221}\Bigg[& \left(d_y^1\right)\frac{-1+\zeta}{4ab^2}+\left(d_y^2\right)\frac{1-\zeta}{4ab^2}+\left(d_y^3\right)\frac{1-\zeta}{4ab^2}+\left(d_y^4\right)\frac{-1+\zeta}{4ab^2}+\\
& \left(d_y^5\right)\frac{-1-\zeta}{4ab^2}+\left(d_y^6\right)\frac{1+\zeta}{4ab^2}+\left(d_y^7\right)\frac{1+\zeta}{4ab^2}+\left(d_y^8\right)\frac{-1-\zeta}{4ab^2}+\\
& \left(d_y^{10}\right)\frac{-1+\zeta}{2ab^2}+\left(d_y^{12}\right)\frac{1-\zeta}{2ab^2}+\left(d_y^{14}\right)\frac{-1-\zeta}{2ab^2}+\left(d_y^{16}\right)\frac{-1-\zeta}{2ab^2}\Bigg]+\\
\tilde{f}_{2223}\Bigg[& \left(d_y^1\right)\frac{-1+\xi}{4b^2c}+\left(d_y^2\right)\frac{-1-\xi}{4b^2c}+\left(d_y^3\right)\frac{-1-\xi}{4b^2c}+\left(d_y^4\right)\frac{-1+\xi}{4b^2c}+\\
& \left(d_y^5\right)\frac{1-\xi}{4b^2c}+\left(d_y^6\right)\frac{1+\xi}{4b^2c}+\left(d_y^7\right)\frac{1+\xi}{4b^2c}+\left(d_y^8\right)\frac{1-\xi}{4b^2c}+\\
& \left(d_y^{10}\right)\frac{1+\xi}{2b^2c}+\left(d_y^{12}\right)\frac{1-\xi}{2b^2c}+\left(d_y^{14}\right)\frac{-1-\xi}{2b^2c}+\left(d_y^{16}\right)\frac{-1+\xi}{2b^2c}\Bigg]+
\end{aligned}
$$

$$
\begin{aligned}
\tilde{f}_{2331}\Bigg[& \left(d_z^1\right)\frac{-1+2\xi+2\eta+2\zeta}{8abc}+\left(d_z^2\right)\frac{1+2\xi-2\eta-2\zeta}{8abc}+\\
& \left(d_z^3\right)\frac{-1-2\xi-2\eta+2\zeta}{8abc}+\left(d_z^4\right)\frac{1-2\xi+2\eta-2\zeta}{8abc}+\\
& \left(d_z^5\right)\frac{1-2\xi-2\eta+2\zeta}{8abc}+\left(d_z^6\right)\frac{-1-2\xi+2\eta-2\zeta}{8abc}+\\
& \left(d_z^7\right)\frac{1+2\xi+2\eta+2\zeta}{8abc}+\left(d_z^8\right)\frac{-1+2\xi-2\eta-2\zeta}{8abc}+\\
& \left(d_z^9\right)\frac{-\xi}{2abc}+\left(d_z^{10}\right)\frac{\eta}{2abc}+\left(d_z^{11}\right)\frac{\xi}{2abc}+\left(d_z^{12}\right)\frac{-\eta}{2abc}+\\
& \left(d_z^{13}\right)\frac{\xi}{2abc}+\left(d_z^{14}\right)\frac{-\eta}{2abc}+\left(d_z^{15}\right)\frac{-\xi}{2abc}+\left(d_z^{16}\right)\frac{\eta}{2abc}+\\
& \left(d_z^{17}\right)\frac{-\zeta}{2abc}+\left(d_z^{18}\right)\frac{\zeta}{2abc}+\left(d_z^{19}\right)\frac{-\zeta}{2abc}+\left(d_z^{20}\right)\frac{\zeta}{2abc}\Bigg]+\\
\tilde{f}_{2332}\Bigg[& \left(d_z^1\right)\frac{-1+\xi}{4b^2c}+\left(d_z^2\right)\frac{-1-\xi}{4b^2c}+\left(d_z^3\right)\frac{-1-\xi}{4b^2c}+\left(d_z^4\right)\frac{-1+\xi}{4b^2c}+\\
& \left(d_z^5\right)\frac{1-\xi}{4b^2c}+\left(d_z^6\right)\frac{1+\xi}{4b^2c}+\left(d_z^7\right)\frac{1+\xi}{4b^2c}+\left(d_z^8\right)\frac{1-\xi}{4b^2c}+\\
& \left(d_z^{10}\right)\frac{1+\xi}{2b^2c}+\left(d_z^{12}\right)\frac{1-\xi}{2b^2c}+\left(d_z^{14}\right)\frac{-1-\xi}{2b^2c}+\left(d_z^{16}\right)\frac{-1+\xi}{2b^2c}\Bigg]+\\
\tilde{f}_{2333}\Bigg[& \left(d_z^1\right)\frac{-1+\xi}{4bc^2}+\left(d_z^2\right)\frac{-1-\xi}{4bc^2}+\left(d_z^3\right)\frac{1+\xi}{4bc^2}+\left(d_z^4\right)\frac{1-\xi}{4bc^2}+\\
& \left(d_z^5\right)\frac{-1+\xi}{4bc^2}+\left(d_z^6\right)\frac{-1-\xi}{4bc^2}+\left(d_z^7\right)\frac{1+\xi}{4bc^2}+\left(d_z^8\right)\frac{1-\xi}{4bc^2}+\\
& \left(d_z^{17}\right)\frac{1-\xi}{2bc^2}+\left(d_z^{18}\right)\frac{1+\xi}{2bc^2}+\left(d_z^{19}\right)\frac{-1-\xi}{2bc^2}+\left(d_z^{20}\right)\frac{-1+\xi}{2bc^2}\Bigg]+
\end{aligned}
$$

$$
\begin{aligned}
\tilde{f}_{2121}\Bigg[& \left(d_x^1\right)\frac{-1+\zeta}{4ab^2}+\left(d_y^1\right)\frac{-1+\zeta}{4a^2b}+\left(d_x^2\right)\frac{1-\zeta}{4ab^2}+\left(d_y^2\right)\frac{-1+\zeta}{4a^2b}+\\
& \left(d_x^3\right)\frac{1-\zeta}{4ab^2}+\left(d_y^3\right)\frac{1-\zeta}{4a^2b}+\left(d_x^4\right)\frac{-1+\zeta}{4ab^2}+\left(d_y^4\right)\frac{1-\zeta}{4a^2b}+\\
& \left(d_x^5\right)\frac{-1-\zeta}{4ab^2}+\left(d_y^5\right)\frac{-1-\zeta}{4a^2b}+\left(d_x^6\right)\frac{1+\zeta}{4ab^2}+\left(d_y^6\right)\frac{-1-\zeta}{4a^2b}+\\
& \left(d_x^7\right)\frac{1+\zeta}{4ab^2}+\left(d_y^7\right)\frac{1+\zeta}{4a^2b}+\left(d_x^8\right)\frac{-1-\zeta}{4ab^2}+\left(d_y^8\right)\frac{1+\zeta}{4a^2b}+\\
& \left(d_y^9\right)\frac{1-\zeta}{2a^2b}+\left(d_x^{10}\right)\frac{-1+\zeta}{2ab^2}+\left(d_y^{11}\right)\frac{-1+\zeta}{2a^2b}+\left(d_x^{12}\right)\frac{1-\zeta}{2ab^2}+\\
& \left(d_y^{13}\right)\frac{1+\zeta}{2a^2b}+\left(d_x^{14}\right)\frac{-1-\zeta}{2ab^2}+\left(d_y^{15}\right)\frac{-1-\zeta}{2a^2b}+\left(d_x^{16}\right)\frac{1+\zeta}{2ab^2}\Bigg]+\\
\tilde{f}_{2122}\Bigg[& \left(d_y^1\right)\frac{-1+\zeta}{4ab^2}+\left(d_y^2\right)\frac{1-\zeta}{4ab^2}+\left(d_y^3\right)\frac{1-\zeta}{4ab^2}+\left(d_y^4\right)\frac{-1+\zeta}{4ab^2}+\\
& \left(d_y^5\right)\frac{-1-\zeta}{4ab^2}+\left(d_y^6\right)\frac{1+\zeta}{4ab^2}+\left(d_y^7\right)\frac{1+\zeta}{4ab^2}+\left(d_y^8\right)\frac{-1-\zeta}{4ab^2}+\\
& \left(d_y^{10}\right)\frac{-1+\zeta}{2ab^2}+\left(d_y^{12}\right)\frac{1-\zeta}{2ab^2}+\left(d_y^{14}\right)\frac{-1-\zeta}{2ab^2}+\left(d_y^{16}\right)\frac{1+\zeta}{2ab^2}\Bigg]+
\end{aligned}
$$

$$
\begin{aligned}
\tilde{f}_{2123}\Bigg[& \left(d_x^1\right)\frac{-1+\xi}{4b^2c}+\left(d_y^1\right)\frac{-1+2\xi+2\eta+2\zeta}{8abc}+\left(d_x^2\right)\frac{-1-\xi}{4ab^2c}+\\
& \left(d_y^2\right)\frac{1+2\xi-2\eta-2\zeta}{8abc}+\left(d_x^3\right)\frac{-1-\xi}{4b^2c}+\left(d_y^3\right)\frac{-1-2\xi-2\eta+2\zeta}{8abc}+\\
& \left(d_x^4\right)\frac{-1+\xi}{4b^2c}+\left(d_y^4\right)\frac{1-2\xi+2\eta-2\zeta}{8abc}+\left(d_x^5\right)\frac{1-\xi}{4b^2c}+\\
& \left(d_y^5\right)\frac{1-2\xi-2\eta+2\zeta}{8abc}+\left(d_x^6\right)\frac{1+\xi}{4b^2c}+\left(d_y^6\right)\frac{-1-2\xi+2\eta-2\zeta}{8abc}+\\
& \left(d_x^7\right)\frac{1+\xi}{4b^2c}+\left(d_y^7\right)\frac{1+2\xi+2\eta+2\zeta}{8abc}+\left(d_x^8\right)\frac{1-\xi}{4b^2c}+\\
& \left(d_y^8\right)\frac{-1+2\xi-2\eta-2\zeta}{8abc}+\left(d_y^9\right)\frac{-\xi}{2abc}+\left(d_x^{10}\right)\frac{1+\xi}{2b^2c}+\left(d_y^{10}\right)\frac{\eta}{2abc}+\\
& \left(d_y^{11}\right)\frac{\xi}{2abc}+\left(d_x^{12}\right)\frac{1-\xi}{2b^2c}+\left(d_y^{12}\right)\frac{-\eta}{2abc}+\left(d_y^{13}\right)\frac{\xi}{2abc}+\\
& \left(d_x^{14}\right)\frac{-1-\xi}{2b^2c}+\left(d_y^{14}\right)\frac{-\eta}{2abc}+\left(d_y^{15}\right)\frac{-\xi}{2abc}+\left(d_x^{16}\right)\frac{-1+\xi}{2b^2c}+\\
& \left(d_y^{16}\right)\frac{\eta}{2abc}+\left(d_y^{17}\right)\frac{-\zeta}{2abc}+\left(d_y^{18}\right)\frac{\zeta}{2abc}+\left(d_y^{19}\right)\frac{-\zeta}{2abc}+\left(d_y^{20}\right)\frac{\zeta}{2abc}\Bigg]+\\
\tilde{f}_{2131}\Bigg[& \left(d_x^1\right)\frac{-1+2\xi+2\eta+2\zeta}{8abc}+\left(d_z^1\right)\frac{-1+\zeta}{4a^2b}+\left(d_x^2\right)\frac{1+2\xi-2\eta-2\zeta}{8abc}+\\
& \left(d_z^2\right)\frac{-1+\zeta}{4a^2b}+\left(d_x^3\right)\frac{-1-2\xi-2\eta+2\zeta}{8abc}+\left(d_z^3\right)\frac{1-\zeta}{4a^2b}+\\
& \left(d_x^4\right)\frac{1-2\xi+2\eta-2\zeta}{8abc}+\left(d_z^4\right)\frac{1-\zeta}{4a^2b}+\left(d_x^5\right)\frac{1-2\xi-2\eta+2\zeta}{8abc}+\\
& \left(d_z^5\right)\frac{-1-\zeta}{4a^2b}+\left(d_x^6\right)\frac{-1-2\xi+2\eta-2\zeta}{8abc}+\left(d_z^6\right)\frac{-1-\zeta}{4a^2b}+\\
& \left(d_x^7\right)\frac{1+2\xi+2\eta+2\zeta}{8abc}+\left(d_z^7\right)\frac{1+\zeta}{4a^2b}+\left(d_x^8\right)\frac{-1+2\xi-2\eta-2\zeta}{8abc}+\\
& \left(d_z^8\right)\frac{1+\zeta}{4a^2b}+\left(d_x^9\right)\frac{-\xi}{2abc}+\left(d_z^9\right)\frac{1-\zeta}{2a^2b}+\left(d_x^{10}\right)\frac{\eta}{2abc}+\\
& \left(d_x^{11}\right)\frac{\xi}{2abc}+\left(d_z^{11}\right)\frac{-1+\zeta}{2a^2b}+\left(d_x^{12}\right)\frac{-\eta}{2abc}+\left(d_x^{13}\right)\frac{\xi}{2abc}+\\
& \left(d_z^{13}\right)\frac{1+\zeta}{2a^2b}+\left(d_x^{14}\right)\frac{-\eta}{2abc}+\left(d_x^{15}\right)\frac{-\xi}{2abc}+\left(d_z^{15}\right)\frac{-1-\zeta}{2a^2b}+\\
& \left(d_x^{16}\right)\frac{\eta}{2abc}+\left(d_x^{17}\right)\frac{-\zeta}{2abc}+\left(d_x^{18}\right)\frac{\zeta}{2abc}+\left(d_x^{19}\right)\frac{-\zeta}{2abc}+\left(d_x^{20}\right)\frac{\zeta}{2abc}\Bigg]+
\end{aligned}
$$

$$
\begin{aligned}
\tilde{f}_{2132}\Bigg[& \left(d_x^1\right)\frac{-1+\xi}{4b^2c}+\left(d_z^1\right)\frac{-1+\zeta}{4ab^2}+\left(d_x^2\right)\frac{-1-\xi}{4b^2c}+\left(d_z^2\right)\frac{1-\zeta}{4ab^2}+\\
& \left(d_x^3\right)\frac{-1-\xi}{4b^2c}+\left(d_z^3\right)\frac{1-\zeta}{4ab^2}+\left(d_x^4\right)\frac{-1+\xi}{4b^2c}+\left(d_z^4\right)\frac{-1+\zeta}{4ab^2}+\\
& \left(d_x^5\right)\frac{1-\xi}{4b^2c}+\left(d_z^5\right)\frac{-1-\zeta}{4ab^2}+\left(d_x^6\right)\frac{1+\xi}{4b^2c}+\left(d_z^6\right)\frac{1+\zeta}{4ab^2}+\\
& \left(d_x^7\right)\frac{1+\xi}{4b^2c}+\left(d_z^7\right)\frac{1+\zeta}{4ab^2}+\left(d_x^8\right)\frac{1-\xi}{4b^2c}+\left(d_z^8\right)\frac{-1-\zeta}{4ab^2}+\\
& \left(d_x^{10}\right)\frac{1+\xi}{2b^2c}+\left(d_z^{10}\right)\frac{-1+\zeta}{2ab^2}+\left(d_x^{12}\right)\frac{1-\xi}{2b^2c}+\left(d_z^{12}\right)\frac{1-\zeta}{2ab^2}+\\
& \left(d_x^{14}\right)\frac{-1-\xi}{2b^2c}+\left(d_z^{14}\right)\frac{-1-\zeta}{2ab^2}+\left(d_x^{16}\right)\frac{-1+\xi}{2b^2c}+\left(d_z^{16}\right)\frac{1+\zeta}{2ab^2}\Bigg]+\\
\tilde{f}_{2133}\Bigg[& \left(d_x^1\right)\frac{-1+\xi}{4bc^2}+\left(d_z^1\right)\frac{-1+2\xi+2\eta+2\zeta}{8abc}+\left(d_x^2\right)\frac{-1-\xi}{4bc^2}+\\
& \left(d_z^2\right)\frac{1+2\xi-2\eta-2\zeta}{8abc}+\left(d_x^3\right)\frac{1+\xi}{4bc^2}+\left(d_z^3\right)\frac{-1-2\xi-2\eta+2\zeta}{8abc}+\\
& \left(d_x^4\right)\frac{1-\xi}{4bc^2}+\left(d_z^4\right)\frac{1-2\xi+2\eta-2\zeta}{8abc}+\left(d_x^5\right)\frac{-1+\xi}{4bc^2}+\\
& \left(d_z^5\right)\frac{1-2\xi-2\eta+2\zeta}{8abc}+\left(d_x^6\right)\frac{-1-\xi}{4bc^2}+\left(d_z^6\right)\frac{-1-2\xi+2\eta-2\zeta}{8abc}+\\
& \left(d_x^7\right)\frac{1+\xi}{4bc^2}+\left(d_z^7\right)\frac{1+2\xi+2\eta+2\zeta}{8abc}+\left(d_x^8\right)\frac{1-\xi}{4bc^2}+\\
& \left(d_z^8\right)\frac{-1+2\xi-2\eta-2\zeta}{8abc}+\left(d_z^9\right)\frac{-\xi}{2abc}+\left(d_z^{10}\right)\frac{\eta}{2abc}+\left(d_z^{11}\right)\frac{\xi}{2abc}+\\
& \left(d_z^{12}\right)\frac{-\eta}{2abc}+\left(d_z^{13}\right)\frac{\xi}{2abc}+\left(d_z^{14}\right)\frac{-\eta}{2abc}+\left(d_z^{15}\right)\frac{-\xi}{2abc}+\\
& \left(d_z^{16}\right)\frac{\eta}{2abc}+\left(d_x^{17}\right)\frac{1-\xi}{2bc^2}+\left(d_z^{17}\right)\frac{-\zeta}{2abc}+\left(d_x^{18}\right)\frac{1+\xi}{2bc^2}+\\
& \left(d_z^{18}\right)\frac{\zeta}{2abc}+\left(d_x^{19}\right)\frac{-1-\xi}{2bc^2}+\left(d_z^{19}\right)\frac{-\zeta}{2abc}+\left(d_x^{20}\right)\frac{-1+\xi}{2bc^2}+\left(d_z^{20}\right)\frac{\zeta}{2abc}\Bigg]+
\end{aligned}
$$

$$
\begin{aligned}
\tilde{f}_{2231}\Bigg[& \left(d_y^1\right)\frac{-1+2\xi+2\eta+2\zeta}{8abc}+\left(d_z^1\right)\frac{-1+\zeta}{4ab^2}+\left(d_y^2\right)\frac{1+2\xi-2\eta-2\zeta}{8abc}+\\
& \left(d_z^2\right)\frac{1-\zeta}{4ab^2}+\left(d_y^3\right)\frac{-1-2\xi-2\eta+2\zeta}{8abc}+\left(d_z^3\right)\frac{1-\zeta}{4ab^2}+\\
& \left(d_y^4\right)\frac{1-2\xi+2\eta-2\zeta}{8abc}+\left(d_z^4\right)\frac{-1+\zeta}{4ab^2}+\left(d_y^5\right)\frac{1-2\xi-2\eta+2\zeta}{8abc}+\\
& \left(d_z^5\right)\frac{-1-\zeta}{4ab^2}+\left(d_y^6\right)\frac{-1-2\xi+2\eta-2\zeta}{8abc}+\left(d_z^6\right)\frac{1+\zeta}{4ab^2}+\\
& \left(d_y^7\right)\frac{1+2\xi+2\eta+2\zeta}{8abc}+\left(d_z^7\right)\frac{1+\zeta}{4ab^2}+\left(d_y^8\right)\frac{-1+2\xi-2\eta-2\zeta}{8abc}+\\
& \left(d_z^8\right)\frac{-1-\zeta}{4ab^2}+\left(d_y^9\right)\frac{-\xi}{2abc}+\left(d_y^{10}\right)\frac{\eta}{2abc}+\left(d_z^{10}\right)\frac{-1+\zeta}{2ab^2}+\\
& \left(d_y^{11}\right)\frac{\xi}{2abc}+\left(d_y^{12}\right)\frac{-\eta}{2abc}+\left(d_z^{12}\right)\frac{1-\zeta}{2ab^2}+\left(d_y^{13}\right)\frac{\xi}{2abc}+\\
& \left(d_y^{14}\right)\frac{-\eta}{2abc}+\left(d_z^{14}\right)\frac{-1-\zeta}{2ab^2}+\left(d_y^{15}\right)\frac{-\xi}{2abc}+\left(d_y^{16}\right)\frac{\eta}{2abc}+\\
& \left(d_z^{16}\right)\frac{1+\zeta}{2ab^2}+\left(d_y^{17}\right)\frac{-\zeta}{2abc}+\left(d_y^{18}\right)\frac{\zeta}{2abc}+\left(d_y^{19}\right)\frac{-\zeta}{2abc}+\left(d_y^{20}\right)\frac{\zeta}{2abc}\Bigg]+\\
\tilde{f}_{2232}\Bigg[& \left(d_y^1\right)\frac{-1+\xi}{4b^2c}+\left(d_y^2\right)\frac{-1-\xi}{4b^2c}+\left(d_y^3\right)\frac{-1-\xi}{4b^2c}+\left(d_y^4\right)\frac{-1+\xi}{4b^2c}+\\
& \left(d_y^5\right)\frac{1-\xi}{4b^2c}+\left(d_y^6\right)\frac{1+\xi}{4b^2c}+\left(d_y^7\right)\frac{1+\xi}{4b^2c}+\left(d_y^8\right)\frac{1-\xi}{4b^2c}+\\
& \left(d_y^{10}\right)\frac{1+\xi}{2b^2c}+\left(d_y^{12}\right)\frac{1-\xi}{2b^2c}+\left(d_y^{14}\right)\frac{-1-\xi}{2b^2c}+\left(d_y^{16}\right)\frac{-1+\xi}{2b^2c}\Bigg]+\\
\tilde{f}_{2233}\Bigg[& \left(d_y^1\right)\frac{-1+\xi}{4bc^2}+\left(d_z^1\right)\frac{-1+\xi}{4b^2c}+\left(d_y^2\right)\frac{-1-\xi}{4bc^2}+\left(d_z^2\right)\frac{-1-\xi}{4b^2c}+\\
& \left(d_y^3\right)\frac{1+\xi}{4bc^2}+\left(d_z^3\right)\frac{-1-\xi}{4b^2c}+\left(d_y^4\right)\frac{1-\xi}{4bc^2}+\left(d_z^4\right)\frac{-1+\xi}{4b^2c}+\\
& \left(d_y^5\right)\frac{-1+\xi}{4bc^2}+\left(d_z^5\right)\frac{1-\xi}{4b^2c}+\left(d_y^6\right)\frac{-1-\xi}{4bc^2}+\left(d_z^6\right)\frac{1+\xi}{4b^2c}+\\
& \left(d_y^7\right)\frac{1+\xi}{4bc^2}+\left(d_z^7\right)\frac{1+\xi}{4b^2c}+\left(d_y^8\right)\frac{1-\xi}{4bc^2}+\left(d_z^8\right)\frac{1-\xi}{4b^2c}+\\
& \left(d_z^{10}\right)\frac{1+\xi}{2b^2c}+\left(d_z^{12}\right)\frac{1-\xi}{2b^2c}+\left(d_z^{14}\right)\frac{-1-\xi}{2b^2c}+\left(d_z^{16}\right)\frac{-1+\xi}{2b^2c}+\\
& \left(d_y^{17}\right)\frac{1-\xi}{2bc^2}+\left(d_y^{18}\right)\frac{1+\xi}{2bc^2}+\left(d_y^{19}\right)\frac{-1-\xi}{2bc^2}+\left(d_y^{20}\right)\frac{-1+\xi}{2bc^2}\Bigg]+
\end{aligned}
$$

$$
\begin{aligned}
\tilde{f}_{3111}\Bigg[& \left(d_x^1\right)\frac{-1+\eta}{4a^2c}+\left(d_x^2\right)\frac{-1+\eta}{4a^2c}+\left(d_x^3\right)\frac{-1-\eta}{4a^2c}+\left(d_x^4\right)\frac{-1-\eta}{4a^2c}+\\
& \left(d_x^5\right)\frac{1-\eta}{4a^2c}+\left(d_x^6\right)\frac{1-\eta}{4a^2c}+\left(d_x^7\right)\frac{1+\eta}{4a^2c}+\left(d_x^8\right)\frac{1+\eta}{4a^2c}+\\
& \left(d_x^9\right)\frac{1-\eta}{2a^2c}+\left(d_x^{11}\right)\frac{1+\eta}{2a^2c}+\left(d_x^{13}\right)\frac{-1+\eta}{2a^2c}+\left(d_x^{15}\right)\frac{-1-\eta}{2a^2c}\Bigg]+\\
\tilde{f}_{3112}\Bigg[& \left(d_x^1\right)\frac{-1+2\xi+2\eta+2\zeta}{8abc}+\left(d_x^2\right)\frac{1+2\xi-2\eta-2\zeta}{8abc}+\\
& \left(d_x^3\right)\frac{-1-2\xi-2\eta+2\zeta}{8abc}+\left(d_x^4\right)\frac{1-2\xi+2\eta-2\zeta}{8abc}+\\
& \left(d_x^5\right)\frac{1-2\xi-2\eta+2\zeta}{8abc}+\left(d_x^6\right)\frac{-1-2\xi+2\eta-2\zeta}{8abc}+\\
& \left(d_x^7\right)\frac{1+2\xi+2\eta+2\zeta}{8abc}+\left(d_x^8\right)\frac{-1+2\xi-2\eta-2\zeta}{8abc}+\\
& \left(d_x^9\right)\frac{-\xi}{2abc}+\left(d_x^{10}\right)\frac{\eta}{2abc}+\left(d_x^{11}\right)\frac{\xi}{2abc}+\left(d_x^{12}\right)\frac{-\eta}{2abc}+\\
& \left(d_x^{13}\right)\frac{\xi}{2abc}+\left(d_x^{14}\right)\frac{-\eta}{2abc}+\left(d_x^{15}\right)\frac{-\xi}{2abc}+\left(d_x^{16}\right)\frac{\eta}{2abc}+\\
& \left(d_x^{17}\right)\frac{-\zeta}{2abc}+\left(d_x^{18}\right)\frac{\zeta}{2abc}+\left(d_x^{19}\right)\frac{-\zeta}{2abc}+\left(d_x^{20}\right)\frac{\zeta}{2abc}\Bigg]+\\
\tilde{f}_{3113}\Bigg[& \left(d_x^1\right)\frac{-1+\eta}{4ac^2}+\left(d_x^2\right)\frac{1-\eta}{4ac^2}+\left(d_x^3\right)\frac{1+\eta}{4ac^2}+\left(d_x^4\right)\frac{-1-\eta}{4ac^2}+\\
& \left(d_x^5\right)\frac{-1+\eta}{4ac^2}+\left(d_x^6\right)\frac{1-\eta}{4ac^2}+\left(d_x^7\right)\frac{1+\eta}{4ac^2}+\left(d_x^8\right)\frac{-1-\eta}{4ac^2}+\\
& \left(d_x^{17}\right)\frac{1-\eta}{2ac^2}+\left(d_x^{18}\right)\frac{-1+\eta}{2ac^2}+\left(d_x^{19}\right)\frac{-1-\eta}{2ac^2}+\left(d_x^{20}\right)\frac{1+\eta}{2ac^2}\Bigg]+
\end{aligned}
$$

$$
\begin{aligned}
\tilde{f}_{3221}\Bigg[& \left(d_y^1\right)\frac{-1+2\xi+2\eta+2\zeta}{8abc}+\left(d_y^2\right)\frac{1+2\xi-2\eta-2\zeta}{8abc}+\\
& \left(d_y^3\right)\frac{-1-2\xi-2\eta+2\zeta}{8abc}+\left(d_y^4\right)\frac{1-2\xi+2\eta-2\zeta}{8abc}+\\
& \left(d_y^5\right)\frac{1-2\xi-2\eta+2\zeta}{8abc}+\left(d_y^6\right)\frac{-1-2\xi+2\eta-2\zeta}{8abc}+\\
& \left(d_y^7\right)\frac{1+2\xi+2\eta+2\zeta}{8abc}+\left(d_y^8\right)\frac{-1+2\xi-2\eta-2\zeta}{8abc}+\\
& \left(d_y^9\right)\frac{-\xi}{2abc}+\left(d_y^{10}\right)\frac{\eta}{2abc}+\left(d_y^{11}\right)\frac{\xi}{2abc}+\left(d_y^{12}\right)\frac{-\eta}{2abc}+\\
& \left(d_y^{13}\right)\frac{\xi}{2abc}+\left(d_y^{14}\right)\frac{-\eta}{2abc}+\left(d_y^{15}\right)\frac{-\xi}{2abc}+\left(d_y^{16}\right)\frac{\eta}{2abc}+\\
& \left(d_y^{17}\right)\frac{-\zeta}{2abc}+\left(d_y^{18}\right)\frac{\zeta}{2abc}+\left(d_y^{19}\right)\frac{-\zeta}{2abc}+\left(d_y^{20}\right)\frac{\zeta}{2abc}\Bigg]+\\
\tilde{f}_{3222}\Bigg[& \left(d_y^1\right)\frac{-1+\xi}{4b^2c}+\left(d_y^2\right)\frac{-1-\xi}{4b^2c}+\left(d_y^3\right)\frac{-1-\xi}{4b^2c}+\left(d_y^4\right)\frac{-1+\xi}{4b^2c}+\\
& \left(d_y^5\right)\frac{1-\xi}{4b^2c}+\left(d_y^6\right)\frac{1+\xi}{4b^2c}+\left(d_y^7\right)\frac{1+\xi}{4b^2c}+\left(d_y^8\right)\frac{1-\xi}{4b^2c}+\\
& \left(d_y^{10}\right)\frac{1+\xi}{2b^2c}+\left(d_y^{12}\right)\frac{1-\xi}{2b^2c}+\left(d_y^{14}\right)\frac{-1-\xi}{2b^2c}+\left(d_y^{16}\right)\frac{-1+\xi}{2b^2c}\Bigg]+\\
\tilde{f}_{3223}\Bigg[& \left(d_y^1\right)\frac{-1+\xi}{4bc^2}+\left(d_y^2\right)\frac{-1-\xi}{4bc^2}+\left(d_y^3\right)\frac{1+\xi}{4bc^2}+\left(d_y^4\right)\frac{1-\xi}{4bc^2}+\\
& \left(d_y^5\right)\frac{-1+\xi}{4bc^2}+\left(d_y^6\right)\frac{-1-\xi}{4bc^2}+\left(d_y^7\right)\frac{1+\xi}{4bc^2}+\left(d_y^8\right)\frac{1-\xi}{4bc^2}+\\
& \left(d_y^{17}\right)\frac{1-\xi}{2bc^2}+\left(d_y^{18}\right)\frac{1+\xi}{2bc^2}+\left(d_y^{19}\right)\frac{-1-\xi}{2bc^2}+\left(d_y^{20}\right)\frac{-1+\xi}{2bc^2}\Bigg]+\\
\tilde{f}_{3331}\Bigg[& \left(d_z^1\right)\frac{-1+\eta}{4ac^2}+\left(d_z^2\right)\frac{1-\eta}{4ac^2}+\left(d_z^3\right)\frac{1+\eta}{4ac^2}+\left(d_z^4\right)\frac{-1-\eta}{4ac^2}+\\
& \left(d_z^5\right)\frac{-1+\eta}{4ac^2}+\left(d_z^6\right)\frac{1-\eta}{4ac^2}+\left(d_z^7\right)\frac{1+\eta}{4ac^2}+\left(d_z^8\right)\frac{-1-\eta}{4ac^2}+\\
& \left(d_z^{17}\right)\frac{1-\eta}{2ac^2}+\left(d_z^{18}\right)\frac{-1+\eta}{2ac^2}+\left(d_z^{19}\right)\frac{-1-\eta}{2ac^2}+\left(d_z^{20}\right)\frac{1+\eta}{2ac^2}\Bigg]+
\end{aligned}
$$

$$
\begin{aligned}
\tilde{f}_{3332}\Bigg[& \left(d_z^1\right)\frac{-1+\xi}{4bc^2}+\left(d_z^2\right)\frac{-1-\xi}{4bc^2}+\left(d_z^3\right)\frac{1+\xi}{4bc^2}+\left(d_z^4\right)\frac{1-\xi}{4bc^2}+\\
& \left(d_z^5\right)\frac{-1+\xi}{4bc^2}+\left(d_z^6\right)\frac{-1-\xi}{4bc^2}+\left(d_z^7\right)\frac{1+\xi}{4bc^2}+\left(d_z^8\right)\frac{1-\xi}{4bc^2}+\\
& \left(d_z^{17}\right)\frac{1-\xi}{2bc^2}+\left(d_z^{18}\right)\frac{1+\xi}{2bc^2}+\left(d_z^{19}\right)\frac{-1-\xi}{2bc^2}+\left(d_z^{20}\right)\frac{-1+\xi}{2bc^2}\Bigg]+\\
\tilde{f}_{3121}\Bigg[& \left(d_x^1\right)\frac{-1+2\xi+2\eta+2\zeta}{8abc}+\left(d_y^1\right)\frac{-1+\eta}{4a^2c}+\left(d_x^2\right)\frac{1+2\xi-2\eta-2\zeta}{8abc}+\\
& \left(d_y^2\right)\frac{-1+\eta}{4a^2c}+\left(d_x^3\right)\frac{-1-2\xi-2\eta+2\zeta}{8abc}+\left(d_y^3\right)\frac{-1-\eta}{4a^2c}+\\
& \left(d_x^4\right)\frac{1-2\xi+2\eta-2\zeta}{8abc}+\left(d_y^4\right)\frac{-1-\eta}{4a^2c}+\left(d_x^5\right)\frac{1-2\xi-2\eta+2\zeta}{8abc}+\\
& \left(d_y^5\right)\frac{1-\eta}{4a^2c}+\left(d_x^6\right)\frac{-1-2\xi+2\eta-2\zeta}{8abc}+\left(d_y^6\right)\frac{1-\eta}{4a^2c}+\\
& \left(d_x^7\right)\frac{1+2\xi+2\eta+2\zeta}{8abc}+\left(d_y^7\right)\frac{1+\eta}{4a^2c}+\left(d_x^8\right)\frac{-1+2\xi-2\eta-2\zeta}{8abc}+\\
& \left(d_y^8\right)\frac{1+\eta}{4a^2c}+\left(d_x^9\right)\frac{-\xi}{2abc}+\left(d_y^9\right)\frac{1-\eta}{2a^2c}+\left(d_x^{10}\right)\frac{\eta}{2abc}+\\
& \left(d_x^{11}\right)\frac{\xi}{2abc}+\left(d_y^{11}\right)\frac{1+\eta}{2a^2c}+\left(d_x^{12}\right)\frac{-\eta}{2abc}+\left(d_x^{13}\right)\frac{\xi}{2abc}+\\
& \left(d_y^{13}\right)\frac{-1+\eta}{2a^2c}+\left(d_x^{14}\right)\frac{-\eta}{2abc}+\left(d_x^{15}\right)\frac{-\xi}{2abc}+\left(d_y^{15}\right)\frac{-1-\eta}{2a^2c}+\\
& \left(d_x^{16}\right)\frac{\eta}{2abc}+\left(d_x^{17}\right)\frac{-\zeta}{2abc}+\left(d_x^{18}\right)\frac{\zeta}{2abc}+\left(d_x^{19}\right)\frac{-\zeta}{2abc}+\left(d_x^{20}\right)\frac{\zeta}{2abc}\Bigg]+
\end{aligned}
$$

$$
\begin{aligned}
\tilde{f}_{3122}\Bigg[& \left(d_x^1\right)\frac{-1+\xi}{4b^2c}+\left(d_y^1\right)\frac{-1+2\xi+2\eta+2\zeta}{8abc}+\left(d_x^2\right)\frac{-1-\xi}{4b^2c}+\\
& \left(d_y^2\right)\frac{1+2\xi-2\eta-2\zeta}{8abc}+\left(d_x^3\right)\frac{-1-\xi}{4b^2c}+\left(d_y^3\right)\frac{-1-2\xi-2\eta+2\zeta}{8abc}+\\
& \left(d_x^4\right)\frac{-1+\xi}{4b^2c}+\left(d_y^4\right)\frac{1-2\xi+2\eta-2\zeta}{8abc}+\left(d_x^5\right)\frac{1-\xi}{4b^2c}+\\
& \left(d_y^5\right)\frac{1-2\xi-2\eta+2\zeta}{8abc}+\left(d_x^6\right)\frac{1+\xi}{4b^2c}+\left(d_y^6\right)\frac{-1-2\xi+2\eta-2\zeta}{8abc}+\\
& \left(d_x^7\right)\frac{1+\xi}{4b^2c}+\left(d_y^7\right)\frac{1+2\xi+2\eta+2\zeta}{8abc}+\left(d_x^8\right)\frac{1-\xi}{4b^2c}+\\
& \left(d_y^8\right)\frac{-1+2\xi-2\eta-2\zeta}{8abc}+\left(d_y^9\right)\frac{-\xi}{2abc}+\left(d_x^{10}\right)\frac{1+\xi}{2b^2c}+\left(d_y^{10}\right)\frac{\eta}{2abc}+\\
& \left(d_y^{11}\right)\frac{\xi}{2abc}+\left(d_x^{12}\right)\frac{1-\xi}{2b^2c}+\left(d_y^{12}\right)\frac{-\eta}{2abc}+\left(d_y^{13}\right)\frac{\xi}{2abc}+\\
& \left(d_x^{14}\right)\frac{-1-\xi}{2b^2c}+\left(d_y^{14}\right)\frac{-\eta}{2abc}+\left(d_y^{15}\right)\frac{-\xi}{2abc}+\left(d_x^{16}\right)\frac{-1+\xi}{2b^2c}+\\
& \left(d_y^{16}\right)\frac{\eta}{2abc}+\left(d_y^{17}\right)\frac{-\zeta}{2abc}+\left(d_y^{18}\right)\frac{\zeta}{2abc}+\left(d_y^{19}\right)\frac{-\zeta}{2abc}+\left(d_y^{20}\right)\frac{\zeta}{2abc}\Bigg]+\\
\tilde{f}_{3123}\Bigg[& \left(d_x^1\right)\frac{-1+\xi}{4bc^2}+\left(d_y^1\right)\frac{-1+\eta}{4ac^2}+\left(d_x^2\right)\frac{-1-\xi}{4bc^2}+\left(d_y^2\right)\frac{1-\eta}{4ac^2}+\\
& \left(d_x^3\right)\frac{1+\xi}{4bc^2}+\left(d_y^3\right)\frac{1+\eta}{4ac^2}+\left(d_x^4\right)\frac{1-\xi}{4bc^2}+\left(d_y^4\right)\frac{-1-\eta}{4ac^2}+\\
& \left(d_x^5\right)\frac{-1+\xi}{4bc^2}+\left(d_y^5\right)\frac{-1+\eta}{4ac^2}+\left(d_x^6\right)\frac{-1-\xi}{4bc^2}+\left(d_y^6\right)\frac{1-\eta}{4ac^2}+\\
& \left(d_x^7\right)\frac{1+\xi}{4bc^2}+\left(d_y^7\right)\frac{1+\eta}{4ac^2}+\left(d_x^8\right)\frac{1-\xi}{4bc^2}+\left(d_y^8\right)\frac{-1-\eta}{4ac^2}+\\
& \left(d_x^{17}\right)\frac{1-\xi}{2bc^2}+\left(d_y^{17}\right)\frac{1-\eta}{2ac^2}+\left(d_x^{18}\right)\frac{1+\xi}{2bc^2}+\left(d_y^{18}\right)\frac{-1+\eta}{2ac^2}+\\
& \left(d_x^{19}\right)\frac{-1-\xi}{2bc^2}+\left(d_y^{19}\right)\frac{-1-\eta}{2ac^2}+\left(d_x^{20}\right)\frac{-1+\xi}{2bc^2}+\left(d_y^{20}\right)\frac{1+\eta}{2ac^2}\Bigg]+
\end{aligned}
$$

$$
\begin{aligned}
\tilde{f}_{3131}\Bigg[& \left(d_x^1\right)\frac{-1+\eta}{4ac^2}+\left(d_z^1\right)\frac{-1+\eta}{4a^2c}+\left(d_x^2\right)\frac{1-\eta}{4ac^2}+\left(d_z^2\right)\frac{-1+\eta}{4a^2c}+\\
& \left(d_x^3\right)\frac{1+\eta}{4ac^2}+\left(d_z^3\right)\frac{-1-\eta}{4a^2c}+\left(d_x^4\right)\frac{-1-\eta}{4ac^2}+\left(d_z^4\right)\frac{-1-\eta}{4a^2c}+\\
& \left(d_x^5\right)\frac{-1+\eta}{4ac^2}+\left(d_z^5\right)\frac{1-\eta}{4a^2c}+\left(d_x^6\right)\frac{1-\eta}{4ac^2}+\left(d_z^6\right)\frac{1-\eta}{4a^2c}+\\
& \left(d_x^7\right)\frac{1+\eta}{4ac^2}+\left(d_z^7\right)\frac{1+\eta}{4a^2c}+\left(d_x^8\right)\frac{-1-\eta}{4ac^2}+\left(d_z^8\right)\frac{1+\eta}{4a^2c}+\\
& \left(d_z^9\right)\frac{1-\eta}{2a^2c}+\left(d_z^{11}\right)\frac{1+\eta}{2a^2c}+\left(d_z^{13}\right)\frac{-1+\eta}{2a^2c}+\left(d_z^{15}\right)\frac{-1-\eta}{2a^2c}+\\
& \left(d_x^{17}\right)\frac{1-\eta}{2ac^2}+\left(d_x^{18}\right)\frac{-1+\eta}{2ac^2}+\left(d_x^{19}\right)\frac{-1-\eta}{2ac^2}+\left(d_x^{20}\right)\frac{1+\eta}{2ac^2}\Bigg]+\\
\tilde{f}_{3132}\Bigg[& \left(d_x^1\right)\frac{-1+\xi}{4bc^2}+\left(d_z^1\right)\frac{-1+2\xi+2\eta+2\zeta}{8abc}+\left(d_x^2\right)\frac{-1-\xi}{4bc^2}+\\
& \left(d_z^2\right)\frac{1+2\xi-2\eta-2\zeta}{8abc}+\left(d_x^3\right)\frac{1+\xi}{4bc^2}+\left(d_z^3\right)\frac{-1-2\xi-2\eta+2\zeta}{8abc}+\\
& \left(d_x^4\right)\frac{1-\xi}{4bc^2}+\left(d_z^4\right)\frac{1-2\xi+2\eta-2\zeta}{8abc}+\left(d_x^5\right)\frac{-1+\xi}{4bc^2}+\\
& \left(d_z^5\right)\frac{1-2\xi-2\eta+2\zeta}{8abc}+\left(d_x^6\right)\frac{-1-\xi}{4bc^2}+\left(d_z^6\right)\frac{-1-2\xi+2\eta-2\zeta}{8abc}+\\
& \left(d_x^7\right)\frac{1+\xi}{4bc^2}+\left(d_z^7\right)\frac{1+2\xi+2\eta+2\zeta}{8abc}+\left(d_x^8\right)\frac{1-\xi}{4bc^2}+\\
& \left(d_z^8\right)\frac{-1+2\xi-2\eta-2\zeta}{8abc}+\left(d_z^9\right)\frac{-\xi}{2abc}+\left(d_z^{10}\right)\frac{\eta}{2abc}+\left(d_z^{11}\right)\frac{\xi}{2abc}+\\
& \left(d_z^{12}\right)\frac{-\eta}{2abc}+\left(d_z^{13}\right)\frac{\xi}{2abc}+\left(d_z^{14}\right)\frac{-\eta}{2abc}+\left(d_z^{15}\right)\frac{-\xi}{2abc}+\\
& \left(d_z^{16}\right)\frac{\eta}{2abc}+\left(d_x^{17}\right)\frac{1-\xi}{2bc^2}+\left(d_z^{17}\right)\frac{-\zeta}{2abc}+\left(d_x^{18}\right)\frac{1+\xi}{2bc^2}+\\
& \left(d_z^{18}\right)\frac{\zeta}{2abc}+\left(d_x^{19}\right)\frac{-1-\xi}{2bc^2}+\left(d_z^{19}\right)\frac{-\zeta}{2abc}+\left(d_x^{20}\right)\frac{-1+\xi}{2bc^2}+\left(d_z^{20}\right)\frac{\zeta}{2abc}\Bigg]+\\
\tilde{f}_{3133}\Bigg[& \left(d_z^1\right)\frac{-1+\eta}{4ac^2}+\left(d_z^2\right)\frac{1-\eta}{4ac^2}+\left(d_z^3\right)\frac{1+\eta}{4ac^2}+\left(d_z^4\right)\frac{-1-\eta}{4ac^2}+\\
& \left(d_z^5\right)\frac{-1+\eta}{4ac^2}+\left(d_z^6\right)\frac{1-\eta}{4ac^2}+\left(d_z^7\right)\frac{1+\eta}{4ac^22}+\left(d_z^8\right)\frac{-1-\eta}{4ac^2}+\\
& \left(d_z^{17}\right)\frac{1-\eta}{1ac^2}+\left(d_z^{18}\right)\frac{-1+\eta}{2ac^2}+\left(d_z^{19}\right)\frac{-1-\eta}{2ac^2}+\left(d_z^{20}\right)\frac{1+\eta}{2ac^2}\Bigg]+
\end{aligned}
$$

$$
\begin{aligned}
\tilde{f}_{3231}\Bigg[& \left(d_y^1\right)\frac{-1+\eta}{4ac^2}+\left(d_z^1\right)\frac{-1+2\xi+2\eta+2\zeta}{8abc}+\left(d_y^2\right)\frac{1-\eta}{4ac^2}+\\
& \left(d_z^2\right)\frac{1+2\xi-2\eta-2\zeta}{8abc}+\left(d_y^3\right)\frac{1+\eta}{4ac^2}+\left(d_z^3\right)\frac{-1-2\xi-2\eta+2\zeta}{8abc}+\\
& \left(d_y^4\right)\frac{-1-\eta}{4ac^2}+\left(d_z^4\right)\frac{1-2\xi+2\eta-2\zeta}{8abc}+\left(d_y^5\right)\frac{-1+\eta}{4ac^2}+\\
& \left(d_z^5\right)\frac{1-2\xi-2\eta+2\zeta}{8abc}+\left(d_y^6\right)\frac{1-\eta}{4ac^2}+\left(d_z^6\right)\frac{-1-2\xi+2\eta-2\zeta}{8abc}+\\
& \left(d_y^7\right)\frac{1+\eta}{4ac^2}+\left(d_z^7\right)\frac{1+2\xi+2\eta+2\zeta}{8abc}+\left(d_y^8\right)\frac{-1-\eta}{4ac^2}+\\
& \left(d_z^8\right)\frac{-1+2\xi-2\eta-2\zeta}{8abc}+\left(d_z^9\right)\frac{-\xi}{2abc}+\left(d_z^{10}\right)\frac{\eta}{2abc}+\left(d_z^{11}\right)\frac{\xi}{2abc}+\\
& \left(d_z^{12}\right)\frac{-\eta}{2abc}+\left(d_z^{13}\right)\frac{\xi}{2abc}+\left(d_z^{14}\right)\frac{-\eta}{2abc}+\left(d_z^{15}\right)\frac{-\xi}{2abc}+\\
& \left(d_z^{16}\right)\frac{\eta}{2abc}+\left(d_y^{17}\right)\frac{1-\eta}{2ac^2}+\left(d_z^{17}\right)\frac{-\zeta}{2abc}+\left(d_y^{18}\right)\frac{-1+\eta}{2ac^2}+\\
& \left(d_z^{18}\right)\frac{\zeta}{2abc}+\left(d_y^{19}\right)\frac{-1-\eta}{2ac^2}+\left(d_z^{19}\right)\frac{-\zeta}{2abc}+\left(d_y^{20}\right)\frac{1+\eta}{2ac^2}+\left(d_z^{20}\right)\frac{-\zeta}{2abc}\Bigg]+\\
\tilde{f}_{3232}\Bigg[& \left(d_y^1\right)\frac{-1+\xi}{4bc^2}+\left(d_z^1\right)\frac{-1+\xi}{4b^2c}+\left(d_y^2\right)\frac{-1-\xi}{4bc^2}+\left(d_z^2\right)\frac{-1-\xi}{4b^2c}+\\
& \left(d_y^3\right)\frac{1+\xi}{4bc^2}+\left(d_z^3\right)\frac{-1-\xi}{4b^2c}+\left(d_y^4\right)\frac{1-\xi}{4bc^2}+\left(d_z^4\right)\frac{-1+\xi}{4b^2c}+\\
& \left(d_y^5\right)\frac{-1+\xi}{4bc^2}+\left(d_z^5\right)\frac{1-\xi}{4b^2c}+\left(d_y^6\right)\frac{-1-\xi}{4bc^2}+\left(d_z^6\right)\frac{1+\xi}{4b^2c}+\\
& \left(d_y^7\right)\frac{1+\xi}{4bc^2}+\left(d_z^7\right)\frac{1+\xi}{4b^2c}+\left(d_y^8\right)\frac{1-\xi}{4bc^2}+\left(d_z^8\right)\frac{1-\xi}{4b^2c}+\\
& \left(d_z^{10}\right)\frac{1+\xi}{2b^2c}+\left(d_z^{12}\right)\frac{1-\xi}{2b^2c}+\left(d_z^{14}\right)\frac{-1-\xi}{2b^2c}+\left(d_z^{16}\right)\frac{-1+\xi}{2b^2c}+\\
& \left(d_y^{17}\right)\frac{1-\xi}{2bc^2}+\left(d_y^{18}\right)\frac{1+\xi}{2bc^2}+\left(d_y^{19}\right)\frac{-1-\xi}{2bc^2}+\left(d_y^{20}\right)\frac{-1+\xi}{2bc^2}\Bigg]+
\end{aligned}
$$

$$\tilde{f}_{3233}\Bigg[\left(d_z^1\right)\frac{-1+\xi}{4bc^2}+\left(d_z^2\right)\frac{-1-\xi}{4bc^2}+\left(d_z^3\right)\frac{1+\xi}{4bc^2}+\left(d_z^4\right)\frac{1-\xi}{4bc^2}+$$
$$\left(d_z^5\right)\frac{-1+\xi}{4bc^2}+\left(d_z^6\right)\frac{-1-\xi}{4bc^2}+\left(d_z^7\right)\frac{1+\xi}{4bc^2}+\left(d_z^8\right)\frac{1-\xi}{4bc^2}+$$
$$\left(d_z^{17}\right)\frac{1-\xi}{2bc^2}+\left(d_z^{18}\right)\frac{1+\xi}{2bc^2}+\left(d_z^{19}\right)\frac{-1-\xi}{2bc^2}+\left(d_z^{20}\right)\frac{-1+\xi}{2bc^2}\Bigg] \tag{B.7}$$

When the value of the integrand in the centre of the element i.e., at $(\xi,\eta,\zeta)=(0,0,0)$ is taken, Equation (B.7) changes to:

$$\nabla\cdot\tilde{\mathbf{P}}=\tilde{f}_{1112}\Bigg[\left(d_x^1\right)\frac{-1}{4a^2b}+\left(d_x^2\right)\frac{-1}{4a^2b}+\left(d_x^3\right)\frac{1}{4a^2b}+\left(d_x^4\right)\frac{1}{4a^2b}+$$
$$\left(d_x^5\right)\frac{-1}{4a^2b}+\left(d_x^6\right)\frac{-1}{4a^2b}+\left(d_x^7\right)\frac{1}{4a^2b}+\left(d_x^8\right)\frac{1}{4a^2b}+$$
$$\left(d_x^9\right)\frac{1}{2a^2b}+\left(d_x^{11}\right)\frac{-1}{2a^2b}+\left(d_x^{13}\right)\frac{1}{2a^2b}+\left(d_x^{15}\right)\frac{-1}{2a^2b}\Bigg]+$$
$$\tilde{f}_{1113}\Bigg[\left(d_x^1\right)\frac{-1}{4a^2c}+\left(d_x^2\right)\frac{-1}{4a^2c}+\left(d_x^3\right)\frac{-1}{4a^2c}+\left(d_x^4\right)\frac{-1}{4a^2c}+$$
$$\left(d_x^5\right)\frac{1}{4a^2c}+\left(d_x^6\right)\frac{1}{4a^2c}+\left(d_x^7\right)\frac{1}{4a^2c}+\left(d_x^8\right)\frac{1}{4a^2c}+$$
$$\left(d_x^9\right)\frac{1}{2a^2c}+\left(d_x^{11}\right)\frac{1}{2a^2c}+\left(d_x^{13}\right)\frac{-1}{2a^2c}+\left(d_x^{15}\right)\frac{-1}{2a^2c}\Bigg]+$$
$$\tilde{f}_{1221}\Bigg[\left(d_y^1\right)\frac{-1}{4a^2b}+\left(d_y^2\right)\frac{-1}{4a^2b}+\left(d_y^3\right)\frac{1}{4a^2b}+\left(d_y^4\right)\frac{1}{4a^2b}+$$
$$\left(d_y^5\right)\frac{-1}{4a^2b}+\left(d_y^6\right)\frac{-1}{4a^2b}+\left(d_y^7\right)\frac{1}{4a^2b}+\left(d_y^8\right)\frac{1}{4a^2b}+$$
$$\left(d_y^9\right)\frac{1}{2a^2b}+\left(d_y^{11}\right)\frac{-1}{2a^2b}+\left(d_y^{13}\right)\frac{1}{2a^2b}+\left(d_y^{15}\right)\frac{-1}{2a^2b}\Bigg]+$$

$$
\begin{aligned}
\tilde{f}_{1222}\Bigg[& \left(d_y^1\right)\frac{-1}{4ab^2}+\left(d_y^2\right)\frac{1}{4ab^2}+\left(d_y^3\right)\frac{1}{4ab^2}+\left(d_y^4\right)\frac{-1}{4ab^2}+ \\
& \left(d_y^5\right)\frac{-1}{4ab^2}+\left(d_y^6\right)\frac{1}{4ab^2}+\left(d_y^7\right)\frac{1}{4ab^2}+\left(d_y^8\right)\frac{-1}{4ab^2}+ \\
& \left(d_y^{10}\right)\frac{-1}{2ab^2}+\left(d_y^{12}\right)\frac{1}{2ab^2}+\left(d_y^{14}\right)\frac{-1}{2ab^2}+\left(d_y^{16}\right)\frac{1}{2ab^2}\Bigg]+ \\
\tilde{f}_{1223}\Bigg[& \left(d_y^1\right)\frac{-1}{8abc}+\left(d_y^2\right)\frac{1}{8abc}+\left(d_y^3\right)\frac{-1}{8abc}+\left(d_y^4\right)\frac{1}{8abc}+ \\
& \left(d_y^5\right)\frac{1}{8abc}+\left(d_y^6\right)\frac{-1}{8abc}+\left(d_y^7\right)\frac{1}{8abc}+\left(d_y^8\right)\frac{-1}{8abc}\Bigg]+ \\
\tilde{f}_{1331}\Bigg[& \left(d_z^1\right)\frac{-1}{4a^2c}+\left(d_z^2\right)\frac{-1}{4a^2c}+\left(d_z^3\right)\frac{-1}{4a^2c}+\left(d_z^4\right)\frac{-1}{4a^2c}+ \\
& \left(d_z^5\right)\frac{1}{4a^2c}+\left(d_z^6\right)\frac{1}{4a^2c}+\left(d_z^7\right)\frac{1}{4a^2c}+\left(d_z^8\right)\frac{1}{4a^2c}+ \\
& \left(d_z^9\right)\frac{1}{2a^2c}+\left(d_z^{11}\right)\frac{1}{2a^2c}+\left(d_z^{13}\right)\frac{-1}{2a^2c}+\left(d_z^{15}\right)\frac{-1}{2a^2c}\Bigg]+ \\
\tilde{f}_{1332}\Bigg[& \left(d_z^1\right)\frac{-1}{8abc}+\left(d_z^2\right)\frac{1}{8abc}+\left(d_z^3\right)\frac{-1}{8abc}+\left(d_z^4\right)\frac{1}{8abc}+ \\
& \left(d_z^5\right)\frac{1}{8abc}+\left(d_z^6\right)\frac{-1}{8abc}+\left(d_z^7\right)\frac{1}{8abc}+\left(d_z^8\right)\frac{-1}{8abc}\Bigg]+ \\
\tilde{f}_{1333}\Bigg[& \left(d_z^1\right)\frac{-1}{4ac^2}+\left(d_z^2\right)\frac{1}{4ac^2}+\left(d_z^3\right)\frac{1}{4ac^2}+\left(d_z^4\right)\frac{-1}{4ac^2}+ \\
& \left(d_z^5\right)\frac{-1}{4ac^2}+\left(d_z^6\right)\frac{1}{4ac^2}+\left(d_z^7\right)\frac{1}{4ac^2}+\left(d_z^8\right)\frac{-1}{4ac^2}+ \\
& \left(d_z^{17}\right)\frac{1}{2ac^2}+\left(d_z^{18}\right)\frac{-1}{2ac^2}+\left(d_z^{19}\right)\frac{-1}{2ac^2}+\left(d_z^{20}\right)\frac{1}{2ac^2}\Bigg]+
\end{aligned}
$$

$$
\begin{aligned}
\tilde{f}_{1121}\Bigg[& \left(d_x^1\right)\frac{-1}{4a^2b}+\left(d_x^2\right)\frac{-1}{4a^2b}+\left(d_x^3\right)\frac{1}{4a^2b}+\left(d_x^4\right)\frac{1}{4a^2b}+\\
& \left(d_x^5\right)\frac{-1}{4a^2b}+\left(d_x^6\right)\frac{-1}{4a^2b}+\left(d_x^7\right)\frac{1}{4a^2b}+\left(d_x^8\right)\frac{1}{4a^2b}+\\
& \left(d_x^9\right)\frac{1}{2a^2b}+\left(d_x^{11}\right)\frac{-1}{2a^2b}+\left(d_x^{13}\right)\frac{1}{2a^2b}+\left(d_x^{15}\right)\frac{-1}{2a^2b}\Bigg]+\\
\tilde{f}_{1122}\Bigg[& \left(d_x^1\right)\frac{-1}{4ab^2}+\left(d_y^1\right)\frac{-1}{4a^2b}+\left(d_x^2\right)\frac{1}{4ab^2}+\left(d_y^2\right)\frac{-1}{4a^2b}+\\
& \left(d_x^3\right)\frac{1}{4ab^2}+\left(d_y^3\right)\frac{1}{4a^2b}+\left(d_x^4\right)\frac{-1}{4ab^2}+\left(d_y^4\right)\frac{1}{4a^2b}+\\
& \left(d_x^5\right)\frac{-1}{4ab^2}+\left(d_y^5\right)\frac{-1}{4a^2b}+\left(d_x^6\right)\frac{1}{4ab^2}+\left(d_y^6\right)\frac{-1}{4a^2b}+\\
& \left(d_x^7\right)\frac{1}{4ab^2}+\left(d_y^7\right)\frac{1}{4a^2b}+\left(d_x^8\right)\frac{-1}{4ab^2}+\left(d_y^8\right)\frac{1}{4a^2b}+\\
& \left(d_y^9\right)\frac{1}{2a^2b}+\left(d_x^{10}\right)\frac{-1}{2ab^2}+\left(d_y^{11}\right)\frac{-1}{2a^2b}+\left(d_x^{12}\right)\frac{1}{2ab^2}+\\
& \left(d_y^{13}\right)\frac{1}{2a^2b}+\left(d_x^{14}\right)\frac{-1}{2ab^2}+\left(d_y^{15}\right)\frac{-1}{2a^2b}+\left(d_x^{16}\right)\frac{1}{2ab^2}\Bigg]+\\
\tilde{f}_{1123}\Bigg[& \left(d_x^1\right)\frac{-1}{8abc}+\left(d_y^1\right)\frac{-1}{4a^2c}+\left(d_x^2\right)\frac{1}{8abc}+\left(d_y^2\right)\frac{-1}{4a^2c}+\\
& \left(d_x^3\right)\frac{-1}{8abc}+\left(d_y^3\right)\frac{-1}{4a^2c}+\left(d_x^4\right)\frac{1}{8abc}+\left(d_y^4\right)\frac{-1}{4a^2c}+\\
& \left(d_x^5\right)\frac{1}{8abc}+\left(d_y^5\right)\frac{1}{4a^2c}+\left(d_x^6\right)\frac{-1}{8abc}+\left(d_y^6\right)\frac{1}{4a^2c}+\\
& \left(d_x^7\right)\frac{1}{8abc}+\left(d_y^7\right)\frac{1}{4a^2c}+\left(d_x^8\right)\frac{-1}{8abc}+\left(d_y^8\right)\frac{1}{4a^2c}+\\
& \left(d_y^9\right)\frac{1}{2a^2c}+\left(d_y^{11}\right)\frac{1}{2a^2c}+\left(d_y^{13}\right)\frac{-1}{2a^2c}+\left(d_y^{15}\right)\frac{-1}{2a^2c}\Bigg]+\\
\tilde{f}_{1131}\Bigg[& \left(d_x^1\right)\frac{-1}{4a^2c}+\left(d_x^2\right)\frac{-1}{4a^2c}+\left(d_x^3\right)\frac{-1}{4a^2c}+\left(d_x^4\right)\frac{-1}{4a^2c}+\\
& \left(d_x^5\right)\frac{1}{4a^2c}+\left(d_x^6\right)\frac{1}{4a^2c}+\left(d_x^7\right)\frac{1}{4a^2c}+\left(d_x^8\right)\frac{1}{4a^2c}+\\
& \left(d_x^9\right)\frac{1}{2a^2c}+\left(d_x^{11}\right)\frac{1}{2a^2c}+\left(d_x^{13}\right)\frac{-1}{2a^2c}+\left(d_x^{15}\right)\frac{-1}{2a^2c}\Bigg]+
\end{aligned}
$$

$$
\begin{aligned}
\tilde{f}_{1132}\Bigg[& \left(d_x^1\right)\frac{-1}{8abc}+\left(d_z^1\right)\frac{-1}{4a^2b}+\left(d_x^2\right)\frac{1}{8abc}+\left(d_z^2\right)\frac{-1}{4a^b}+\\
& \left(d_x^3\right)\frac{-1}{8abc}+\left(d_z^3\right)\frac{1}{4a^2b}+\left(d_x^4\right)\frac{1}{8abc}+\left(d_z^4\right)\frac{1}{4a^2b}+\\
& \left(d_x^5\right)\frac{1}{8abc}+\left(d_z^5\right)\frac{-1}{4a^2b}+\left(d_x^6\right)\frac{-1}{8abc}+\left(d_z^6\right)\frac{-1}{4a^2b}+\\
& \left(d_x^7\right)\frac{1}{8abc}+\left(d_z^7\right)\frac{1}{4a^2b}+\left(d_x^8\right)\frac{-1}{8abc}+\left(d_z^8\right)\frac{1}{4a^2b}+\\
& \left(d_z^9\right)\frac{1}{2a^2b}+\left(d_z^{11}\right)\frac{-1}{2a^2b}+\left(d_z^{13}\right)\frac{1}{2a^2b}+\left(d_z^{15}\right)\frac{-1}{2a^2b}\Bigg]+\\
\tilde{f}_{1133}\Bigg[& \left(d_x^1\right)\frac{-1}{4ac^2}+\left(d_z^1\right)\frac{-1}{4a^2c}+\left(d_x^2\right)\frac{1}{4ac^2}+\left(d_z^2\right)\frac{-1}{4a^2c}+\\
& \left(d_x^3\right)\frac{1}{4ac^2}+\left(d_z^3\right)\frac{-1}{4a^2c}+\left(d_x^4\right)\frac{-1}{4ac^2}+\left(d_z^4\right)\frac{-1}{4a^2c}+\\
& \left(d_x^5\right)\frac{-1}{4ac^2}+\left(d_z^5\right)\frac{1}{4a^2c}+\left(d_x^6\right)\frac{1}{4ac^2}+\left(d_z^6\right)\frac{1}{4a^2c}+\\
& \left(d_x^7\right)\frac{1}{4ac^2}+\left(d_z^7\right)\frac{1}{4a^2c}+\left(d_x^8\right)\frac{-1}{4ac^2}+\left(d_z^8\right)\frac{1}{4a^2c}+\\
& \left(d_z^9\right)\frac{1}{2a^2c}+\left(d_z^{11}\right)\frac{1}{2a^2c}+\left(d_z^{13}\right)\frac{-1}{2a^2c}+\left(d_z^{15}\right)\frac{-1}{2a^2c}+\\
& \left(d_x^{17}\right)\frac{1}{2ac^2}+\left(d_x^{18}\right)\frac{-1}{2ac^2}+\left(d_x^{19}\right)\frac{-1}{2ac^2}+\left(d_x^{20}\right)\frac{1}{2ac^2}\Bigg]+\\
\tilde{f}_{1231}\Bigg[& \left(d_y^1\right)\frac{-1}{4a^2c}+\left(d_z^1\right)\frac{-1}{4a^2b}+\left(d_y^2\right)\frac{-1}{4a^2c}+\left(d_z^2\right)\frac{-1}{4a^2b}+\\
& \left(d_y^3\right)\frac{-1}{4a^2c}+\left(d_z^3\right)\frac{1}{4a^2b}+\left(d_y^4\right)\frac{-1}{4a^2c}+\left(d_z^4\right)\frac{1}{4a^2b}+\\
& \left(d_y^5\right)\frac{1}{4a^2c}+\left(d_z^5\right)\frac{-1}{4a^2b}+\left(d_y^6\right)\frac{1}{4a^2c}+\left(d_z^6\right)\frac{-1}{4a^2b}+\\
& \left(d_y^7\right)\frac{1}{4a^2c}+\left(d_z^7\right)\frac{1}{4a^2b}+\left(d_y^8\right)\frac{1}{4a^2c}+\left(d_z^8\right)\frac{1}{4a^2b}+\\
& \left(d_y^9\right)\frac{1}{2a^2c}+\left(d_z^9\right)\frac{1}{2a^2b}+\left(d_y^{11}\right)\frac{1}{2a^2c}+\left(d_z^{11}\right)\frac{-1}{2a^2b}+\\
& \left(d_y^{13}\right)\frac{-1}{2a^2c}+\left(d_z^{13}\right)\frac{1}{2a^2b}+\left(d_y^{15}\right)\frac{-1}{2a^2c}+\left(d_z^{15}\right)\frac{-1}{2a^2b}\Bigg]+
\end{aligned}
$$

$$
\begin{aligned}
\tilde{f}_{1232}\Bigg[& \left(d_y^1\right)\frac{-1}{8abc}+\left(d_z^1\right)\frac{-1}{4ab^2}+\left(d_y^2\right)\frac{1}{8abc}+\left(d_z^2\right)\frac{1}{4ab^2}+\\
& \left(d_y^3\right)\frac{-1}{8abc}+\left(d_z^3\right)\frac{1}{4ab^2}+\left(d_y^4\right)\frac{1}{8abc}+\left(d_z^4\right)\frac{-1}{4ab^2}+\\
& \left(d_y^5\right)\frac{1}{8abc}+\left(d_z^5\right)\frac{-1}{4ab^2}+\left(d_y^6\right)\frac{-1}{8abc}+\left(d_z^6\right)\frac{1}{4ab^2}+\\
& \left(d_y^7\right)\frac{1}{8abc}+\left(d_z^7\right)\frac{1}{4ab^2}+\left(d_y^8\right)\frac{-1}{8abc}+\left(d_z^8\right)\frac{-1}{4ab^2}+\\
& \left(d_z^{10}\right)\frac{-1}{2ab^2}+\left(d_z^{12}\right)\frac{1}{2ab^2}+\left(d_z^{14}\right)\frac{-1}{2ab^2}+\left(d_z^{16}\right)\frac{1}{2ab^2}\Bigg]+\\
\tilde{f}_{1233}\Bigg[& \left(d_y^1\right)\frac{-1}{4ac^2}+\left(d_z^1\right)\frac{-1}{8abc}+\left(d_y^2\right)\frac{1}{4ac^2}+\left(d_z^2\right)\frac{1}{8abc}+\\
& \left(d_y^3\right)\frac{1}{4ac^2}+\left(d_z^3\right)\frac{-1}{8abc}+\left(d_y^4\right)\frac{-1}{4ac^2}+\left(d_z^4\right)\frac{1}{8abc}+\\
& \left(d_y^5\right)\frac{-1}{4ac^2}+\left(d_z^5\right)\frac{1}{8abc}+\left(d_y^6\right)\frac{1}{4ac^2}+\left(d_z^6\right)\frac{-1}{8abc}+\\
& \left(d_y^7\right)\frac{1}{4ac^2}+\left(d_z^7\right)\frac{1}{8abc}+\left(d_y^8\right)\frac{-1}{4ac^2}+\left(d_z^8\right)\frac{-1}{8abc}+\\
& \left(d_y^{17}\right)\frac{1}{2ac^2}+\left(d_y^{18}\right)\frac{-1}{2ac^2}+\left(d_y^{19}\right)\frac{-1}{2ac^2}+\left(d_y^{20}\right)\frac{1}{2ac^2}\Bigg]+\\
\tilde{f}_{2111}\Bigg[& \left(d_x^1\right)\frac{-1}{4a^2b}+\left(d_x^2\right)\frac{-1}{4a^2b}+\left(d_x^3\right)\frac{1}{4a^2b}+\left(d_x^4\right)\frac{1}{4a^2b}+\\
& \left(d_x^5\right)\frac{-1}{4a^2b}+\left(d_x^6\right)\frac{-1}{4a^2b}+\left(d_x^7\right)\frac{1}{4a^2b}+\left(d_x^8\right)\frac{1}{4a^2b}+\\
& \left(d_x^9\right)\frac{1}{2a^2b}+\left(d_x^{11}\right)\frac{-1}{2a^2b}+\left(d_x^{13}\right)\frac{1}{2a^2b}+\left(d_x^{15}\right)\frac{-1}{2a^2b}\Bigg]+\\
\tilde{f}_{2112}\Bigg[& \left(d_x^1\right)\frac{-1}{4ab^2}+\left(d_x^2\right)\frac{1}{4ab^2}+\left(d_x^3\right)\frac{1}{4ab^2}+\left(d_x^4\right)\frac{-1}{4ab^2}+\\
& \left(d_x^5\right)\frac{-1}{4ab^2}+\left(d_x^6\right)\frac{1}{4ab^2}+\left(d_x^7\right)\frac{1}{4ab^2}+\left(d_x^8\right)\frac{-1}{4ab^2}+\\
& \left(d_x^{10}\right)\frac{-1}{2ab^2}+\left(d_x^{12}\right)\frac{1}{2ab^2}+\left(d_x^{14}\right)\frac{-1}{2ab^2}+\left(d_x^{16}\right)\frac{1}{2ab^2}\Bigg]+
\end{aligned}
$$

$$
\begin{aligned}
\tilde{f}_{2113}\Bigg[& \left(d_x^1\right)\frac{-1}{8abc}+\left(d_x^2\right)\frac{1}{8abc}+\left(d_x^3\right)\frac{-1}{8abc}+\left(d_x^4\right)\frac{1}{8abc}+ \\
& \left(d_x^5\right)\frac{1}{8abc}+\left(d_x^6\right)\frac{-1}{8abc}+\left(d_x^7\right)\frac{1}{8abc}+\left(d_x^8\right)\frac{-1}{8abc}\Bigg]+ \\
\tilde{f}_{2221}\Bigg[& \left(d_y^1\right)\frac{-1}{4ab^2}+\left(d_y^2\right)\frac{1}{4ab^2}+\left(d_y^3\right)\frac{1}{4ab^2}+\left(d_y^4\right)\frac{-1}{4ab^2}+ \\
& \left(d_y^5\right)\frac{-1}{4ab^2}+\left(d_y^6\right)\frac{1}{4ab^2}+\left(d_y^7\right)\frac{1}{4ab^2}+\left(d_y^8\right)\frac{-1}{4ab^2}+ \\
& \left(d_y^{10}\right)\frac{-1}{2ab^2}+\left(d_y^{12}\right)\frac{1}{2ab^2}+\left(d_y^{14}\right)\frac{-1}{2ab^2}+\left(d_y^{16}\right)\frac{-1}{2ab^2}\Bigg]+ \\
\tilde{f}_{2223}\Bigg[& \left(d_y^1\right)\frac{-1}{4b^2c}+\left(d_y^2\right)\frac{-1}{4b^2c}+\left(d_y^3\right)\frac{-1}{4b^2c}+\left(d_y^4\right)\frac{-1}{4b^2c}+ \\
& \left(d_y^5\right)\frac{1}{4b^2c}+\left(d_y^6\right)\frac{1}{4b^2c}+\left(d_y^7\right)\frac{1}{4b^2c}+\left(d_y^8\right)\frac{1}{4b^2c}+ \\
& \left(d_y^{10}\right)\frac{1}{2b^2c}+\left(d_y^{12}\right)\frac{1}{2b^2c}+\left(d_y^{14}\right)\frac{-1}{2b^2c}+\left(d_y^{16}\right)\frac{-1}{2b^2c}\Bigg]+ \\
\tilde{f}_{2331}\Bigg[& \left(d_z^1\right)\frac{-1}{8abc}+\left(d_z^2\right)\frac{1}{8abc}+\left(d_z^3\right)\frac{-1}{8abc}+\left(d_z^4\right)\frac{1}{8abc}+ \\
& \left(d_z^5\right)\frac{1}{8abc}+\left(d_z^6\right)\frac{-1}{8abc}+\left(d_z^7\right)\frac{1}{8abc}+\left(d_z^8\right)\frac{-1}{8abc}\Bigg]+ \\
\tilde{f}_{2332}\Bigg[& \left(d_z^1\right)\frac{-1}{4b^2c}+\left(d_z^2\right)\frac{-1}{4b^2c}+\left(d_z^3\right)\frac{-1}{4b^2c}+\left(d_z^4\right)\frac{-1}{4b^2c}+ \\
& \left(d_z^5\right)\frac{1}{4b^2c}+\left(d_z^6\right)\frac{1}{4b^2c}+\left(d_z^7\right)\frac{1}{4b^2c}+\left(d_z^8\right)\frac{1}{4b^2c}+ \\
& \left(d_z^{10}\right)\frac{1}{2b^2c}+\left(d_z^{12}\right)\frac{1}{2b^2c}+\left(d_z^{14}\right)\frac{-1}{2b^2c}+\left(d_z^{16}\right)\frac{-1}{2b^2c}\Bigg]+
\end{aligned}
$$

$$
\begin{aligned}
\tilde{f}_{2333}\Bigg[& \left(d_z^1\right)\frac{-1}{4bc^2}+\left(d_z^2\right)\frac{-1}{4bc^2}+\left(d_z^3\right)\frac{1}{4bc^2}+\left(d_z^4\right)\frac{1}{4bc^2}+\\
& \left(d_z^5\right)\frac{-1}{4bc^2}+\left(d_z^6\right)\frac{-1}{4bc^2}+\left(d_z^7\right)\frac{1}{4bc^2}+\left(d_z^8\right)\frac{1}{4bc^2}+\\
& \left(d_z^{17}\right)\frac{1}{2bc^2}+\left(d_z^{18}\right)\frac{1}{2bc^2}+\left(d_z^{19}\right)\frac{-1}{2bc^2}+\left(d_z^{20}\right)\frac{-1}{2bc^2}\Bigg]+\\
\tilde{f}_{2121}\Bigg[& \left(d_x^1\right)\frac{-1}{4ab^2}+\left(d_y^1\right)\frac{-1}{4a^2b}+\left(d_x^2\right)\frac{1}{4ab^2}+\left(d_y^2\right)\frac{-1}{4a^2b}+\\
& \left(d_x^3\right)\frac{1}{4ab^2}+\left(d_y^3\right)\frac{1}{4a^2b}+\left(d_x^4\right)\frac{-1}{4ab^2}+\left(d_y^4\right)\frac{1}{4a^2b}+\\
& \left(d_x^5\right)\frac{-1}{4ab^2}+\left(d_y^5\right)\frac{-1}{4a^2b}+\left(d_x^6\right)\frac{1}{4ab^2}+\left(d_y^6\right)\frac{-1}{4a^2b}+\\
& \left(d_x^7\right)\frac{1}{4ab^2}+\left(d_y^7\right)\frac{1}{4a^2b}+\left(d_x^8\right)\frac{-1}{4ab^2}+\left(d_y^8\right)\frac{1}{4a^2b}+\\
& \left(d_y^9\right)\frac{1}{2a^2b}+\left(d_x^{10}\right)\frac{-1}{2ab^2}+\left(d_y^{11}\right)\frac{-1}{2a^2b}+\left(d_x^{12}\right)\frac{1}{2ab^2}+\\
& \left(d_y^{13}\right)\frac{1}{2a^2b}+\left(d_x^{14}\right)\frac{-1}{2ab^2}+\left(d_y^{15}\right)\frac{-1}{2a^2b}+\left(d_x^{16}\right)\frac{1}{2ab^2}\Bigg]+\\
\tilde{f}_{2122}\Bigg[& \left(d_y^1\right)\frac{-1}{4ab^2}+\left(d_y^2\right)\frac{1}{4ab^2}+\left(d_y^3\right)\frac{1}{4ab^2}+\left(d_y^4\right)\frac{-1}{4ab^2}+\\
& \left(d_y^5\right)\frac{-1}{4ab^2}+\left(d_y^6\right)\frac{1}{4ab^2}+\left(d_y^7\right)\frac{1}{4ab^2}+\left(d_y^8\right)\frac{-1}{4ab^2}+\\
& \left(d_y^{10}\right)\frac{-1}{2ab^2}+\left(d_y^{12}\right)\frac{1}{2ab^2}+\left(d_y^{14}\right)\frac{-1}{2ab^2}+\left(d_y^{16}\right)\frac{1}{2ab^2}\Bigg]+\\
\tilde{f}_{2123}\Bigg[& \left(d_x^1\right)\frac{-1}{4b^2c}+\left(d_y^1\right)\frac{-1}{8abc}+\left(d_x^2\right)\frac{-1}{4ab^2c}+\left(d_y^2\right)\frac{1}{8abc}+\\
& \left(d_x^3\right)\frac{-1}{4b^2c}+\left(d_y^3\right)\frac{-1}{8abc}+\left(d_x^4\right)\frac{-1}{4b^2c}+\left(d_y^4\right)\frac{1}{8abc}+\\
& \left(d_x^5\right)\frac{1}{4b^2c}+\left(d_y^5\right)\frac{1}{8abc}+\left(d_x^6\right)\frac{1}{4b^2c}+\left(d_y^6\right)\frac{-1}{8abc}+\\
& \left(d_x^7\right)\frac{1}{4b^2c}+\left(d_y^7\right)\frac{1}{8abc}+\left(d_x^8\right)\frac{1}{4b^2c}+\left(d_y^8\right)\frac{-1}{8abc}+\\
& \left(d_x^{10}\right)\frac{1}{2b^2c}+\left(d_x^{12}\right)\frac{1}{2b^2c}+\left(d_x^{14}\right)\frac{-1}{2b^2c}+\left(d_x^{16}\right)\frac{-1}{2b^2c}\Bigg]+
\end{aligned}
$$

$$
\begin{aligned}
\tilde{f}_{2131}\Bigg[& \left(d_x^1\right)\frac{-1}{8abc}+\left(d_z^1\right)\frac{-1}{4a^2b}+\left(d_x^2\right)\frac{1}{8abc}+\left(d_z^2\right)\frac{-1}{4a^2b}+\\
& \left(d_x^3\right)\frac{-1}{8abc}+\left(d_z^3\right)\frac{1}{4a^2b}+\left(d_x^4\right)\frac{1}{8abc}+\left(d_z^4\right)\frac{1}{4a^2b}+\\
& \left(d_x^5\right)\frac{1}{8abc}+\left(d_z^5\right)\frac{-1}{4a^2b}+\left(d_x^6\right)\frac{-1}{8abc}+\left(d_z^6\right)\frac{-1}{4a^2b}+\\
& \left(d_x^7\right)\frac{1}{8abc}+\left(d_z^7\right)\frac{1}{4a^2b}+\left(d_x^8\right)\frac{-1}{8abc}+\left(d_z^8\right)\frac{1}{4a^2b}+\\
& \left(d_z^9\right)\frac{1}{2a^2b}+\left(d_z^{11}\right)\frac{-1}{2a^2b}+\left(d_z^{13}\right)\frac{1}{2a^2b}+\left(d_z^{15}\right)\frac{-1}{2a^2b}\Bigg]+\\
\tilde{f}_{2132}\Bigg[& \left(d_x^1\right)\frac{-1}{4b^2c}+\left(d_z^1\right)\frac{-1}{4ab^2}+\left(d_x^2\right)\frac{-1}{4b^2c}+\left(d_z^2\right)\frac{1}{4ab^2}+\\
& \left(d_x^3\right)\frac{-1}{4b^2c}+\left(d_z^3\right)\frac{1}{4ab^2}+\left(d_x^4\right)\frac{-1}{4b^2c}+\left(d_z^4\right)\frac{-1}{4ab^2}+\\
& \left(d_x^5\right)\frac{1}{4b^2c}+\left(d_z^5\right)\frac{-1}{4ab^2}+\left(d_x^6\right)\frac{1}{4b^2c}+\left(d_z^6\right)\frac{1}{4ab^2}+\\
& \left(d_x^7\right)\frac{1}{4b^2c}+\left(d_z^7\right)\frac{1}{4ab^2}+\left(d_x^8\right)\frac{1}{4b^2c}+\left(d_z^8\right)\frac{-1}{4ab^2}+\\
& \left(d_x^{10}\right)\frac{1}{2b^2c}+\left(d_z^{10}\right)\frac{-1}{2ab^2}+\left(d_x^{12}\right)\frac{1}{2b^2c}+\left(d_z^{12}\right)\frac{1}{2ab^2}+\\
& \left(d_x^{14}\right)\frac{-1}{2b^2c}+\left(d_z^{14}\right)\frac{-1}{2ab^2}+\left(d_x^{16}\right)\frac{-1}{2b^2c}+\left(d_z^{16}\right)\frac{1}{2ab^2}\Bigg]+\\
\tilde{f}_{2133}\Bigg[& \left(d_x^1\right)\frac{-1}{4bc^2}+\left(d_z^1\right)\frac{-1}{8abc}+\left(d_x^2\right)\frac{-1}{4bc^2}+\left(d_z^2\right)\frac{1}{8abc}+\\
& \left(d_x^3\right)\frac{1}{4bc^2}+\left(d_z^3\right)\frac{-1}{8abc}+\left(d_x^4\right)\frac{1}{4bc^2}+\left(d_z^4\right)\frac{1}{8abc}+\\
& \left(d_x^5\right)\frac{-1}{4bc^2}+\left(d_z^5\right)\frac{1}{8abc}+\left(d_x^6\right)\frac{-1}{4bc^2}+\left(d_z^6\right)\frac{-1}{8abc}+\\
& \left(d_x^7\right)\frac{1}{4bc^2}+\left(d_z^7\right)\frac{1}{8abc}+\left(d_x^8\right)\frac{1}{4bc^2}+\left(d_z^8\right)\frac{-1}{8abc}+\\
& \left(d_x^{17}\right)\frac{1}{2bc^2}+\left(d_x^{18}\right)\frac{1}{2bc^2}+\left(d_x^{19}\right)\frac{-1}{2bc^2}+\left(d_x^{20}\right)\frac{-1}{2bc^2}\Bigg]+
\end{aligned}
$$

$$
\begin{aligned}
\tilde{f}_{2231}\Bigg[& \left(d_y^1\right)\frac{-1}{8abc}+\left(d_z^1\right)\frac{-1}{4ab^2}+\left(d_y^2\right)\frac{1}{8abc}+\left(d_z^2\right)\frac{1}{4ab^2}+\\
& \left(d_y^3\right)\frac{-1}{8abc}+\left(d_z^3\right)\frac{1}{4ab^2}+\left(d_y^4\right)\frac{1}{8abc}+\left(d_z^4\right)\frac{-1}{4ab^2}+\\
& \left(d_y^5\right)\frac{1}{8abc}+\left(d_z^5\right)\frac{-1}{4ab^2}+\left(d_y^6\right)\frac{-1}{8abc}+\left(d_z^6\right)\frac{1}{4ab^2}+\\
& \left(d_y^7\right)\frac{1}{8abc}+\left(d_z^7\right)\frac{1}{4ab^2}+\left(d_y^8\right)\frac{-1}{8abc}+\left(d_z^8\right)\frac{-1}{4ab^2}+\\
& \left(d_z^{10}\right)\frac{-1}{2ab^2}+\left(d_z^{12}\right)\frac{1}{2ab^2}+\left(d_z^{14}\right)\frac{-1}{2ab^2}+\left(d_z^{16}\right)\frac{1}{2ab^2}\Bigg]+\\
\tilde{f}_{2232}\Bigg[& \left(d_y^1\right)\frac{-1}{4b^2c}+\left(d_y^2\right)\frac{-1}{4b^2c}+\left(d_y^3\right)\frac{-1}{4b^2c}+\left(d_y^4\right)\frac{-1}{4b^2c}+\\
& \left(d_y^5\right)\frac{1}{4b^2c}+\left(d_y^6\right)\frac{1}{4b^2c}+\left(d_y^7\right)\frac{1}{4b^2c}+\left(d_y^8\right)\frac{1}{4b^2c}+\\
& \left(d_y^{10}\right)\frac{1}{2b^2c}+\left(d_y^{12}\right)\frac{1}{2b^2c}+\left(d_y^{14}\right)\frac{-1}{2b^2c}+\left(d_y^{16}\right)\frac{-1}{2b^2c}\Bigg]+\\
\tilde{f}_{2233}\Bigg[& \left(d_y^1\right)\frac{-1}{4bc^2}+\left(d_z^1\right)\frac{-1}{4b^2c}+\left(d_y^2\right)\frac{-1}{4bc^2}+\left(d_z^2\right)\frac{-1}{4b^2c}+\\
& \left(d_y^3\right)\frac{1}{4bc^2}+\left(d_z^3\right)\frac{-1}{4b^2c}+\left(d_y^4\right)\frac{1}{4bc^2}+\left(d_z^4\right)\frac{-1}{4b^2c}+\\
& \left(d_y^5\right)\frac{-1}{4bc^2}+\left(d_z^5\right)\frac{1}{4b^2c}+\left(d_y^6\right)\frac{-1}{4bc^2}+\left(d_z^6\right)\frac{1}{4b^2c}+\\
& \left(d_y^7\right)\frac{1}{4bc^2}+\left(d_z^7\right)\frac{1}{4b^2c}+\left(d_y^8\right)\frac{1}{4bc^2}+\left(d_z^8\right)\frac{1}{4b^2c}+\\
& \left(d_z^{10}\right)\frac{1}{2b^2c}+\left(d_z^{12}\right)\frac{1}{2b^2c}+\left(d_z^{14}\right)\frac{-1}{2b^2c}+\left(d_z^{16}\right)\frac{-1}{2b^2c}+\\
& \left(d_y^{17}\right)\frac{1}{2bc^2}+\left(d_y^{18}\right)\frac{1}{2bc^2}+\left(d_y^{19}\right)\frac{-1}{2bc^2}+\left(d_y^{20}\right)\frac{-1}{2bc^2}\Bigg]+\\
\tilde{f}_{3111}\Bigg[& \left(d_x^1\right)\frac{-1}{4a^2c}+\left(d_x^2\right)\frac{-1}{4a^2c}+\left(d_x^3\right)\frac{-1}{4a^2c}+\left(d_x^4\right)\frac{-1}{4a^2c}+\\
& \left(d_x^5\right)\frac{1}{4a^2c}+\left(d_x^6\right)\frac{1}{4a^2c}+\left(d_x^7\right)\frac{1}{4a^2c}+\left(d_x^8\right)\frac{1}{4a^2c}+\\
& \left(d_x^9\right)\frac{1}{2a^2c}+\left(d_x^{11}\right)\frac{1}{2a^2c}+\left(d_x^{13}\right)\frac{-1}{2a^2c}+\left(d_x^{15}\right)\frac{-1}{2a^2c}\Bigg]+
\end{aligned}
$$

$$
\begin{aligned}
\tilde{f}_{3112}\Bigg[& \left(d_x^1\right)\frac{-1}{8abc}+\left(d_x^2\right)\frac{1}{8abc}+\left(d_x^3\right)\frac{-1}{8abc}+\left(d_x^4\right)\frac{1}{8abc}+ \\
& \left(d_x^5\right)\frac{1}{8abc}+\left(d_x^6\right)\frac{-1}{8abc}+\left(d_x^7\right)\frac{1}{8abc}+\left(d_x^8\right)\frac{-1}{8abc}\Bigg]+ \\
\tilde{f}_{3113}\Bigg[& \left(d_x^1\right)\frac{-1}{4ac^2}+\left(d_x^2\right)\frac{1}{4ac^2}+\left(d_x^3\right)\frac{1}{4ac^2}+\left(d_x^4\right)\frac{-1}{4ac^2}+ \\
& \left(d_x^5\right)\frac{-1}{4ac^2}+\left(d_x^6\right)\frac{1}{4ac^2}+\left(d_x^7\right)\frac{1}{4ac^2}+\left(d_x^8\right)\frac{-1}{4ac^2}+ \\
& \left(d_x^{17}\right)\frac{1}{2ac^2}+\left(d_x^{18}\right)\frac{-1}{2ac^2}+\left(d_x^{19}\right)\frac{-1}{2ac^2}+\left(d_x^{20}\right)\frac{1}{2ac^2}\Bigg]+ \\
\tilde{f}_{3221}\Bigg[& \left(d_y^1\right)\frac{-1}{8abc}+\left(d_y^2\right)\frac{1}{8abc}+\left(d_y^3\right)\frac{-1}{8abc}+\left(d_y^4\right)\frac{1}{8abc}+ \\
& \left(d_y^5\right)\frac{1}{8abc}+\left(d_y^6\right)\frac{-1}{8abc}+\left(d_y^7\right)\frac{1}{8abc}+\left(d_y^8\right)\frac{-1}{8abc}\Bigg]+ \\
\tilde{f}_{3222}\Bigg[& \left(d_y^1\right)\frac{-1}{4b^2c}+\left(d_y^2\right)\frac{-1}{4b^2c}+\left(d_y^3\right)\frac{-1}{4b^2c}+\left(d_y^4\right)\frac{-1}{4b^2c}+ \\
& \left(d_y^5\right)\frac{1}{4b^2c}+\left(d_y^6\right)\frac{1}{4b^2c}+\left(d_y^7\right)\frac{1}{4b^2c}+\left(d_y^8\right)\frac{1}{4b^2c}+ \\
& \left(d_y^{10}\right)\frac{1}{2b^2c}+\left(d_y^{12}\right)\frac{1}{2b^2c}+\left(d_y^{14}\right)\frac{-1}{2b^2c}+\left(d_y^{16}\right)\frac{-1}{2b^2c}\Bigg]+ \\
\tilde{f}_{3223}\Bigg[& \left(d_y^1\right)\frac{-1}{4bc^2}+\left(d_y^2\right)\frac{-1}{4bc^2}+\left(d_y^3\right)\frac{1}{4bc^2}+\left(d_y^4\right)\frac{1}{4bc^2}+ \\
& \left(d_y^5\right)\frac{-1}{4bc^2}+\left(d_y^6\right)\frac{-1}{4bc^2}+\left(d_y^7\right)\frac{1}{4bc^2}+\left(d_y^8\right)\frac{1}{4bc^2}+ \\
& \left(d_y^{17}\right)\frac{1}{2bc^2}+\left(d_y^{18}\right)\frac{1}{2bc^2}+\left(d_y^{19}\right)\frac{-1}{2bc^2}+\left(d_y^{20}\right)\frac{-1}{2bc^2}\Bigg]+
\end{aligned}
$$

$$
\begin{aligned}
\tilde{f}_{3331}\Bigg[& \left(d_z^1\right)\frac{-1}{4ac^2}+\left(d_z^2\right)\frac{1}{4ac^2}+\left(d_z^3\right)\frac{1}{4ac^2}+\left(d_z^4\right)\frac{-1}{4ac^2}+\\
& \left(d_z^5\right)\frac{-1}{4ac^2}+\left(d_z^6\right)\frac{1}{4ac^2}+\left(d_z^7\right)\frac{1}{4ac^2}+\left(d_z^8\right)\frac{-1}{4ac^2}+\\
& \left(d_z^{17}\right)\frac{1}{2ac^2}+\left(d_z^{18}\right)\frac{-1}{2ac^2}+\left(d_z^{19}\right)\frac{-1}{2ac^2}+\left(d_z^{20}\right)\frac{1}{2ac^2}\Bigg]+\\
\tilde{f}_{3332}\Bigg[& \left(d_z^1\right)\frac{-1}{4bc^2}+\left(d_z^2\right)\frac{-1}{4bc^2}+\left(d_z^3\right)\frac{1}{4bc^2}+\left(d_z^4\right)\frac{1}{4bc^2}+\\
& \left(d_z^5\right)\frac{-1}{4bc^2}+\left(d_z^6\right)\frac{-1}{4bc^2}+\left(d_z^7\right)\frac{1}{4bc^2}+\left(d_z^8\right)\frac{1}{4bc^2}+\\
& \left(d_z^{17}\right)\frac{1}{2bc^2}+\left(d_z^{18}\right)\frac{1}{2bc^2}+\left(d_z^{19}\right)\frac{-1}{2bc^2}+\left(d_z^{20}\right)\frac{-1}{2bc^2}\Bigg]+\\
\tilde{f}_{3121}\Bigg[& \left(d_x^1\right)\frac{-1}{8abc}+\left(d_y^1\right)\frac{-1}{4a^2c}+\left(d_x^2\right)\frac{1}{8abc}+\left(d_y^2\right)\frac{-1}{4a^2c}+\\
& \left(d_x^3\right)\frac{-1}{8abc}+\left(d_y^3\right)\frac{-1}{4a^2c}+\left(d_x^4\right)\frac{1}{8abc}+\left(d_y^4\right)\frac{-1}{4a^2c}+\\
& \left(d_x^5\right)\frac{1}{8abc}+\left(d_y^5\right)\frac{1}{4a^2c}+\left(d_x^6\right)\frac{-1}{8abc}+\left(d_y^6\right)\frac{1}{4a^2c}+\\
& \left(d_x^7\right)\frac{1}{8abc}+\left(d_y^7\right)\frac{1}{4a^2c}+\left(d_x^8\right)\frac{-1}{8abc}+\left(d_y^8\right)\frac{1}{4a^2c}+\\
& \left(d_y^9\right)\frac{1}{2a^2c}+\left(d_y^{11}\right)\frac{1}{2a^2c}+\left(d_y^{13}\right)\frac{-1}{2a^2c}+\left(d_y^{15}\right)\frac{-1}{2a^2c}\Bigg]+\\
\tilde{f}_{3122}\Bigg[& \left(d_x^1\right)\frac{-1}{4b^2c}+\left(d_y^1\right)\frac{-1}{8abc}+\left(d_x^2\right)\frac{-1}{4b^2c}+\left(d_y^2\right)\frac{1}{8abc}+\\
& \left(d_x^3\right)\frac{-1}{4b^2c}+\left(d_y^3\right)\frac{-1}{8abc}+\left(d_x^4\right)\frac{-1}{4b^2c}+\left(d_y^4\right)\frac{1}{8abc}+\\
& \left(d_x^5\right)\frac{1}{4b^2c}+\left(d_y^5\right)\frac{1}{8abc}+\left(d_x^6\right)\frac{1}{4b^2c}+\left(d_y^6\right)\frac{-1}{8abc}+\\
& \left(d_x^7\right)\frac{1}{4b^2c}+\left(d_y^7\right)\frac{1}{8abc}+\left(d_x^8\right)\frac{1}{4b^2c}+\left(d_y^8\right)\frac{-1}{8abc}+\\
& \left(d_x^{10}\right)\frac{1}{2b^2c}+\left(d_x^{12}\right)\frac{1}{2b^2c}+\left(d_x^{14}\right)\frac{-1}{2b^2c}+\left(d_x^{16}\right)\frac{-1}{2b^2c}\Bigg]+
\end{aligned}
$$

$$
\begin{aligned}
\tilde{f}_{3123}\Bigg[& \left(d_x^1\right)\frac{-1}{4bc^2}+\left(d_y^1\right)\frac{-1}{4ac^2}+\left(d_x^2\right)\frac{-1}{4bc^2}+\left(d_y^2\right)\frac{1}{4ac^2}+\\
& \left(d_x^3\right)\frac{1}{4bc^2}+\left(d_y^3\right)\frac{1}{4ac^2}+\left(d_x^4\right)\frac{1}{4bc^2}+\left(d_y^4\right)\frac{-1}{4ac^2}+\\
& \left(d_x^5\right)\frac{-1}{4bc^2}+\left(d_y^5\right)\frac{-1}{4ac^2}+\left(d_x^6\right)\frac{-1}{4bc^2}+\left(d_y^6\right)\frac{1}{4ac^2}+\\
& \left(d_x^7\right)\frac{1}{4bc^2}+\left(d_y^7\right)\frac{1}{4ac^2}+\left(d_x^8\right)\frac{1}{4bc^2}+\left(d_y^8\right)\frac{-1}{4ac^2}+\\
& \left(d_x^{17}\right)\frac{1}{2bc^2}+\left(d_y^{17}\right)\frac{1}{2ac^2}+\left(d_x^{18}\right)\frac{1}{2bc^2}+\left(d_y^{18}\right)\frac{-1}{2ac^2}+\\
& \left(d_x^{19}\right)\frac{-1}{2bc^2}+\left(d_y^{19}\right)\frac{-1}{2ac^2}+\left(d_x^{20}\right)\frac{-1}{2bc^2}+\left(d_y^{20}\right)\frac{1}{2ac^2}\Bigg]+\\
\tilde{f}_{3131}\Bigg[& \left(d_x^1\right)\frac{-1}{4ac^2}+\left(d_z^1\right)\frac{-1}{4a^2c}+\left(d_x^2\right)\frac{1}{4ac^2}+\left(d_z^2\right)\frac{-1}{4a^2c}+\\
& \left(d_x^3\right)\frac{1}{4ac^2}+\left(d_z^3\right)\frac{-1}{4a^2c}+\left(d_x^4\right)\frac{-1}{4ac^2}+\left(d_z^4\right)\frac{-1}{4a^2c}+\\
& \left(d_x^5\right)\frac{-1}{4ac^2}+\left(d_z^5\right)\frac{1}{4a^2c}+\left(d_x^6\right)\frac{1}{4ac^2}+\left(d_z^6\right)\frac{1}{4a^2c}+\\
& \left(d_x^7\right)\frac{1}{4ac^2}+\left(d_z^7\right)\frac{1}{4a^2c}+\left(d_x^8\right)\frac{-1}{4ac^2}+\left(d_z^8\right)\frac{1}{4a^2c}+\\
& \left(d_z^9\right)\frac{1}{2a^2c}+\left(d_z^{11}\right)\frac{1}{2a^2c}+\left(d_z^{13}\right)\frac{-1}{2a^2c}+\left(d_z^{15}\right)\frac{-1}{2a^2c}+\\
& \left(d_x^{17}\right)\frac{1}{2ac^2}+\left(d_x^{18}\right)\frac{-1}{2ac^2}+\left(d_x^{19}\right)\frac{-1}{2ac^2}+\left(d_x^{20}\right)\frac{1}{2ac^2}\Bigg]+\\
\tilde{f}_{3132}\Bigg[& \left(d_x^1\right)\frac{-1}{4bc^2}+\left(d_z^1\right)\frac{-1}{8abc}+\left(d_x^2\right)\frac{-1}{4bc^2}+\left(d_z^2\right)\frac{1}{8abc}+\\
& \left(d_x^3\right)\frac{1}{4bc^2}+\left(d_z^3\right)\frac{-1}{8abc}+\left(d_x^4\right)\frac{1}{4bc^2}+\left(d_z^4\right)\frac{1}{8abc}+\\
& \left(d_x^5\right)\frac{-1}{4bc^2}+\left(d_z^5\right)\frac{1}{8abc}+\left(d_x^6\right)\frac{-1}{4bc^2}+\left(d_z^6\right)\frac{-1}{8abc}+\\
& \left(d_x^7\right)\frac{1}{4bc^2}+\left(d_z^7\right)\frac{1}{8abc}+\left(d_x^8\right)\frac{1}{4bc^2}+\left(d_z^8\right)\frac{-1}{8abc}+\\
& \left(d_x^{17}\right)\frac{1}{2bc^2}+\left(d_x^{18}\right)\frac{1}{2bc^2}+\left(d_x^{19}\right)\frac{-1}{2bc^2}+\left(d_x^{20}\right)\frac{-1}{2bc^2}\Bigg]+
\end{aligned}
$$

$$
\begin{aligned}
\tilde{f}_{3133}\Bigg[& \left(d_z^1\right)\frac{-1}{4ac^2}+\left(d_z^2\right)\frac{1}{4ac^2}+\left(d_z^3\right)\frac{1}{4ac^2}+\left(d_z^4\right)\frac{-1}{4ac^2}+\\
& \left(d_z^5\right)\frac{-1}{4ac^2}+\left(d_z^6\right)\frac{1}{4ac^2}+\left(d_z^7\right)\frac{1}{4ac^22}+\left(d_z^8\right)\frac{-1}{4ac^2}+\\
& \left(d_z^{17}\right)\frac{1}{1ac^2}+\left(d_z^{18}\right)\frac{-1}{2ac^2}+\left(d_z^{19}\right)\frac{-1}{2ac^2}+\left(d_z^{20}\right)\frac{1}{2ac^2}\Bigg]+\\
\tilde{f}_{3231}\Bigg[& \left(d_y^1\right)\frac{-1}{4ac^2}+\left(d_z^1\right)\frac{-1}{8abc}+\left(d_y^2\right)\frac{1}{4ac^2}+\left(d_z^2\right)\frac{1}{8abc}+\\
& \left(d_y^3\right)\frac{1}{4ac^2}+\left(d_z^3\right)\frac{-1}{8abc}+\left(d_y^4\right)\frac{-1}{4ac^2}+\left(d_z^4\right)\frac{1}{8abc}+\\
& \left(d_y^5\right)\frac{-1}{4ac^2}+\left(d_z^5\right)\frac{1}{8abc}+\left(d_y^6\right)\frac{1}{4ac^2}+\left(d_z^6\right)\frac{-1}{8abc}+\\
& \left(d_y^7\right)\frac{1}{4ac^2}+\left(d_z^7\right)\frac{1}{8abc}+\left(d_y^8\right)\frac{-1}{4ac^2}+\left(d_z^8\right)\frac{-1}{8abc}+\\
& \left(d_y^{17}\right)\frac{1}{2ac^2}+\left(d_y^{18}\right)\frac{-1}{2ac^2}+\left(d_y^{19}\right)\frac{-1}{2ac^2}+\left(d_y^{20}\right)\frac{1}{2ac^2}\Bigg]+\\
\tilde{f}_{3232}\Bigg[& \left(d_y^1\right)\frac{-1}{4bc^2}+\left(d_z^1\right)\frac{-1}{4b^2c}+\left(d_y^2\right)\frac{-1}{4bc^2}+\left(d_z^2\right)\frac{-1}{4b^2c}+\\
& \left(d_y^3\right)\frac{1}{4bc^2}+\left(d_z^3\right)\frac{-1}{4b^2c}+\left(d_y^4\right)\frac{1}{4bc^2}+\left(d_z^4\right)\frac{-1}{4b^2c}+\\
& \left(d_y^5\right)\frac{-1}{4bc^2}+\left(d_z^5\right)\frac{1}{4b^2c}+\left(d_y^6\right)\frac{-1}{4bc^2}+\left(d_z^6\right)\frac{1}{4b^2c}+\\
& \left(d_y^7\right)\frac{1}{4bc^2}+\left(d_z^7\right)\frac{1}{4b^2c}+\left(d_y^8\right)\frac{1}{4bc^2}+\left(d_z^8\right)\frac{1}{4b^2c}+\\
& \left(d_z^{10}\right)\frac{1}{2b^2c}+\left(d_z^{12}\right)\frac{1}{2b^2c}+\left(d_z^{14}\right)\frac{-1}{2b^2c}+\left(d_z^{16}\right)\frac{-1}{2b^2c}+\\
& \left(d_y^{17}\right)\frac{1}{2bc^2}+\left(d_y^{18}\right)\frac{1}{2bc^2}+\left(d_y^{19}\right)\frac{-1}{2bc^2}+\left(d_y^{20}\right)\frac{-1}{2bc^2}\Bigg]+\\
\tilde{f}_{3233}\Bigg[& \left(d_z^1\right)\frac{-1}{4bc^2}+\left(d_z^2\right)\frac{-1}{4bc^2}+\left(d_z^3\right)\frac{1}{4bc^2}+\left(d_z^4\right)\frac{1}{4bc^2}+\\
& \left(d_z^5\right)\frac{-1}{4bc^2}+\left(d_z^6\right)\frac{-1}{4bc^2}+\left(d_z^7\right)\frac{1}{4bc^2}+\left(d_z^8\right)\frac{1}{4bc^2}+\\
& \left(d_z^{17}\right)\frac{1}{2bc^2}+\left(d_z^{18}\right)\frac{1}{2bc^2}+\left(d_z^{19}\right)\frac{-1}{2bc^2}+\left(d_z^{20}\right)\frac{-1}{2bc^2}\Bigg]
\end{aligned}
\tag{B.8}
$$

References

O. S. Adrianov, N. I. Vykhodtseva, V. F. Fokin, N. A. Uranova, and V. M. Avirom. Reversible functional shutdown of the optic tract on exposure to focused ultrasound. *Bulletin of Experimental Biology and Medicine*, 97(6):760–762, 1984.

B. Agnes and E. Nandor. *Flexoelectricity In Liquid Crystals: Theory, Experiments And Applications*. Imperial College Press, 2013.

F. Ahmadpoor and P. Sharma. Flexoelectricity in two-dimensional crystalline and biological membranes. *Nanoscale*, 7(40):16555–16570, 2015. doi: https://doi.org/10.1039/C5NR04722F.

F. Ahmadpoor, Q. Deng, L. P. Liu, and P. Sharma. Apparent flexoelectricity in lipid bilayer membranes due to external charge and dipolar distributions. *Physical Review E*, 88(5):1–5, 2013. doi: https://doi.org/10.1103/PhysRevE.88.050701.

L. Ai, J. K. Mueller, A. Grant, Y. Eryaman, and W. Legon. Transcranial focused ultrasound for bold fmri signal modulation in humans. *Annual International Conference of the IEEE Engineering in Medicine and Biology Society*, 2016. doi: https://doi.org/10.1109/EMBC.2016.7591057.

R. D. Airan and K. Butts Pauly. Hearing out ultrasound neuromodulation. *Neuron*, 98(5):875–877, 2018. doi: https://doi.org/10.1016/j.neuron.2018.05.031.

R. D. Airan, R. A. Meyer, N. P. K. Ellens, K. R. Rhodes, K. Farahani, M. G. Pomper, S. D. Kadam, and J. J. Green. Noninvasive targeted transcranial neuromodulation via focused ultrasound gated drug release from nanoemulsions.

Nano Letters, 17(2):652–659, 2017. doi: https://doi.org/10.1021/acs.nanolett.6b03517.

R. R. Aliev and A. V. Panfilov. A simple two-variable model of cardiac excitation. *Chaos, Solitons and Fractals*, 7(3):293–301, 1996. doi: https://doi.org/10.1016/0960-0779(95)00089-5.

A. Alonso, E. Reinz, B. Leuchs, J. Kleinschmidt, M. Fatar, B. Fatar, B. Geers, I. Lentacker, M. G. Hennerici, S. C. de Smedt, and S. Meairs. Focal delivery of aav2/1-transgenes into the rat brain by localized ultrasound-induced bbb opening. *Molecular Therapy Nucleic Acids*, 2(e73):1–7, 2013. doi: https://doi.org/10.1038/mtna.2012.64.

C. Amiez, J. P. Joseph, and E. Procyk. Reward encoding in the monkey anterior cingulate cortex. *Cerebral Cortex*, 16(7):1040–1055, 2006. doi: https://doi.org/10.1093/cercor/bhj046.

S. S. Anderson, A. D. Jackson, and T. Heimburg. Towards a thermodynamic theory of nerve pulse propagation. *Progress in Neurobiology*, 88(2):104–113, 2009. doi: 10.1016/j.pneurobio.2009.03.002.

R. Appali, U. van Rienen, and T. R. Heimburg. A comparison of the hodgkin-huxley model and the soliton theory for the action potential in nerves. *Advances in Planar Lipid Bilayers and Liposomes*, 16:275–299, 2012. doi: https://doi.org/10.1016/B978-0-12-396534-9.00009-X.

L. V. Azaroff and J. J. Brophy. *Electronic Processes in Materials*. McGraw-Hill Book Company, 1963.

H. Baek, K. J. Pahk, and H. Kim. A review of low-intensity focused ultrasound for neuromodulation. *Biomedical Engineering Letters*, 7:135–142, 2017. doi: 10.1007/s13534-016-0007-y.

M. Barbarisi, E. Pantelis, C. Antypas, and P. Romanelli. Radiosurgery for movement disorders. *Computer Aided Surgery*, 16(3):101–111, 2011. doi: https://doi.org/10.3109/10929088.2011.569127.

J. W. Barnard, W. J. Fry, F. J. Fry, and R. F. Krumins. Effects of high intensity ultrasound on the central nervous system of the cat. *Journal of Comparative Neurology*, 103(3), 1955. doi: https://doi.org/10.1002/cne.901030304.

E. Berberoglu, H. O. Solmaz, and S. G oktepe. Computational modeling of coupled cardiac electromechanics incorporating cardiac dysfunctions. *European Journal of Mechanics A/Solids*, 48:60–73, 2014. doi: https://doi.org/10.1016/j.euromechsol.2014.02.021.

J.-P. Berenger. Three-dimensional perfectly matched layer for the absorption of electromagnetic waves. *Journal of Computational Physics*, 127(2):363–379, 1996. doi: https://doi.org/10.1006/jcph.1996.0181.

A. Beyder, J. L. Rae, C. Bernard, P. R. Strege, F. Sachs, and G. Farrugia. Mechanosensitivity of nav1.5, a voltage-sensitive sodium channel. *The Journal of Physiology*, 588(24):4969–4985, 2010. doi: 10.1113/jphysiol.2010.199034.

Y. Bing, D. Garcia-Gonzalez, and A. Jérusalem. Medical imaging based in silico head model for ischaemic stroke simulation. *Journal of the Mechanical Behavior of Biomedical Materials*, 101:103442, 2020. doi: https://doi.org/10.1016/j.jmbbm.2019.103442.

R. J. Biondi, M. J. Levy, and P. A. Weiss. An engineering study of the peristaltic drive of axonal flow. *PNAS*, 69(7):1732–1736, 1972. doi: https://doi.org/10.1073/pnas.69.7.1732.

G. H. Bishop. Natural history of the nerve impulse. *Physiological Reviews*, 36 (3):376–399, 1956. doi: 10.1152/physrev.1956.36.3.376.

J. Blackmore, S. Shrivastava, J. Sallet, C. R. Butler, and R. O. Cleveland. Ultrasound neuromodulation: A review of results, mechanisms and safety. *Ultrasound in Medicine and Biology*, 45(7):1509–1536, 2019. doi: 10.1016/j.ultrasmedbio.2018.12.015.

P. S. Boggio, R. Ferrucci, S. P. Rigonatti, P. Covre, M. Nitsche, A. Pascual-Leone, and F. Fregni. Effects of transcranial direct current stimulation on working memory in patients with parkinson's disease. *Journal of Neurological Sciences*, 249(1):31–38, 2006. doi: 10.1016/j.jns.2006.05.062.

J. Boonzaier, G. A. F. van Tilborg, M. Straathof, P. I. Petrov, C. L. Heijningen, G. van Vliet, N. Smirnov, A. van der Toorn, S. F. Neggers, and R. M. Dijkhuizen. Differential outcomes of rtms and anesthesia effects on functional connectivity in the rat brain. *Brain Stimulation*, 10(2):418, 2017. doi: https://doi.org/10.1016/j.brs.2017.01.241.

M. J. Borrelli, K. I. Bailey, and F. Dunn. Early ultrasonic effects upon mammalian cns structures (chemical synapses). *The Journal of the Acoustical Society of America*, 69(5):1514–1416, 1981. doi: 10.1121/1.385791.

K. D. Breneman, W. E. Brownell, and R. D. Rabbitt. Hair cell bundles: flexoelectric motors of the inner ear. *PLoS One*, 4(4):1–9, 2009. doi: https://doi.org/10.1371/journal.pone.0005201.

W. E. Brownell, A. A. Spector, R. M. Raphael, and A. S. Popel. Micro- and nanomechanics of the cochlear outer hair cell. *Annual Review of Biomedical Engineering*, 3:169–194, 2001. doi: https://doi.org/10.1146/annurev.bioeng.3.1.169.

W. E. Brownell, F. Qian, and B. Anvari. Cell membrane tethers generate me-

chanical force in response to electrical stimulation. *Biophysical Journal*, 99(3): 845–852, 2010. doi: https://doi.org/10.1016/j.bpj.2010.05.025.

D. S. Bruhn, M. A. Lomholt, and H. Khandelia. Quantifying the relationship between curvature and electric potential in lipid bilayers. *The Journal of Physical Chemistry B*, 120(21):4812–4817, 2016. doi: 10.1021/acs.jpcb.6b03439.

A. Bystritsky and A. S. Korb. A review of low-intensity transcranial focused ultrasound for clinical applications. *Current Behavioral Neuroscience Reports*, 2:60–66, 2015. doi: 10.1007/s40473-015-0039-0.

A. Bystritsky, A. S. Korb, P. K. Douglas, M. S. Cohen, W. P. Melega, A. P. Mulgaonkar, A. DeSalles, B. K. Min, and S. S. Yoo. A review of low-intensity focused ultrasound pulsation. *Brain Stimulation*, 4(3):125–136, 2011. doi: https://doi.org/10.1016/j.brs.2011.03.007.

R. A. Casarotto, J. C. Adamowski, F. Fallopa, and F. Bacanelli. Coupling agents in therapeutic ultrasound: acoustic and thermal behavior. *Physical Medicine and Rehabilitation*, 85(1):162–165, 2004. doi: https://doi.org/10.1016/S0003-9993(03)00293-4.

W. A. Catterall, I. A. Raman, H. P. C. Robinson, T. J. Sejnowski, and O. Paulson. The hodgkin-huxley heritage: From channels to circuits. *Journal of Neuroscience*, 32(41):14064–14073, 2012. doi: https://doi.org/10.1523/JNEUROSCI.3403-12.2012.

R. Chakrabarti, M. Ghazanwy, and A. Tewari. Anesthetic challenges for deep brain stimulation: a systematic approach. *North American Journal of Medical Sciences*, 6(8):359–369, 2014. doi: 10.4103/1947-2714.139281.

W. S. Chang, H. H. Jung, E. Zadicario, I. Rachmilevitch, T. Tlusty, and S. Vitek. Factors associated with successful magnetic resonance-guided focused ultra-

sound treatment: efficiency of acoustic energy delivery through the skull. *Journal of Neurosurgery*, 124(2):411–416, 2016. doi: https://doi.org/10.3171/2015.3.jns142592.

R. A. Chapman. Dependence on temperature of the conduction velocity of the action potential of the squid giant axon. *Nature*, 213:1143–1144, 1967. doi: https://doi.org/10.1038/2131143a0.

S. Chatelin, C. Deck, and R. Willinger. An anisotropic viscous hyperelastic constitutive law for brain material finite-element modelling. *Biorheology*, 27:26–37, 2012. doi: https://doi.org/10.1007/s12573-012-0055-6.

H. Chen, D. Garcia-Gonzalez, and A. Jérusalem. Computational model of the mechanoelectrophysiological coupling in axons with application to neuromodulation. *Physical Review E*, 99(3):1–18, 2019. doi: 10.1103/PhysRevE.99.032406.

J. J. Choi, M. Pernot, S. A. Small, and E. E. Konofagou. Noninvasive, transcranial and localized opening of the blood-brain barrier using focused ultrasound in mice. *Ultrasound in Medicine and Biology*, 33(1):95–104, 2007. doi: https://doi.org/10.1016/j.ultrasmedbio.2006.07.018.

P. C. Chu, H. L. Liu, H. Y. Lai, C. Y. Lin, H. C. Tsai, and Y. C. Pei. Neuromodulation accompanying focused ultrasound-induced blood-brain barrier opening. *Scientific Reports*, 5(15477):1–12, 2015. doi: 10.1038/srep15477.

I. Cinelli, M. Destrade, M. Duffy, and P. McHugh. Electro-mechanical response of a 3d nerve bundle model to mechanical loads leading to axonal injury. *Conference proceedings - IEEE engineering in medicine and biology society*, 34(3):978–981, 2018. doi: 10.1109/EMBC.2017.8036989.

G. T. Clement. Perspectives in clinical uses of high-intensity focused ultrasound. *Ultrasonics*, 42(10):1087–1093, 2004. doi: 10.1016/j.ultras.2004.04.003.

G. T. Clement and K. Hynynen. A non-invasive method for focusing ultrasound through the human skull. *Physics in Medicine and Biology*, 47(8), 2002. doi: https://iopscience.iop.org/article/10.1088/0031-9155/47/8/301/pdf.

K. S. Cole. Rectification and inductance in the squid giant axon. *Journal of General Physiology*, 25(1):29–51, 1941. doi: 10.1085/jgp.25.1.29.

V. Colucci, G. Strichartz, F. Jolesz, N. Vykhodtseva, and K. Hynynen. Focused ultrasound effects on nerve action potential in vitro. *Ultrasound in Medicine and Biology*, 35(10):1737–1747, 2009. doi: 10.1016/j.ultrasmedbio.2009.05.002.

C. Constans, T. Deffieux, P. Pouget, M. Tanter, and A. F. Aubry. 200-1380 khz quadrifrequency focused ultrasound transducer for neurostimulation in rodents and primates: Transcranial in vitro calibration and numerical study of the influence of skull cavity. *IEEE Transactions on Ultrasonics, Ferroelectrics, and Frequency Control*, 64(4):717–724, 2017. doi: 10.1109/TUFFC.2017.2739840.

C. Constans, H. Ahnine, M. Santin, S. Lehericy, M. Tanter, P. Puoget, and A. F. Aubry. Non-invasive ultrasonic modulation of visual evoked response by gaba delivery through the blood brain barrier. *Journal of Controlled Release*, 318:223–231, 2020. doi: 10.1016/j.jconrel.2019.12.006.

B. T. Cox, S. Kara, S. R. Arridge, and P. C. Beard. k-space propagation models for acoustically heterogeneous media: Application to biomedical photoacoustics. *The Journal of the Acoustical Society of America*, 121(3453):3453–3464, 2007. doi: https://doi.org/10.1121/1.2717409.

M. O. Culjat, D. Goldenberg, P. Tewari, and R. S. Singh. A review of tissue

substitutes for ultrasound imaging. *Ultrasound in Medicine and Biology*, 36 (6):861–873, 2010. doi: 10.1016/j.ultrasmedbio.2010.02.012.

D. Dalecki. Mechanical bioeffects of ultrasound. *Annual Review of Biomedical Engineering*, 6:229–248, 2004. doi: https://doi.org/10.1146/annurev.bioeng.6.040803.140126.

R. F. Dallapiazza, K. F. Timbie, S. Holmberg, J. Gatesman, M. Beatriz Lopes, R. J. Price, G. Wilson Miller, and W. J. Elias. Noninvasive neuromodulation and thalamic mapping with low-intensity focused ultrasound. *Journal of Neurosurgery*, 128:875–884, 2018. doi: https://doi.org/10.3171/2016.11.JNS16976.

D. P. Darrow. Focused ultrasound for neuromodulation. *Neurotherapeutics*, 16: 88–99, 2019. doi: https://doi.org/10.1007/s13311-018-00691-3.

D. P. Darrow, P. O'Brien, T. J. Richner, T. I. Netoff, and E. S. Ebbini. Reversible neuroinhibition by focused ultrasound is mediated by a thermal mechanism. *Brain Stimulation*, 12:1439–1447, 2019. doi: https://doi.org/10.1016/j.brs.2019.07.015.

Dassault. Abaqus/cae 6.14-5, 2017.

E. Dayan, N. Censor, E. R. Buch, M. Sandrini, and L. G. Cohen. Noninvasive brain stimulation: from physiology to network dynamics and back. *Nature Neuroscience*, 16(7):838–844, 2013. doi: 10.1038/nn.3422.

T. Deffieux, Y. Younan, M. Tanter, J. F. Aubry, N. Wattiez, and P. Pouget. Transcranial ultrasound neuromodulation of the contralateral visual field in awake monkey. *Institute of Electrical and Electronics Engineers*, 2013 IEEE International Ultrasonics Symposium (IUS), 2013a. doi: 10.1109/ULTSYM.2013.0001.

T. Deffieux, Y. Younan, N. Wattiez, M. Tanter, P. Pouget, and J. F. Aubry. Low-

intensity focused ultrasound modulates monkey visuomotor behavior. *Current Biology*, 23(23):2430–2433, 2013b. doi: https://doi.org/10.1016/j.cub.2013.10.029.

M. Dehghan and F. Fakhar-Izadi. Pseudospectral methods for nagumo equation. *International Journal for Numerical Methods in Biomedical Engineering*, 27 (4):553–561, 2011. doi: https://doi.org/10.1002/cnm.1319.

L. Demi, B. E. Treeby, and M. D. Verweij. Comparison between two different full-wave methods for the computation of nonlinear ultrasound fields in inhomogeneous and attenuating tissue. *Proceedings of the 2014 IEEE International Ultrasonics Symposium*, pages 1464–1467, 2014. doi: 10.1109/ULTSYM.2014.0362.

Q. Deng, L. Liu, and P. Sharma. Flexoelectricity in soft materials and biological membranes. *Journal of the Mechanics and Physics of Solids*, 62:209–227, 2014. doi: http://dx.doi.org/10.1016/j.jmps.2013.09.021.

L. di Biase, E. Falato, and V. Di Lazzaro. Transcranial focused ultrasound (tfus) and transcranial unfocused ultrasound (tus) neuromodulation: From theoretical principles to stimulation practices. *frontiers in Neurology*, 10:1–12, 2019. doi: 10.3389/fneur.2019.00549.

M. Di Luca, D. Nutt, W. Oertel, P. Boyer, J. Jaarsma, F. Destrebecq, G. Esposito, and V. Quoidbach. Towards earlier diagnosis and treatment of disorders of the brain. *Bull World Health Organ*, 96:298–298A, 2018. doi: http://dx.doi.org/10.2471/BLT.17.206599.

P. P. Dobrakowski, A. K. Machowska-Majchrzak, B. Labuz-Roszak, K. G. Majchrzak, E. Kluczewska, and K. B. Pierzchala. Mr-guided focused ultrasound: a new generation treatment of parkinson's disease, essential tremor and neu-

ropathic pain. *Interventional Neuroradiology*, 20(3):275–282, 2014. doi: https://doi.org/10.15274/INR-2014-10033.

M. E. Downs, T. Teichert, A. Buch, M. E. Karakatsani, C. Sierra, and S. Chen. Toward a cognitive neural prosthesis using focused ultrasound. *frontiers in Neuroscience*, 2017. doi: https://doi.org/10.3389/fnins.2017.00607.

C. S. Drapaca. An electromechanical model of neuronal dynamics using hamilton's principle. *Frontiers in Cellular Neuroscience*, 9(271):1–8, 2015. doi: https://doi.org/10.3389/fncel.2015.00271.

B. Drukarch, H. A. Holland, M. Velichkov, J. J. G. Geurts, P. Voorn, G. Glas, and H. W. de Regt. Thinking about the nerve impulse: A critical analysis of the electricity-centered conception of nerve excitability. *Progress in Neurobiology*, 169:172–185, 2018. doi: https://doi.org/10.1016/j.pneurobio.2018.06.009.

H. Duffau. Stimulation mapping of white matter tracts to study brain functional connectivity. *Nature Reviews Neurology*, 11:255–265, 2015. doi: https://doi.org/10.1038/nrneurol.2015.51.

M. Eames, A. Hananel, J. W. Snell, N. F. Kasell, and J. F. Aubry. Trans-cranial focused ultrasound without hair shaving: Feasibility study in an ex-vivo cadaver model. *Journal of Therapeutic Ultrasound*, 1(24):1–6, 2014. doi: 10.1186/2050-5736-1-24.

K. Easson, C. V. Rohlicek, J. C. Houde, G. Gilbert, C. Saint-Martin, K. Fontes, A. Majnemer, A. Marelli, P. Wintermark, M. Descoteaux, and M. Brossard-Racine. Quantification of apparent axon density and orientation dispersion in the white matter of youth born with congenital heart disease. *NeuroImage*, 205, 2020. doi: https://doi.org/10.1016/j.neuroimage.2019.116255.

L. J. Edwards, K. J. Pine, I. Ellerbrock, N. Weiskopf, and S. Mohammadi. Noddi-

dti: Estimating neurite orientation and dispersion parameters from a diffusion tensor in healthy white matter. *frontiers in Neuroscience*, 11(720):1–15, 2017. doi: https://doi.org/10.3389/fnins.2017.00720.

A. El Hady and B. B. Machta. Mechanical surface waves accompany action potential propagation. *Nature Communications*, 6(6697):1–7, 2015. doi: 10.1038/ncomms7697.

W. J. Elias, D. Huss, T. Voss, J. Loomba, M. Khaled, E. Zadicario, R. C. Frysinger, S. A. Sperling, S. Wylie, S. J. Monteith, J. Druzgal, B. B. Shah, M. Harrison, and M. Wintermark. A pilot study of focused ultrasound thalamotomy for essential tremor. *The New England Journal of Medicine*, 369:640–648, 2013. doi: 10.1056/NEJMoa1300962.

E. A. Eliseev and A. N. Morozovska. Hidden symmetry of flexoelectric coupling. *Physical Review B*, 98:12, 2018. doi: 10.1103/PhysRevB.98.094108.

H. Ellis. Anatomy of head injury. *Surgery (Oxford)*, 25(12):505–507, 2007. doi: https://doi.org/10.1016/j.mpsur.2007.10.008.

J. Engelbrecht, T. Peets, K. Tamm, M. Laasmaa, and M. Vendelin. On modelling of physical effects accompanying the propagation of action potentials in nerve fibres. *Biological Physics*, pages 1–10, 2016. doi: https://arxiv.org/abs/1601.01867.

J. Engelbrecht, T. Peets, and K. Tamm. Electromechanical coupling of waves in nerve fibres. *Biological Physics*, pages 1–18, 2018a. doi: 10.1007/s10237-018-1055-2.

J. Engelbrecht, T. Peets, K. Tamm, M. Laasmaa, and M. Vendelin. On the complexity of signal propagation in nerve fibres. *The Proceedings of the Estonian*

Academy of Sciences, 67(1):28–38, 2018b. doi: https://doi.org/10.3176/proc.2017.4.28.

J. Eyckmans, T. Boudou, X. Yu, and C. S. Chen. A hitchhiker's guide to mechanobiology. *Developmental Cell*, 21(1):35–47, 2011. doi: 10.1016/j.devcel.2011.06.015.

A. I. Farrer, H. Odéen, J. de Bever, B. Coats, D. L. Parker, and A. Payne. Characterization and evaluation of tissue-mimicking gelatin phantoms for use with mrgfus. *Journal of Therapeutic Ultrasound*, 3(9), 2015. doi: 10.1186/s40349-015-0030-y.

A. Fatemi-Ardekani. Transcranial magnetic stimulation: physics, electrophysiology, and applications. *Critical Reviews in Biomedical Engineering*, 36(5-6):375–412, 2008. doi: 10.1615/critrevbiomedeng.v36.i5-6.30.

Y. Feng, R. J. Okamoto, R. Namani, G. M. Genin, and P. V. Bayly. Measurements of mechanical anisotropy in brain tissue and implications for transversely isotropic material models of white matter. *Journal of the Mecahnical Behavior of Biomedical Materials*, 23:117–132, 2013. doi: https://doi.org/10.1016/j.jmbbm.2013.04.007.

M. A. Fernandez-Gil, R. Palacios-Bote, M. Leo-Barahona, and J. P. Mora-Encinas. Anatomy of the brainstem: a gaze into the stem of life. *Seminars in Ultrasound*, 31(3):196–219, 2010. doi: 10.1053/j.sult.2010.03.006.

D. Field, Y. Ammouche, J. M. Pẽna, and A. Jérusalem. Machine learning based multiscale calibration of mesoscopic constitutive models for composite materials: application to brain white matter. *Computational Mechanics*, 67:1629–1643, 2021. doi: https://doi.org/10.1007/s00466-021-02009-1.

R. D. Fields. A new mechanism of nervous system plasticity: activity-dependent

myelination. *Nature Reviews Neuroscience*, 16:756–767, 2015. doi: 10.1038/nrn4023.

M. Fini and W. J. Tyler. Transcranial focused ultrasound: a new tool for non-invasive neuromodulation. *International Review of Psychiatry*, 29(2):168–177, 2017. doi: 10.1080/09540261.2017.1302924.

K. Firouzi and N. Saffari. A numerical model for the study of photoacoustic imaging of brain tumours. *arXiv: Medical Physics*, 2015. doi: https://arxiv.org/ftp/arxiv/papers/1512/1512.06792.pdf.

R. Fitzhugh. Impulses and physiological states in theoretical models of nerve membrane. *Biophysical Journal*, 1(6):445–466, 1961. doi: https://doi.org/10.1016/S0006-3495(61)86902-6.

A. Fletcher. Action potential: Generation and propagation. *Anaesthesia and Intensive Care Medicine*, 9(6):251–255, 2008. doi: 10.1016/j.mpaic.2008.04.004.

A. Fletcher. Nerve cell function and synaptic mechanisms. *Anaesthesia and Intensive Care Medicine*, 15(6):282–286, 2014. doi: https://doi.org/10.1016/j.mpaic.2014.03.003.

J. L. Foley, J. W. Little, and S. Vaezy. Effects of high-intensity focused ultrasound on nerve conduction. *Muscle Nerve*, 37(2):241–250, 2008. doi: 10.1002/mus.20932.

R. Follmann, E. Rosa, and W. Stein. Dynamics of signal propagation and collision in axons. *Physical Review E: Statistical, Nonlinear, and Soft Matter Physics*, 92(3):1–11, 2015. doi: 10.1103/PhysRevE.92.032707.

D. Folloni, J. Sallet, A. A. Khrapitchev, N. Sibson, L. Verhagen, and R. B. Mars. Dichotomous organization of amygdala/temporal-prefrontal bundles in both humans and monkeys. *eLife*, pages 1–23, 2019a. doi: 10.7554/eLife.47175.

D. Folloni, L. Verhagen, R. B. Mars, E. Fouragnan, C. Constans, J. F. Aubry, M. F. Rushworth, and J. Sallet. Manipulation of subcortical and deep cortical activity in the primate brain using transcranial focused ultrasound stimulation. *Neuron*, 101(6):1109–1116, 2019b. doi: https://doi.org/10.1016/j.neuron.2019.01.019.

A. Fomenko, C. Neudorfer, R. F. Dallapiazza, S. K. Kalia, and A. M. Lozano. Low-intensity ultrasound neuromodulation: An overview of mechanisms and emerging human applications. *Brain Stimulation*, 11:1209–1217, 2018. doi: https://doi.org/10.1016/j.brs.2018.08.013.

B. Fornberg. High-order finite differences and the pseudospectral method on staggered grids. *SIAM Journal on Numerical Analysis*, 27(4):904–918, 1990. doi: https://doi.org/10.1137/0727052.

E. F. Fouragnan, B. K. Chau, D. Folloni, N. Kolling, L. Verhagen, M. Klein-Flügge, L. Tankelevitch, G. K. Papageorgiou, J. F. Aubry, J. Sallet, and M. F. Rushworth. The macaque anterior cingulate cortex translates counterfactual choice value into actual behavioral change. *Nature Neuroscience*, 22:797–808, 2019. doi: https://doi.org/10.1038/s41593-019-0375-6.

F. J. Fry. Acoustical properties of the human skull. *The Journal of the Acoustical Society of America*, 63(5):1576–1590, 1978. doi: https://doi.org/10.1121/1.381852.

F. J. Fry, H. W. Ades, and W. J. Fry. Production of reversible changes in the central nervous system by ultrasound. *Science*, 127(3289):83–84, 1958. doi: 10.1126/science.127.3289.83.

W. J. Fry. Intense ultrasound - a new tool for neurological research. *Journal of Mental Science*, 100(418):85–96, 1954. doi: https://doi.org/10.1192/bjp.100.418.85.

W. J. Fry. Electrical stimulation of brain localized without probes–theoretical analysis of a proposed method. *The Journal of the Acoustical Society of America*, 44(4):919–931, 1968. doi: 10.1121/1.1911230.

A. Galvan, M. J. Caiola, and D. L. Albaugh. Advances in optogenetic and chemogenetic methods to study brain circuits in non-human primates. *Journal of Neural Transmission*, 125:547–563, 2018. doi: https://doi.org/10.1007/s00702-017-1697-8.

S. Ganpule, N. P. Daphalapurkar, M. Pirtini Cetingul, and K. T. Ramesh. Effect of bulk modulus on deformation of the brain under rotational accelerations. *Shock Waves*, 28(1):127–139, 2018. doi: https://doi.org/10.1007/s00193-017-0791-z.

L. T. Gao, X. Q. Feng, Y. Yin, and H. Gao. An electromechanical liquid crystal model of vesicles. *Journal of the Mechanics and Physics of Solids*, 56(9):2844–2862, 2008. doi: 10.1016/j.jmps.2008.04.006.

D. Garcia-Gonzalez and A. Jérusalem. Energy based mechano-electrophysiological model of cns damage at the tissue scale. *Journal of the Mechanics and Physics of Solids*, 125(22):22–37, 2019. doi: https://doi.org/10.1016/j.jmps.2018.12.009.

D. Garcia-Gonzalez, A. Jérusalem, S. Garzon-Hernandez, R. Zaera, and A. Arias. A continuum mechanics constitutive framework for transverse isotropic tissues. *Journal of the Mechanics and Physics of Solids*, 112:209–224, 2018. doi: https://doi.org/10.1016/j.jmps.2017.12.001.

J. A. García-Grajales, G. Rucabado, A. García-Dopico, J. M. Peña, and A. Jérusalem. Neurite, a finite difference large scale parallel program for the simulation of electrical signal propagation in neurites under mechanical load-

ing. *PLoS One*, 10(2):1–22, 2015. doi: https://doi.org/10.1371/journal.pone.0116532.

A. N. Gasser, R. W. Ogden, and G. A. Holzapfel. Hyperelastic modelling of arterial layers with distributed collagen fiber orientations. *PLoS One*, 3(6), 2006. doi: https://doi.org/10.1098/rsif.2005.0073.

L. R. Gavrilov. Use of focused ultrasound for stimulation of nerve structures. *Ultrasonics*, 22(3):132–138, 1984. doi: https://doi.org/10.1016/0041-624X(84)90008-8.

L. R. Gavrilov and E. Tsirulnikov. Focused ultrasound as a tool to input sensory information to humans (review). *Acoustical Physics*, 58(1):3–27, 2012. doi: 10.1134/S1063771012010083.

GBD 2015 Neurological Disorders Collaborator Group. Global, regional, and national burden of neurological disorders during 1990-2015: a systematic analysis for the global burden of disease study 2015. *The Lancet Neurology*, 16(11):877–897, 2017. doi: https://doi.org/10.1016/S1474-4422(17)30299-5.

GBD 2016 Neurology Collaborators. Global, regional, and national burden of neurological disorders, 1990-2016: a systematic analysis for the global burden of disease study 2016. *The Lancet Neurology*, 18(5):459–480, 2019. doi: 10.1016/S1474-4422(18)30499-X.

R. M. Gibbs, S. Lipnick, J. W. Bateman, L. Chen, H. C. Cousins, E. G. Hubbard, G. Jowett, D. S. LaPointe, M. J. McGredy, O. M. N., G. Repetti, E. Thomas, and L. L. Rubin. Toward precision medicine for neurological and neuropsychiatric disorders. *Europe PMC*, 23(1):21–24, 2018. doi: 10.1016/j.stem.2018.05.019.

D. S. Gilbert. Axoplasm architecture and physical properties as seen in the

myxicola giant axon. *The Journal of Physiology*, 253(1), 1975. doi: https://doi.org/10.1113/jphysiol.1975.sp011190.

E. Glassinger, A. C. Lee, and R. M. Raphael. Electromechanical effects on tether formation from lipid membranes: A theoretical analysis. *Physical Review E*, 72(4), 2005. doi: 10.1103/PhysRevE.72.041926.

A. Gonzalez-Perez, R. Buvytyte, L. D. Mosgaard, S. Nissen, and T. Heimburg. Penetration of action potentials during collision in the median and lateral giant axons of invertebrates. *Physical Review X*, 4(3):1–12, 2014. doi: https://doi.org/10.1103/PhysRevX.4.031047.

A. Gonzalez-Perez, L. D. Mosgaard, R. Budvytyte, E. Villagran-Vargas, A. D. Jackson, and T. Heimburg. Solitary electromechanical pulses in lobster neurons. *Biophysical Chemistry*, 216:51–59, 2016. doi: https://doi.org/10.1016/j.bpc.2016.06.005.

S. A. Goss, R. L. Johnston, and F. Dunn. Comprehensive compilation of empirical ultrasonic properties of mammalian tissues. *The Journal of the Acoustical Society of America*, 64(2):423–457, 1978. doi: https://doi.org/10.1121/1.382016.

I. S. Grant and W. R. Phillips. *Electromagnetism (2nd Edition)*. John Wiley and Sons, 2008.

R. Grant, S. E. Gruenbaum, and J. Gerrard. Anaesthesia for deep brain stimulation. *Current Opinion in Anaesthesiology*, 28(5):505–510, 2015. doi: 10.1097/ACO.0000000000000230.

D. A. Groves and B. V. J. Vagal nerve stimulation: a review of its applications and potential mechanisms that mediate its clinical effects. *Neuroscience and Biobehavioral Reviews*, 29(3):493–500, 2005. doi: 10.1016/j.neubiorev.2005.01.004.

H. Guo, M. Hamilton 2nd, S. J. Offutt, C. D. Gloeckner, T. Li, Y. Kim, W. Legon, J. K. Alford, and H. H. Lim. Ultrasound produces extensive brain activation via a cochlear pathway. *Neuron*, 98(5):1020–1030, 2018. doi: https://doi.org/10.1016/j.neuron.2018.04.036.

R. Guttman. Temperature characteristics of excitation in space-clamped squid axons. *Journal of General Physiology*, 49(5):1007–1018, 1966. doi: https://doi.org/10.1085/jgp.49.5.1007.

H. Hakimova, S. Kim, K. Chu, S. K. Lee, B. Jeong, and D. Jeon. Ultrasound stimulation inhibits recurrent seizures and improves behavioral outcome in an experimental model of mesial temporal lobe epilepsy. *Epilepsy and Behavior*, 49:26–32, 2015. doi: https://doi.org/10.1016/j.yebeh.2015.04.008.

C. Hamani, H. Mayberg, S. Stone, A. Laxton, S. Haber, and A. M. Lozano. The subcallosal cingulate gyrus in the context of major depression. *Biological Psychiatry*, 69(4):301–308, 2011. doi: https://doi.org/10.1016/j.biopsych.2010.09.034.

S. Hameroff, M. Trakas, C. Duffield, E. Annabi, M. B. Gerace, P. Boyle, A. Lucas, Q. Amos, A. Buadu, and J. J. Badal. Transcranial ultrasound (tus) effects on mental states: a pilot study. *Brain Stimulation*, 6(3):409–415, 2013. doi: 10.1016/j.brs.2012.05.002.

S. Han, M. Kim, H. Kim, H. Shin, and I. Youn. Ketamine inhibits ultrasound stimulation-induced neuromodulation by blocking cortical neuron activity. *Ultrasound in Medicine and Biology*, 44(3):635–646, 2018. doi: https://doi.org/10.1016/j.ultrasmedbio.2017.11.008.

J. Harden, B. Mbanga, N. Éber, K. Fodor-Csorba, S. Sprunt, and J. T. Gleeson.

Giant flexoelectricity of bent-core nematic liquid crystals. *Physical Review Letters*, 97(15), 2006. doi: https://doi.org/10.1103/PhysRevLett.97.157802.

J. Harden, R. Teeling, J. T. Gleeson, S. Sprunt, and A. Jákli. Converse flexoelectric effect in a bent-core nematic liquid crystal. *Physical Review E*, 78(3), 2008. doi: https://doi.org/10.1103/PhysRevE.78.031702.

A. Haritonova, D. Liu, and E. S. Ebbini. In vivo application and localization of transcranial focused ultrasound using dual-mode ultrasound arrays. *IEEE Transactions on Ultrasonics, Ferroelectrics, and Frequency Control*, 62(12): 2031–2042, 2015. doi: 10.1109/TUFFC.2014.006882.

E. N. Harvey. The effect of high frequency sound waves on heart muscle and other irritable tissues. *American Journal of Physiology*, 91(1):284–290, 1929. doi: https://doi.org/10.1152/ajplegacy.1929.91.1.284.

P. A. Hasgall, F. Di Gennaro, C. Baumgartner, E. Neufeld, B. Lloyd, M. C. Gosselin, D. Payne, A. Kingenb ock, and N. Kuster. It'is database for thermal and electromagnetic parameters for biological tissues - version 4.0, 2021.

T. Heimburg and A. D. Jackson. On soliton propagation in biomembranes and nerves. *PNAS*, 102(28):9790–9795, 2005. doi: https://doi.org/10.1073/pnas.0503823102.

S. Herculano-Houzel. The remarkable, yet not extraordinary, human brain as a scaled-up primate brain and its associated cost. *PNAS*, 109:10661–10668, 2012. doi: https://doi.org/10.1073/pnas.1201895109.

B. C. Hill, E. D. Schubert, M. A. Nokes, and R. P. Michelson. Laser interferometer measurement of changes in crayfish axon diameter concurrent with action potential. *Science*, 196(4288):426–428, 1977. doi: 10.1126/science.850785.

D. K. Hill. The volume change resulting from stimulation of a giant nerve fibre.

The Journal of Physiology, 111(3-4):304–327, 1950. doi: 10.1113/jphysiol.1950.sp004481.

M. H. Histed, V. Bonin, and R. C. Reid. Direct activation of sparse, distributed populations of cortical neurons by electrical microstimulation. *Neuron*, 63(4): 508–522, 2009. doi: https://doi.org/10.1016/j.neuron.2009.07.016.

A. L. Hodgkin and A. F. Huxley. Action potentials recorded from inside a nerve fibre. *Nature*, 144:710–711, 1939. doi: https://doi.org/10.1038/144710a0.

A. L. Hodgkin and A. F. Huxley. A quantitative description of membrane current and its application to conduction and excitation in nerve. *The Journal of Physiology*, 117:500–544, 1952. doi: 10.1113/jphysiol.1952.sp004764.

L. Holland, H. W. de Regt, and B. Drukarch. Thinking about the nerve impulse: The prospects for the development of a comprehensive account of nerve impulse propagation. *frontiers in Cellular Neuroscience*, 13:208, 2019. doi: https://doi.org/10.3389/fncel.2019.00208.

M. M. Horder, S. B. Barnett, G. J. Vella, M. J. Edwards, and A. K. W. Wood. In vivo heating of the guinea-pig fetal brain by pulsed ultrasound and estimates of thermal index. *Ultrasound in Medicine and Biology*, 24(9):1467–1474, 1998. doi: https://doi.org/10.1016/S0301-5629(98)00111-2.

C. Howard, C. H. Hansen, and A. C. Zander. A review of current airborne ultrasound exposure limits. *Journal of Occupational Health and Safety - Australia and New Zealand*, 21(3):253–257, 2005. doi: https://www.researchgate.net/publication/235923211_A_review_of_current_airborne_ultrasound_exposure_limits.

J. V. Howarth, R. D. Keynes, and J. M. Ritchie. The origin of the initial heat associated with a single impulse in mammalian non-myelinated nerve fibres.

The Journal of Physiology, 194(3):745–793, 1968. doi: 10.1113/jphysiol.1968.sp008434.

K. H. Huebner. *The Finite Element Method for Engineers*. J. Wiley, New York; Chichester, 2001.

F. Hyder, E. A. Phelps, C. J. Wiggins, K. S. Labar, A. M. Blamire, and R. G. Shulman. "willed action": A functional mri study of the human prefrontal cortex during a sensorimotor task. *PNAS*, 94(13):6989–6994, 1997. doi: 10.1073/pnas.94.13.6989.

K. Hynynen and F. A. Jolesz. Demonstration of potential noninvasive ultrasound brain therapy through an intact skull. *Ultrasound in Medicine and Biology*, 24 (2):275–283, 1998. doi: 10.1016/s0301-5629(97)00269-x.

K. Hynynen, G. T. Clement, N. McDannold, N. Vykhodtseva, R. King, and P. J. White. 500-element ultrasound phased array system for non-invasive focal surgery of the brain: a preliminary rabbit study with ex vivo human skulls. *Magnetic Resonance in Medicine*, 52(1), 2004. doi: https://doi.org/10.1002/mrm.20118.

K. Hynynen, N. McDannold, N. A. Sheikov, F. A. Jolesz, and N. Vykhodtseva. Local and reversible blood-brain barrier disruption by noninvasive focused ultrasound at frequencies suitable for trans-skull sonications. *NeuroImage*, 24(1): 12–20, 2005. doi: https://doi.org/10.1016/j.neuroimage.2004.06.046.

K. Hynynen, N. McDannold, G. Clement, F. A. Jolesz, E. Zadicario, R. K. T. Moore, and D. Rosen. Pre-clinical testing of a phased array ultrasound system for mri-guided noninvasive surgery of the brain. *European Journal of Radiology*, 59(2):149–156, 2006. doi: https://doi.org/10.1016/j.ejrad.2006.04.007.

K. Iwasa and I. Tasaki. Mechanical changes in squid giant axons associ-

ated with production of action potentials. *Biochemical and Biophysical Research Communications*, 95(3):1328–1331, 1980. doi: https://doi.org/10.1016/0006-291X(80)91619-8.

K. Iwasa, I. Tasaki, and R. C. Gibbons. Swelling of nerve fibers associated with action potentials. *Science*, 210(4467):338–339, 1980. doi: 10.1126/science.7423196.

M. Jenkinson, C. F. Beckmann, T. E. J. Behrens, M. W. Woolrich, and S. M. Smith. Fsl. *NeuroImage*, 62(2):782–790, 2012. doi: https://doi.org/10.1016/j.neuroimage.2011.09.015.

A. Jérusalem, J. A. García-Grajales, A. Merchán-Pérez, and J. M. Peña. A computational model coupling mechanics and electrophysiology in spinal cord injury. *Biomechanics and Modeling in Mechanobiology*, 13:883–896, 2013. doi: 10.1007/s10237-013-0543-7.

A. Jérusalem, Z. Al-Rekabi, H. Chen, A. Ercole, M. Malboubi, M. Tamayo-Elizalde, L. Verhagen, and S. Contera. Electrophysiological-mechanical coupling in the neuronal membrane and its role in ultrasound neuromodulation and general anaesthesia. *Acta Biomaterialia*, 97(1):116–140, 2019. doi: https://doi.org/10.1016/j.actbio.2019.07.041.

L. D. Johns. Nonthermal effects of therapeutic ultrasound: The frequency resonance hypothesis. *Journal of Athletic Training*, 37(3):293–299, 2002. doi: https://www.ncbi.nlm.nih.gov/pmc/articles/PMC164359/pdf/attr_37_03_0293.pdf.

D. Johnston and S. M. S. Wu. *Foundations of Cellular Neurophysiology*. The MIT Press, 1994.

H. A. S. Kamimura. Focused ultrasound neuromodulation of cortical and sub-

cortical brain structures using 1.9 mhz. *Medical Physics*, 43(10):5730–5735, 2016. doi: 10.1118/1.4963208.

H. A. S. Kamimura, S. Wang, H. Y. Chen, Q. Wang, C. Aurup, C. J. Acosta, A. Carneiro, and E. E. Konofagou. Pupil dilation and motor response elicitation by ultrasound neuromodulation. *IEEE International Ultrasonics Symposium*, 2015. doi: 10.1109/ULTSYM.2015.0070.

H. A. S. Kamimura, A. Conti, N. Toschi, and E. E. Konofagou. Ultrasound neuromodulation: Mechanisms and the potential of multimodal stimualtion for neuronal function assessment. *frontiers in Physics*, 8(150), 2020. doi: https://doi.org/10.3389/fphy.2020.00150.

J. T. Kevenaar and C. C. Hoogenraad. The axonal cytoskeleton: from organization to function. *frontiers in Medical Neuroscience*, 8(44), 2016. doi: http://dx.doi.org/10.3389/fnmol.2015.00044.

N. Khanna, D. Gandhi, A. Steven, V. Frenkel, and E. R. Melhem. Intracranial applications of mr imaging-guided focused ultrasound. *American Journal of Neuroradiology*, 38(3):426–431, 2017. doi: https://doi.org/10.3174/ajnr.A4902.

M. L. Khraiche, W. B. Phillips, N. Jackson, and J. Muthuswamy. Ultrasound induced increase in excitability of single neurons. *Conference Proceedings - IEEE Engineering in Medicine and Biology Society*, pages 4246–4249, 2008. doi: 10.1109/IEMBS.2008.4650147.

H. Kim, A. Chiu, S. D. Lee, K. Fischer, and S. S. Yoo. Focused ultrasound-mediated non-invasive brain stimulation: Examination of sonication parameters. *Brain Stimulation*, 7(5):748–756, 2014a. doi: https://doi.org/10.1016/j.brs.2014.06.011.

H. Kim, S. D. Lee, A. Chiu, S. S. Yoo, and S. Park. Estimation of the spatial profile

of neuromodulation and the temporal latency in motor responses induced by focused ultrasound brain stimulation. *Neuroreport*, 25(7):475–479, 2014b. doi: 10.1097/WNR.0000000000000118.

H. Kim, M. Y. Park, S. D. Lee, W. Lee, A. Chiu, and S. S. Yoo. Suppression of eeg visual-evoked potentials in rats through neuromodulatory focused ultrasound. *Neuroreport*, 26(4):211–215, 2015. doi: 10.1097/WNR.0000000000000330.

R. L. King, J. R. Brown, W. T. Newsome, and K. Butts Pauly. Effective parameters for ultrasound-induced in vivo neurostimulation. *Ultrasound in Medicine and Biology*, 39(2):312–331, 2013. doi: 10.1016/j.ultrasmedbio.2012.09.009.

R. L. King, J. R. Brown, and K. B. Pauly. Localization of ultrasound-induced in vivo neurostimulation in the mouse model. *Ultrasound in Medicine and Biology*, 40(7):1512–1522, 2014. doi: 10.1016/j.ultrasmedbio.2014.01.020.

A. Kirton and D. Gilbert. *Pediatric Brain Stimulation (Mapping and Modulating the Developing Brain)*. Academic Press, 2016.

M. Kotikanyadanam, S. Göktepe, and E. Kuhl. Computational modeling of electrocardiograms: A finite element approach toward cardiac excitation. *International Journal for Numerical Methods in Biomedical Engineering*, 26:524–533, 2010. doi: 10.1002/cnm.1273.

B. Krasovitski, V. Frenkel, S. Shoham, and E. Kimmel. Intramembrane cavitation as a unifying mechanism for ultrasound-induced bioeffects. *PNAS*, 108(8): 3258–3263, 2011. doi: https://doi.org/10.1073/pnas.1015771108.

S. Krichen and P. Sharma. Flexoelectricity: A perspective on an unusual electromechanical coupling. *Journal of Applied Mechanics*, 83(3):1–5, 2016. doi: https://doi.org/10.1115/1.4032378.

V. Krishna, F. Sammartino, P. Agrawal, B. K. Changizi, E. Bourekas, M. V.

Knopp, and A. Rezai. Prospective tractography-based targeting for improved safety of focused ultrasound thalamotomy. *Neurosurgery*, 84(1):160–168, 2019. doi: https://doi.org/10.1093/neuros/nyy020.

J. D. Kropotov. *Functional Neuromarkers for Psychiatry (Applications for Diagnosis and Treatment)*. Academic Press, 2016.

K. Krug, C. D. Salzman, and S. Waddell. Understanding the brain by controlling neural activity. *Philosophical Transaction B*, 370:1–4, 2015. doi: http://dx.doi.org/10.1098/rstb.2014.0201.

J. Kubanek. Neuromodulation with transcranial focused ultrasound. *Neurosurgical Focus*, 44(2):1–12, 2018. doi: 10.3171/2017.11.FOCUS17621.

J. Kubanek, J. Shi, J. Marsh, D. Chen, C. Deng, and J. Cui. Ultrasound modulates ion channel currents. *Scientific Reports*, 6(24170):1–14, 2016. doi: 10.1038/srep24170.

J. Kusunose, W. Rodriguez, H. Luo, M. A. Phipps, W. Grissom, P. E. Konrad, B. M. Dawant, and C. Caskey. Patient-specific stereotactic frame for transcranial ultrasound therapy. *IEEE International Ultrasonics Symposium*, 2021. doi: 10.1109/IUS52206.2021.9593641.

M. T. Kwong, F. Bianchi, M. Malboubi, J. A. García-Grajales, L. Homsi, M. Thompson, H. Ye, L. Noels, and A. Jérusalem. 3d finite element formulation for mechanical-electrophysiological coupling in axonopathy. *Computer Methods in Applied Mechanics and Engineering*, 346(1025):1025–1050, 2019. doi: https://doi.org/10.1016/j.cma.2018.09.006.

A. Kyriakou, E. Neufeld, B. Werner, M. M. Paulides, G. Szekely, and N. Kuster. A review of numerical and experimental compensation techniques for skull-induced phase aberrations in transcranial focused ultrasound. *International*

Journal of Hyperthermia, 30(1):36–46, 2014. doi: https://doi.org/10.3109/02656736.2013.861519.

J. Latikka, T. Kuurne, and H. Eskola. Conductivity of living intracranial tissues. *Physics in Medicine and Biology*, 46(6):1611–1616, 2001. doi: https://doi.org/10.1088/0031-9155/46/6/302.

B. Lautrup, R. Appali, A. D. Jackson, and T. Heimburg. The stability of solitons in biomembranes and nerves. *The European Physical Journal E*, 34(57):1–9, 2011. doi: 10.1140/epje/i2011-11057-0.

D. Le Bihan. The 'wet mind': water and functional neuroimaging. *Physics in Medicine and Biology*, 52(7):57–90, 2007. doi: 10.1088/0031-9155/52/7/R02.

H. Le Quang and Q. C. He. The number and types of all possible rotational symmetries for flexoelectric tensors. *Proceedings of the Royal Society A*, 467:2369–2386, 2011. doi: 10.1098/rspa.2010.0521.

J. C. Lee, D. M. Blumnerger, P. B. Fitzgerald, Z. J. Daskalakis, and A. J. Levinson. The role of transcranial magnetic stimulation in treatment-resistant depression: a review. *Current Pharmaceutical Design*, 18(36):5846–5852, 2012. doi: 10.2174/138161212803523644.

J. C. F. Lee, J. C. Callaway, and R. C. Foehring. Effects of temperature on calcium transients and ca2+-dependent afterhyperpolarizations in neocortical pyramidal neurons. *Journal of Neurophysiology*, 93:2012–2020, 2005. doi: https://doi.org/10.1152/jn.01017.2004.

W. Lee, H. Kim, Y. Jung, I. U. Song, Y. A. Chung, and S. S. Yoo. Image-guided transcranial focused ultrasound stimulates human primary somatosensory cortex. *Scientific Reports*, 5(8743):1–10, 2015a. doi: 10.1038/srep08743.

W. Lee, H. Kim, S. D. Lee, M. Y. Park, and S. S. Yoo. Fus-mediated functional

neuromodulation for neurophysiologic assessment in a large animal model. *Journal of Therapeutic Ultrasound*, 3(1), 2015b. doi: https://doi.org/10.1186/2050-5736-3-S1-O23.

W. Lee, H. C. Kim, Y. Jung, Y. A. Chung, I. U. Song, J. H. Lee, and S. S. Yoo. Transcranial focused ultrasound stimulation of human primary visual cortex. *Scientific Reports*, 6(34026):1–12, 2016a. doi: 10.1038/srep34026.

W. Lee, S. D. Lee, M. Y. Park, L. Foley, E. Purcell-Estabrook, H. Kim, K. Fischer, L. S. Maeng, and S. S. Yoo. Image-guided focused ultrasound-mediated regional brain stimulation in sheep. *Ultrasound in Medicine and Biology*, 42 (2):459–470, 2016b. doi: https://doi.org/10.1016/j.ultrasmedbio.2015.10.001.

W. Legon, A. Rowlands, A. Opitz, T. F. Sato, and W. J. Tyler. Pulsed ultrasound differentially stimulates somatosensory circuits in humans as indicated by eeg and fmri. *PLoS One*, 7(12):1–14, 2012. doi: https://doi.org/10.1371/journal.pone.0051177.

W. Legon, T. F. Sato, A. Opitz, J. Mueller, A. Barbour, A. Williams, and W. J. Tyler. Transcranial focused ultrasound modulates the activity of primary somatosensory cortex in humans. *Nature Neuroscience*, 17(2):322–329, 2014. doi: 10.1038/nn.3620.

W. Legon, L. Ai, P. Bansal, and J. K. Mueller. Neuromodulation with single-element transcranial focused ultrasound in human thalamus. *Human Brain Mapping*, 39(5):1995–2006, 2018a. doi: 10.1002/hbm.23981.

W. Legon, P. Bansal, R. Tyshybsky, L. Ai, and J. K. Mueller. Transcranial focused ultrasound neuromodulation of the human primary motor cortex. *Scientific Reports*, 8(10007):1–14, 2018b. doi: 10.1038/s41598-018-28320-1.

J. F. Lehman, B. D. Greenberg, C. C. McIntyre, S. A. Rasmussen, and S. N.

Haber. Rules ventral prefrontal cortical axons use to reach their targets: Implications for diffusion tensor imaging tractography and deep brain stimulation for psychiatric illness. *Journal of Neuroscience*, 31(28):10392–10402, 2011. doi: https://doi.org/10.1523/JNEUROSCI.0595-11.2011.

G. Leinenga, C. Langton, R. Nisbet, and J. Götz. Ultrasound treatment of neurological diseases - current and emerging applications. *Nature Reviews Neurology*, 12(3):161–174, 2016. doi: 10.1038/nrneurol.2016.13.

P. P. Lele. Effects of focused ultrasonic radiation on peripheral nerve, with observations on local heating. *Experimental Neurology*, 8(1):47–83, 1963. doi: https://doi.org/10.1016/0014-4886(63)90008-6.

R. J. LeVeque. *Finite Difference Methods for Ordinary and Partial Differential Equations: Steady-state and time-dependent Problems*. Siam, Seattle, Washington, 2007.

G. Li, W. Qiu, Z. Zhang, Q. Jiang, M. Su, and R. Cai. Noninvasive ultrasonic neuromodulation in freely moving mice. *IEEE Transactions on Biomedical Engineering*, 66(1):217–224, 2018. doi: https://doi.org/10.1109/TBME.2018.2821201.

G. F. Li, H. X. Zhao, H. Zhou, F. Yan, J. Y. Wang, C. X. Xu, C. Z. Wang, L. L. Niu, L. Meng, S. Wu, H. L. Zhang, W. B. Qiu, and H. R. Zheng. Improved anatomical specificity of non-invasive neurostimulation by high frequency (5 mhz) ultrasound. *Scientific Reports*, 6(24738), 2016. doi: 10.1038/srep24738.

M. C. H. Li and M. J. Cook. Deep brain stimulation for drug-resistant epilepsy. *Epilepsia*, 59(2):273–290, 2018. doi: https://doi.org/10.1111/epi.13964.

D. Liewald, R. Miller, N. Logothetis, H. J. Wagner, and A. Sch uz. Distribution of axon diameter in cortical white matter: an electron-microscopic study on three

human brains and a macaque. *Biological Cybernetics*, 108(5):541–557, 2014. doi: 10.1007/s00422-014-0626-2.

Z. Lin, L. Meng, J. Zou, W. Zhou, X. Huang, S. Xue, T. Bian, T. Yuan, L. Niu, Y. Guo, and H. Zheng. Non-invasive ultrasonic neuromodulation of neuronal excitability for treatment of epilepsy. *Theranostics*, 10(12):5514–5526, 2020. doi: 10.7150/thno.40520.

N. Lipsman, T. G. Mainprize, M. L. Schwartz, K. Hynynen, and A. M. Lozano. Intracranial applications of magnetic resonance-guided focused ultrasound. *Neurotherapeutics*, 11:593–605, 2014. doi: 10.1007/s13311-014-0281-2.

L. P. Liu and P. Sharma. Flexoelectricity and thermal fluctuations of lipid bilayer membranes: Renormalization of flexoelectric, dielectric, and elastic properties. *Physical Review E*, 87:1–8, 2013. doi: https://doi.org/10.1103/PhysRevE.87.032715.

H. Lodish, A. Berk, S. L. Zipursky, P. Matsudaira, D. Baltimore, and J. Darnell. *Molecular Cell Biology*. W. H. Freeman, New York, 2000.

A. M. Lozano, H. S. Mayberg, P. Giacobbe, C. Hamani, R. C. Craddock, and S. H. Kennedy. Subcallosal cingulate gyrus deep brain stimulation for treatment-resistant depression. *Biological Psychiatry*, 64(6):461–467, 2008. doi: https://doi.org/10.1016/j.biopsych.2008.05.034.

G. Maimbourg, A. Houdouin, T. Deffieux, M. Tanter, and J. F. Aubry. 3d-printed adaptive acoustic lens as a disruptive technology for transcranial ultrasound therapy using single-element transducers. *Physics in Medicine and Biology*, 63 (2), 2018. doi: https://doi.org/10.1088/1361-6560/aaa037.

J. S. Manlapaz, K. E. Astrom, H. T. Ballantine, and P. P. Lele. Effects of ultrasonic

radiation in experimental focal epilepsy in the cat. *Experimental Neurology*, 10 (4):345–356, 1964. doi: https://doi.org/10.1016/0014-4886(64)90005-6.

R. B. Mars, L. Verhagen, T. E. Gladwin, F. X. Neubert, J. Sallet, and M. F. S. Rushworth. Comparing brains by matching connectivity profiles. *Neuroscience and Biobehavioral Reviews*, 60:90–97, 2016. doi: https://doi.org/10.1016/j.neubiorev.2015.10.008.

E. Martin, D. Jeanmonod, A. Morel, E. Zadicario, and B. Werner. High-intensity focused ultrasound for noninvasive functional neurosurgery. *Annals of Neurology*, 66(6):858–861, 2009. doi: 10.1002/ana.21801.

E. Martin, B. Werner, R. Bauer, K. van Leyen, D. Coluccia, and J. Fandino. Clinical neurological hifu applications: the zurich experience. *Translational Cancer Research*, 3(5):449–458, 2014. doi: http://tcr.amegroups.com/article/view/3156/3640.

MathWorks. Matlab and statistical toolbox release 2017b, 2017.

H. S. Mayberg, A. M. Lozano, V. Voon, H. E. McNeely, D. Seminowicz, C. Hamani, J. M. Schwalb, and S. H. Kennedy. Deep brain stimulation for treatment-resistant depression. *Neuron*, 45(5):651–660, 2005. doi: https://doi.org/10.1016/j.neuron.2005.02.014.

M. L. McCain and K. K. Parker. Mechanotransduction: the role of mechanical stress, myocyte shape, and cytoskeletal architecture on cardiac function. *Pflugers Archiv: European Journal of Physiology*, 462(1):89–104, 2011. doi: 10.1007/s00424-011-0951-4.

N. McDannold, G. T. Clement, P. Black, F. Jolesz, and K. Hynynen. Transcranial magnetic resonance imaging- guided focused ultrasound surgery of brain

tumors: initial findings in 3 patients. *Neurosurgery*, 66(2):323–332, 2010. doi: 10.1227/01.NEU.0000360379.95800.2F.

N. McDannold, C. D. Arvanitis, N. Vykhodtseva, and M. S. Livingstone. Temporary disruption of the blood-brain barrier by use of ultrasound and microbubbles: Safety and efficacy evaluation in rhesus macaques. *Therapeutics, Targets, and Chemical Biology*, 72(14):3652–3663, 2012. doi: 10.1158/0008-5472.CAN-12-0128.

E. Mehić, J. M. Xu, C. J. Caler, N. K. Coulson, C. T. Moritz, and P. D. Mourad. Increased anatomical specificity of neuromodulation via modulated focused ultrasound. *PLos One*, 9(2):1–13, 2014. doi: 10.1371/journal.pone.0086939.

J. Mendez and A. Keys. Density and composition of mammalian muscle. *Metabolism*, 9:184–188, 1960.

Y. Meng, C. B. Pople, H. Lea-Banks, A. Abrahao, B. Davidson, S. Suppiah, L. M. Vecchio, N. Samuel, F. Mahmud, K. Hynynen, C. Hamani, and N. Lipsman. Safety and efficacy of focused ultrasound induced blood-brain barrier opening, an integrative review of animal and human studies. *Journal of Controlled Release*, 309:25–36, 2019. doi: https://doi.org/10.1016/j.jconrel.2019.07.023.

R. B. Meyer. Piezoelectric effects in liquid crystals. *Physical Review Letters*, 22 (18):918–921, 1969. doi: https://doi.org/10.1103/PhysRevLett.22.918.

R. T. Mihran, F. S. Barnes, and H. Wachtel. Temporally-specific modification of myelinated axon excitability in vitro following a single ultrasound pulse. *Ultrasound in Medicine and Biology*, 16(3):297–309, 1990. doi: 10.1016/0301-5629(90)90008-z.

B. K. Min, A. Bystritsky, K. I. Jung, K. Fischer, Y. Zhang, L. S. Maeng, S. I. Park, Y. A. Chung, F. A. Jolesz, and S. S. Yoo. Focused ultrasound-mediated suppres-

sion of chemically-induced acute epileptic eeg activity. *BMC Neuroscience*, 12 (23):1–12, 2011a. doi: 10.1186/1471-2202-12-23.

B. K. Min, P. S. Yang, M. Bohlke, S. Park, D. R. Vago, T. J. Maher, and S. S. Yoo. Focused ultrasound modulates the level of cortical neurotransmitters: Potential as a new functional brain mapping technique. *International Journal of Imaging Systems and Technology*, 21(2):232–240, 2011b. doi: https://doi.org/10.1002/ima.20284.

R. Min and T. Nevian. Astrocyte signaling controls spike timing-dependent depression at neocortical synapses. *Nature Neuroscience*, 15:746–753, 2012. doi: 10.1038/nn.3075.

L. Minati and W. P. Weglarz. Physical foundations, models, and methods of diffusion magnetic resonance imaging of the brain: A review. *Concepts of Magnetic Resonance Part A*, 30(5):278–307, 2007. doi: https://doi.org/10.1002/cmr.a.20094.

M. Mohammadi, P. P. Ye, A. Xia, J. Brown, G. Popelka, and K. B. Pauly. Elimination of peripheral auditory pathway activation does not affect motor responses from ultrasound neuromodulation. *Brain Stimulation*, 12:901–910, 2019. doi: https://doi.org/10.1016/j.brs.2019.03.005.

M. M. Monti, C. Schnakers, A. S. Korb, and A. Bystritsky. Non-invasive ultrasonic thalamic stimulation in disorders of consciousness after severe brain injury: A first-in-man report. *Brain Stimulation*, 9(6):940–941, 2016. doi: https://doi.org/10.1016/j.brs.2016.07.008.

C. E. Morris. Voltage-gated channel mechanosensitivity: Fact or friction? *frontiers in Physiology*, 2(25):1–10, 2011. doi: 10.3389/fphys.2011.00025.

M.Plaksin, E. Kimmel, and S. Shoham. Cell-type-selective effects of intramem-

brane cavitation as a unifying theoretical framework for ultrasonic neuromodulation. *eNeuro*, 3(3):1–16, 2016. doi: 10.1523/ENEURO.0136-15.2016.

J. Mueller, W. Legon, A. Opitz, T. F. Sato, and W. J. Tyler. Transcranial focused ultrasound modulates intrinsic and evoked eeg dynamics. *Brain Stimulation*, 7 (6):900–908, 2014. doi: https://doi.org/10.1016/j.brs.2014.08.008.

J. K. Mueller and W. J. Tyler. A quantitative overview of biophysical forces impinging on neural function. *Physical Biology*, 11(5):1–15, 2014. doi: 10.1088/1478-3975/11/5/051001.

J. K. Mueller, L. Ai, P. Bansal, and W. Legon. Computational exploration of wave propagation and heating from transcranial focused ultrasound for neuromodulation. *Journal of Neural Engineering*, 13(5), 2016. doi: https://doi.org/10.1088/1741-2560/13/5/056002.

J. K. Mueller, L. Ai, P. Bansal, and W. Legon. Numerical evaluation of the skull for human neuromodulation with transcranial focused ultrasound. *Journal of Neural Engineering*, 14(6), 2017. doi: https://doi.org/10.1088/1741-2552/aa843eJ.

R. Muratore and J. J. Vaitekunas. Ultrasound bioeffects on peripheral nerves. *Acoustics Today*, 8:38–42, 2012. doi: http://quantumnowllc.com/RM_pubs/Muratore_2012_AT.pdf.

R. Muratore, J. LaManna, E. Szulman, A. Kalisz, M. Lamprecht, M. Simon, Z. Yu, N. Xu, and B. Morrison. Bioeffective ultrasound at very low doses: Reversible manipulation of neuronal cell morphology and function in vitro. *AIP Conference Proceedings*, 1113:25–29, 2009. doi: https://doi.org/10.1063/1.3131426.

J. S. Nagumo, S. Arimoto, and S. Yoshizawa. An active pulse transmission line

simulating nerve impulse. *Proceedings of the Institute of Radio Engineers*, 50 (10):2061–2070, 1962. doi: https://doi.org/10.3176/proc.2017.4.28.

O. Naor, S. Krupa, and S. Shoham. Ultrasonic neuromodulation. *Journal of Neural Engineering*, 13(3):1–18, 2016. doi: http://dx.doi.org/10.1088/1741-2560/13/3/031003.

T. Narahashi, J. W. Moore, and W. R. Scott. Tetrodotoxin blockage of sodium conductance increase in lobster giant axons. *Journal of General Physiology*, 47 (5):965–974, 1964. doi: 10.1085/jgp.47.5.965.

J. Narvaez, F. Vasquez-Sancho, and G. Catalan. Enhanced flexoelectric-like response in oxide semiconductors. *Nature*, 538:219–221, 2016. doi: https://doi.org/10.1038/nature19761.

E. A. Newman and K. R. Zahs. Modulation of neuronal activity by glial cells in the retina. *The Journal of Neuroscience*, 18(11):4022–4028, 1998. doi: https://doi.org/10.1523/JNEUROSCI.18-11-04022.1998.

T. D. Nguyen, N. Deshmukh, J. M. Nagarah, T. Kramer, P. K. Purohit, M. J. Berry, and M. C. McAlpine. Piezoelectric nanoribbons for monitoring cellular deformations. *Nature Nanotechnology*, 7(9):587–593, 2012. doi: 10.1038/nnano.2012.112.

M. A. Nitsche, P. S. Boggio, F. Fregni, and A. Pascual-Leone. Treatment of depression with transcranial direct current stimulation (tdcs): a review. *Experimental Neurology*, 219(1):14–19, 2009. doi: 10.1016/j.expneurol.2009.03.038.

S. Oh, C. Fang-Yen, W. Choi, Z. Yaqoob, D. Fu, Y. Park, R. R. Dassari, and M. S. Feld. Label-free imaging of membrane potential using membrane electromotility. *Biophysical Journal*, 103(1):11–18, 2012. doi: 10.1016/j.bpj.2012.05.020.

S. J. Oh, J. M. Lee, H. B. Kim, J. Lee, S. Han, J. Y. Bae, G. S. Hong, W. Koh,

J. Kwon, E. S. Hwang, D. H. Woo, I. Youn, I. J. Cho, Y. C. Bae, S. Lee, J. W. Shim, J. H. Park, and C. J. Lee. Ultrasonic neuromodulation via astrocytic trpa1. *Current Biology*, 29(20):3386–3401, 2019. doi: https://doi.org/10.1016/j.cub.2019.08.021.

J. X. O'Reilly, P. L. Croxson, S. Jbabdi, J. Sallet, M. P. Noonan, R. B. Mars, P. G. Browning, C. R. Wilson, A. S. Mitchell, K. L. Miller, M. F. Rushworth, and M. G. Baxter. Causal effect of disconnection lesions on interhemispheric functional connectivity in rhesus monkeys. *Proceedings of the National Academy of Sciences of the United States of America*, 110(34):13982–13987, 2013. doi: https://doi.org/10.1073/pnas.1305062110.

C. Pasquinelli, L. G. Hanson, H. R. Siebner, H. J. Lee, and A. Thielscher. Safety of transcranial focused ultrasound stimulation: A systematic review of the state of knowledge from both human and animal studies. *Brain Stimulation*, 12(6):1367–1380, 2019. doi: https://doi.org/10.1016/j.brs.2019.07.024.

R. E. Passingham, K. E. Stephan, and R. K otter. The anatomical basis of functional localization in the cortex. *Nature Reviews Neuroscience*, 3:606–616, 2002. doi: https://doi.org/10.1038/nrn893.

J. S. Perlmutter and J. W. Mink. Deep brain stimulation. *Annual Review of Neuroscience*, 29:229–257, 2006. doi: https://doi.org/10.1146/annurev.neuro.29.051605.112824.

A. G. Petrov. *Flexoelectric model for active transport. In Physical and Chemical Basis of Biological Information Transfer*. Plenum Press,, New York, 1975.

A. G. Petrov. *The Lyotropic State of Matter: Molecular Physics and Living Matter Physics*. Gordon and Breach Science Publishers, Amsterdam, The Netherlands, 1999.

A. G. Petrov. Flexoelectricity of model and living membranes. *Biochimica et Biophysica Acta*, 1561(1):1–25, 2002. doi: https://doi.org/10.1016/S0304-4157(01)00007-7.

A. G. Petrov. Electricity and mechanics of biomembrane systems: Flexoelectricity in living membranes. *Analytica Chimica Acta*, 568(1-2):70–83, 2006. doi: https://doi.org/10.1016/j.aca.2006.01.108.

A. G. Petrov and L. Mircevová. Is flexoelectricity the coupling factor between chemical energy and osmotic work in the pump? a model of pump. *General Physiology and Biophysics*, 5(4):391–403, 1986. doi: https://doi.org/10.1016/S0304-4157(01)00007-7.

A. G. Petrov, B. A. Miller, K. Hristova, and P. N. R. Usherwood. Flexoelectric effects in model and native membranes containing ion channels. *European Biophysical Journal*, 22:289–300, 1993. doi: https://doi.org/10.1007/BF00180263.

R. Phillips, J. Kondev, J. Theriot, and H. Garcia. *Physical Biology of the Cell*. Garland Science, 2012.

S. Picardo, V. W. Sin, and K. Hynynen. Multi-frequency characterization of the speed of sound and attenuation coefficient for longitudinal transmission of freshly excised human skulls. *Physics in Medicine and Biology*, 56(1):219–250, 2011. doi: 10.1088/0031-9155/56/1/014.

A. D. Pierce. *An Introduction to its Physical Principles and Applications*. Springer International Publishing, Springer Nature Switzerland AG, 1998.

C. Pierpaoli and P. J. Basser. Toward a quantitative assessment of diffusion anisotropy. *Magnetic Resonance in Medicine*, 36(6):893–906, 1996. doi: 10.1002/mrm.1910360612.

G. F. Pinton, J. F. Aubry, M. Fink, and M. Tanter. Numerical prediction of

frequency dependent 3d maps of mechanical index thresholds in ultrasonic brain therapy. *IEEE Ultrasonics Symposium*, 5935459:2258–2261, 2010. doi: 10.1109/ULTSYM.2010.5935459.

M. Plaksin, S. Shoham, and E. Kimmel. Intramembrane cavitation as a predictive bio-piezoelectric mechanism for ultrasonic brain stimulation. *Physical Review X*, 4:1–10, 2014. doi: 10.1103/PhysRevX.4.011004.

R. Polanía, M. A. Nitsche, and C. C. Ruff. Studying and modifying brain function with non-invasive brain stimulation. *Nature Neuroscience*, 21:174–187, 2018. doi: https://doi.org/10.1038/s41593-017-0054-4.

E. B. Postnikov and O. V. Titkova. A correspondence between the models of hodgkin-huxley and fitzhugh-nagumo revisited. *The European Physical Journal Plus*, 131(411):1–9, 2016. doi: 10.1140/epjp/i2016-16411-1.

P. Pouget, S. Frey, H. Ahnine, D. Attali, J. Claron, C. Constans, J. F. Aubry, and F. Arcizet. Neuronavigated repetitive transcranial ultrasound stimulation induces long-lasting and reversible effects on oculomotor performance in non-human primates. *frontiers in Physiology*, 11(1042), 2020. doi: https://doi.org/10.3389/fphys.2020.01042.

M. L. Prieto, Ö. Oralkan, B. T. Khuri-Yakub, and M. C. Maduke. Dynamic response of model lipid membranes to ultrasonic radiation force. *PLoS One*, 8 (10):1–14, 2013. doi: https://doi.org/10.1371/journal.pone.0077115.

M. L. Prieto, K. Firouzi, B. T. Khuri-Yakub, and M. Maduke. Activation of piezo1 but not nav1.2 channels by ultrasound at 43 mhz. *Ultrasound in Medicine and Biology*, 44(6):1217–1232, 2018. doi: https://doi.org/10.1016/j.ultrasmedbio.2017.12.020.

D. Purves, G. J. Augustine, D. Fitzpatrick, L. C. Katz, A. S. LaMantia, J. O.

McNamara, and S. M. Williams. *Neuroscience*. Sinauer Associates, Sunderland (MA), 2001.

W. Qiu, J. Zhou, Y. Chen, M. Su, G. Li, and H. Zhao. A portable ultrasound system for non-invasive ultrasonic neuro-stimulation. *IEEE Transactions on Neural Systems and Rehabilitation Engineering*, 25(12):2509–2515, 2017. doi: https://doi.org/10.1109/TNSRE.2017.2765001.

Z. Qiu, J. Guo, S. Kala, J. Zhu, Q. Xian, W. Qiu, G. Li, T. Zhu, L. Meng, R. Zhang, H. C. Chan, H. Zheng, and L. Sun. The mechanosensitive ion channel piezo1 significantly mediates in vivo ultrasonic stimulation of neurons. *iScience*, 21: 448–457, 2019. doi: https://doi.org/10.1016/j.isci.2019.10.037.

W. Rall. Theory of physiological properties of dendrites. *Annals of the New York Academy of Sciences*, 96(4):1071–1092, 2010. doi: https://doi.org/10.1111/j.1749-6632.1962.tb54120.x.

R. M. Raphael, A. S. Popel, and W. E. Brownell. A membrane bending model of outer hair cell electromotility. *Biophysical Journal*, 78(6):2844–2862, 2000. doi: https://doi.org/10.1016/S0006-3495(00)76827-5.

P. Riva-Posse, K. S. Choi, P. E. Holtzheimer, C. C. McIntyre, R. E. Gross, A. Chaturvedi, A. L. Crowell, S. J. Garlow, J. K. Rajendra, and H. S. Mayberg. Defining critical white matter pathways mediating succesful subcallosal cingulate deep brain stimulation for treatment-resistant depression. *Biological Psychiatry*, 76(12):963–969, 2014. doi: https://doi.org/10.1016/j.biopsych.2014.03.029.

J. L. B. Robertson, B. T. Cox, J. Jaros, and B. E. Treeby. Accurate simulation of transcranial ultrasound propagation for ultrasonic neuromodulation and stimu-

lation. *The Journal of the Acoustical Society of America*, 141(3), 2017. doi: https://doi.org/10.1121/1.4976339.

M. M. Rvachev. On axoplasmic pressure waves and their possible role in nerve impulse propagation. *Biophysical Reviews and Letters*, 5(2):73–88, 2010. doi: https://doi.org/10.1142/S1793048010001147.

F. Sachs. Stretch-activated ion channels: what are they? *Physiology (Bethesda)*, 25(1):50–56, 2010. doi: 10.1152/physiol.00042.2009.

J. L. Sanguinetti, S. Hameroff, E. E. Smith, T. Sato, C. M. Daft, W. J. Tyler, and J. J. B. Allen. Transcranial focused ultrasound to the right prefrontal cortex improves mood and alters functional connectivity in humans. *frontiers in Human Neuroscience*, 14(52):1–13, 2020. doi: 10.3389/fnhum.2020.00052.

E. Sassaroli and N. Vykhodtseva. Acoustic neuromodulation from a basic science prospective. *Journal of Therapeutic Ultrasound*, 4(17):1–14, 2016. doi: 10.1186/s40349-016-0061-z.

T. Sato, M. G. Shapiro, and D. Y. Tsao. Ultrasonic neuromodulation causes widespread cortical activation via an indirect auditory mechanism. *Neuron*, 6(98):1031–1041, 2018. doi: 10.1016/j.neuron.2018.05.009.

N. Sheikov, N. McDannold, S. Sharma, and K. Hynynen. Effect of focused ultrasound applied with an ultrasound contrast agent on the tight junctional integrity of the brain microvascular endothelium. *Ultrasound in Medicine and Biology*, 34(7):1093–1104, 2008. doi: https://doi.org/10.1016/j.ultrasmedbio.2007.12.015.

L. Shu, X. Wei, T. Pang, X. Yao, and C. Wang. Symmetry of flexoelectric coefficients in crystalline medium. *Journal of Applied Physics*, 110(104106):8, 2011. doi: https://doi.org/10.1063/1.3662196.

W. S. Slaughter. *The Linearized Theory of Elasticity*. Birkh auser, 2002.

J. M. Soares, P. Marques, V. Alves, and N. Sousa. A hitchhiker's guide to diffusion tensor imaging. *frontiers in Neuroscience*, 7(31):1–14, 2013. doi: https://doi.org/10.3389/fnins.2013.00031.

A. A. Spector, N. Deo, K. Grosh, J. T. Ratnanather, and R. M. Raphael. Electromechanical models of the outer hair cell composite membrane. *The Journal of Membrane Biology*, 209:135–152, 2006. doi: https://doi.org/10.1007/s00232-005-0843-7.

S. M. Sternson and B. L. Roth. Chemogenetic tools to interrogate brain functions. *Annual Review of Neuroscience*, 37:387–407, 2014. doi: https://doi.org/10.1146/annurev-neuro-071013-014048.

J. Sun and K. Hynynen. Focusing of therapeutic ultrasound through a human skull: a numerical study. *The Journal of the Acoustical Society of America*, 104 (1705), 1998. doi: https://doi.org/10.1121/1.424383.

M. Tabei, T. D. Mast, and R. C. Waag. A k-space method for coupled first-order acoustic propagation equations. *The Journal of the Acoustical Society of America*, 111(53):53–63, 2002. doi: https://doi.org/10.1121/1.1421344.

A. K. Tagantsev. Piezoelectricity and flexoelectricity in crystalline dielectrics. *Physical Review B*, 34(8):5883–5889, 1986. doi: 10.1103/PhysRevB.34.5883.

M. Tamayo Elizalde. *Action potential alterations induced by single neuron mechanical loading*. PhD thesis, The University of Oxford, Oxford, 2020.

S. C. Tang and G. T. Clement. Standing-wave suppression for transcranial ultrasound by random modulation. *IEEE Transactions on Biomedical Engineering*, 57(1):203–205, 2010. doi: https://doi.org/10.1109/TBME.2009.2028653.

J. Tanji. The supplementary motor area in the cerebral cortex. *Neuroscience Research*, 19(3):251–268, 1994. doi: https://doi.org/10.1016/0168-0102(94)90038-8.

I. Tasaki. A macromolecular approach to excitation phenomena: mechanical and thermal changes in nerve during excitation. *Physiological Chemistry and Physics and Medical NMR*, 20(4):251–268, 1988. doi: https://pubmed.ncbi.nlm.nih.gov/3076013/.

I. Tasaki and S. Hagiwara. Demonstration of two stable potential states in the squid giant axon under tetraethylammonium chloride. *Journal of General Physiology*, 40(6):859–885, 1957. doi: 10.1085/jgp.40.6.859.

I. Tasaki and K. Iwasa. Rapid pressure changes and surface displacements in the squid giant axon associated with production of action potentials. *The Japanese Journal of Physiology*, 32(1):69–81, 1982. doi: 10.2170/jjphysiol.32.69.

I. Tasaki, K. Kusano, and P. M. Byrne. Rapid mechanical and thermal changes in the garfish olfactory nerve associated with a propagated impulse. *Biophysical Journal*, 55(6):1033–1040, 1989. doi: 10.1016/S0006-3495(89)82902-9.

G. ter Haar. Therapeutic applications of ultrasound. *Progress in Biophysics and Molecular Biology*, 93(1-3):111–129, 2007. doi: https://doi.org/10.1016/j.pbiomolbio.2006.07.005.

G. ter Haar, S. Daniels, K. C. Eastaugh, and C. R. Hill. Ultrasonically induced cavitation in vivo. *British Journal of Cancer*, 45:151–155, 1982. doi: https://www.ncbi.nlm.nih.gov/pmc/articles/PMC2149305/pdf/brjcancersuppl00063-0160.pdf.

G. ter Haar, S. Daniels, and K. Morton. Evidence for acoustic cavitation in vivo: Thresholds for bubble formation with 0.75-mhz continuous wave and pulsed

beams. *IEEE transactions on ultrasonics, ferroelectrics, and frequency control*, 33(2):162–164, 1986. doi: 10.1109/t-uffc.1986.26809.

S. Terakawa. Potential-dependent variations of the intracellular pressure in the intracellularly perfused squid giant axon. *The Journal of Physiology*, 369:229–248, 1985. doi: 10.1113/jphysiol.1985.sp015898.

S. M. Thompson, L. M. Masukawa, and D. A. Prince. Temperature dependence of intrinsic membrane properties and synaptic potentials in hippocampal ca1 neurons in vitro. *The Journal of Neuroscience*, 5(3):817–824, 1985. doi: https://doi.org/10.1523/JNEUROSCI.05-03-00817.1985.

A. T. Todorov, A. G. Petrov, and J. H. Fendler. Flexoelectricity of charged and dipolar bilayer lipid membranes studied by stroboscopic interferometry. *Langmuir*, 10(7):2344–2350, 1994a. doi: https://doi.org/10.1021/la00019a053.

A. T. Todorov, A. G. Petrov, and J. H. Fendler. First observation of the converse flexoelectric effect in bilayer lipid membranes. *The Journal of Physical Chemistry*, 98(12):3076–3079, 1994b. doi: https://doi.org/10.1021/j100063a004.

L. H. Treat, N. McDannold, N. Vykhodtseva, Y. Zhang, K. Tam, and K. Hynynen. Targeted delivery of doxorubicin to the rat brain at therapeutic levels using mri-guided focused ultrasound. *International Journal of Cancer Therapy*, 121(4): 901–907, 2007. doi: https://doi.org/10.1002/ijc.22732.

B. T. Treeby and B. T. Cox. k-wave: Matlab toolbox for the simulation and reconstruction of photoacoustic wave fields. *Journal of Biomedical Optics*, 15 (2):021314, 2010. doi: https://doi.org/10.1117/1.3360308.

E. M. Tsirulnikov, I. A. Vartanyan, G. V. Gersuni, A. S. Rosenblyum, V. I. Pudov, and L. R. Gavrilov. Use of amplitude-modulated focused ultrasound for diagno-

sis of hearing disorders. *Ultrasound in Medicine and Biology*, 14(4):277–285, 1988. doi: https://doi.org/10.1016/0301-5629(88)90093-2.

P. H. Tsui, S. H. Wang, and C. C. Huang. In vitro effects of ultrasound with different energies on the conduction properties of neural tissue. *Ultrasonics*, 43 (7):560–565, 2005. doi: https://doi.org/10.1016/j.ultras.2004.12.003.

Y. Tufail, A. Matyushov, N. Baldwin, M. L. Tauchmann, J. Georges, A. Yoshihiro, S. I. Tillery, and T. W. J. Transcranial pulsed ultrasound stimulates intact brain circuits. *Neuron*, 66(5):681–694, 2010. doi: 10.1016/j.neuron.2010.05.008.

Y. Tufail, A. Yoshihiro, S. Pati, M. M. Li, and W. J. Tyler. Ultrasonic neuromodulation by brain stimulation with transcranial ultrasound. *Nature Protocols*, 6: 1453–1470, 2011. doi: doi:10.1038/nprot.2011.371.

W. J. Tyler. Noninvasive neuromodulation with ultrasound: A continuum mechanics hypothesis. *Neuroscientist*, 17(1):25–36, 2011. doi: 10.1177/1073858409348066.

W. J. Tyler. The mechanobiology of brain function. *Nature Reviews Neuroscience*, 13(12):867–878, 2012. doi: 10.1038/nrn3383.

W. J. Tyler, Y. Tufail, M. Finsterwald, M. L. Tauchmann, E. J. Olson, and C. Majestic. Remote excitation of neuronal circuits using low-intensity, low-frequency ultrasound. *PLoS One*, 3(10), 2008. doi: https://doi.org/10.1371/journal.pone.0003511.

W. J. Tyler, S. W. Lani, and G. M. Hwang. Ultrasonic modulation of neural circuit activity. *Current Opinion in Neurobiology*, 50:222–231, 2018. doi: https://doi.org/10.1016/j.conb.2018.04.011.

N. A. Uranova, N. I. Vykhodtseva, V. F. Fokin, A. V. Chepkunov, and V. M. Avirom. Ultrastructure of optic terminals in the superior colliculus after reversible

functional depression of optic tract by focused ultrasound. *Proceedings of International Meeting on Interaction of Ultrasound with Biological Media*, pages 29–30, 1979.

T. Ursell, R. Phillips, J. Kondev, D. Reeves, and P. A. Wiggins. The role of lipid bilayer mechanics in mechanosensation. *Respiratory Physiology and Neurobiology*, pages 1–37, 2007. doi: http://rpdata.caltech.edu/publications/reviewUrselletal2007.pdf.

W. Vanduffel. *In-Vivo Connectivity in Monkeys (Micro-, Meso- and Macro-Connectomics of the Brain)*. Springer, 2016.

F. Vasquez-Sancho, A. Abdollahi, D. Damjanovic, and G. Catalan. Flexoelectricity in bones. *Advanced Materials*, 30(9), 2018. doi: https://doi.org/10.1002/adma.201705316.

L. Verhagen, C. Gallea, D. Folloni, C. Constans, D. E. A. Jensen, H. Ahnine, L. Roumazeilles, M. Santin, B. Ahmed, S. Lehericy, M. C. Klein-Flügge, K. Krug, R. B. Mars, M. F. S. Rushworth, P. Pouget, J. F. Aubry, and J. Sallet. Offline impact of transcranial focused ultrasound on cortical activation in primates. *eLife*, 8:1–28, 2019. doi: 10.7554/eLife.40541.

M. D. Verweij and J. Huijssen. *Computational methods for nonlinear acoustic wavefields (Computational Methods in Nonlinear Acoustics: Current Trends)*. Research Signpost, 2011.

M. D. Verweij, B. E. Treeby, K. W. A. van Dongen, and L. Demi. *Simulation of Ultrasound Fields*. Elsevier B.V., 2014.

J. Vion-Bailly, W. A. N'Djin, I. M. Suarez Castellanos, J. L. Mestas, A. Carpentier, and J. Y. Chapelon. A causal study of the pehnomenon of ultrasound

neurostimulation applied to an in vivo invertebrate nervous model. *Scientific Reports*, 9(13738), 2019. doi: https://doi.org/10.1038/s41598-019-50147-7.

N. I. Vykhodtseva and V. I. Koroleva. Changes in the steady potential in various structures of the rat brain induced by focused ultrasound. *Doklady Akademii Nauk*, 287(1):248–251, 1986.

N. I. Vykhodtseva and V. I. Koroleva. Steady potential changes and spreading depression in rat brains produced by focused ultrasound. *AIP Conference Proceedings*, 829:59–63, 2006. doi: https://doi.org/10.1063/1.2205438.

N. I. Vykhodtseva, I. Konopatskaya, and V. I. Koroleva. Focused ultrasound potential to initiate spreading depression for disruption of blood brain barrier. *IEEE Ultrasonics Symposium*, pages 428–431, 2007.

T. Wagner, A. Valero-Cabre, and A. Pascual-Leone. Noninvasive human brain stimulation. *Annual Review of Biomedical Engineering*, 9:527–565, 2007. doi: 10.1146/annurev.bioeng.9.061206.133100.

R. A. Wahab, M. Choi, Y. Liu, V. Krauthamer, V. Zderic, and M. R. Myers. Mechanical bioeffects of pulsed high intensity focused ultrasound on a simple neural model. *Medical Physics*, 39(7):4274–4283, 2012. doi: 10.1118/1.4729712.

P. D. Wall, D. Tucker, F. J. Fry, and W. H. Mosberg Jr. The use of high intensity ultrasound in experimental neurology. *The Journal of the Acoustical Society of America*, 25(2):281–285, 1953. doi: https://doi.org/10.1121/1.1907032.

H. Wang, X. Zhou, D. Cui, R. Liu, R. Tan, X. Wang, Z. Liu, and T. Yin. Comparative study of transcranial magneto-acoustic stimulation and transcranial ultrasound stimulation of motor cortex. *frontiers in Behavioral Neuroscience*, 13 (241):1–10, 2019. doi: 10.3389/fnbeh.2019.00241.

J. A. Wang, W. Lin, T. Morris, U. Banderali, P. F. Juranka, and C. E. Morris.

Membrane trauma and na+ leak from nav1.6 channels. *AJP Cell Physiology*, 297(4):823–834, 2009. doi: 10.1152/ajpcell.00505.2008.

T. R. Wang, R. Dallapiazza, and W. J. Elias. Neurological applications of transcranial high intensity focused ultrasound. *International Journal of Hyperthermia*, 31(3):285–291, 2015. doi: https://doi.org/10.3109/02656736.2015.1007398.

Y. Wang, C. Xu, Z. Xu, C. Ji, J. Liang, Y. Wang, B. Chen, X. Wu, F. Gao, S. Wang, Y. Guo, X. Li, J. Luo, S. Duan, and C. Z. Depolarized gabaergic signaling in subicular microcircuits mediates generalized seizure in temporal lobe epilepsy. *Neuron*, 95(1):92–105, 2017. doi: 10.1016/j.neuron.2017.06.004.

M. L. Ward, I. A. Williams, Y. Chu, P. J. Cooper, Y. K. Ju, and D. G. Allen. Stretch-activated channels in the heart: contributions to length-dependence and to cardiomyopathy. *Progress in Biophysics and Molecular Biology*, 97(2-3): 232–249, 2008. doi: 10.1016/j.pbiomolbio.2008.02.009.

N. Wattiez, C. Constans, T. Deffieux, P. M. Daye, M. Tanter, J. F. Aubry, and P. Pouget. Transcranial ultrasonic stimulation modulates single-neuron discharge in macaques performing an antisaccade task. *Brain Stimulation*, 10(6): 1024–1031, 2017. doi: https://doi.org/10.1016/j.brs.2017.07.007.

D. N. White, G. R. Curry, and R. J. Stevenson. The acoustic characteristics of the skull. *Ultrasound in Medicine and Biology*, 4(3):225–239, 1978. doi: https://doi.org/10.1016/0301-5629(78)90054-6.

E. Wilke. Das problem der reizleitung im nerven vom standpunkte der wellenlehre aus betrachtet. *Pflüger's Archiv für die gesamte Physiologie des Menschen und der Tiere*, 144:35–38, 1912. doi: https://doi.org/10.1007/BF01681175.

World Health Organisation. Global health estimates 2016: Disease burden by cause, age, sex, by country and by region, 2000-2016, 2018.

URL https://www.who.int/healthinfo/global_burden_disease/estimates/en/index1.html.

A. Wright, T. Graven-Nielsen, I. Davies, and L. Arendt-Nielsen. Temporal summation of pain from skin, muscle and joint following nociceptive ultrasonic stimulation in humans. *Experimental Brain Research*, 144(4):475–482, 2002. doi: 10.1007/s00221-002-1062-4.

C. J. Wright, J. Rothwell, and N. Saffari. Ultrasonic stimulation of peripheral nervous tissue: an investigation into mechanisms. *Journal of Physics: Conference Series*, 581(13th Anglo-French Physical Acoustics Conference):1–12, 2015. doi: 10.1088/1742-6596/581/1/012003.

C. J. Wright, S. R. Hagshenas, J. Rothwell, and N. Saffari. Unmyelinated peripheral nerves can be stimulated in vitro using pulsed ultrasound. *Ultrasound in Medicine and Biology*, 43(10):2269–2283, 2017. doi: 10.1016/j.ultrasmedbio.2017.05.008.

R. M. Wright, A. Post, B. Hoshizaki, and K. T. Ramesh. A multiscale computational approach to estimating axonal damage under inertial loading of the head. *Journal of Neurotrauma*, 30(2):102–118, 2013. doi: 10.1089/neu.2012.2418.

Y. Wu, J. Mo, L. Sui, J. Zhang, W. Hu, C. Zhang, Y. Wang, C. Liu, B. Zhao, X. Wang, K. Zhang, and X. Xie. Deep brain stimulation in treatment-resistant depression: A systematic review and meta-analysis on efficacy and safety. *Frontiers in Neuroscience*, 15(655412), 2021. doi: https://doi.org/10.3389/fnins.2021.655412.

V. J. Wulff, W. J. Fry, D. Tucker, F. J. Fry, and C. Melton. Effect of ultrasonic vibrations on nerve tissues. *Proceedings of the Society for Experimental Biology and Medicine*, 76(2):361–366, 1951. doi: 10.3181/00379727-76-18490.

K. Xu, G. Zhong, and X. Zhuang. Actin, spectrin, and associated proteins form a periodic cytoskeletal structure in axons. *Science*, 339(6118):452–456, 2013. doi: 10.1126/science.1232251.

P. F. Yang, M. A. Phipps, A. T. Newton, V. Chaplin, J. C. Gore, C. F. Caskey, and L. M. Chen. Neuromodulation of sensory networks in monkey brain by focused ultrasound with mri guidance and detection. *Scientific Reports*, 8(1), 2018. doi: doi:10.1038/s41598-018-26287-7.

P. S. Yang, H. Kim, W. Lee, M. Bohlke, S. Park, T. J. Maher, and S. S. Yoo. Transcranial focused ultrasound to the thalamus is associated with reduced extracellular gaba levels in rats. *Neuropsychobiology*, 65(3):153–160, 2012. doi: 10.1159/000336001.

P. P. Ye, J. R. Brown, and K. Butts Pauly. Frequency dependence of ultrasound neurostimulation in the mouse brain. *Ultrasound in Medicine and Biology*, 42 (7):1512–1530, 2016. doi: https://doi.org/10.1016/j.ultrasmedbio.2016.02.012.

S. S. Yoo, K. Jung, Y. Zhang, N. McDannold, A. Bystritsky, and F. A. Jolesz. Noninvasive suppression of animal-model chronic epilepsy using image-guided focused ultrasound. *Proceedings of the SIGCHI Conference on Human Factors in Computing Systems*, pages 1797–1806, 2010. doi: https://doi.org/10.1145/1753326.1753596.

S. S. Yoo, A. Bystritsky, J. H. Lee, Y. Zhang, K. Fischer, B. K. Min, N. J. McDannold, A. Pascual-Leone, and F. A. Jolesz. Focused ultrasound modulates region-specific brain activity. *NeuroImage*, 56(3):1267–1275, 2011a. doi: 10.1016/j.neuroimage.2011.02.058.

S. S. Yoo, H. Kim, B. K. Min, E. Franck, and S. Park. Transcranial focused

ultrasound to the thalamus alters anesthesia time in rats. *NeuroImage*, 22(15): 783–787, 2011b. doi: doi:10.1097/WNR.0b013e32834b2957.

K. Yoon, W. Lee, J. E. Lee, L. Xu, P. Croce, L. Foley, and S. S. Yoo. Effects of sonication parameters on transcranial focused ultrasound brain stimulation in an ovine model. *PloS One*, 14(10):1–31, 2019. doi: https://doi.org/10.1371/journal.pone.0224311.

Y. Younan, T. Deffieux, B. Larrat, M. Fink, M. Tanter, and J. F. Aubry. Influence of the pressure field distribution in transcranial ultrasonic neurostimulation. *Medical Physics*, 40(8):1–10, 2013. doi: 10.1118/1.4812423.

J. Z. Young. The functioning of the giant nerve fibres of the squid. *Journal of Experimental Biology*, 15:170–185, 1938. doi: https://jeb.biologists.org/content/jexbio/15/2/170.full.pdf.

Y. Yuan, J. Yan, Z. Ma, and X. Li. Noninvasive focused ultrasound stimulation can modulate phase-amplitude coupling between neuronal oscillations in the rat hippocampus. *frontiers in Neuroscience*, 10(348), 2016. doi: https://doi.org/10.3389/fnins.2016.00348.

H. Zhang, T. Schneider, C. A. Wheeler-Kingshott, and D. C. Alexander. Noddi: practical in vivo neurite orientation dispersion and density imaging of the human brain. *Neuroimage*, 61(4):1000–1016, 2012. doi: https://doi.org/10.1016/j.neuroimage.2012.03.072.

O. Zohar, M. Ikeda, H. Shinagawa, H. Inoue, H. Nakamura, D. Elbaum, D. L. Alkon, and T. Yoshioka. Thermal imaging of receptor-activated heat production in single cells. *Biophysical Journal*, 74(1):82–89, 1998. doi: https://doi.org/10.1016/S0006-3495(98)77769-0.

J. Zou, L. Meng, Z. Lin, Y. Qiao, C. Tie, Y. Wang, X. Huang, T. Yuan, Y. Chi,

W. Meng, L. Niu, Y. Guo, and H. Zheng. Ultrasound neuromodulation inhibits seizures in acute epileptic monkeys. *iScience*, 23(5), 2020. doi: https://doi.org/10.1016/j.isci.2020.101066.

P. Zubko, G. Catalan, and A. K. Tagantsev. Flexoelectric effect in solids. *Annual Review of Materials Research*, 43:387–421, 2013. doi: https://doi.org/10.1146/annurev-matsci-071312-121634.

Zuse Institute Berlin and Thermo Fisher Scientific. Advanced 3d visualisation and volume modeling version 6.0.1, 2019. URL Softwareanduser'sguideavailablefromwww.amiravis.com.